Université Gustave Eiffel

Semi-Probabilistic Assessment of Existing Structures under Climate Change

Thèse de doctorat à l'Université Gustave Eiffel

École doctorale : Sciences, Ingénierie et Environnement (SIE)
Domaine du doctorat : Génie civil
Unité de recherche : Laboratoire EMGCU - Département MAST
Thèse soutenue à l'Université Gustave Eiffel
à Champs-sur-Marne, le 15 janvier 2026, par :

Lorenzo CASTI

Encadrement de la thèse

Dr. Franziska SCHMIDT Université Gustave Eiffel	Directrice de thèse
Prof. Dr. Fabio BIONDINI Politecnico di Milano	Co-directeur de thèse
Dr. Nisrine MAKHOUL ESTP Paris	Encadrante

Composition du jury

Prof. Emilio BASTIDAS-ARTEAGA La Rochelle Université	Rapporteur
Prof. Frédéric DUPRAT INSA Toulouse	Rapporteur
Prof. Arthur Lebee École nationale des ponts et chaussées	Président du jury
Prof. Dr. Gabriel SAS Luleå University of Technology	Examinateur
Dr. Jean-Bernard KOVARIK Université Gustave Eiffel	Examinateur

Acknowledgment

At the end of this journey, it is difficult to find the proper words to thank all the people who supported and helped me. But I want to try.
I would like to express my gratitude to my supervisors Franziska Schmidt, Fabio Biondini, and Nisrine Makhoul for their contributions, suggestions, and daily exchanges. You made this PhD experience very interesting and I learned a lot from you.
I would like to thank the members of the jury, who helped me greatly with their constructive revisions and comments to improve the quality of this PhD dissertation.
I would like to thank my PhDmate, Midula; we started and finished almost together. Thank you for the help with French administration and bureaucracy, thank you for being a good colleague, friend, and person. Thank you for sharing this journey with me. Thank you also to Silvia, for making me feel closer to home even when I was not. Thank you to the colleguas of my labs for helping me and welcoming me.
Thank you to Romain Pittet and the colleagues of APRR for the support they gave me and the experience in their offices of Saint-Apollinaire. Thank you for showing me the beautiful cable-stayed bridge. Somehow, I find beauty in this human constructions.
I would like to thank my parents, Patrizia and Giuseppe, for allowing me to follow this dream of a PhD, and for always being supportive even in the most difficult choices. This is for them, because without them, none of this would have been possible.
Thank you to Maurizio and Benedetta for being with me in this experience, even if from a distance. You gave me the energy to carry on until the end. Thank you to Luca, Riccardo, Simone, and Simona for being friends I can always rely on.
Thank you to my family, the part that came to Paris for my defense and the ones who could not. You always make me feel loved. Thank you to my Nonna Maria and Nonna Germana for everything you taught to me. Thank you to Marta and Daniele for very different reasons I cannot quite explain. I guess I am just happy to have you in my life.
Thank you to my Parisian friends, especially Eden, Maylisse, Jules, and Jankow, for integrating me into a friend group and welcoming me when I did not know anyone in France.
Thank you to Claudio, Noor, and Liam for the study nights and the nights out, the dinners, the late library sessions, the sports tournaments. Thank you for being my neighbors and now my friends. You made my journey in Paris special.
Thank you to the FEU friends and all the friends I met during these years and before who somehow do not hate me even when I disappear.
Finally, thank you to my two cats, Neko and Gastone, for simply making my life happier. This path was not without obstacles, but the people I met along the way are my greatest gifts.

This project has received funding from the European Union's Horizon 2020 research and innovation program under the Marie Skłodowska-Curie COFUND grant agreement No 101034248.



Funded by
the European Union

"Design is a journey of discovery."
Alvin Huang

"You mistake stars reflected in a pond for the night sky."
Andrzej Sapkowski

Abstract

The assessment of the residual performance of existing structures throughout their life cycle is a critical task for engineers, as it needs to address community demands while limiting the construction sector's emissions. Large stocks of existing structures and infrastructures have already exhibited significant deterioration and structural deficiencies, necessitating substantial investments in maintenance interventions. In the last decades, several structural failures have been observed in France and across Europe, such as the Mirepoix-sur-Tarn bridge and the Genoa viaduct. These failures are usually related to reduction in structural capacity due to deterioration processes, including environmental aging and mechanical degradation, and changes in structural demand, which affect structural systems throughout their service life.

Assessing the residual performance of existing structures typically is significantly different respect to the design of new structures, covering a broader spectrum of uncertainties. The differences arise from several aspects, such as the presence of time-dependent aging and deterioration processes, and the different reference service life. In addition, climate change may have a significant impact on this problem. In order to account for these aspects, full-probabilistic approaches are commonly employed in the assessment of existing structural systems. However, these methodologies are time-consuming and may require significant knowledge and expertise for numerical implementation. Consequently, the development of semi-probabilistic methodologies for existing structures considering the impact of climate change, including proper validation and calibration for incorporation in design codes and standards, is necessary.

This thesis focuses on the elaboration of a framework for the calibration of semi-probabilistic methodologies for the assessment of aging existing reinforced concrete structures under the impact of climate change. Corrosion, identified as the most critical deterioration mechanism in reinforced concrete structures, is analyzed, highlighting the impact of climate change on this process. The time-variant reliability of deteriorating structures is assessed via Monte Carlo simulation, with the aim of evaluating resistance parameters and safety factors.

The features and effectiveness of the proposed framework are presented and discussed with reference to a case study of a RC beam exposed to chloride-induced corrosion. The results demonstrate both the advantages and the limitations of the proposed framework, and the importance of a tailored approach to semi-probabilistic assessment of aging structures under climate change.

Résumé

L'évaluation de la performance résiduelle des structures existantes pendant leur cycle de vie est une tâche essentielle pour les ingénieurs, car elle doit répondre aux besoins de la communauté tout en limitant la contribution du secteur de la construction aux émissions. De nombreux bâtiments et infrastructures existants présentent déjà une détérioration importante et des défauts structurels, ce qui nécessite des investissements considérables dans des travaux d'entretien. Au cours des dernières décennies, plusieurs défaillances structurelles ont été observées en France et dans toute l'Europe, comme le viaduc de Gênes et le pont de Mirepoix-sur-Tarn. Ces défaillances sont généralement liées à des processus de détérioration, notamment le vieillissement environnemental et la dégradation mécanique, ainsi qu'à des changements dans la demande structurelle, qui affectent les systèmes structurels pendant toute leur durée de vie.

L'évaluation de la performance résiduelle des structures existantes implique généralement un éventail d'incertitudes plus large que la conception de nouvelles structures. Ces différences résultent des processus de vieillissement et de détérioration liés au temps, ainsi que des différences dans la durée de vie de référence prise en compte lors de l'évaluation. En outre, le changement climatique a un impact significatif sur cette évolution. Afin de tenir compte de ces aspects, des approches totalement probabilistes sont souvent utilisées dans l'évaluation des systèmes structurels existants. Cependant, ces méthodologies sont coûteuses en temps et peuvent nécessiter des connaissances et une expertise importantes pour leur mise en œuvre numérique. Par conséquent, il est nécessaire de développer des méthodologies semi-probabilistes pour les structures existantes tenant compte de l'impact du changement climatique, y compris une validation et un calibrage appropriés pour leur intégration dans les codes et normes de conception.

Cette thèse se focalise sur l'élaboration d'un cadre pour l'étalonnage de méthodologies semi-probabilistes pour l'évaluation des structures en béton armé existantes vieillissantes sous l'impact du changement climatique. La corrosion, identifiée comme le mécanisme de détérioration le plus critique dans les structures en béton armé, est analysée, en soulignant l'impact du changement climatique sur ce processus. La fiabilité variable dans le temps des structures en détérioration est évaluée à l'aide de la simulation de Monte Carlo, dans le but d'évaluer les paramètres de résistance et les facteurs de sécurité.

Les caractéristiques et l'efficacité du cadre proposé sont présentées et discutées en référence à une étude de cas d'une poutre en béton armé exposée à la corrosion induite par le chlorure. Les résultats démontrent à la fois les avantages et les limites du cadre proposé, ainsi que l'importance d'une approche sur mesure pour l'évaluation semi-probabiliste des structures vieillissantes dans le contexte du changement climatique.

Contents

Acknowledgment **III**

Abstract **VII**

Résumé **VIII**

List of Figures **XV**

List of Tables **XVII**

List of Acronyms **XIX**

1 Introduction **1**

1.1 Background and Motivation for the Research 1

1.2 Objective and Scope 5

1.3 Outline of the Dissertation 8

2 Fundamentals of Climate Change for Civil Engineering **10**

2.1 Fundamentals of Climate Science 10

2.1.1 Earth's energy balance 11

2.1.2 Radiative Forcing 13

2.1.3 Climate Drivers 13

2.2 Climate Change Scenarios 16

2.2.1 Historical development of climate change scenarios 17

2.2.2 Reference Climate Change Scenarios 19

2.3 Climate Models 22

2.3.1 Coupled Model of Intercomparison Project 24

2.3.2 Regional Climate Modeling 25

2.3.3 Uncertainties in Climate Modeling 27

2.4 Climate Change Impact on Civil Structures 28

3 Fundamentals of Semi-Probabilistic Assessment **33**
3.1 Background on Code Calibration . . . 33
3.2 Structural Reliability Analysis . . . 36
3.2.1 First-Order Reliability Methods . . . 37
3.2.2 Second-Order Reliability Methods . . . 41
3.2.3 Simulation Techniques . . . 41
3.3 Reliability-Based Code Calibration . . . 43
3.3.1 Definition of the Reliability Target . . . 43
3.3.2 Reliability-based Optimization Problem . . . 45
3.3.3 Design Value Method for Calibration . . . 49
3.4 Semi-Probabilistic Assessment . . . 51
3.4.1 Partial Safety Format . . . 52
3.4.2 Global Safety Format . . . 53
3.5 Semi-Probabilistic Assessment of Existing Structures . . . 55
3.5.1 Reliability Target for Existing Structures . . . 56
3.5.2 Assessment of Reinforced Concrete Structures . . . 57
3.5.2.1 Partial Safety Format . . . 61
3.5.2.2 Global Safety Format . . . 62
3.5.2.3 Considerations on Deteriorating Structures . . . 63
3.6 Semi-Probabilistic Assessment under Climate Change . . . 64
3.6.1 Characteristic Structural Demand . . . 65
3.6.2 Characteristic Structural Capacity . . . 70
3.7 Research Gaps and Challenges in Semi-Probabilistic Assessment . . . 74

4 Structural Capacity Modeling under Deterioration **76**
4.1 Reliability of Deteriorating Structures . . . 76
4.2 Structural Capacity Modeling under Deterioration . . . 77
4.3 Deterioration Mechanisms in Reinforced Concrete Structure . . . 79
4.3.1 Physical Deterioration . . . 79
4.3.2 Chemical Deterioration . . . 81
4.4 Corrosion of Reinforced Concrete Structures . . . 82
4.4.1 Corrosion Initiation . . . 84
4.4.1.1 Chloride-Induced Corrosion . . . 85
4.4.1.2 Carbonation-Induced Corrosion . . . 86
4.4.1.3 Climate Change Impact on Corrosion Initiation . . . 88
4.4.2 Corrosion Propagation . . . 93
4.4.2.1 Chloride-Induced Corrosion . . . 97
4.4.2.2 Carbonation-Induced Corrosion . . . 98

4.4.2.3 Climate Change Impact on Corrosion Propagation 99
4.4.3 Corrosion Damage 101
4.4.3.1 Steel Mass Reduction 102
4.4.3.2 Steel Strength Reduction 104
4.4.3.3 Steel Ductility Reduction 105
4.4.3.4 Concrete Cover Reduction 106
4.4.3.5 Steel-Concrete Bond Reduction 108
4.5 Remarks on Corrosion Modeling 108

5 Semi-Probabilistic Assessment of Existing Structure under Climate Change-induced Deterioration 112
5.1 Existing Aging Structure under Climate Change 112
5.1.1 Proposed Framework 113
5.1.2 Analytical Methodology 114
5.2 Semi-probabilistic Assessment of a RC beam under climate change-induced corrosion 120
5.2.1 Case Study Description 120
5.2.2 Results and Discussion 136
5.2.2.1 Reference Study 137
5.2.2.2 Impact of Space Variability 149
5.2.2.3 Impact of Corrosion Aggressiveness 159
5.3 Closing Remarks and Practical Implications 165

6 Conclusions and Future Perspectives 168
6.1 Conclusions 169
6.2 Future Perspectives 171

Bibliography 175

List of Figures

1.1 Example of bridge pier with corroded steel bars 2
1.2 Projected change in average mean surface air temperature in France for different climate change scenarios 4
1.3 Projected change in distribution of mean surface air temperature in France 4
1.4 Interconnected research subjects for the PhD dissertation 6

2.1 Scheme of the Earth's annual global mean energy budget. 12
2.2 Change in effective radiative forcing by different climate drivers 17
2.3 The challenge space for the SSPs 20
2.4 SSP-RCP scenario matrix 22
2.5 Representation of a climate model 23
2.6 Downscaling concept for climate models 26
2.7 Impacts of climate change on civil structures 29

3.1 Decision methodologies for structural analysis 35
3.2 Hasofer-Lind reliability index for a linear limit state function. 39
3.3 Principle of Monte Carlo Simulation 43

4.1 Phases of corrosion and damage propagation. 83
4.2 Corrosion consequences in reinforced concrete structure 84
4.3 Impact of temperature and relative humidity on chloride diffusivity in concrete 90
4.4 Impact of temperature and relative humidity on carbonate diffusivity in concrete 93
4.5 Influence of concrete resistivity on corrosion rate 95
4.6 Corrosion rate in carbonated mortar, both for different chloride content and relative humidity 98
4.7 Impact of temperature and relative humidity on the corrosion rate 101
4.8 Cross-section reduction of steel reinforcement. 103
4.9 Reduction of steel ductility for different levels of corrosion 105
4.10 Damage patterns induced by corrosion cracks in reinforced concrete structures 106

5.1 Calibration of semi-probabilistic format for the assessment of existing aging structures under climate change . . . 113
5.2 "Traditional" calibration of safety factors by solving the reliability-based optimization problem . . . 115
5.3 Proposed methodology for calibration of safety factors by solving the reliability-based optimization problem . . . 116
5.4 "Traditional" methodology for the determination of safety factors by using the design value method . . . 116
5.5 Proposed methodology for the determination of safety factors by using the design value method . . . 117
5.6 Static scheme of the clamped-hinged reinforced concrete beam. . . . 121
5.7 Cross-section of the clamped-hinged reinforced concrete beam. . . . 121
5.8 Variation in average mean surface air temperature in France for different climate change scenarios . . . 124
5.9 Variation in relative humidity in France for different climate change scenarios 125
5.10 Evolution of the empirical CDF and PDF of the steel area due to corrosion 127
5.11 Evolution of the empirical CDF and PDF of the steel yielding strength due to corrosion . . . 128
5.12 Evolution of the empirical CDF and PDF of the concrete cover area due to corrosion . . . 128
5.13 Internal forces in the damaged RC section under bending . . . 129
5.14 Evolution of the empirical CDF and PDF of the resisting bending moment due to corrosion . . . 130
5.15 Determination of characteristic values for steel area. . . . 131
5.16 Variation of the characteristic and design values of steel area with sample size . . . 133
5.17 Variation of the characteristic and design values of steel yielding strength with sample size . . . 133
5.18 Variation of characteristic and design values of the concrete cover area with sample size . . . 134
5.19 Variation of the characteristic and design values of ultimate bending moment with sample size . . . 134
5.20 Variation of empirical CDF for the critical, cracking, and failure time with sample size . . . 135
5.21 Detail of the variation of empirical CDF failure time with sample size . . . 135
5.22 Variation of the reliability index with sample size . . . 136

5.23 Scenarios for projected mean surface air temperature in France for the 2000-2100 period . . . 137
5.24 Scenarios for projected relative humidity in France for the 2000-2100 period 138
5.25 Evolution of the reliability index for different climate change scenarios . . . 138
5.26 Evolution of the characteristic value and the correction function of the steel area for different climate change scenarios . . . 139
5.27 Evolution of the characteristic value and the correction function of the steel yielding strength for different climate change scenarios . . . 140
5.28 Evolution of the characteristic value and the correction function of the concrete cover area for different climate change scenarios . . . 140
5.29 Evolution of the design value and the correction function of the steel area for different climate change scenarios . . . 141
5.30 Evolution of the design value and the correction function of the steel yielding strength for different climate change scenarios . . . 142
5.31 Evolution of the design value and the correction function of the concrete cover area for different climate change scenarios . . . 142
5.32 Evolution of the partial safety factor and the correction function of the steel area for different climate change scenarios. . . . 143
5.33 Evolution of the partial safety factor and the correction function of the steel yielding strength for different climate change scenarios. . . . 144
5.34 Evolution of the partial safety factor and the correction function of the concrete cover area for different climate change scenarios. . . . 144
5.35 Comparison between the reference and modified PSF for different climate change scenarios . . . 145
5.36 Evolution of the mean value and the correction function of the ultimate bending moment for different climate change scenarios . . . 146
5.37 Evolution of the design value and the correction function of the ultimate bending moment for different climate change scenarios . . . 147
5.38 Evolution of the global safety factor and the correction function of the ultimate bending moment for different climate change scenarios . . . 147
5.39 Evolution of the design value of the ultimate bending moment for different semi-probabilistic formats . . . 149
5.40 Projected temperature and relative humidity in Poitou-Charentes VS France 150
5.41 Projected temperature and relative humidity in Ile-de-France VS France . . 151
5.42 Projected temperature and relative humidity in Alsace VS France . . . 151
5.43 Projected temperature and relative humidity in Rhone-Alpes VS France . . 152
5.44 Projected temperature and relative humidity in Corse VS France . . . 152

5.45 Evolution of the reliability index of the aging reinforced concrete beam under climate change for different French regions. 153
5.46 Evolution of the mean value and the design value of the ultimate bending moment for selected French climates 154
5.47 Evolution of the correction functions for the mean value and for the design value of the ultimate bending moment under climate change for selected French climates 154
5.48 Evolution of the safety factor and correction function of the ultimate bending moment for selected French climates 155
5.49 Evolution of the normalized correction function for the mean values and for the design values of the ultimate bending moment for selected French climates 157
5.50 Evolution of the normalized correction function for the safety factors of the ultimate bending moment for selected French climates 158
5.51 Evolution of the reliability index of the aging reinforced concrete beam for the selected corrosion scenarios 160
5.52 Evolution of the mean value and the design value of the ultimate bending moment for the selected environmental aggressiveness scenarios 161
5.53 Evolution of the correction function for mean values and design values of the ultimate bending moment for the selected environmental aggressiveness scenarios 161
5.54 Evolution of the safety factor and correction function of the ultimate bending moment the selected environmental aggressiveness scenarios 162
5.55 Evolution of the normalized correction function for the mean values and for the design values of the ultimate bending moment for selected environmental aggressiveness scenarios 164
5.56 Evolution of the normalized correction function for the safety factors of the ultimate bending moment for environmental aggressiveness scenarios 164

List of Tables

2.1 Characteristics of the Representative Concentration Pathways 18
2.2 Summary of Shared Socio-economic Pathways narratives. 21

3.1 Levels of decision methodologies for structural analysis 36
3.2 Target reliability for 1-year reference period at the ULS according to the international standard ISO2394 44
3.3 Target Reliability for 1-year and 50-year reference period at the ULS according to the Eurocode 44
3.4 Reference FORM sensitivity factors 50
3.5 Research lines for calibration of safety factors in civil engineering 55
3.6 Research findings on reliability target values for existing structures. 58
3.7 Analytical formulation of reliability target tailored for existing bridges. . . 59
3.8 Partial safety format for the assessment of existing reinforced concrete structures. 62
3.9 Characteristic and design values of loadings considering climate change in the European standardization 69
3.10 Impact of climate change on the capacity of reinforced concrete structures under corrosion 73

4.1 Main deterioration mechanisms in reinforced concrete structures. 80
4.2 Surface chloride content for different exposure classes 86
4.3 Classifications of corrosion rate severity 94
4.4 Summary of Corrosion Rate Models 96
4.5 Chloride-induced corrosion rates for various exposures. 97
4.6 Carbonation-induced corrosion rates for various exposures. 99
4.7 Corrosion penetration rate considering different exposure scenarios 99

5.1 Geometrical characteristics of the clamped-hinged beam. 120
5.2 Statistical characteristics of the considered random variables 123
5.3 Comparison of the correction functions for selected regions under different climate scenarios 156

5.4 Exposure classes related to corrosion induced by chlorides. 159
5.5 Selected corrosion aggressiveness scenarios 160
5.6 Comparison of the correction functions for selected environmental aggressiveness scenarios and climate scenarios 163

Acronyms

AAR Alkali-Aggregate Reaction. 81

AFOSM Advanced First-Order Second-Moment. 37, 38

AM Approximate Methods. 48, 49

APFM Adjusted Partial Factor Method. 57, 60–62

CC Consequences Class. 57, 59

CDF Cumulative Density Function. 42, 50, 52, 53, 59, 118, 119, 127, 130, 131, 133

DVM Design Value Method. 49, 51, 57, 58, 60–62, 115, 117, 171

EMICs Earth System Models of Intermediate Complexity. 24

ERF Effective Radiative Forcing. 13, 16, 17

ESMs Earth System Models. 23, 24

FORM First Order Reliability Method. 37, 41, 48–50, 54, 66, 78, 79, 171

FOSM First-Order Second-Moment. 37

GCMs General Circulation Models. 24, 25

GHGs Greenhouse Gases. 10–12, 14, 18, 28, 33

GOM Global Optimization Methods. 48

GSF Global Safety Format. 51, 53, 62, 63, 117, 119, 121, 130, 131, 136, 148, 165, 166, 170

IPCC Intergovernmental Panel on Climate Change. 17, 19

NCC No Climate Change. 122, 123, 137, 139, 146, 157

NLSA Non-Linear Structural Analysis. 62, 63

PDF Probability Density Function. 41, 42, 51, 127, 130, 171

PSF Partial Safety Format. 51, 52, 62, 63, 117, 119, 121, 131, 136, 139, 146, 148, 165, 166, 170

RC Reinforced Concrete. 6–8, 29, 45, 57, 61–64, 70–73, 77–86, 91, 100–102, 106, 108, 110, 111, 114, 117, 119, 120, 146, 148, 152, 153, 159, 160, 165, 169, 171

RCPs Representative Concentration Pathways. 18, 19, 22

RF Radiative Forcing. 11, 13–16, 18

RV Random Variable. 132

SLS Serviceability Limit State. 45

SORM Second Order Reliability Method. 37, 41, 48, 78, 79

SSPs Shared Socio-economic Pathways. 19, 21, 22, 113, 122

ULS Ultimate Limit State. 44, 45

Chapter 1

Introduction

1.1 Background and Motivation for the Research

Civil structures are conventionally designed and maintained to ensure a specified level of functionality, durability, and safety over a period of time. In particular, strategic structures, such as bridges and infrastructural networks, are expected to satisfy the prescribed performance criteria throughout their service life, which typically spans from 50 to 100 years (ASCE, 1999; CEN, 2002). In this context, the evaluation of the residual structural performance is currently a key issue, as a substantial number of existing structures is approaching the end of their design service life (Belin, 2022; ASCE, 2025).

The assessment of existing structures can be perform at different level respect with the complexity of the problem, the uncertainties involved, and the consequences of failure (ISO2394, 2015). For the usual cases in terms of uncertainty and consequences of failure, the semi-probabilistic methodology is generally recommended and preferred especially by practitioners for the sake of repeatability and simplicity. Nevertheless, most of the current structural codes, such as the Eurocodes (CEN, 2002), propose reference values for the application of this methodology only for the design of new structures.

The exploitation of the semi-probabilistic methodology tailored for the design of new structures may, in several cases, lead to unnecessary and costly repair interventions due to intrinsic differences in the evaluation of existing systems (Luechinger et al., 2015). For this reason, significant efforts have been made concerning the calibration of semi-probabilistic methodology for the assessment of existing structures (Diamantidis and Bazzurro, 2007; Steenbergen and Vrouwenvelder, 2010; Caspeele et al., 2013; fib, 2016), leading to the development of tailored regulations in the last decade (SIA, 2011; AS, 2017; fib, 2023; CEN, 2024). Nevertheless, the methodology is generally applicable under the assumption of undamaged structure without deterioration evidence and stationary climate conditions, highlighting a gap in the current research proposal.

Environmental deterioration may have a major influence on the performance and durability of civil structures, as highlighted by several reports on the condition of existing infrastructure (Cerema, 2024; ASCE, 2025). The Infrastructure Report Card of the American Society of Civil Engineers (ASCE, 2025) shows that among more than 623,000 bridges in the United States, about 6.8% are currently rated in "poor" structural condition (Figure 1.1). Furthermore, it is estimated that approximately 191 billion dollars would be needed to restore the national bridge network to a satisfactory condition.



Figure 1.1: Example of bridge pier with corroded steel bars, from ASCE (2025)

A similar situation is observed in Europe. For instance, in France, 63,180 structures have been assessed, revealing that 25% of bridges and 14% of retaining walls exhibit significant structural defects (Chaize and Dagbert, 2019; Cerema, 2024). The estimated annual cost for maintenance of these structures is around 140 million euros, while the complete repair would require nearly 3.3 billion euros.

These reports highlight the increasing necessity of assessing existing structures, considering the impact of deterioration processes, if identified, combined with strategic maintenance planning. Evaluation of the residual structural performance allows engineers and practitioners to estimate the actual structural behavior and to preserve the designed performance, avoiding costly repair and rehabilitation activities.

Over the past decades, substantial changes in global climate trends have been doc-

umented by the scientific community (IPCC, 1990, 2007, 2013, 2023a). Unsustainable energy and land use practices, coupled with lifestyles and production–consumption patterns, have driven greenhouse gas emissions to unprecedented levels between 2010 and 2019, leading to anthropogenic climate change.

Human-induced climate change is expected to influence human communities in several ways, such as adversely affecting food and water security (Gregory et al., 2005; Misra, 2014) and posing increasing risks to human health (Ascione and Valdano, 2025; Patz et al., 2005). In addition, it is predicted to impact the frequency and intensity of numerous extreme weather and climate events worldwide (Seneviratne et al., 2021; Stott, 2016). Observed impacts include rising atmospheric and ocean temperatures, more severe droughts and wildfires, increased extreme precipitation, and accelerated global sea-level rise—trends that are projected to intensify throughout the 21st century.

Figure 1.2 presents the projections of the mean surface air temperature in France over the 21st century under different climate change scenarios. The results consistently indicate a significant warming trend compared to the historical reference period (1995–2014). Even under moderate emission pathways, temperatures are expected to rise continuously, while high-emission scenarios may lead to increases exceeding 4°C by 2100. In addition to this trend, the evolution of probabilistic distributions for different time windows is represented in Figure 1.3, indicating a clear progression toward higher temperature regimes, accompanied by an widening distribution spread. This reflects not only a sustained long-term increase, but also enhanced variability, which means more frequent and intense warm periods.

The uncertainties in future climate conditions depend on several complex natural and social factors, and their interactions which are expected to be observed in a long-term horizon. In this context, the exact prediction of the future state of the Earth's climate is practically very difficult if not impossible. For these reasons, the problem should be treated considering decision-making under deep uncertainty. Under these conditions, the future may be represented by a large set of scenarios for which decision-makers cannot agree on specific probabilities (Marchau et al., 2019). Moreover, Further, the structure of the models used to represent the climate, its parameters, its inputs and outputs, and the criteria to rank the preference of possible outcomes may be also different. Deep uncertainty poses additional challenges to the evaluation of future structural performance since decision-makers first need to decide on the most likely future conditions and then assess the systems for those particular conditions, adding a safety margin to account for uncertainty (Yousefpour and Hanewinkel, 2016).

Changes in climate directly affect not only human society but also the performance of civil infrastructure. Firstly, climate change is expected to affect structural resistance due

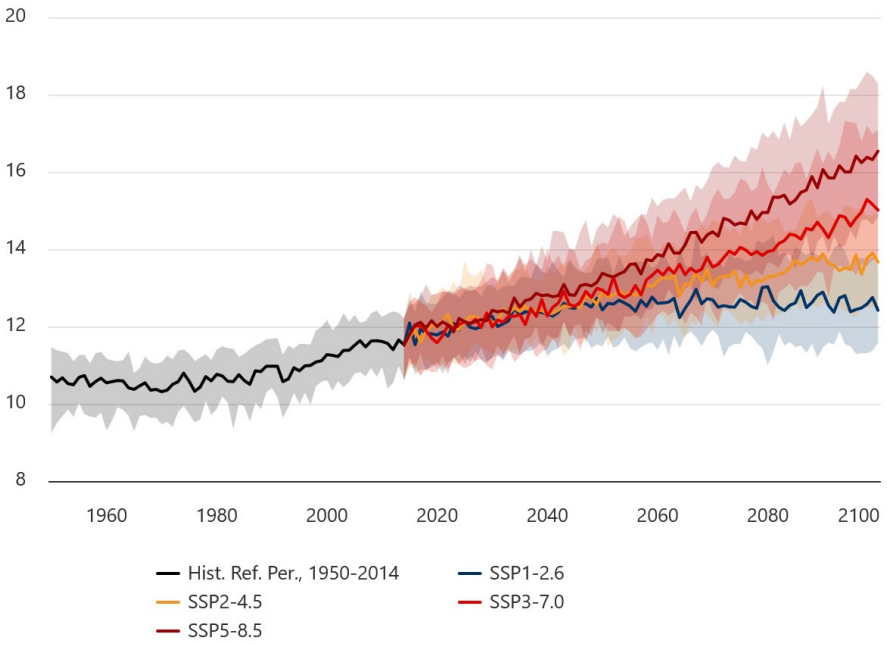

Figure 1.2: Projected change in average mean surface air temperature in France for different climate change scenarios (WorldBankGroup, 2025)

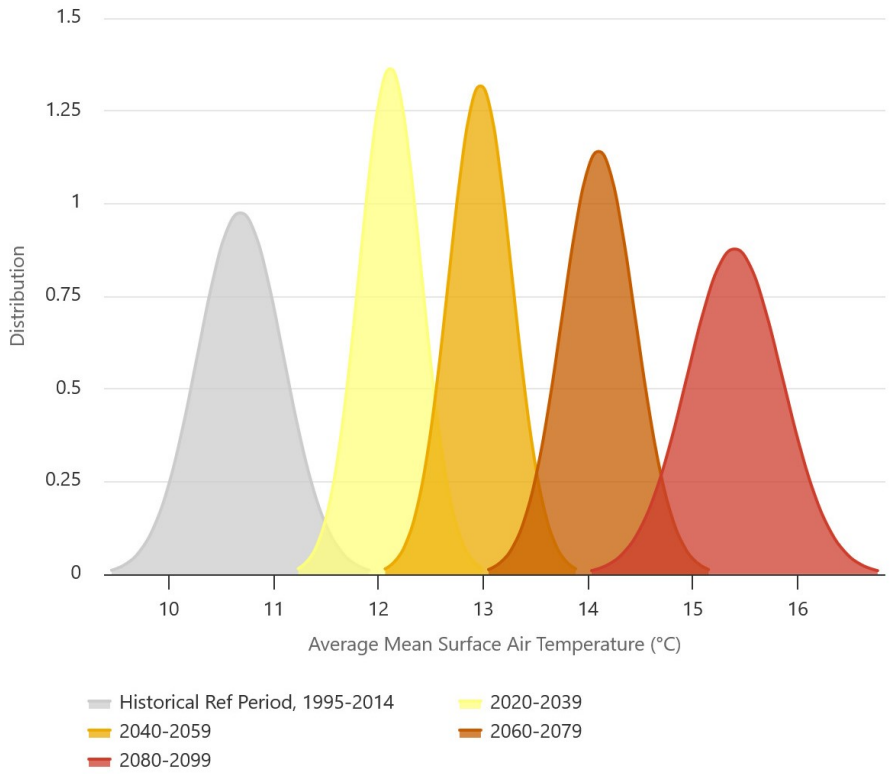

Figure 1.3: Projected change in distribution of mean surface air temperature in France for the SSP5-8.5 (WorldBankGroup, 2025)

to the exacerbation of deterioration processes (Raposo De M. Do N. E S. De Sotto Mayor et al., 2020; Nasr et al., 2021) and the consequent damage associated with these mechanisms, such as corrosion (Stewart et al., 2011; Bastidas-Arteaga et al., 2013). Secondly, climatic loads are expected to be altered by climate change (Croce et al., 2019; Mishra and Sadhu, 2023), resulting in an evolution of structural demand.

The mentioned impacts of future climate conditions further highlights the need to incorporate time-dependent and climate-sensitive methodologies for the performance assessment of the existing built environment.

Current standards and codes for structural design and assessment are still based on historical climatic data and associated loads, operating under the assumption of stationarity. Changes in climate affecting the built environment are proving the hypothesis of stationarity questionable, highlighting the need to redefine the characteristic values of climatic loadings, (Croce et al., 2019), the safety factors, and the concept of the return period (Cooley, 2012; Kovarik, 2024). Moreover, the actual regulation does not provide specific guidance regarding the semi-probabilistic methodology when the structure is subject to deterioration processes, which may severely impact the characteristic values of capacity and the associated safety factors.

Consequently, nowadays, one of the main challenges for civil engineers involves the life-cycle assessment, prediction, and optimal management of aging structures and infrastructure systems under uncertainty, while taking into account the effects of climate change. This implies the incorporation of non-stationarity consideration for loadings definition and damaged structures in code regulations. The goal is to provide engineers and practitioners with the tools to analyze the aging existing structural systems, considering the impact of climate change both on resistance and demand.

For this reasons, the calibration of an appropriate semi-probabilistic format for assessing the aging of existing structures in a changing climate represents a critical issue that practitioners and researchers must address.

1.2 Objective and Scope

The main purpose of this PhD dissertation is to define a methodological and analytical framework for the calibration of semi-probabilistic methodology for the assessment of existing structures subjected to environmental aging under climate change. Three main research spheres are investigated and interconnected for this purpose: climate change, environmental aggressiveness, and life-cycle reliability (Figure 1.4).

1. **Climate change** may influence structural capacity and demand over time. To

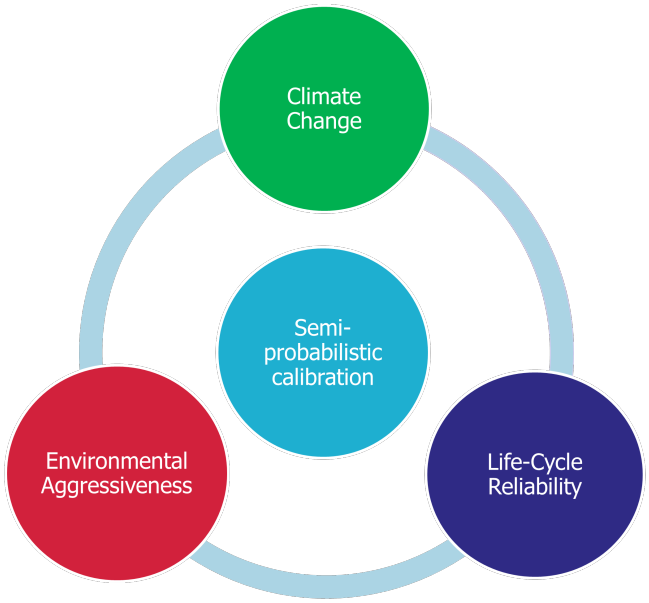

Figure 1.4: Interconnected research subjects for the PhD dissertation

evaluate this impact, future projections of environmental parameters should be taken into account. The definition of these projections depends on the considered climate change scenarios, which are based on assumptions about socio-economic drivers and possible future policies. These scenarios are used in climate models to predict future environmental parameters on a specific temporal and spatial scale.

2. **Environmental aggressiveness** is significantly influenced by surrounding climate conditions; therefore, the integration of deterioration processes, such as corrosion, with future climate projections is fundamental for accurately estimating structural damage over time. Indeed, the assessment of structural safety can be considered a decision problem involving uncertainties, wherein the resistance $R = R(t)$ should not be lower than the demand $S = S(t)$ over time t; consequently, the uncertainties involved in this problem evolve during the system's lifetime, primarily due to aging and structural deterioration. This evolution leads to a decay of the resistance and to possible alterations of the demand, which relate to changes in external loadings or internal stress redistribution. Climate change is observed to impact both structural loadings (Mishra and Sadhu, 2023), such as snow, temperature, and wind loads, and to enhance deterioration mechanisms, including chloride- and carbonate-induced corrosion (Stewart et al., 2011; Stewart et al., 2012; Bastidas-Arteaga and Stewart, 2016). Given its diffusion and severity in existing Reinforced Concrete (RC) infrastructure, and its strong sensitivity to environmental conditions, corrosion-induced deterioration is expected to intensify under future climate scenarios. Rising tem-

peratures, increasing atmospheric carbon dioxide concentrations, evolving humidity and chloride exposure conditions are likely expected to accelerate both carbonation and chloride ingress. Therefore, corrosion represents a critical phenomenon to investigate when assessing the long-term reliability of reinforced concrete structures subjected to climate change, constituting the primary degradation mechanism addressed in this thesis.

3. In this context, **life-cycle reliability** analysis of existing aging structures, considering the long-term evolution of environmental parameters, may be used to estimate the time-variant safety of the considered structural system. Eventually, these results may be used for the calibration of tailored the semi-probabilistic methodology, which is generally based on reliability considerations.

The proposed methodology aims to address the integration of climate change and deterioration processes considerations into the calibration of semi-probabilistic formats. In fact, regarding structural demand, efforts are already ongoing to integrate the impact of climate change into future standards (Croce et al., 2016; Athanasopoulou et al., 2020; Arnold and Kraus, 2022), while a research gap has been identified concerning the evolution of structural capacity.

The methodology is then applied for the life-cycle analysis of an aging RC clamped-hinged beam under climate change. The purpose of this evaluation is to underline the peculiar benefits and drawbacks of the framework, highlighting the potential interests of this investigation. The impact of climate change and environmental degradation on the evolution of resistance uncertainty over time using simulation-based techniques.

The developed methodology enables the estimation of the impact of climate change on the evolution of structural performance, highlighting the modification of the reliability elements of the semi-probabilistic methodology and the importance of these aspects in its calibration. In addition, these results highlight the need to consider, on the one hand, deterioration processes and the consequent induced damage, and on the other, environmental parameters and climate evolution over time for an appropriate semi-probabilistic assessment of aging RC structures under climate change and a life-cycle-informed approach to optimally manage infrastructure systems.

1.3 Outline of the Dissertation

The proposed dissertation is organized into six chapters. The content and structure are summarized concisely in the following sections.

In **Chapter 2** the impact of climate change on civil engineering is presented, focusing on civil structures. Section 2.1 presents the fundamental concept of climate science and the basics of climate change. The reference climate change scenarios are described in Section 2.2 with particular attention to their conception. The modeling of climate is briefly introduced in Section 2.3, assessing as well the involved uncertainties. Eventually, the impact of climate change and the connected risks respect to civil structures are addressed and reported in Section 2.4.

Chapter 3 presents the fundamental aspects of code calibration strategies, focusing on the definition of semi-probabilistic methodologies. The main differences between the design of new structures and the assessment of existing ones are highlighted, while also considering the possible impact of climate change. In Section 3.1, the background of code calibration is presented, focusing on the initial attempts and the historical development of code calibration. Section 3.2 details the fundamental concepts of reliability analysis, including the definition of the reliability index, its calculation using various techniques. In Section 3.3, the concept of reliability target is introduced and the peculiarities of reliability-based calibration are discussed. Section 3.4 illustrates the fundamental notions and components of semi-probabilistic formats. Eventually, Section 3.5 focuses on the semi-probabilistic assessment of existing structures, highlighting its peculiarities respect to design of new structures and discussing several studies which addressed this subject. Section 3.6 analyzes the challenges and perspectives regarding the integration of climate change impacts into semi-probabilistic standards. A summary of the research gaps and challenges in semi-probabilistic assessment, especially for the integration of climate-change induced deterioration, are eventually discussed in Section 3.7.

In **Chapter 4**, the emphasis is placed on time-variant structural capacity and its modeling under deterioration. Firstly, in Section 4.1, a general discussion of time-variant reliability analysis of deteriorating systems is delineated. Section 4.2 describes the primary challenges for modeling uncertainties and performing reliability analysis in the context of deterioration and climate change. Focusing on civil structures, Section 4.3 provides a comprehensive overview of the deterioration phenomena that may affect RC systems. In Section 4.4, the phenomena of chloride and carbonate-induced corrosion are discussed in detail. The primary features of corrosion initiation, propagation, and damage in RC structures are emphasized, taking into account the possible influence of climate change on each of these phases. Concluding remarks on more advanced corrosion modeling and

the limitation of the models proposed are addressed in Section 4.5.

Chapter 5 presents the proposed framework and methodology for the semi-probabilistic assessment of existing structures under climate change-induced deterioration, as well as the benefits and drawbacks of its application. The framework and analytical methodology are detailed in Section 5.1. Section 5.2 proposes the application of the methodology to a benchmark case study. A summary of the obtained results, limitation and benefits of the proposed methodology, as well as remarks on its applicability in civil engineering practice are discussed in Section 5.3.

Ultimately, the principal contributions and accomplishments of this thesis, along with the possible future perspectives, are summarized in **Chapter 6** .

Chapter 2

Fundamentals of Climate Change for Civil Engineering

2.1 Fundamentals of Climate Science

Climate has always influenced any aspect of human life. In turn, human activities, especially after the industrial revolution, are influencing the evolution of the climate. The evidence of climate change is described in a conspicuous number of studies (IPCC, 2022, 2023b). This is recognized to be principally related to human activities, especially those related to the release of Greenhouse Gases (GHGs) into the atmosphere. These changes in climate can pose significant risks to the ecosystem and human life.
In order to understand this complex phenomenon and its impact, it is instrumental to introduce some fundamental concepts regarding climate science. Firstly, it is important to underline the distinction between weather and climate:

- the description of the atmospheric state at a specific time and place is referred to as **weather**;
- the average weather over a period of time ranging from months to millions of years is referred to as **climate**.

In this sense, the parameters of interest for the description of climate are usually quantities related to the surface of the Earth, such as wind, temperature, or precipitation, averaged over 30 years following the guidelines of the World Meteorological Organization (WMO, 2017, 2023). A change in the state of climate, which may be recognized by observing a modification in the statistical descriptors of its properties, persistent over a significantly extended period of time (decades or longer) is referred to as climate change.

Both natural processes and anthropogenic activities affecting the atmosphere, biosphere, cryosphere, land, and oceans can drive substantial modifications in the climate

system, when influencing the Earth's energy balance. These changes can be described through variations in Radiative Forcing (RF), defined as the net change in the Earth's energy balance caused by an external perturbation, such as greenhouse gas emissions, aerosols, or land-surface transformations (IPCC, 2013).

Anthropogenic activities are recognized as the main driver of the modifications that the climate of the Earth is experiencing during the last century (IPCC, 2023a). For instance, the emission of GHGs is directly related to the enhancement of the greenhouse effect and consequently to the modification of the Earth's energy balance.

Furthermore, changes in the concentration of key atmospheric gases, such as ozone (O_3), resulting from anthropogenic emissions and air pollutants have been shown to exert an indirect influence on the greenhouse effect, altering radiative forcing and affecting the Earth's energy balance (WMO, 2018; IPCC, 2023a).

In addition, Earth's energy and water budgets are significantly influenced by changes in land-use and land-cover. The energy budget refers to the balance between incoming solar radiation and outgoing longwave radiation, while the water budget describes the continuous exchange of water between the surface, atmosphere, and subsurface through processes such as evaporation, transpiration, precipitation, and runoff.

Alterations in land-cover, such as the replacement of forests with agricultural fields or urban areas, modify surface albedo and evapotranspiration rates. These changes reduce the carbon storage capacity of vegetation and increase atmospheric CO_2 concentrations through biomass removal and soil carbon release, thereby perturbing the surface energy and moisture fluxes (Bonan, 2008; Pielke Sr et al., 2011; IPCC, 2023a).

In order to provide a basic overview of climate science for engineering practice, the concept of Earth's energy balance is delineated in Section 2.1.1 by means of a simple zero-dimensional radiation balance model. Moreover, a brief description of the notion of radiative forcing and of the main climate drivers is provided in sections 2.1.2 and 2.1.3, respectively.

2.1.1 Earth's energy balance

The climate of the Earth is determined by the flows or fluxes of radiative energy entering and leaving the planet. The balance between incoming and outgoing energy is known as Earth's energy budget, and understanding these phenomena is strictly related to understanding the climate and its changes. Indeed, the climate remains unchanged when the Earth's energy budget is balanced. In contrast, the energy budget may become unbalanced due to the modification of the so-called climate drivers, leading to changes in the climate. For example, referring to the temperature, if the outgoing energy is smaller than the incoming energy, the average temperature of the Earth increases.

Research on the Earth's energy balance still involves significant challenges, both in accurately quantifying it at the global scale and in understanding its spatial variability at regional scales (Stephens and L'Ecuyer, 2015). Nevertheless, in the following, a simplified conceptual description is presented to clarify how the energy balance is related to climate change and its underlying physical mechanisms.

Solar energy reaches the Earth primarily in the form of shortwave radiations emitted by the Sun. A fraction of this incoming radiation is absorbed or scattered by atmospheric gases, aerosols, and clouds, while the remaining part penetrates the atmosphere and reaches the surface. In turn, the Earth' surface emits longwave (infrared) radiations towards the space and it re-radiates part of the absorbed energy. A substantial portion of this outgoing longwave radiation is absorbed by GHGs and clouds within the atmosphere and subsequently re-emitted in all directions. Part of this re-emitted infrared radiation travels downward to the surface, referred to as downward longwave radiation or back-radiation, providing an additional source of energy to the Earth system. This mechanism, referred to as the natural greenhouse effect, is fundamental to maintain the climate of the Earth and, consequently, the environmental conditions necessary to sustain human life. A scheme of the Earth's energy budget is provided in Figure 2.1.

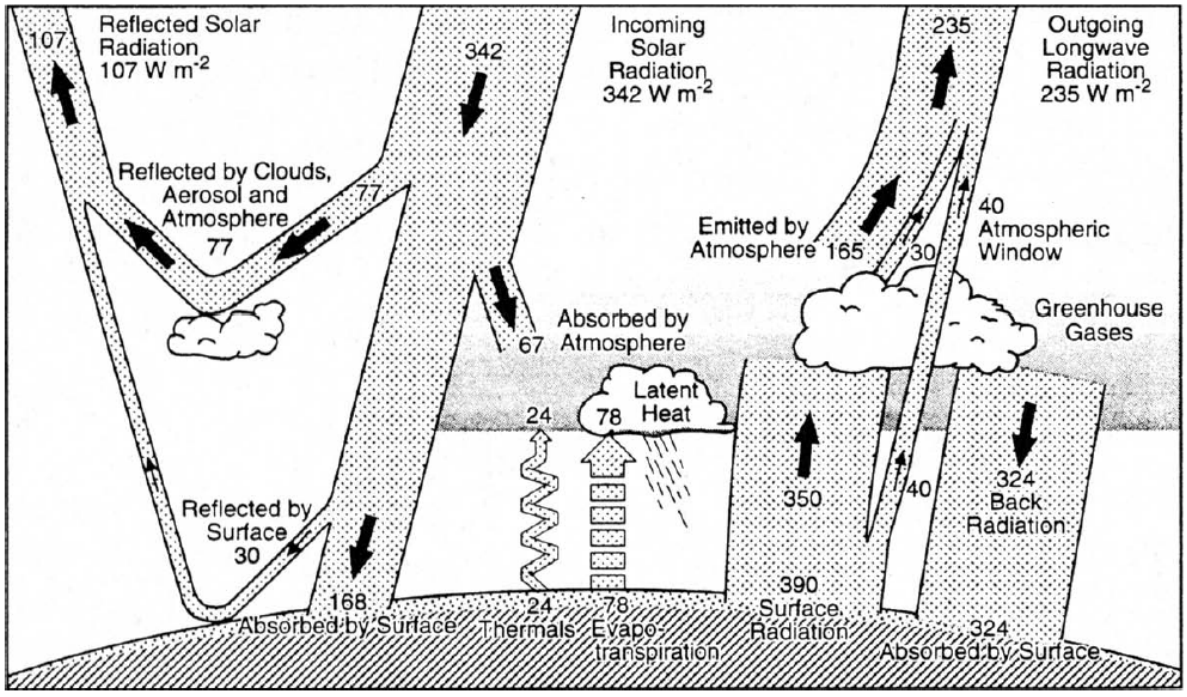

Figure 2.1: Scheme of the Earth's annual global mean energy budget, from Kiehl and Trenberth (1997).

Human activities, mainly due to the exploitation of fossil fuels and the change in land-use, have significantly increased atmospheric concentrations of GHGs. This has intensified

the absorption and re-emission of infrared radiation and led to an enhanced greenhouse effect, modifying the energy budget and, consequently, leading to climate modifications (IPCC, 2013).

In general, the energy balance of the Earth may be modified by changes in physical, chemical, and biological processes, also known as climate drivers or forcings. Their effect is expressed through changes in the net radiative energy received, absorbed, or emitted by the planet, which may be estimated through the concept of radiative forcing, which is the focus of the following section.

2.1.2 Radiative Forcing

The Radiative Forcing is a measure of the change in the energy budget of the Earth-atmosphere system due to variations in particular climate drivers, such as the total solar irradiance or the atmospheric concentration of carbon dioxide (Shine, 2000). The RF is measured in Wm^{-2} and a positive value is related to warming, while a negative value is related to cooling of the climate. Evaluation of radiative energy fluxes provides essential information on how different forcing agents influence Earth's radiation balance.

Although RF is a useful metric for assessing perturbations in the energy budget of the planet, it does not account for rapid adjustments within the atmosphere that occur before the climate system reaches a new equilibrium. To address this, the concept of Effective Radiative Forcing (ERF) is often used. The ERF includes not only the instantaneous change in radiative fluxes caused by a forcing agent, but also the associated rapid atmospheric adjustments that occur independently of changes in surface temperature. These rapid adjustments involve processes in the troposphere, which are held constant in the traditional RF definition. As a result, ERF provides a more complete and physically sounded measure of the influence of anthropogenic and natural agents on the Earth's energy balance. Since these metrics allow for the quantitative assessment of how different forcing agents perturb the Earth's energy balance, it is important to evaluate not only their global mean, but also their spatial and temporal evolution.

A brief description of the climate drivers, how their variation can impact the energy balance and, consequently, the RF and ERF is provided in the following Section.

2.1.3 Climate Drivers

Climate drivers are the physical, chemical, and biological processes that can influence the Earth's energy balance and, consequently, the climate system. Their effect is expressed through changes in the net radiative energy received, absorbed, or emitted by the planet, ultimately affecting atmospheric temperature, circulation patterns, and the behavior of

the oceans and cryosphere.
Climate drivers are generally categorized into natural and anthropogenic.

Natural climate drivers

The only significant natural climate drivers recognized in the industrial era are changes in solar irradiance, volcanic eruptions, and the El Niño–Southern Oscillation (Fahey et al., 2017). Changes in solar irradiance directly impact the climate system since it is the primary energy source directed to the Earth (Lean, 1997). However, according to the IPCC (2013), the contribution of solar irradiance to the change in radiative forcing is relatively small compared to the one driven by anthropogenic GHGs throughout the industrial period. Volcanic eruptions represent the largest natural driver in the industrial era. In the last millennium, eruptions caused several transient episodes of negative RF, but the value of multiple episodic eruptions is negligible compared to other climate drivers. According to Robock (2000), only if a sufficient number of non-explosive eruptions would occur over an extended time period in the future, the consequent average changes in atmospheric composition or circulation could yield to a significant RF change.

Anthropogenic climate drivers

Anthropogenic drivers are recognized as the principal reason for the current changes in climate. They can be distinguished into:

- **Well-Mixed Greenhouse Gases** (WMGHGs):
  - the main WMGHGs are carbon dioxide (CO_2), methane (CH_4), and nitrous oxide (N_2O). Their atmospheric abundances have increased substantially over the industrial era, leading to an increase in the corresponding RF. This is mainly due to fossil fuel combustion, cement manufacturing, and land-use change (Ciais et al., 2013). It is important to highlight that a substantial fraction of industrial-era emissions (43 %) is connected to cement production, as reported by Xi et al. (2016). Over at least the last 50 years, CO_2 has shown the highest annual increases in RF among all WMGHGs. The global mean concentration of methane CH_4 and the connected RF have also increased substantially in the industrial era, while the trend is less significant for nitrous oxide N_2O (Ciais et al., 2013).
  - Other WMGHGs include several categories of synthetic gases that are collectively referred to as halocarbons. During the industrial era, the anthropogenic emissions of these gases have exceeded those deriving from natural sources,

making human activities their dominant contributor. A notable example is the widespread use of chlorofluorocarbons (CFCs) as refrigerants and in other industrial applications. CFCs contribute strongly to positive RF through high infrared absorption efficiency and long atmospheric lifetimes, while also causing stratospheric ozone depletion.

- **Short Lived Climate Forcers** (SLCFs):
  - Hydrofluorocarbons (HFCs), developed as ozone-safe substitutes to CFCs, exert significant positive RF due to high global warming potentials and increasing atmospheric concentrations, although they do not deplete ozone.
  - Ozone is a naturally occurring GHG in the troposphere which is influenced by a variety of natural and anthropogenic emissions, leading to an increase in the RF. The abundance of ozone has high spatial and temporal variability due to its nature, which adds complexity to RF calculations.
  - Atmospheric aerosols are probably the most complex and uncertain component of climate drivers due to anthropogenic activities (IPCC, 2013). Aerosols have several natural and anthropogenic sources, and their emissions interact in complex ways (Boucher et al., 2013).

    Aerosols from anthropogenic activities influence RF in three primary ways: through aerosol–radiation interactions, aerosol–cloud interactions, and albedo changes from absorbing-aerosol deposition in snow and ice (Boucher et al., 2013). Nevertheless, their net radiative forcing is assessed to be negative, indicating an overall cooling effect on the climate system. The primary reason for this negative forcing is that most of the anthropogenic aerosols scatter the incoming shortwave solar radiation back to space, increasing the planetary albedo and producing a cooling effect (IPCC, 2023a). In addition to these interactions, aerosols also modify cloud physical properties. By increasing cloud droplet number concentrations, aerosols lead to brighter (higher-albedo) clouds and longer cloud lifetimes, which further enhance the reflection of solar radiation. Although some aerosol species, such as black carbon, absorb solar radiation and therefore contribute a positive (warming) forcing, their effect is outweighed by the much larger magnitude of cooling associated with scattering aerosols and cloud adjustments.

- **Water vapor** plays a key role in increasing the Earth's equilibrium temperature. In the stratosphere, its concentration is controlled primarily by transport from the troposphere and by the oxidation of methane (CH_4). As anthropogenic activities

increase atmospheric methane levels, more CH_4 is transported and oxidized in the stratosphere, leading to higher stratospheric water vapor concentrations. This additional water vapor contributes to a positive radiative forcing, which further enhances warming (Hegglin et al., 2014).

- Line-shaped **contrails** are a special type of cirrus cloud that forms in the wake of jet engine aircraft operating in the mid to upper troposphere under conditions of high ambient humidity (Fahey et al., 2017). These are additional forms of cirrus cloudiness that interact with solar and thermal radiation to provide a global net positive RF due to human activities (Burkhardt and Kärcher, 2011).

- Changes in land-cover due to anthropogenic activities modify the brightness of the land surface (**albedo**), principally through deforestation and afforestation. There is strong evidence that these changes have increased the global surface albedo of the Earth, creating a negative RF, although in specific regions the opposite effect is observed (IPCC, 2013). Absorbing aerosols, particularly black carbon, can be deposited onto snow and ice surfaces, darkening them and, thereby, reducing their albedo. This albedo reduction increases the absorption of solar radiation, producing a positive radiative forcing that accelerates surface warming.

The IPCC (2023a) provides values of the ERF of the main anthropogenic and natural climate drivers, as shown in Figure 2.2. As primary determinants of the scale, rate, and direction of environmental change, assumptions on the evolution of climate drivers provide the conceptual and quantitative foundation from which climate scenarios are formulated and distinguished.

2.2 Climate Change Scenarios

Climate change scenarios are widely used to explore the long-term environmental consequences of human activities. This includes assessing future emissions and mitigation potential, modeling climate system responses to changing atmospheric composition, and, more generally, studying impact, adaptation, and vulnerability with respect to climate change.

Possible climate change scenarios defined according to assumptions on the socio-economic evolution and their impact on climate drivers (Section 2.1.3). The development of reference scenarios plays a key role in transferring information between the different research communities. Moreover, these also allow for the comparability of results obtained by different research groups. A brief description of the past and current reference climate change scenarios is provided in Section 2.2.1 and 2.2.2, respectively.

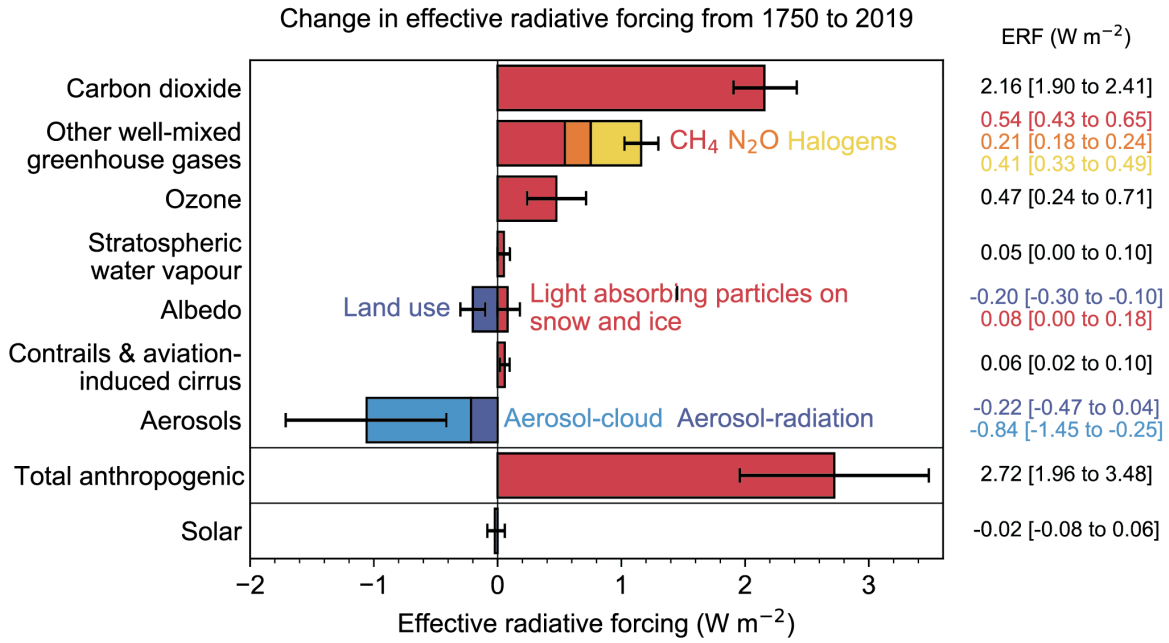

Figure 2.2: Change in ERF by different climate drivers, from IPCC (2023a).

2.2.1 Historical development of climate change scenarios

Originally, the use of scenarios can be related to military planning, gaming, and economics (Bradfield et al., 2005). The purpose of scenarios is not to exactly predict the future, but to improve the understanding of the uncertainties involved in order to make robust decisions under a wide range of possibilities (Schwartz, 1997).

In general, the climate research community develops scenarios to refine the knowledge on the interactions between climate systems, ecosystems, and human activities. Specifically, climate change scenarios can be used to evaluate the impact of anthropogenic activities on the climate and the consequent response of the Earth system. In addition, climate change scenarios attempt to describe the effect of different future climates, considering possible mitigation and adaptation strategies.

The Intergovernmental Panel on Climate Change (IPCC) gathered researchers for the definition of reference scenarios through a work process that took several years. In 1990, the IPCC proposed a set of four emission pathways, called SA90 emission scenarios (IPCC, 1990), including a 'business-as-usual' future and three policy scenarios. This first set of scenarios was followed by the IS92 scenarios (IPCC, 1992), which introduced the implications of uncertainties in economic growth, population, and technology in a number of 'business-as-usual' energy and economic forecasts.

In the Special Report on Emission Scenarios (SRES, IPCC, 2000), the IPCC proposed a set of 40 scenarios associated with 4 qualitative "families" or future storylines,

which facilitated the interpretation of the scenarios. The uncertainty of futureGHGs and short-lived pollutant emissions was investigated given a wide range of driving forces, e.g. assumptions on global population, gross world product and energy consumption. In addition, 6 different modeling teams produced the SRES scenarios, unlike previous scenarios that were based on only one or two climate models. Similarly to the IS92 scenarios, the SRES did not consider policy actions to mitigate climate change.

Afterward, the Representative Concentration Pathways (RCPs) were defined from the necessity to consider a decade of new data and observations, to obtain more detailed information with respect to previous scenarios, to directly implement the consequences of the application of different climate policies, and to consider adaptation strategies (van Vuuren et al., 2011). Different criteria were used for the selection of a proper number of RCPs to accommodate the needs of both user and climate scenario developers, leading to the definition of 4 scenarios representative of a much broader set reported in the literature (Moss et al., 2008). The choice of a even number of scenarios is linked to the decision of avoiding a "middle" RCP, although providing a manageable set of scenarios able to describe extreme projections. The name was selected according to the RF level predicted in 2100, where the RCP2.6 is a mitigation scenario, the RCP4.5 and the RCP6 are medium stabilization scenarios and the RCP8.5 is a very high baseline emission scenario. The RPC2.6 is also known as RPC3PD highlighting that the peak forcing level is 3 W/m^{-2} followed by a decline (Peak-Decline (PD)). The characteristics of the different RCPs in terms of radiative forcing and CO_2 concentration are reported in Table 2.1.

A timeline highlighting the main development in the reference scenarios is reported in Moss et al. (2010).

Scenario	Radiative Forcing	CO_2 Concentration	Reference
RCP2.6	$\sim$ 2.6 Wm^{-2} in 2100	Peak at $\sim$ 490 p.p.m. CO_2-equiv. before 2100	Vuuren et al. (2006); Van Vuuren et al. (2007).
RCP4.5	$\sim$ 4.5 Wm^{-2} at stabilization after 2100	$\sim$ 650 p.p.m. CO_2-equiv. at stabilization after 2100	Smith and Wigley (2006).
RCP6.0	$\sim 6\, Wm^{-2}$ at stabilization after 2100	$\sim$ 850 p.p.m. CO_2-equiv. at stabilization after 2100	Fujino et al. (2006); Hijioka et al. (2008).
RCP8.5	$>$ 8.5 Wm^{-2} in 2100	$>$ 1.370 p.p.m. CO_2-equiv. in 2100	Rao and Riahi (2006); Riahi et al. (2007).

Table 2.1: Characteristics of the RCPs, based on Moss et al. (2010).

2.2.2 Reference Climate Change Scenarios

In the last IPCC Assessment Report (AR6, IPCC, 2023b), a new set of scenarios was proposed. These scenarios were developed incorporating the RCPs and different socio-economic reference assumptions, described by Shared Socio-economic Pathways (SSPs) (O'Neill et al., 2014) to explore future emissions, climate change, related impacts and risks, possible mitigation and adaptation strategies.

The SSPs are a set of scenarios developed to describe plausible trends in the evolution of society and ecosystems over the 21st century. They do not assume any change in climate or impact, as well as no new climate policies (Kriegler et al., 2012); in this sense, SSPs are considered "reference" pathways. These consist of two elements: a narrative storyline and a set of quantified measures of development, related to socio-economic factors or drivers like demography, social, cultural, and technological change.

One of the primary purposes of these scenarios is to represent the range of uncertainties associated with future mitigation and adaptation strategies. Mitigation scenarios explore the different pathways required to achieve specific climate outcomes, while adaptation scenarios describe how societies may respond to the projected climate changes and their associated impacts. In Figure 2.3, the socio-economic challenges for mitigation and adaptation are represented in an outcome space, also defined as "Challenge space" (O'Neill et al., 2014), which is divided into five domains. Consequently, five SSPs were selected as a representative number of pathways to describe the challenges space, connected to five different narratives (O'Neill et al., 2017). Several pathways could fall within a given domain, while the SSPs represent a single socio-economic pathway within each domain developed as a reference for common use in a wide range of studies within the overall scenario framework. These are indicated by the stars in Figure 2.3.

The four narratives of the SSP1, the SSP3, the SSP4, and the SSP5 depict the different combinations of high or low challenges to adaptation and mitigation. In addition, a fifth narrative related to the SSP2 describes moderate challenges in both adaptation and mitigation, representing a future in which development trends are not extreme. A summary of the main characteristics of the narratives is provided in Table 2.2.

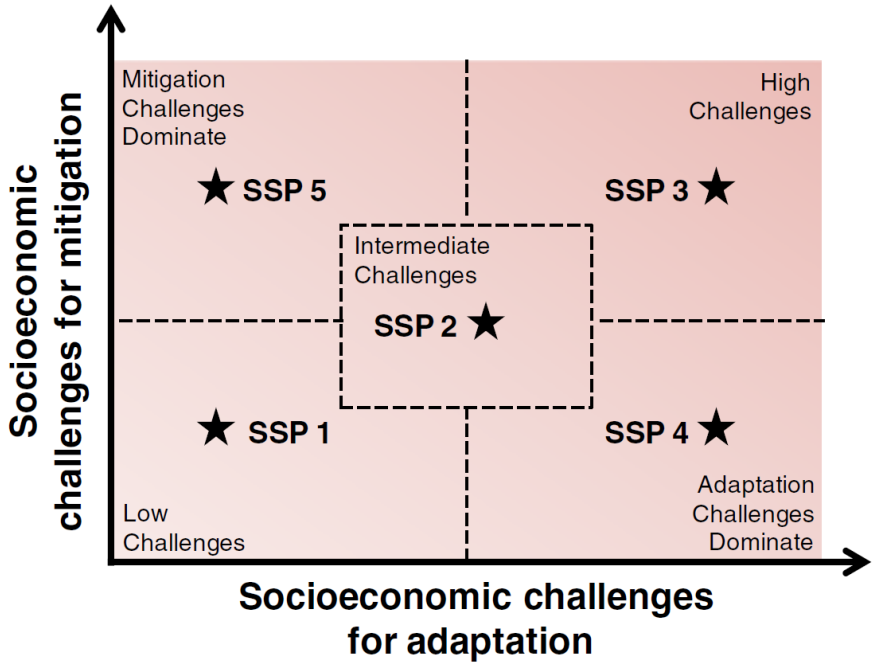

Figure 2.3: The challenge space for the SSPs from O'Neill et al. (2014), based on Kriegler et al. (2012)

SSP	Challenges	Narrative
SSP1	Low for mitigation and adaptation	*Sustainability - Taking the green road*: the world shifts gradually toward a more sustainable path. Management of the global commons slowly improves, educational and health investments accelerate the demographic transition, and the emphasis on economic growth shifts toward a broader emphasis on human well-being. Driven by an increasing commitment to achieving development goals, inequality is reduced. Consumption is oriented towards low material growth, lower resources and energy intensity.
SSP2	Moderate for mitigation and adaptation	*Middle of the road*: the world follows a path in which social, economic, and technological trends do not shift markedly from historical patterns. Development and income growth proceed unevenly. Global and national institutions work toward but make slow progress in achieving sustainable development goals. Environmental systems experience degradation, although there are some improvements, and overall, the intensity of resources and energy use declines. Global population growth is moderate.
SSP3	High for mitigation and adaptation	*Regional rivalry - A rocky road*: policies shift over time to become increasingly oriented towards national and regional security issues. Countries focus on achieving energy and food security goals within their own regions at the expense of broader-based development. Investments in education and technological development decline. Economic development is slow, consumption is material-intensive, and inequalities persist or worsen over time. Population growth is low in industrialized and high in developing countries.
SSP4	Low for mitigation and high for adaptation	*Inequality - A road divided*: increasing inequalities and stratification both across and within countries. Larger gap between internationally connected and a fragmented collection of lower-income, poorly educated societies, low-tech economy. Social cohesion degrades, and conflicts become increasingly common. Technology development is high in the high-tech economy and sectors. The globally connected energy sector diversifies, with investments in both carbon-intensive fuels like coal and unconventional oil, but also low-carbon energy sources.
SSP5	High for mitigation and low for adaptation	*Fossil-fueled development - Taking the highway*: the world places increasing faith in competitive markets, innovation and participatory societies to produce rapid technological progress and development of human capital as the path to sustainable development. There are also strong investments in health, education, and institutions. At the same time, the exploitation of fossil fuel resources is abundant. All these factors lead to rapid growth of the global economy, while the global population peaks and declines in the 21st century.

Table 2.2: Summary of SSPs, based on O'Neill et al. (2017) and Riahi et al. (2017).

Eventually, the SSPs are integrated with different radiative forcing scenarios, including an updated 4 SSP-based versions of the RCPs and different "Gap scenarios", new forcing pathways not covered by the RCPs. This integration process may be represented by the SSP-RCP scenario matrix proposed by O'Neill et al. (2016) and reported in Figure 2.4.

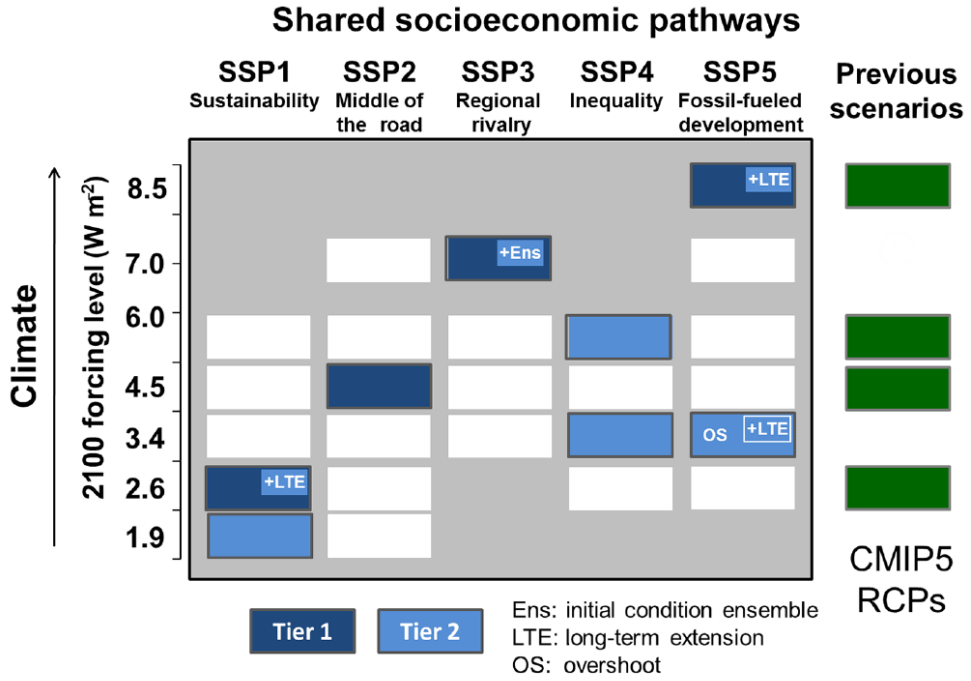

Figure 2.4: SSP-RCP scenario matrix (O'Neill et al., 2016)

Each cell of the matrix indicates a possible combination of an SSP and a climate outcome based on a particular forcing pathway. Dark blue cells (Tier 1) indicate scenarios intended as the basis for climate model projections; light blue cells (Tier 2) include additional scenarios of interest, as well as additional ensemble members and long-term extensions. The white cells indicate other possible outcomes for the matrix. The RCPs, which were developed from previous socio-economic scenarios rather than SSPs, are also shown in Figure 2.4 for comparison.

2.3 Climate Models

Climate models are the principal tools for the evaluation of the climate response to perturbations. They are computerized representations of the atmosphere, ocean, sea, land surface, and other processes, which describe the climate system with mathematical equations based on laws of physics (Figure 2.5). Climate scientists exploit climate scenarios and models to obtain climatic parameters from the past and to project their future evo-

lution.

Climate models support a wide range of applications, including simulating historical climate, conducting sensitivity analyses for attribution and physical understanding, predicting near-term climate variability and change on seasonal to decadal time scales, and projecting long-term climate change over the coming century. Several types of these models are used in climate research, and the choice of model depends on the specific goals of the project (Held, 2005), ranging from simple energy-balance models to highly complex Earth System Models (ESMs) that require high-performance computing.

Considering that climate models can be computationally expensive, the choice of model often involves balancing complexity against cost. Simplified models with reduced complexity or lower spatial resolution are therefore commonly used when large ensembles or long simulation periods are needed. On the other hand, more complex, high-resolution models are essential when the objective is to resolve fine-scale processes, capture nonlinear feedback mechanisms, and provide physically consistent projections of regional climate dynamics and extreme events.

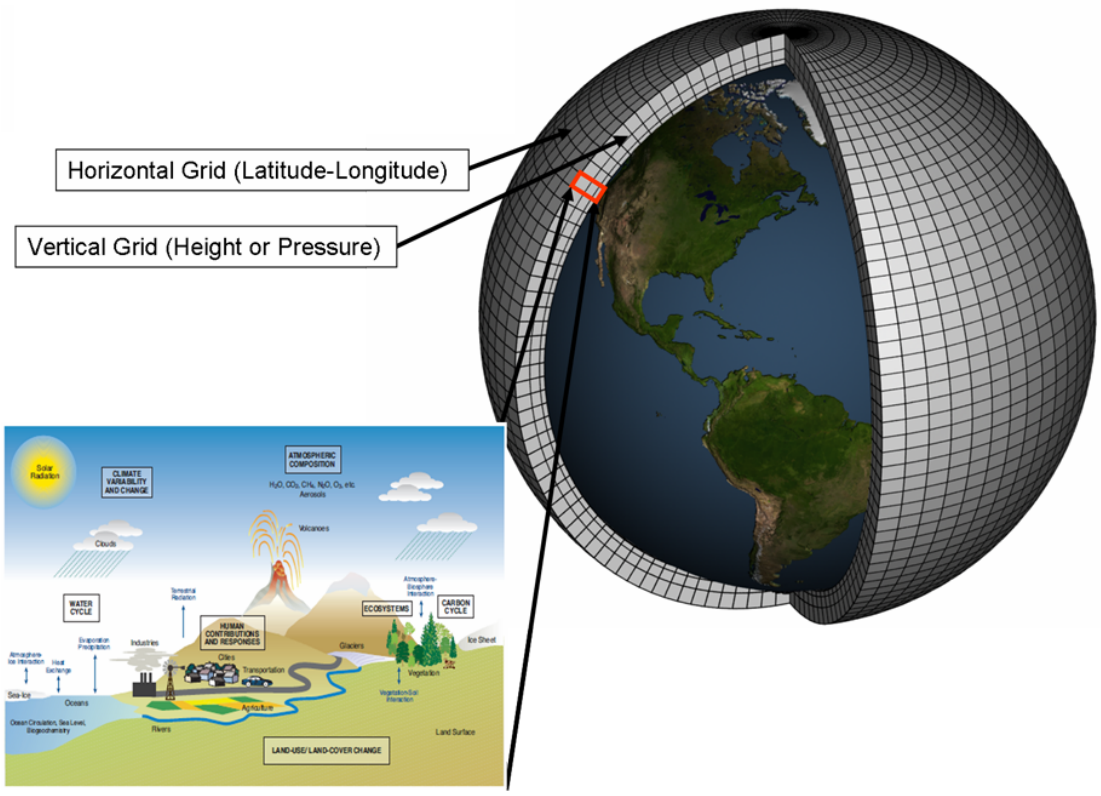

Figure 2.5: Representation of a climate model, from the National Oceanic and Atmospheric Administration (NOAA, 2026)

Among the different climate models, the following are extensively used to assess the climate:

- **General Circulation Models (GCMs)** (Randall, 2000; Weart, 2010): GCMs are designed to represent the dynamics of the major physical components of the climate system, i.e., atmosphere, ocean, land, and sea ice. They are frequently used to make projections under different forcing scenarios. A particular class of GCMs, the Atmosphere–Ocean General Circulation Models (AOGCMs), explicitly couples atmospheric and oceanic processes. The AOGCMs served as the reference models in the fourth Assessment Report of the IPCC (2007) and continue to be used extensively for seasonal to decadal climate prediction, where biogeochemical feedbacks are less critical. High-resolution or variable-resolution AOGCMs are also employed for process studies or applications with a strong regional focus.

- **Earth System Models (ESMs)** (Flato, 2011): the ESMs extend the AOGCMs by incorporating representations of key biogeochemical processes, such as carbon, sulfur, and ozone cycles. Because they simulate interactions between physical climate dynamics and biogeochemical feedbacks, ESMs provide the most comprehensive tools for studying both past climate evolution and future climate change under external forcing.

- **Earth System Models of Intermediate Complexity (EMICs)** (Claussen et al., 2002; Petoukhov et al., 2005): the EMICs capture the essential components of the Earth system, but often at reduced spatial resolution or with idealized formulations compared to ESMs. They may also include components not yet consistently represented in full ESMs, such as dynamic ice sheets. The EMICs are particularly suitable for scientific questions that require long integration times, large ensemble simulations, or the exploration of long-term climate feedbacks on millennial time scales.

Resolution is a fundamental feature of climate models. Due to the complexity of the analyzed phenomena, significant computing tools are requested; for this reason, a trade-off between model resolution, number of simulations, climate processes implemented, and available computational resources is generally required. Moreover, it is important to underline that higher model resolution involves more accurate mathematical models and consequently higher computational cost, nevertheless not necessarily leading to more reliable simulations.

2.3.1 Coupled Model of Intercomparison Project

Several research groups and scientific organizations employ climate scenarios and models to obtain future climate projections. Nevertheless, the reliability of the retrieved data may

be difficult to assess when the hypothesis, boundaries, and methodology are not consistent between the different groups. In this context, the Working Group on Coupled Modelling (WGCM) of the World Climate Research Programme (WCRP) established the Coupled Model of Intercomparison Project (CMIP), intending to provide climate scientists with a database of coupled GCM simulations under standardized boundary conditions and benchmark experiments. Moreover, the objective of CMIP is to better understand past, present, and future climate change arising from natural, unforced variability or in response to changes in radiative forcings in a multi-model context (Eyring et al., 2016).

The CMIP has progressed in five phases into a major international multi-model research activity , introducing a new era to climate science research and becoming a central element of national and international assessments of climate change , e.g. IPCC (2013) with the CMIP5 (Taylor et al., 2012). The current phase is represented by CMIP6, which is exploited in sixth assessment report of the IPCC (2022). An overview of the experimental design of CMIP6 is provided by Eyring et al. (2016).

2.3.2 Regional Climate Modeling

Several problems, such as those associated with civil engineering activities, require information at the local scale. To this end, a variety of reports, tools, and datasets provide climate projections that are downscaled to finer spatial and temporal resolutions than those of the original global projections. In this context, the Coordinated Regional Downscaling Experiment (CORDEX; Giorgi et al., 2006) provides an internationally coordinated framework to improve regional climate projections. As part of the global CORDEX framework, the EURO-CORDEX initiative (; Jacob, Petersen, Eggert, Alias, Christensen, et al., 2014) provides regional climate projections for Europe with a resolution of 50 km (EUR-44) and 12.5 km (EUR-11).

The main tools used to project the climate are GCMs. The processes represented in the GCMs are generally well known but often cannot be fully represented in the models due to limitations on computing resources and input data. Thus, the results of GCMs should only be considered on global or continental scales for climatic conditions averaged on monthly, seasonal, annual, and longer time scales (Trzaska and Schnarr, 2014).

Indeed, GCMs cannot account for fine-scale heterogeneity of climate variability and change due to their coarse resolution (100–500 kilometers). To retrieve climate projections on scales of 10–50 km and on finer temporal scales than monthly, the data considered should undergo a downscaling process. Nevertheless, this process involves additional information, data, and assumptions, leading to further uncertainties and limitations of the results.

In fact, downscaling is based on the assumption that local climate is a combination of

large-scale climatic/atmospheric features and local conditions such as topography, water bodies, and land surface properties (Figure 2.6). Moreover, the derivation of climate projections at local scales is a multi-step process, in which assumptions and approximations are made at each step. Several downscaling methods are often combined to obtain climate change information at desired spatial and temporal scales.

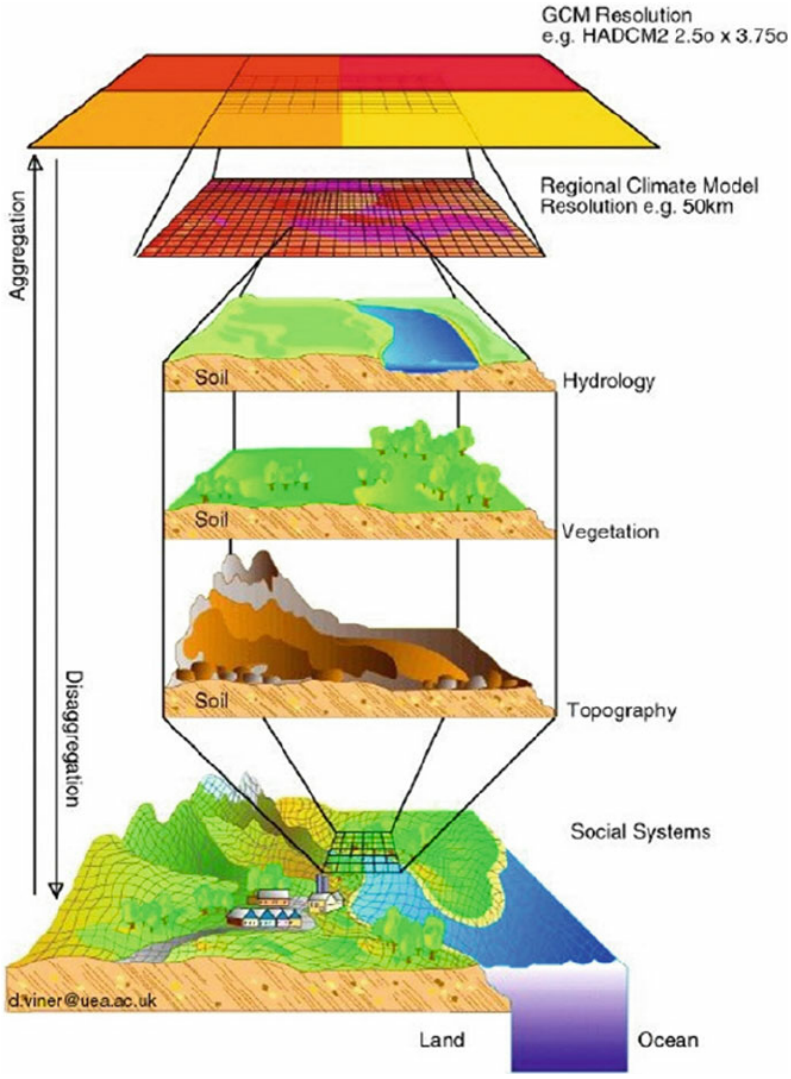

Figure 2.6: Downscaling concept for climate models, from Adem et al. (2014).

The local conditions may be combined with large-scale climate projections using mainly two down-scaling techniques:

- **Dynamical Down-scaling** (Fowler et al., 2007; Giorgi and Gutowski Jr, 2015): includes additional data and physical processes in models similar to GCMs but at higher resolution and select only specific portions of the globe, i.e., Regional Climate Models (RCMs). This method has numerous advantages, but is computationally intensive, requires large volumes of data and a high level of expertise to implement

and interpret results. The overall quality of the downscaled output is related to the accuracy of the large-scale forcing of the GCM and its biases (Seaby et al., 2013).

- **Statistical downscaling** (Wilby et al., 2004; Fowler et al., 2007) establishes statistical relationships between large-scale climate features and local climate characteristics. With respect to dynamical down-scaling, the statistical methods are easier to implement and interpret. They require minimal computing resources, but they rely significantly on historical climate observations and the assumption that currently observed relationships will hold into the future (Zorita and Von Storch, 1999).

Dynamical and statistical downscaling techniques are often used in combination, resulting in a more complex approach than statistical downscaling but less computationally demanding compared to dynamical downscaling, showing improvements in regional climate modeling (Fuentes and Heimann, 2000; Guyennon et al., 2013). A discussion of the benefits and drawbacks of these techniques is provided by Trzaska and Schnarr (2014).

Finally, it is important to note that the selection of downscaling methods depends on the desired spatial and temporal resolution and the climate characteristics of the investigated outputs.

2.3.3 Uncertainties in Climate Modeling

Confidence in climate projections is based on the understanding of physical processes and laws at the basis of the models, the ability to accurately simulate past climate, and the agreement in results across models. For instance, multiple model comparisons project warming of globally averaged near-surface temperature over the next two decades in response to increased GHG emissions. However, the magnitude of this increase varies from model to model. Additionally, in certain regions, different models project opposite changes in certain environmental parameters, e.g., rainfall amount. These aspects highlight the inherent uncertainty of future climate projections even when sophisticated models are exploited.

According to Trzaska and Schnarr (2014), the main sources of uncertainty in climate projections are:

- Uncertainty in future levels of anthropogenic and natural drivers;
- Uncertainty in model representation of climate processes;
- Epistemic uncertainty: imperfect knowledge of climate conditions;
- Uncertainty in representing inter-annual variability in long-term projections.

The future evolution of GHGs emissions is highly uncertain because it depends on many interacting drivers, including socio-economic development, population trends, and technological change. To account for these uncertainties, climate models are run under alternative emissions scenarios, each representing a plausible future pathway.

In addition to scenario uncertainty, climate models require initial conditions to start a simulation. Because these initial conditions cannot be specified with perfect accuracy, projections are generated from slightly perturbed initial states. This produces a collection of simulations known as an initial-condition ensemble, that reflects the influence of internal climate variability on future outcomes.

A third source of uncertainty arises from differences among climate models themselves. No single model can represent all climate processes perfectly; each model incorporates different assumptions, parameterizations, and numerical schemes. To capture this "model uncertainty," many research centers run simulations using different climate models. Collectively, these simulations form a multi-model ensemble (Tebaldi and Knutti, 2007; Knutti et al., 2010). A multi-model ensemble is created by combining simulations from multiple independently developed models, such as those participating in CMIP projects (Eyring et al., 2016). Each model typically contributes several runs for each scenario. The multi-model ensemble mean, computed by averaging across all model outputs, is often used because it tends to reduce individual model biases and provides a more robust estimate of the most likely climate trajectory. The spread of the ensemble, meanwhile, provides insight into the range of plausible future outcomes driven by model structural differences.

Uncertainty is compounded by downscaling due to assumptions that are inherent in models. With each modeling stage, uncertainties are naturally added because more assumptions are made. Although downscaling can provide decision makers with the ability to visualize relevant, fine-resolution climate features, a drawback is that uncertainty and error are difficult to quantify. Thus, evaluating tradeoffs in error created by the downscaling process versus uncertainties in GCM outputs is crucial.

2.4 Climate Change Impact on Civil Structures

The impacts of climate change are not limited only to the natural sphere; indeed, influencing the Earth's environment, these impacts may be recognized in several anthropogenic sectors. Focusing on the built environment and infrastructure systems, several risks can be enhanced due to climate change. Nasr et al. (2021) proposed a wide categorization of the potential impacts of future climatic conditions on bridges. Nevertheless, these impacts may be extended to different types of structural system (Figure 2.7). In the following, an

overview of the possible impacts of climate change on civil structures is provided.

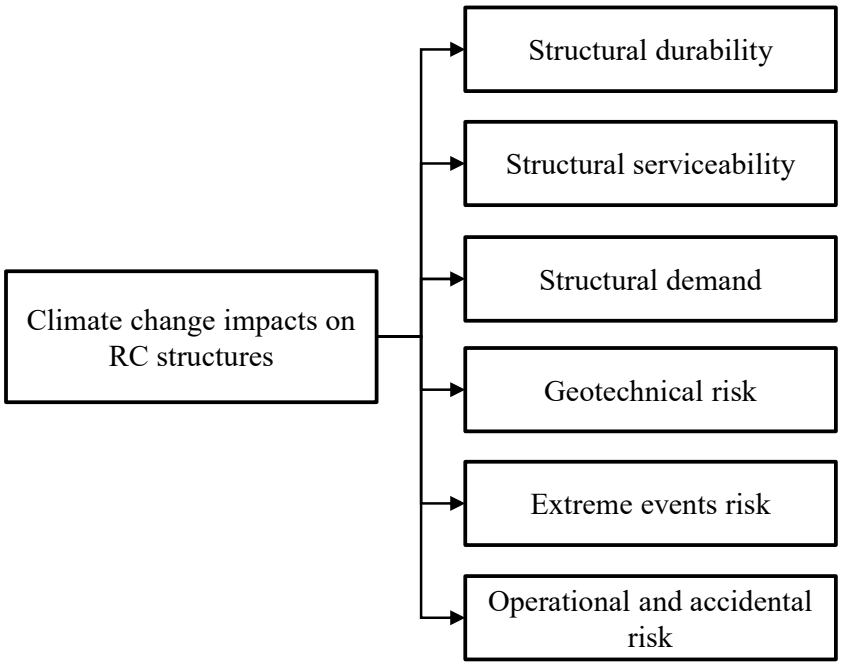

Figure 2.7: Impacts of climate change on civil structures.

Structural Durability

The enhancement of degradation processes is recognized as one of the main impacts of climate change on structural systems. For example, Stewart et al. (2002) evaluated the probability of the initiation and damage of corrosion, considering existing concrete infrastructures located in Australia, under projections of climate change defined in the period 2000-2100, concluding that the risk of carbonation-induced corrosion damage may increase by over 400% in specific Australian Regions. Bastidas-Arteaga et al. (2013) highlighted that global warming can increase the effect of chloride-induced corrosion on RC structures; specifically the study analyzed a bridge girder and showed an anticipation of the failure time up to 31%, corresponding to a shortening in service life of about 15 years for moderate level of aggressiveness. Although an increase in temperature and the abundance of carbon dioxide may have a detrimental effect on RC structures, as highlighted in the studies mentioned above, Bastidas-Arteaga and Stewart (2015) demonstrated that a decrease in relative humidity may lead to a reduction in the corrosion rate. Furthermore, in several regions, the projected increase in snowfall is expected to lead to a more frequent application of de-icing salt, leading to a higher probability of chloride-induced

deterioration.

Corrosion-induced deterioration is not the only detrimental process that can affect structural systems; for example, photo-degradation may be enhanced by increasing solar radiation in specific regions, significantly affecting materials such as plastics, rubber, and timber, as documented by Andrady et al. (2003). Furthermore, Kumar and Imam (2013) evidenced that also composite materials are inclined to photo-degradation. Increase in temperature, precipitation and relative humidity may also impact the growth of organism causing biodegradation, especially in timber (Shupe et al., 2008).

Moreover, a possible increase in the freeze-thaw cycle due to climate change is predicted according to TRB (2008) and Meyer and Weigel (2011). Deterioration of structural foundations may also be impacted by projected change environmental variables, particularly considering the acidification of the ocean and salification of soil.

Structural Serviceability

Climate change may affect not only the durability of structural systems, but also their serviceability. In particular, pavements and railways can be prone to the impact of projected temperature rise and more frequent heatwaves (Schwartz Jr, 2010; Anyala et al., 2011; Mallick et al., 2018; Qiao et al., 2020). Higher pavement distresses and premature failure are likely to be observed due to higher future temperature according to Gudipudi et al. (2017); on the other hand, the impact of increased precipitation is found to be negligible with respect to pavement performance.

Long term deformations, such as creep, are also expected to be influenced by modification in climate, being one of the main factors governing these phenomena of concrete. In particular, a higher creep deformation rate is predicted for higher temperature and lower relative humidity conditions (Geymayer, 1970; Vandamme et al., 2013).

Structural Demand

One of the main effects of climate change is related to the modification of climatic structural demand. For instance, the increase in wind speed is expected in several regions, leading to significantly affect the structural system sensitive to wind excitations (Meyer et al., 2008; Steenbergen et al., 2012; Cui and Caracoglia, 2016; Hintermaier and Lin, 2024). Especially, the possible enhancement of wind induced mechanisms on bridges as galloping, flutter, vortex shedding, buffeting on both shallow deck and cables should be considered. For example, Seo and Caracoglia (2015) concluded that climate change is likely to impact the risk of flutter for long span bridges.

The IPCC (2023a) predicted increase in frequency and height of waves, which can directly impact the safety of bridges (Snaiki et al., 2020). The structural demand related to

drainage capacity is also predicted to increase, respectively, due to the projected increase in precipitation (Berggren et al., 2012; Berggren et al., 2014).

Beyond the impacts mentioned above, structural demand can be influenced by climate change enhancing several other mechanisms, such as increase in thermal stresses and ice-induced loads, and reduction of prestressing forces.

Geotechnincal Risk

Scour is reported to be one of the most common causes of bridge failure (Briaud et al., 2014; Cook et al., 2015; Flint et al., 2017). An increase in sea level and precipitation can lead to higher future flow depths and/or velocities, and consequently faster scour rates (Arnell and Gosling, 2013); in addition, a decrease in the kinematic viscosity of water is expected for higher temperature, and therefore the risk of scour could be further increased. Several studies address this risk under climate change (e.g. Kallias and Imam, 2016; Habeeb et al., 2024). Climate change may also impact slope failure (Hultén et al., 2007) and stability, which can lead to more frequent landslides (Ciabatta et al., 2016; Robinson et al., 2017).

The increase or decrease in precipitation is expected to lead to a rise or drop in the groundwater table (GWT), increasing the risk related to settlement (Toll et al., 2012) and the risk of soil liquefaction (Nath et al., 2018).

Eventually, higher temperatures may trigger rockfalls (Collins and Stock, 2016) and increase the risk of avalanches (Harris et al., 2009).

Extreme Events

Climate change, whether driven by natural or human forcings, may induce variations in the likelihood of the occurrence or strength of extreme events. Considering probability theory, an event may be categorized as extreme if its occurrence is rarer than the 10th or 90th percentile of the estimated probability density function. When a pattern of extreme weather persists in time, it may be classified as an extreme climatic event (e.g. flood, heat waves, and drought).

An increase in intensity and/or frequency of extreme events is expected due to climate change (Clarke et al., 2022). Between natural hazard threatening structural systems, one of the main concerns is with respect to flooding. For example, projected future sea level rise and an increase in precipitation are expected to cause more frequent flood events. In addition, the decrease in ocean pH, the increase in ocean temperature, and the intensity and frequency of tropical cyclones can adversely affect the growth of coral reefs (World Bank, 2012), which are natural barriers to floods. The absence of coral reefs would lead to double annual damage caused by floods according to Beck et al. (2018).

Furthermore, an increase in the intensity and frequency of storms is also expected due to climate change. Storm events associated with a return period of 100 years may be related to a return period of only 20 years nowadays, according to Schwartz Jr (2010). The hurricane hazard is also expected to be impacted by climate change (Mudd et al., 2014a; Mudd et al., 2014b; Rosowsky, 2018). Similarly, due to projected increases in temperature and precipitation decrease in some regions, the increase in the frequency and intensity of wildfires is predictable (Lozano et al., 2017; Kerr et al., 2018).

Operational and Accidental Risk

Climate change may also influence operational and accidental risk. The enhanced operational risk could be related to the additional cost for snow removal (Karl et al., 2009), the more frequent temporary restriction for bridges, and the increased risk of power shortage (Carvalho et al., 2017; Davy et al., 2018). Concerning the accidental risk, the projected future warming is expected to increase the in-cloud liquid water content of marine fogs (Kawai et al., 2016), leading to a higher risk of ship collisions due to lower visibility (Houghton and Radford, 1938). Moreover, the reduced visibility during fogs and the projected increase in precipitation may increase the risk of vehicle-pier collisions or more frequent vehicle accidents (Nasr et al., 2021).

Risk Interconnection

The different risks have been presented individually in the previous discussion for the sake of clarity. Nevertheless, in reality several environmental risks are interconnected, creating a compound effect where individual hazards converge to trigger systemic structural failure. Indeed, structural failures are really imputable to a single cause. For instance, J.-H. Hong et al. (2012) studied the failure of a Bridge in Taiwan observing that the collapse is connected by different compound hazards, e.g., scour enhanced by an earthquake and typhoon. Another example is represented by the increased hydrostatic pressure behind bridge abutments which may combine with the risk of accelerated scour rates and the durability risks to cause failure (Nasr et al., 2021). Concerning extreme events, for example, prolonged drought acts as a primary stressor by dehydrating vegetation and reducing soil moisture, which significantly lowers the ignition threshold for wildfires. An analysis of compound and cascading hazards for climate extetreme event is proposed by AghaKouchak et al. (2020).

Chapter 3

Fundamentals of Semi-Probabilistic Assessment

3.1 Background on Code Calibration

Civil structural and infrastructural facilities are critical assets for human society. Their functionality and safety in time need to be ensured by civil engineers for the sake of the users. Moreover, the built environment is a fundamental resource for the societal economy and growth. Nevertheless, the natural and economic resources for the maintenance and development of structural systems are limited. For this reason, the decision-making process related to these activities should be optimized, maximizing the benefit for society, as well as minimizing the exploitation of resources and the possible number of fatalities.

Structural codes and standards are essential in this context, providing a reference for the design or assessment of safe, durable, and functional structures. They constitute a support for decisions in civil engineering practice, implying the satisfaction of different prescriptions which influence the quality and quantity of the material used and consequently the embodied GHGs. The employment and continuous development of these references is therefore fundamental not only for assuring a certain safety level and functionality to the built environment but also to mitigate the impact of climate change and to enforce sustainable development.

Code calibration is the procedure to determine all the different elements of the code, based on the associated risk or the related probability of failure. Code calibration is defined as ¨the particular activity exercised by some authority, such as code committee, say when it applies some superior method to assign values to the variables of the code format such that a specific design code is formulated¨, according to Ditlevsen and Madsen (1996), or ”the determination of the values of all the parameters in a given code format”, according to ISO2394 (2015). For a semi-probabilistic format, the elements of the code

to be calibrated are the nominal values (i.e., characteristic or mean values dependent on the used format) design values, the safety factors, and the load-reduction factors.

Judgment, fitting, optimization, or a combination of these is usually used to calibrate structural codes (Ditlevsen and Madsen, 1996; ISO2394, 2015; Madsen et al., 2006). Judgment was the main procedure for calibration until the early 1960s, before the employment of structural reliability theories. The definition of the code elements was based on previous experience, implementing the values that led to safe design and increasing the ones that led to structural weakness or failure. However, this strategy has significant drawbacks and limitations concerning the application of new technologies, materials, and structural solutions, since in these cases very limited experience is available. Moreover, the resulting design could lead to expensive and unnecessary safe structures.

In order to overcome the drawbacks of the experience-based calibration, at the end of 1960, structural reliability and decision theory were employed to develop codes and standards. Specifically, calibration by optimization consists in the definition of the elements of the code to satisfy a certain risk-acceptance criterion or reliability requirement, maximizing the expected benefits for society. Calibration by fitting consists of defining the elements of the new code to achieve the same safety level or design that was prescribed in the old code. In Henderson and Blockley (1982) and Sørensen et al. (2002), examples of the calibration process by fitting concerning the British and Danish standards, respectively.

Even if optimization and fitting are analytical methodologies based on the achievement of a certain goal, calibration also needs the contribution of engineering judgment. For this reason, the calibration of design codes is addressed by code committees, which are composed of recognized experts in the field, since the decisions involved in this complex problem can only be faced by combining experience with optimization or fitting.

Levels of Decision for Code Calibration

Code calibration may be considered as a decision problem involving risk and uncertainties (Baravalle and Köhler, 2019), and structural codes may be treated as standardized tools to guide the work of civil engineers. In general, standards are strictly interrelated with other regulations concerning connected subjects, e.g., material production and testing; consequently, they should be considered as part of a regulatory framework.

In ISO2394 (2015), three different decision methodologies are defined for the design and assessment of structures, involving different complexity and approximation levels: risk-informed, reliability-based, and semi-probabilistic approaches (Figure 3.1).

The risk-informed decision represents the highest level of detail (Level 4). In this case, the decision-making process explicitly considers economic and safety consequences,

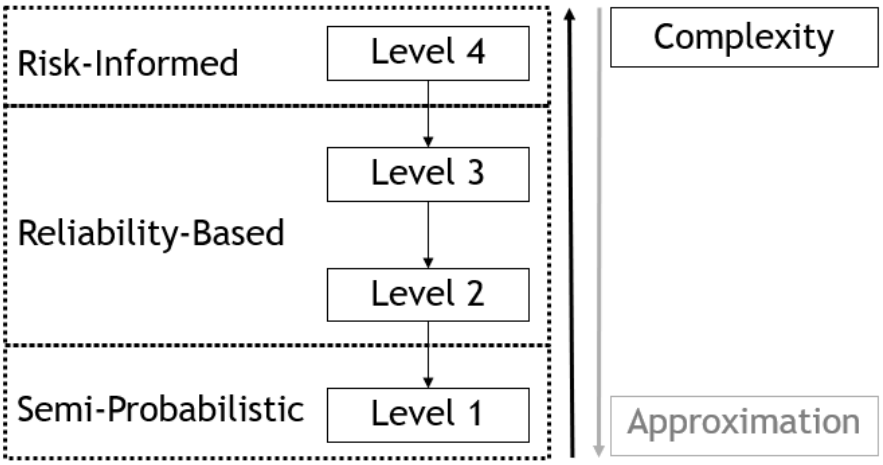

Figure 3.1: Decision methodologies for structural analysis.

as well as the modeling of uncertainties, with the aim of minimizing the associated risk. The analysis is performed by considering the effects of different decision alternatives and choosing the one that maximizes the expected utility. General guidance on the risk-informed decision approach is provided in ISO2394 (2015). Although this approach is very powerful and flexible, it is usually not applied in engineering practice due to complexity and time constraints. Furthermore, in the context of code regulation, standardization and replicability are important aspects that are hardly achievable at this level of detail.

A simpler alternative is represented by a reliability-based decision (Level 3). This approach relies on the satisfaction of predefined reliability requirements, e.g., the reliability target, which can be based on past experience, judgment, or formal calibration through the Level 4 approach (Ditlevsen, 1997). The requirements may depend on the consequences and the cost of the implementation of a specific decision, although these are not explicitly evaluated in the reliability considerations. Guidance on this approach can be found in ISO2394 (2015) and JCSS (2001). In the latter, detailed recommendations for the representation of uncertainties in civil engineering are provided. Similarly, a reliability-based decision problem can be formulated involving a simplified representation of uncertainties and reliability computation (Level 2).

Eventually, the semi-probabilistic approach corresponds to the lowest level of detail (Level 1). This approach relies on the satisfaction of the safety deterministic criterion stating that the design capacity R_d must be greater than the design demand E_d. The design values are generally determined by multiplying or dividing the nominal values by the partial safety factors, which are calibrated to meet the prescribed reliability requirements. The semi-probabilistic format was originally implemented through the so-called Allowable Stress Design (ASD) where the safety factors were applied only to capacity

variables. Nowadays, several national and international design standards, such as the Eurocodes (CEN, 2002) and the American Association of State Highway and Transportation Officials standard (AASHTO, 2020), propose this format following the Load and Resistance Factor Design (LRFD) (Allen, 1975; Ravindra and Galambos, 1978), where the safety factors are applied to both demand and capacity variables, when dealing with common situations in terms of uncertainties and consequences.

The different levels of decision-making strategies are reported in Table 3.1.

Approach	Applicability	Objective	Norm
Risk-Informed (Level IV)	Exceptional design situations with respect to uncertainties and consequences.	Maximization of the expected utility for the decision maker.	Guidelines, e.g., ISO2394 (2015).
Reliability-Based (Level III and II)	Unusual design situations with respect to uncertainties and consequences.	Fulfillment of reliability requirements.	Probabilistic codes, e.g., JCSS (2001).
Semi-Probabilistic (Level I)	Usual design situations with respect to uncertainties and consequences.	Achievement of deterministic design criteria.	Semi-Probabilistic codes, e.g., CEN (2002).

Table 3.1: Levels of decision methodologies according to ISO2394 (2015), based on Baravalle and Köhler (2016) and Köhler and Baravalle (2019).

It should be noted that all the different decision-making approaches, even if related to a different complexity, are strongly interconnected; indeed, higher-level methodologies should be compliant and used to calibrate the lower levels.

For the sake of standardization at the regulatory level, semi-probabilistic format is usually preferred because of its low level of complexity, its generalization and replicability. The semi-probabilistic format is based on reliability analysis and, for this reason, the fundamental concepts of structural reliability are introduced in the following Section.

3.2 Structural Reliability Analysis

The reliability of a structural system may be defined as a function of its capacity and demand. Indeed, considering the structural capacity R and demand S, the probability of failure at a given time t can be evaluated by integration of the joint density function $f_{R,S}(r,s)$ within the failure domain or the limit state function $\Im = \{r, s | r < s\}$:

$$p_f = P[R < S] = \int_{\Im} f_{(R,S)}(r,s) dr ds \tag{3.1}$$

where r and s are the outcomes of the random variables R and S.

Since probability of failure in civil engineering are in general very small ($p_f = 10^{-6} - 10^{-7}$), it is instrumental to introduce an alternative measure of structural safety through the definition of the reliability index β. Equation (3.2) provides an exact relationship only if the capacity and demand are normal variates, even if it is often generalized and applied to estimate the reliability index for non-normal variates:

$$p_f = \Phi(-\beta) \tag{3.2}$$

in which, $\Phi(\cdot)$ is standard normal cumulative density function.

The analytical solution of the integral reported in Equation (3.1) may not always be achievable. For this reason, methods involving analytical approximations are often used to estimate the reliability index β and, consequently, the probability of failure p_f. These methods can be classified into First Order Reliability Method (FORM), Second Order Reliability Method (SORM), and Simulation-Based Methods. In the following Sections, the focus is dedicated to these methodologies, with particular focus on FORM, which is the method usually used for code calibration of semi-probabilistic formats, which is instead detailed in the Section 3.3.

3.2.1 First-Order Reliability Methods

The development of FORM is historically related to the so-called second-moment methods, such as the First-Order Second-Moment (FOSM) and the Advanced First-Order Second-Moment (AFOSM) methods. These use the first and second moments (means and variances) of the random variables to find the approximation of the probability of failure.

First-Order Second-Moment (FOSM) method

FOSM method is based on the first-order Taylor series approximation of the limit state function, linearized at the mean values of the random variables using only the second-moment statistics. For this reason, it is also referred to as the Mean Value First-Order Second-Moment (MVFOSM) method.

The original formulation uses the simple two-variable approach representing structural resistance R and demand S (Cornell, 1969a), where the limit state function can be described as:

$$Z = R - S \tag{3.3}$$

Assuming that R and S are statistically independent normally distributed random variables, Z is also normally distributed. In this case, the reliability index β may be computed as:

$$\beta = \frac{\mu_Z}{\sigma_Z} = \frac{\mu_R - \mu_S}{\sqrt{\sigma_R^2 - \sigma_S^2}} \tag{3.4}$$

This formulation can be easily extended to n random variables X, and the obtained reliability index is often defined as the Cornell reliability index β_C. However, the exact probability of failure may be retrieved just for the cases of statistically independent normal or lognormal random variables and if the limit state function is a summation or a product of these variables, respectively.

Several early versions of reliability-based design formats, such as the Canadian Standard Association (CSA, 1974) and the European Committee for Concrete (CEB, 1976), used the FOSM method to derive reliability elements of the code such as safety factors.

Nevertheless, the FOSM method has several limitations: it is not dependent on the distribution of the random variables $\mathbf{X}$ and the limit state function $g(\mathbf{X})$ is linearized at the mean values of $\mathbf{X}$. When $g(\mathbf{X})$ is non-linear, a significant error may arise by neglecting higher order terms. Moreover, the reliability index may be different under distinct, but mechanically equivalent formulations of the limit state function. In the early 1970s, Hasofer and Lind (1974) proposed the AFOSM method for normal variables.

Advanced First-Order Second-Moment (AFOSM) method

The Hasofer-Lind or AFOSM method is based on the transformation of the original limit state function $g(\mathbf{X})$ into a reduced space $g(\mathbf{Z})$, where the reduced variables Z_i, with zero mean μ_{Z_i} and unit standard deviation σ_{Z_i}, are defined as:

$$Z = \frac{X - \mu_X}{\sigma_X} \tag{3.5}$$

The Hasofer-Lind reliability index β_{HL} is defined as the minimum distance from the origin of the axes to the limit state surface in the reduced coordinate system, and can be expressed as:

$$\beta_{HL} = \sqrt{(\mathbf{z}^*)'(\mathbf{z}^*)} \tag{3.6}$$

where $\mathbf{z}^*$ is the vector containing the value of the variables in the reduced space that minimize the distance between the origin and the limit state surface. The transformation of the limit state function from the original to the reduced coordinate system is depicted in Figure 3.2.

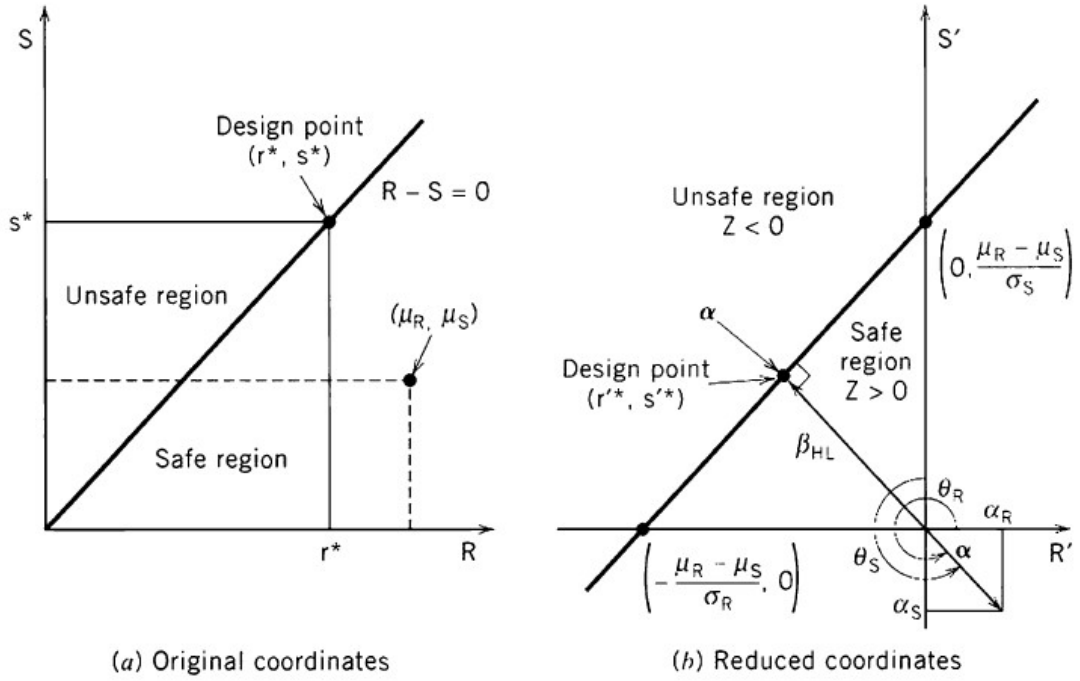

Figure 3.2: Hasofer-Lind reliability index for a linear limit state function, from Haldar and Mahadevan (2000).

The Cornell reliability index β_C defined by the FOSM method coincides with the reliability index β_{HL} obtained by the AFOSM if the random variables X_i are normally distributed and the limit state function is linear. However, the Hasofer-Lind reliability index is obtained following a completely different procedure based on geometry. Considering this definition, β_{HL} is invariant respect to the definition of the limit state function because, regardless of the form in which $g(\mathbf{X})$ is depicted, its geometric shape and the distance from the origin remain constant.

In general, the limit state $g(\mathbf{Z})$ may be a non-linear function; in this case, an optimization problem needs to be solved to find the minimum distance between the origin of the axis in the reduced space and $g(\mathbf{Z})$ under constraints:

$$\begin{aligned} \min D &= \sqrt{(\mathbf{z}^*)'(\mathbf{z}^*)} \\ \text{constraint to:} \quad & g(\mathbf{X}) = g(\mathbf{Z}) = 0 \end{aligned} \tag{3.7}$$

This optimization problem can be solved using the method of Lagrange multipliers, obtaining:

$$z_i^* = -\alpha_i \beta_{HL} \tag{3.8}$$

$$\alpha_i = \frac{\left(\frac{\partial g}{\partial z_i}\right)^*}{\sqrt{\sum_{i=1}^{n}\left(\frac{\partial g}{\partial z_i}\right)^{2*}}} \tag{3.9}$$

where z_i^* and α_i are the design value and the direction cosine in the transformed space $\mathbf{Z}$ for the random variable Z_i, respectively; $\frac{\partial g}{\partial z_i}$ is the partial derivative evaluated at the design point.

The α_i, defined in Equation (3.9), are also referred to as sensitivity factors and provide an indication of the importance of the random variable with respect to the definition of the reliability index.

Rackwitz (1976) formulated an algorithm to compute β_{HL}, which can be summarized in the following procedure:

1. Define the limit state equation $g(\mathbf{X})$;
2. Assume the initial values of the design point x_i^*; a typical assumption is to consider the initial design point at the mean values of the random variables.
3. Transform x_i^* into the reduced variates z_i^*;
4. Evaluate the partial derivatives $\frac{\partial g}{\partial z_i}$ at the design value z_i^*;
5. Evaluate the sensitivity factors α_i, using equation 3.9;
6. Obtain the new design point $z_i'^*$ in terms of the reliability index β_{HL};
7. Substitute the new design point $z_i'^*$ in the limit state function $g(z_i'^*) = 0$ and obtain the reliability index β_{HL};
8. Input the β_{HL} computed in the previous step to reevaluate $z_i''^*$, using equation 3.8;
9. Repeat the procedure from step 4 to 8 until the convergence in terms of β_{HL}.

It is important to highlight that, considering a non-linear limit state surface, the value of β_{HL} computed by the AFOSM may not be consistent with the actual reliability level of the considered structure (Ditlevsen, 1979). In fact, the Hasofer-Lind reliability index can provide the exact result only in the case of statistically independent normally distributed random variables and a linear limit state surface. In any other case, the information on the probability of failure is retrieved with a certain degree of approximation.

The Rosenblatt transformation (Rosenblatt, 1952) may be used to transform a set of statistically independent non-normal variables into normal standard random variables, if the joint CDF is available. Moreover, an algorithm to estimate the mean and standard

deviation of the equivalent normal distribution was proposed by Rackwitz and Fiessler (1976, 1978). The Rackwitz–Fiessler method has proven to be computationally efficient, yet it often fails to converge for a variety of nonlinear or non-Gaussian reliability problems. Consequently, significant research efforts have been devoted to improve its stability, robustness, and overall convergence performance (P. L. Liu and Der Kiureghian, 1991; Santos et al., 2012; D. Zhang et al., 2022).

An extension of the Rackwitz-Fiessler algorithm using a three-parameter approximation was proposed by Chen and Lind (1982). Concerning the Chen-Lind method, Y.-T. Wu and Wirsching (1987) reported an alternative procedure to obtain an equivalent normal transformation of three parameters.

3.2.2 Second-Order Reliability Methods

In many practical applications, the limit state function could be non-linear. Moreover, a linear limit state in the original space becomes non-linear when transformed to the standard normal space if any of the variables is non-normal. If the joint Probability Density Function (PDF) of the random variables rapidly decays far from the minimum distance point, then the first-order estimate of the failure probability is quite accurate. If the decay is slow and the limit state is highly non-linear, it is necessary to use a higher-order approximation for an accurate estimation of the failure probability. In these cases, the SORM improves the estimation obtained by the FORM including additional information about the curvature of the limit state. This is possible considering the second-order terms of the Taylor series approximation. SORM was first proposed by Fiessler et al. (1979) and then studied in several research (Breitung, 1984; Der Kiureghian et al., 1987; Tvedt, 1990; Melchers and Beck, 2018). Nevertheless, it is less efficient than FORM and for highly non-linear limit state function the approximation at the second-order may not be sufficient. For these reasons, FORM is often preferred, especially in the context of code calibration.

3.2.3 Simulation Techniques

The concept of numerical simulation is based on the representation of each random variable in the problem considered as a sample of several realizations to represent the real distribution according to the assumed probabilistic characteristics (Melchers, 1989; Au and Beck, 2001; Christiane, 2009). The problem is solved deterministically for each realization, and this step is known as a simulation cycle or run. The precision of the solution increases with the number of simulations N, as well as the computational cost. The method generally used for numerical simulation is called Monte Carlo Simulation and it

was used for the first time by Von Neumann during World War II as a code word for nuclear weapons work. The Monte Carlo simulation technique may be resumed by 6 essential steps:

1. The definition of all the random variables involved in the problem;

2. The quantification of the probabilistic parameters of the random variables and their PDFs;

3. The generation of the realizations of the random variables;

4. The solution of the problem deterministically for each realization;

5. The extraction of the probabilistic information from the realizations of the researched parameter, e.g., the probability of failure or reliability index;

6. The determination of the accuracy and efficiency of the simulation.

The principal feature of Monte Carlo simulation is the generation of random numbers according to a specific distribution. The first step consists of generating N uniformly distributed random numbers u_i between 0 and 1. Eventually, the inverse transformation technique is used to transform u_i into random numbers x_i with the appropriate probability characteristics (Equation 3.10).

$$x_i = F_X^{-1}(u_i) \tag{3.10}$$

The sampling procedure of a random variable with a generic Cumulative Density Function (CDF) is depicted in Figure 3.3.

The principal drawbacks of MCS are related to the computational cost required to estimate very small probabilities, leading to the impossibility of solving specific problems. For this reason, different techniques have been developed in the last decades to perform simulations, reducing the computational cost (Haldar and Mahadevan, 2000; Rubinstein and Kroese, 2008). The general goal of these techniques is to select the samples to efficiently cover the sample space of the basic random variables, exploiting alternative sampling strategies, such as Rejection Sampling and Latin Hypercube Sampling, or alternative formulations of the reliability problem aiming to reduce the variance of the probability estimator, such as Importance Sampling (Melchers, 1989) and Subset Simulation (Au and Beck, 2001).

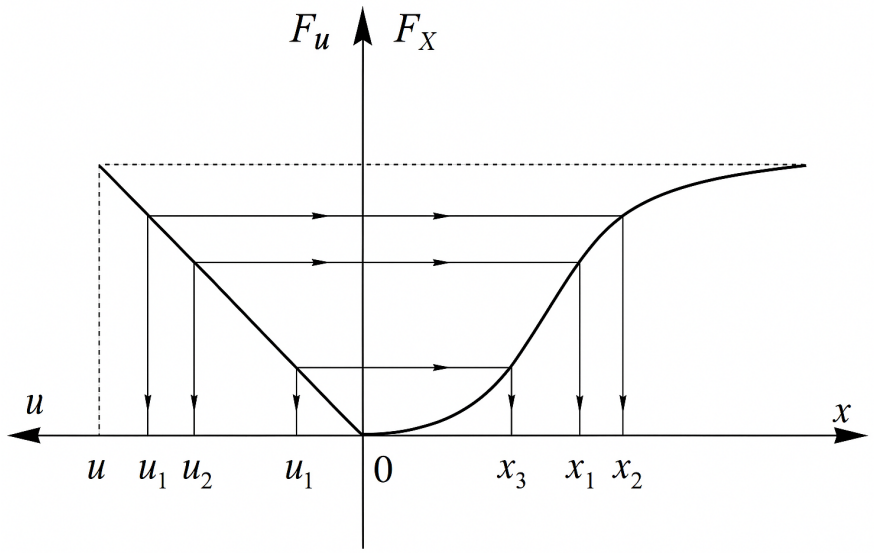

Figure 3.3: Principle of Monte Carlo Simulation.

3.3 Reliability-Based Code Calibration

Code calibration has been systematically researched in the past decades by several research groups, e.g., Cornell (1969b), Allen (1975), Ravindra and Galambos (1978), Ellingwood et al. (1980), Galambos et al. (1982), Thoft-Cristensen and Baker (1982), Ditlevsen and Madsen (1996), Faber and Sørensen (2003), and Madsen et al. (2006). Based on the sustained effort on this research line, a standardized procedure for calibration of the semi-probabilistic formats is reported in ISO2394 (2015), specifically with respect to reliability-based calibration. This procedure is based on the achievement and satisfaction of reliability requirements usually represented by the reliability target β_T. A focus on the definition of β_T is proposed in Section 3.3.1, while the code-calibration procedure is depicted in Sections 3.3.2 and 3.3.3.

3.3.1 Definition of the Reliability Target

In general, the reliability a structure can be described as the ability to fulfill it design purpose during a specified reference period (Thoft-Christensen and Murotsu, 2012). The concept of reliability target translates this into a specific threshold defining the maximum acceptable likelihood for the failure of a system.

In the context of reliability-based code calibration, the selection of the reliability target β_T is a fundamental step, since it implicitly defines the minimum safety level to be ensured by the design or evaluation of a structural system. The optimal decision for structural target reliability levels is related to economical, social, political aspects in addition to the

technical aspects (G. Li and Cheng, 2001). These aspects include the importance of the structure, economic considerations, such as the costs related to the repair and interruption of the activities, and considerations of the potential historic or cultural value.

Nevertheless, β_T is often incoherent between different regulations and referred to prescribed lifetimes common to civil structures, e.g., 50 or 100 years for buildings and bridges, respectively. For example, in the international standard ISO2394 (2015), different values of the reliability target are proposed considering the relative cost of safety measures and the possible consequence of failure for a 1-year reference period. The values, defined at the Ultimate Limit State (ULS), are reported in Table 3.2:

Relative cost of safety measure	Consequences of failure		
	Small	Medium	Large
Large	3.1	3.3	3.7
Medium	3.7	4.2	4.4
Small	4.2	4.4	4.7

Table 3.2: Target Reliability for 1-year reference period at the ULS according to the international standard ISO2394 (JCSS, 2001; ISO2394, 2015).

In the European context, the values of the reliability target proposed by the Eurocode (CEN, 2002) consider only the importance of the structure with respect to a possible collapse in terms of consequence classes, without including the cost for the implementation of the eventual safety measure, as depicted in Table 3.3.

Consequence Level	Minimum β_T	
	1-year reference period	50-year reference period
Large	5.2	4.3
Medium	4.7	3.8
Small	4.2	4.4

Table 3.3: Target Reliability for 1-year and 50-year reference period at the ULS according to the Eurocode (CEN, 2002).

Several studies tried to address the problem of incoherency related to the defintion of the reliability target. Baravalle and Köhler (2017) and Köhler et al. (2019) provide a discussion regarding the selection of β_T for the design codes, addressing the benefits and drawbacks of the current methodology used for calibration. In Köhler et al. (2019), the calibration of design codes is studied, comparing the obtained results with respect to the propositions of the Eurocode (CEN, 2002). The average reliability levels retrieved in the

study are observed to be significantly lower than the reliability target $\beta_T = 4.7$ assumed in the Eurocodes (CEN, 2002) for the medium consequence level and the yearly reference period, highlighting the need for a revision of the current regulations (M/515, 2012).

Furthermore, Baravalle and Köhler (2019) proposed a comprehensive approach to code calibration of the reliability target through all design levels, providing the background to the selection of β_T and defining a possible alternative to reliability-based calibration. In the study, a risk-based calibration problem is formulated, where economic considerations are explicitly considered in the optimization problem through the definition of a minimum expected cost. This is observed to be more consistent with respect to reliability-based optimization, for which the definition of a generally accepted reliability target is observed to be hardly achievable.

Concerning the Serviceability Limit State (SLS), the value of 1.5 for the reliability target is recommended in the Eurocode (CEN, 2002) for irreversible states and a 50-year reference period. In fib (2013) and ISO2394 (2015), the same value is proposed for the remaining service life and the reference design lifetime, respectively, while the JCSS (2001) proposes a set of values for the reliability target at the SLS considering the relative costs of safety measures and 1-year reference time. In Van Nierop et al. (2017), β_T for SLS is defined by exploiting reliability-based calibration and considering different consequence classes and costs. The general procedure proposed by Van Nierop et al. (2017) is adopted by Lenner et al. (2019) for the specific case of a water retaining structure. Quan and Gengwei (2002) discusses the definition of the reliability target at the SLS for RC beams considering the maximum crack width.

A review of reliability levels for ULS, SLS, and fatigue considering different standards is provided by Ghosn et al. (2016).

3.3.2 Reliability-based Optimization Problem

The international standard ISO2394 (2015) describes calibration as an optimization problem consisting of 7 steps. However, other descriptions, such as the 5-step procedure proposed by Ditlevsen and Madsen (1996), may be found in the literature. The 7-step procedure is discussed below.

1. **Definition of the scope of the code**
   It consists of the definition of the structural classes addressed by the code; this definition should highlight very clearly the domain and the limitation of the code, for instance the selection of materials, loadings, and geometries as well as the geographic areas where the code is applicable (Ditlevsen and Madsen, 1996). In general, if the scope of the code is related to a very specific class of structures, its validity is more

limited but the adherence with the code objective is higher, while for a broader class the adherence to the code objective of each structures is, on average, less optimal.

2. **Definition of the code objective**
   The objective of the code depends on the decision-making level used for calibration. For risk-based calibration (Level 4), the code objective is to minimize the risk maximizing the expected utility. A guideline and framework for risk assessment in civil engineering is provided by JCSS (2008).

   For reliability-based calibration of semi-probabilistic code formats, the objective consist of the target reliability β_T, which may be defined from life safety-cost risk analysis, for instance based on the Life Quality Index (LQI) criterion (Nathwani et al. (1997), Faber and Virguez Rodriguez (2011), Fischer et al. (2012)), or assumed equal to other existing design codes covering similar domains. The values of the reliability target are usually not unique since they depend on several aspects such as the considered failure mode, the possible consequence of failure, and the lifetime of the structure.

3. **Definition of code format**
   A code format is a formal system of variables together with a set of rules (Ditlevsen and Madsen, 1996). The rules define the relations between these variables, their relations with respect to the mechanical modeling and the actions on the structure. In practice, firstly, the set of rules is defined and, eventually, the elements of the codes are selected and calibrated. Considering semi-probabilistic code format, the elements of the code are safety factors, nominal and design values of resistance and demand, and load combination factors. According to ISO2394 (2015), the code format should define:

   - the number of safety factors and load combination factors to be used;
   - the independence of load safety factors with respect to material ones and vice versa;
   - the use of the safety factors in the design equations rules for load combinations.

   In general, the number of code elements is an indicator of the code's complexity; the larger the number of code elements, the more optimal the structures designed, although the same set of elements can address fewer design situations.

4. **Identification of typical failure modes and probabilistic models**
   Typical failure modes are identified for the selected structural classes. Consequently,

the related limit state and design equation are formulated. The limit states equations may be more general, covering several failure modes governed by the same set of random variables, or just representative of a very specific failure mode. For a generic design situation j, the limit state equation is a function of a set of random variables $\mathbf{X}$ and the design parameters p, which depends on the calibrated elements of the code $\mathbf{r}$.

$$g_j = g_j(p(\mathbf{r}), \mathbf{X}) \tag{3.11}$$

The selection of the uncertainty is a crucial step for code calibration. These models may be adopted from probabilistic codes, such as the JCSS (2001), or from measurements and experiments reported in the literature (Holicky and Sykora, 2011). The selected models should represent the different sources of uncertainty associated with geometry, material characteristics, the load effects, measurements, and models used to represent the structural capacity and demand. Moreover, the load representation is often dependent on the geographical location limiting the validity of its application to specific areas. Eventually, the stochastic models representing the material properties and geometrical imperfections are related to habits, production methods and quality control routines specific to every country. Therefore, the model uncertainties should be tailored for each design code.

5. **Definition of a measure of closeness**

   The measure of closeness or penalty function is a mathematical tool used to minimize the difference between the prescribed code objective and the actual objective resulting from the calibration. The definition of the measure of closeness depends on the selected calibration approach. Indeed, for reliability-based calibration, the measure is generally defined with respect to the reliability target. For risk-informed calibration the measure is instead formulated considering risk or expected utility functions. Different utility functions have been defined in literature (Rosenblueth and Mendoza, 1971; Sørensen et al., 1994; Rackwitz, 2000) and detail on the risk optimization problem are provided and discussed in Baravalle (2017) and Köhler and Baravalle (2019).

   Focusing on reliability-based calibration, several measures of closeness or penalty functions may be defined in terms of the reliability target β_T, reliability element of the code to be defined and other eventual parameters (Lind, 1977; Nowak and Lind, 1979; Vrouwenvelder and Siemes, 1987; Sørensen et al., 1994; Ditlevsen and Madsen, 1996; Faber and Sørensen, 2003; ISO2394, 2015). In ISO2394 (2015), the measure of closeness W_j is proposed according to Equation 3.12:

$$W_j(\mathbf{r}, \beta_T) = \sum_{j=1}^{L} w_j(\beta_j(\mathbf{r}) - \beta_T)^2 \tag{3.12}$$

where j is the generic design scenario, L is the total number of scenarios, $(\mathbf{r})$ is the reliability level corresponding to the given elements of the code $\mathbf{r}$ for the scenario j, β_T is the target reliability, and w_j are the weights indicating the relative frequency of the appearance or importance of the different design situations. The sum of all w_j must be equal to 1.

In general, the result of calibration is not strongly sensitive to the selection of the penalty function (Ditlevsen, 1997), even if for significantly asymmetric ones around the target value (skewed functions) and for structures with very different reliability level the result may be impacted (Baravalle, 2017).

6. **Determination of the optimal reliability elements for the chosen code format**

   The optimal reliability elements $\mathbf{r_{opt}}$ of the codes are defined by solving an optimization problem. For the penalty function defined in equation (3.12), $\mathbf{r_{opt}}$ is computed according to Equation (3.13):

$$\mathbf{r_{opt}} = \arg\min_{r} \left\{ \frac{1}{\sum_{j=1}^{L} w_j} W_j(\mathbf{r}, \beta_T) \right\} \tag{3.13}$$

   where j is the generic design scenario, L is the total number of scenarios, $W_j(\mathbf{r}, \beta_T)$ is the measure of closeness for the scenario j, β_T is the target reliability, and w_j are the weights indicating the relative frequency of the appearance or importance of the different design situations.

   The solution of equation 3.13 may be obtained using 2 types of methodologies (Gayton et al., 2004): Global Optimization Methods (GOM) and Approximate Methods (AM), which may be preferable in case of high complexity and computational cost. In order to solve the optimization problem with the GOM, for each scenario j, firstly, the design is defined just to satisfy the safety requirement for a given set of $\mathbf{r}$. Secondly, the reliability index $\beta_j(\mathbf{r})$ is evaluated using the reliability methods discussed in Section 3.2. Usually, for reliability-based code calibration, FORM is used due to the reduced computational cost with respect to SORM and simulation-based techniques. Eventually, the minimization problem is solved in order to obtain the optimal set of reliability elements $\mathbf{r_{opt}}$. The number of iterations n needed to solve the problem corresponds to the times the reliability index $\beta_j(\mathbf{r})$ is calculated.

In the case of AM, the design scenarios are prescribed to satisfy, at first instance, the reliability requirement $\beta_j(\mathbf{r}) = \beta_T$. Eventually, the safety factors γ_{X_j} are retrieved knowing the nominal and design values $x_{n,j}, x_{d,j}$ for the considered variable X_j at the design scenario j. The optimal safety factors are selected considering the most conservative value or exploiting a weighted mean. One of the AM is the Design Value Method (DVM), which is detailed in Section 3.3.3, and proposed in several works concerning the update of the safety factors for existing structures (Ditlevsen, 1997; CEN, 2002; fib, 2016). It is important to highlight that AM are capable of defining only safety factors and not other reliability elements of the code as the combination factors.

In general, the optimization problem is subordinate to a series of constraints, concerning the limit value of reliability level, the reliability target, the lower and upper bounds for reliability elements of the code, and the general requirements for the design variables.

7. **Examination and verification of the reliability elements**
   The obtained $\mathbf{r_{opt}}$ is evaluated by standardization committees, which establish the final values for the reliability elements involving engineering judgment, past experience, and other eventual considerations. This process may result in different values with respect to the optimal ones, due to several reasons; for example, the changes to subsequent code versions should be gradual, in order to assure a certain continuity among the users, as reported by Vrouwenvelder and Siemes (1987).

3.3.3 Design Value Method for Calibration

The design value method is based on direct evaluation of relevant design situations and corresponding design equations using design values for basic variables (ISO2394, 2015) determined by direct reliability methods, such as FORM. Considering two random variables, R and S, with cumulative density functions $F_R(r)$ and $F_S(s)$, which describe structural resistance and the demand, respectively, the limit state function $g(\mathbf{z})$ can be formulated as Equation 3.14.

$$g(\mathbf{z}) = R - S \tag{3.14}$$

According to the FORM, the design values R_d and S_d can then be calculated following Equations 3.15 and 3.16, respectively.

$$R_d = F_R^{-1}[\Phi(-\alpha_R \beta)] \tag{3.15}$$

$$S_d = F_S^{-1}[\Phi(-\alpha_S \beta)] \tag{3.16}$$

Consequently, the design value $X_{i,d}$ of a generic variable X_i depends on the statistical descriptors of X_i, the assumed CDF F_{X_i}, the reliability index β for the limit state, and the FORM sensitivity factor α_{X_i} (Equation 3.9) describing the sensitivity of β to variations in X_i with respect to the limit state $g(\mathbf{z})$.

If the random variables are statistically independent, the sensitivity factors α_{X_i} have the following properties:

$$-1 \leq \alpha_{X_i} \leq 1 \tag{3.17}$$

$$\sum \alpha_{X_i}^2 = 1 \tag{3.18}$$

In principle, the values of the sensitivity factors should be found from a number of representative FORM calculations, which require several iterations. However, a set of standardized values α_{X_i} has been defined based on the combination of actual calibration and experience, assuming statistical independence between the resisting and demand random variables (König and Hosser, 1982). These values are presented in Table 3.4 .

Random Variable X_i	**Sensitivity Factor** α_i
Dominating resistance parameter	0.8
Other resistance parameters	$0.4 \times 0.8 = 0.32$
Dominating load parameter	-0.7
Other load parameters	$-0.4 \times 0.7 = -0.28$

Table 3.4: Reference FORM sensitivity factors (ISO2394, 2015).

According to the ISO2394 (2015), the ratio of the standard deviations σ_S and σ_R of the dominating demand S and resistance R random variables needs to be bounded between $0,16 < \sigma_S/\sigma_R < 6,6$ to limit the error when using Table 3.4.

The safety factors may be derived from this methodology knowing the design and nominal values as reported in Equations 3.19 and 3.20 for a generic resistance and demand variable.

$$\gamma_{R,i} = \frac{R_{n,i}}{R_{d,i}} \tag{3.19}$$

$$\gamma_{S,i} = \frac{S_{d,i}}{S_{n,i}} \tag{3.20}$$

$\gamma_{R,i}$ and $\gamma_{S,i}$ are the safety factors, $R_{n,i}$ and $S_{n,i}$ are the nominal values, and $R_{d,i}$ and

$S_{d,i}$ are the design values for capacity and demand variables, respectively.

The safety factors obtained with the presented methodology, also addressed as DVM, are valid only for the considered design scenarios and limit state function, while safety factors applicable to different design scenarios should be retrieved by solving the reliability-based optimization problem (Section 3.3.2).

3.4 Semi-Probabilistic Assessment

The semi-probabilistic approach relies on the satisfaction of the safety criterion stating that the design resistance R_d must be greater than the design demand E_d:

$$g(\mathbf{z}) = R_d(\mathbf{z}) - E_d(\mathbf{z}) > 0 \tag{3.21}$$

where $\mathbf{z}$ is the vector of the design parameters and $g(\mathbf{z})$ is the design or limit state equation.

Design values are generally determined through the multiplication or division of the nominal values by safety factors γ which are calibrated to meet the prescribed reliability requirements, usually represented by the target reliability index β_T. Several international design standards, e.g., Eurocodes (CEN, 2002), exploiting the partial factors concepts, American Association of State Highway and Transportation Officials AASHTO (2020) and American Society of Civil Engineers ASCE ASCE (2022), implementing the so-called Load and Resistance Factor Design (LRFD) formulation (Ravindra and Galambos, 1978), propose the semi-probabilistic approach for the design of new structures. when dealing with common situations in terms of uncertainties and consequences.

The satisfaction of the criterion, defined by Equation 3.21, should be checked for all significant design scenarios and failure modes by evaluating R_d and E_d for the different structural components. The design value of capacity R_d can be estimated using one of the following safety formats (fib, 2023):

- Partial Safety Format (PSF);
- Global Safety Format (GSF);
- Sampling-based Method.

In the PSF, the design capacity is determined using local partial factors applied to individual random variables affecting the overall structural capacity, while in GSF, a global factor is applied directly to the overall capacity. In the Sampling-based Method, R_d is estimated from the PDF of the capacity using simulation-based techniques. The

choice of one of these methods depends on experts' judgment, taking into account the capacity model and possible uncertainties.

3.4.1 Partial Safety Format

In the PSF , the design resistance R_d is evaluated as a function of different parameters:

$$R_d = R\left\{\eta_i \frac{X_{k,i}}{\gamma_{M,i}}; a_d\right\} \ , \ i \ \geq 1 \tag{3.22}$$

where η_i are conversion factors, exploited to relate possible test results to the actual behavior of the considered member, $X_{k,i}$ are the characteristic values of the materials' property, a_d is the value of the geometrical data and $\gamma_{M,i}$ is the partial safety factor. $\gamma_{M,i}$ may be defined as a product of three partial factors $\gamma_{R_{d,1}}$, $\gamma_{R_{d,2}}$, and $\gamma_{m,i}$ incorporating model, geometrical, and material uncertainties, respectively (Equation 3.23).

$$\gamma_{M,i} = \gamma_{Rd,1} \cdot \gamma_{Rd,2} \cdot \gamma_{m,i} \tag{3.23}$$

The partial factor $\gamma_{m,i}$ is usually calibrated based on reliability considerations (3.3).

The characteristic value $X_{k,i}$ is usually defined in terms of the percentile q_R and the inverse CDF $F_{X_i}^{-1}$ of X_i:

$$X_{k,i} = F_{X_i}^{-1}(q_R) \tag{3.24}$$

For example, assuming the material strength described by a lognormal distribution, $X_{k,i}$ can be defined as follows:

$$X_{k,i} = \mu_{X_i} \cdot exp(-\Phi^{-1}(q_R)V_{X_i}) \tag{3.25}$$

where V_{X_i} is the coefficient of variation of the material property X_i, Φ^{-1} is the inverse standard normal CDF, and q_R is generally assumed to be equal to the 5th percentile for the characteristic values of the resisting parameters (JCSS, 2001).

The design demand E_d is generally evaluated as a function of different parameters considering the effect of external loadings (Equation 3.26).

$$E_d = E\left\{\gamma_{G,i} \cdot G_{k,i}; \gamma_P \cdot P; \gamma_{Q,1} \cdot Q_{k,1}; \gamma_{Q,j} \cdot \psi_{0,j} \cdot Q_{k,j}\right\} \quad i \ \geq 1; j \ \geq 2 \tag{3.26}$$

$G_{k,i}$, P, $Q_{k,1}$, and $Q_{k,j}$ are the characteristic values of permanent actions, prestressing, dominant variable loading, and non-dominant variable loadings, respectively; $\psi_{k,j}$ are

the combination factors related to the selected loading configuration; eventually, $\gamma_{G,i}$, γ_P and $\gamma_{Q,j}$ are the partial safety factors for permanent actions, prestressing, and variable loadings, respectively. Specifically, the factors γ_{G_i} and γ_{Q_j} can be defined as a product of two safety factors accounting for the model uncertainty, e.g., $\gamma_{E_{d,G}}$ and $\gamma_{E_{d,Q}}$, and the intrinsic aleatory uncertainties of permanent actions γ_{g_i} and variable loadings γ_{q_j} (Equations 3.27).

$$\gamma_{G,i} = \gamma_{Ed,G} \cdot \gamma_{g,i} \quad ; \quad \gamma_{Q,i} = \gamma_{Ed,Q} \cdot \gamma_{q,i} \tag{3.27}$$

Analogously to the resistance, the partial factors $\gamma_{g,i}$ and $\gamma_{q,i}$ are usually calibrated based on reliability considerations (Section 3.3).

The characteristic value of the permanent load $G_{k,i}$ is usually defined in terms of the percentile q_G and the inverse CDF $F_{G_i}^{-1}$ of G_i:

$$G_{k,i} = F_{G_i}^{-1}(q_G) \tag{3.28}$$

Assuming that the permanent loading follows a normal distribution, $G_{k,i}$ can be defined as:

$$G_{k,i} = \mu_{G_i} \cdot (1 - \Phi^{-1}(q_G) \cdot V_{G_i}) \tag{3.29}$$

where V_{G_i} is the coefficient of variation of the permanent loading and Φ^{-1} is the inverse standard normal CDF, and q_G is generally assumed equal to the 50th percentile for the characteristic values of the permanent loading (JCSS, 2001).

The characteristic value of the variable loading $Q_{k,i}$ is defined in terms of the percentile q_q and the inverse CDF $F_{Q_i}^{-1}$ of Q_i:

$$Q_{k,i} = F_{Q_i}^{-1}(q_Q) \tag{3.30}$$

Variable loadings, imposed and environmental, may be modeled in several ways. For example, considering the random variable modeling the largest load within the reference period (often one year), this is generally represented by an extreme distribution such as the Gumbel distribution. The characteristic value can be chosen by assuming q_Q as the 98th percentile in the distribution function for the annual maximum load (JCSS, 2001).

3.4.2 Global Safety Format

In the GSF, the design value of resistance R_d is defined by Equation 3.31:

$$R_d = \frac{R_m}{\gamma_R \gamma_{Rd}} = \frac{R(X_m; a_{nom})}{\gamma_R \gamma_{Rd}} \tag{3.31}$$

where R_m is the mean value of the resistance, which may be computed based on the mean value of the basic variables X_m and the nominal values of the geometrical parameters a_{nom}; γ_R is the global resistance factor and γ_{Rd} is the model uncertainty factor.

In fib (2013), γ_R equal to 1.2 is proposed. According to the estimation of the coefficient of variation of resistance (ECOV) and based on the assumption that the resistance R is modeled by a log-normal random variable, γ_R may be also evaluated from Equation 3.32:

$$\gamma_R = \exp\left(\alpha_R \beta_T V_R\right) \tag{3.32}$$

where α_R is the FORM sensitivity factor for the capacity, β_T is the target reliability index of the limit state of interest, and V_R is the coefficient of variation of the global resistance.

Assuming R to be a lognormal random variable, the global coefficient of variation may be estimated as:

$$V_R = \frac{1}{1.65} \ln\left(\frac{R_m}{R_k}\right) \tag{3.33}$$

where R_m and R_k are the mean and characteristic resistance values based on the materials' properties.

If in situ measurements are available, the design resistance R_d is derived from the resistance computed using the mean in situ resistance measurements, the nominal values of geometric dimensions a_{nom} and the global resistance factor γ_R (Schlune et al., 2011, 2012; fib, 2023):

$$R_d = \frac{R(f_{ym}, f_{cm,is}, a_{nom})}{\gamma_R} \tag{3.34}$$

where γ_R is defined according to Equation 3.35:

$$\gamma_R = \frac{1}{\mu_\theta} \exp\left(\alpha_R \beta_T V_R\right) \tag{3.35}$$

μ_θ is the bias factor, i.e., the mean ratio of experimental to predicted strength for the chosen modeling approach. Its value varies between 0.7 and 1.2 for failure in compression, bending, and shear (Allaix et al., 2013). It is important to highlight that the bias factor μ_θ and the model uncertainty factor γ_{Rd} are different parameters, although both take into account model uncertainties. The coefficient of variation V_R is defined in this case by Schlune et al. (2011) as follows:

$$V_R = \sqrt{V_g^2 + V_m^2 + V_f^2} \tag{3.36}$$

where V_g, V_m, and V_f are the coefficients of variation of the geometrical, model, and material uncertainties, respectively. Suggestions for V_g and V_m are also proposed by Schlune et al. (2011, 2012) and for V_f by Allaix et al. (2013).

3.5 Semi-Probabilistic Assessment of Existing Structures

Assessing existing structural systems is a complex task that has gained importance over the last decades because large stocks of structures are reaching the end of the prescribed service life (Belin, 2022; ASCE, 2025). Due to the uncertainties related to this problem, it is generally preferable to perform a full-probabilistic study to appropriately evaluate the residual structural performance of the analyzed system. Nevertheless, full-probabilistic methodologies require a high level of expertise and are often significantly time consuming. In this context, semi-probabilistic approaches may be simple and reliable tools for practitioners to assess existing structures, if properly calibrated. Different research groups explored the calibration of safety factors for several research lines in the context of civil engineering, as reported in Table 3.5.

Subject	References
Loading of special vehicles on road bridges.	Lenner et al. (2014) and Lenner and Sýkora (2016).
Design of submerged floating tunnels.	Baravalle and Köhler (2016).
Imposed loads in areas for storage and industrial use.	Lenner and Sykora (2017).
Offshore concrete wind turbine subjected to fatigue.	Velarde et al. (2020).

Table 3.5: Research lines for calibration of safety factors in civil engineering.

Nevertheless, this problem is often addressed following codes and regulations that are defined for the design of new structures, without considering the peculiarities related to the evaluation of existing structures. Nevertheless, structural systems are subjected to an evolution in time of their resistance R, e.g., due to aging and deterioration processes such as corrosion (Bertolini et al., 2013), as well as the modification of the originally assumed structural demand S, e.g., due to the increase in traffic volume (X. Y. Zhou et al., 2012) and to the change of climatic conditions (Retief, 2022). Moreover, the remaining

service life t_{ref} associated with existing structures may be significantly different from the original design service life, usually equal to 50-100 years (ISO2394, 2015), and the cost of repair or upgrading to provide a certain safety performance is usually higher than the cost of applying the same measure in the design phase of a new structure (CEN, 2020). For these reasons, the assessment of existing structures should be performed with tailored methodologies, different from the conservative approaches calibrated for the design of new structures, considering the different types of uncertainties involved and avoiding possible expensive and unnecessary repair activities (Luechinger et al., 2015).

Specifically, the semi-probabilistic assessment of existing structures is a critical issue to be addressed by researchers and an essential need for practitioners. Significant effort has been made along these research line (Diamantidis and Bazzurro, 2007; Steenbergen and Vrouwenvelder, 2010; Caspeele et al., 2013; Sykora et al., 2017). In the last decade, the growing interest in this subject led to the proposal of specific regulations for existing structures, e.g., the Swiss Society of Engineers and Architects SIA 269 (SIA, 2011), the Australian Standard AS 5100.7 (AS, 2017), the Czech Technical Standard CSN 73 0038 (ČSN, 2019), and the Royal Netherlands Standardization Institute NEN 8700 (NEN, 2020).

In the European context, the second generation of Eurocodes is answering this need through the CEN (2024) along with the new Model Code 2020 (Matthews et al., 2018; Walraven and Dieteren, 2023; fib, 2023). Moreover, general guidance on the definition of safety factors for the evaluation of existing structures is provided in the fib Bulletin N°80 (fib, 2016).

The calibration of semi-probabilistic formats for existing structures should account for:

- reduced reference period t_{ref}, related to the remaining lifetime;
- tailored safety level, i.e., reliability target β_T, considering changes in economic and human safety considerations in the case of existing structures. This aspect is discussed in Section 3.5.1;
- adjusted probabilistic models for basic variables; for example, by modifying their coefficient of variation and model uncertainties. Examples and discussion on these aspects are provided in Section 3.5.2.

3.5.1 Reliability Target for Existing Structures

The discussion provided in Section 3.3.1 addressed the definition of the reliability target β_T for new structures. In the case of existing systems, the target probability of failure could be higher than the one accepted for the design of new structures within the considered time interval $t = [t_i, t_{ref}]$ due to the higher cost of upgrading, the shorter remaining

lifetime, and the possible increased level of information with respect to the new structural systems (Vrouwenvelder, 2002; Val and Stewart, 2002; Vrouwenvelder and Scholten, 2010). Consequently, the reliability target for existing structures should be tailored considering these aspects to avoid misleading maintenance decisions and interventions. In this context, different studies have proposed methodologies for the definition of β_T for existing structures (Table 3.6).

Eventually, the definition of analytical equations exploitable by practitioners for the definition of an appropriate value of the reliability target is an important step for the achievement of an integrated semi-probabilistic methodology for existing structures.

For instance, based on the study of more than 100 collapses of buildings, Tanner and Hingorani (2010) and Tanner and Hingorani (2015) proposed an empirical relationship between the number of casualties n and the collapsed area A_{col} related to the failure of the structural member. Considering the study mentioned above and the research by Steenbergen et al. (2015), a formulation of β_T for existing buildings in terms of the Consequences Class (CC), collapsed area A_{col} and the remaining or reference lifetime t_{ref} is provided in fib (2016). The consequence classes are defined with respect to the probability of loss of human life, distinguishing low, medium, and high consequences as CC1, CC2, and CC3, respectively.

Different formulations for the definition of the reliability target β_T concerning the assessment of existing bridges are reported in Table 3.7.

3.5.2 Assessment of Reinforced Concrete Structures

Guidance for the application of semi-probabilistic approaches explicitly addressing the assessment of existing RC structures can be found in the fib Bulletin N°80 (fib, 2016). The described methodologies consider residual service life, information from in situ and laboratory tests, measurements of variable actions, and reduced target reliability levels according to both economical and human safety criteria, focusing on standard RC structures.

Specifically, two methodologies devoted to the redefinition of partial safety factors for existing structures are presented: the DVM and the Adjusted Partial Factor Method (APFM). The DVM, which has been introduced in the ISO2394 (2015) and adopted in the Eurocodes (CEN, 2002), provides formulas for the calibration of the safety factors of both material resistances and actions, exploiting the appropriate probabilistic models derived from prior knowledge, test results, and observations related to the existing structure under investigation. APFM (Caspeele and Taerwe, 2012) is a simpler approach that allows updating the partial safety factors defined by Eurocodes for new structures, using "adjustment coefficients". A brief description of the DVM and APFM is provided in the

Findings	References
Discussion on the difference between the reliability target for new and existing structures. Proposition of a reduction factor $\Delta\beta = 1.5$ when existing structures are considered. Optimization of the value $\Delta\beta$ is recommended if specific cases are analyzed.	Vrouwenvelder and Scholten (2010); Vrouwenvelder (2012)
Specification of two different reliability levels for existing buildings and bridges: the minimum target β_{T_0} for a reliable structure and the level $\beta_{T_{up}}$ for an optimum upgrade strategy. The reliability target values are defined based on the analysis of historically collapsed buildings and bridges.	Steenbergen et al. (2015)
Discussion on unambiguous recommendations for values of reliability target considering existing civil engineering systems. Introduction of minimum reliability target for minimum safety level and optimal upgrading. Limitations of the proposal are discussed.	Sýkora et al. (2016); Sykora et al. (2017)
General framework for the definition of annual reliability target for new and existing structures, independently of the design working life.	Steenbergen et al. (2015)
Definition of reliability target values considering different risk criteria: individual, societal, and marginal lifesaving cost principle. A parametric study is proposed for assessing the impact of different factors on the definition of β_T, i.e., probabilistic distributions, uncertainties in structural demand and resistance, and probability of potential fatalities.	L. Liu et al. (2021)
General framework for the definition of reliability target for non-stationary time series, i.e., incorporating the impact of climate change, compliant with European standardization. The time window concept is exploited for the incorporation of the non-stationarity and the evaluation of the target reliability for the entire lifetime of the structure.	Arnold and Kraus (2022)

Table 3.6: Research findings on reliability target values for existing structures.

following. Different research assessing existing structures using the partial safety format, the global safety format, and considering deterioration processes are discusses in Sections 3.5.2.1, 3.5.2.2, and 3.5.2.3, respectively.

Design Value Method

The principles of the DVM are detailed in Section 3.3.3. Taking into account the definition for the semi-probabilistic approach given in Section 3.4, the safety factor for the material

Formula	**Parameters**	**References**
$\beta_T = \Phi^{-1}\{\Phi(\beta_{1y})\}^{\frac{t_{ref}}{t_0}}$ · $t_0 = 1$ year in the case of dominant climatic or traffic actions; · $t_0 = 5$–10 years for dominant imposed loads; · $t_0 = t_{ref}$ for dominant permanent loadings.	· Remaining lifetime t_{ref}; · basic period t_0 for independent failure.	Sýkora et al. (2016).
$\beta_T = \begin{cases} 1.8 & \text{for CC1} \\ \max(2.3; \beta_{T,hs}) & \text{for CC2} \\ \max(2.8; \beta_{T,hs}) & \text{for CC3} \end{cases}$ where $\beta_{T,hs} = -\Phi^{-1}\left[\frac{2.75 \cdot 10^{-5} \cdot (0.09S)^{-2} \cdot t_{ref}}{0.055}\right]$	· Span length S; · remaining lifetime t_{ref}.	Steenbergen et al. (2015); fib (2016).
$\beta_T = \begin{cases} 4.7 & \text{for } 0 \leq t_{ref} \leq 14 \\ 4.63 + 0.03^{\frac{t_{ref}}{25.74}} & 14 < t_{ref} \leq T \end{cases}$ Calibrated considering carbonate-induced corrosion.	· Remaining lifetime t_{ref}.	Z. Zhang et al. (2022).

Table 3.7: Analytical formulation of reliability target tailored for existing bridges.

properties may be derived as follows:

$$\gamma_{m,i} = \frac{X_{k,i}}{X_{d,i}} = \frac{F_{X_i}^{-1}(q_R)}{F_{X_i}^{-1}[\Phi(-\alpha_{X_i}\beta_T)]} \tag{3.37}$$

where $\gamma_{m,i}$ is the safety factor for the material, $X_{k,i}$ is the characteristic value and $X_{d,i}$ is the design value of the random variable X_i; $F_{X_i}^{-1}$ is the inverse CDF of X_i, V_{X_i} is the coefficient of variation, Φ^{-1} is the inverse standard normal CDF, and q_R is generally assumed to be equal to the 5th percentile for the characteristic values of the resisting parameters (JCSS, 2001).

The safety factor for the permanent $\gamma_{g,i}$ and variable loadings $\gamma_{q,i}$ may be eventually defined as:

$$\gamma_{g,i} = \frac{G_{d,i}}{G_{k,i}} = \frac{F_{G_i}^{-1}[\Phi(-\alpha_{G_i}\beta_T)]}{F_{G_i}^{-1}(q_G)} \tag{3.38}$$

$$\gamma_{q,i} = \frac{Q_{d,i}}{Q_{k,i}} = \frac{F_{Q_i}^{-1}[\Phi(-\alpha_{Q_i}\beta_T)]}{F_{Q_i}^{-1}(q_Q)} \tag{3.39}$$

where $G_{k,i}$, $Q_{k,i}$ are the characteristic values and $G_{d,i}$, $Q_{d,i}$ are the design values of the random variables G_i and Q_i; $F_{G_i}^{-1}$ and $F_{Q_i}^{-1}$ are the inverse CDFs of G_i and Q_i; V_{G_i} and V_{Q_i} are the coefficient of variations; Φ^{-1} is the inverse standard normal CDF; q_G and q_Q

are generally assumed to be equal to the 50th and 98th percentiles, respectively (JCSS, 2001).

Adjusted Partial Factor Method

The APFM is based on the computation of the adjusted partial factor γ_X^{exist} for a certain variable X multiplying the partial factor γ_X^{ref}, provided in the standard for new structures, by an adjustment factor ω_γ. The adjustment factor need to account for the actual values of the reference period t_{ref}, e.g., remaining lifetime, the target reliability index β_T, and the updated coefficient of variation V_X. For a given variable X this partial factor is established according to Equation 3.40 :

$$\gamma_X^{exist} = \omega_\gamma(t_{ref}, \beta, V_X) \cdot \gamma_X^{ref} \tag{3.40}$$

Due to the "adjustment" of the safety factors' values for new structures, the proposed methodology is fully compatible with the current Standards. Specifically, APFM was developed in the context of European standardization (Caspeele et al., 2013; fib, 2016).

The main difference of the APFM with respect to the DVM is that the "adjusted" partial factors are chosen only partly based on optimization of statistical models considering updated data, since the starting point is represented by the reference safety factors used for new structures. The methodology might be suitable for practical investigations, especially when additional information or/and financial resources for further investigations are limited.

Assuming lognormal distribution for material properties, normal distribution for permanent actions, Gumbel distribution and basic reference period equal to 1 year for variable actions, the adjustment factors may be defined by Equations 3.41, 3.42 and 3.43:

$$\omega_{\gamma_m} = \frac{\gamma_m(\beta'')}{\gamma_m(\beta')} \exp\left(\alpha_R \beta' V_X' \left(\frac{\beta''}{\beta'} \frac{V_X''}{V_X'} - 1\right) + \Phi^{-1}(q_R)\, V_X' \left(\frac{V_X''}{V_X'} - 1\right)\right) \tag{3.41}$$

$$\omega_{\gamma_g} = \frac{\gamma_g(\beta'')}{\gamma_g(\beta')} \frac{1 - \alpha_E \beta'' V_G''}{1 - \alpha_E \beta' V_G'} \tag{3.42}$$

$$\omega_{\gamma_q} = \frac{\gamma_q(\beta'')}{\gamma_q(\beta')} \frac{1 + V_{Q,t_{\text{ref}}}'' \left[0.78 \ln(t'_{\text{ref}}/t_{\text{ref}}) - 0.45 - 0.78 \ln(-\ln(\Phi(-\alpha_E \beta'')))\right]}{1 + V_{Q,t_{\text{ref}}}' \left[0.78 \ln(t'_{\text{ref}}/t_{\text{ref}}) - 0.45 - 0.78 \ln(-\ln(\Phi(-\alpha_E \beta')))\right]} \tag{3.43}$$

3.5.2.1 Partial Safety Format

In the past years, several research have assessed existing structures using the partial safety format. Specifically, DVM and APFM have been widely applied for the evaluation of residual structural performance. In the following a review of significant studies on this subject is provided.

In Sykora et al. (2013), the DVM is applied to the pier and the slab of an existing RC bridge subjected to permanent and traffic loading. The results show that the partial safety format recommended for structural design in current codes may lead to conservative results and non-optimal decisions concerning the rehabilitation of existing RC bridges.

Caspeele et al. (2013) exploited the DVM and the APFM for the evaluation of an existing RC beam and short column subjected separately to wind and imposed variable loads. The study also provides a framework for the application of the methodologies. The influence on the evaluation of existing structures using different approaches for the estimation of concrete strength is studied in Caspeele and Taerwe (2014), analyzing a concrete column both with APFM and standard partial factors for new structures.

Gino et al. (2020) used DVM and APFM, following the recommendations provided in the fib Bulletin N°80 (fib, 2016), to evaluate the residual safety of an existing prestressed RC bridge. The results obtained are eventually compared with the results based on Eurocodes (CEN, 2002), showing that the recalibration of partial safety factors accounting for updated information may avoid expensive and ineffective interventions. Nevertheless, the authors highlighted the absence of a definition for the probabilistic models to update partial safety factors for prestressing and imposed deformations in the fib Bulletin N°80 (fib, 2016) and the need for further research on this issue.

The DVM and APFM methodologies are applied in Orcesi et al. (2021) for the assessment of two different existing RC bridges. The study illustrates the procedure for the application of the methodologies and provides a discussion on the assumptions involved in both approaches. It is shown that major simplifications rely on the consideration of statistical uncertainty associated with the new measurements only in the estimate of characteristic values of basic variables and on the assumption of standardized sensitivity factors or types of probabilistic distributions. Following the previously discussed contribution Orcesi et al. (2023) provided an analysis of the current state of the art in the definition of partial factors for the assessment of existing structures, discussing the benefits and drawbacks between the use of prescribed fixed partial factors, partial factors tailored for the case considered, and full-probabilistic methodology.

The European Committee for Standardization provided a Technical Specification CEN (2020) on the assessment of existing structures, suggesting the use of the partial safety format of the Eurocodes (CEN, 2002) as the initial method for the verification of struc-

tural safety. In Lara et al. (2021), the assessment of RC beams of an existing industrial building is performed, following the indication of the technical specification CEN (2020) and applying both the DVM and APFM to compare the results with the outcomes of a full-probabilistic analysis. The comparison shows that DVM incorporates the updated information more accurately than APFM. Furthermore, the full-probabilistic assessment is reported to be in good agreement with the results obtained from both DVM and APFM.

A parametric study addressing the influence of uncertainties on the calculation of partial safety factors for an existing RC bridge girder under bending is provided by Alam et al. (2023). The study highlighted the traffic load and the yielding strength of steel as the most dominant parameters for the considered bridge.

Finally, an overview of recent achievements on semi-probabilistic methods for the assessment of existing concrete structures is provided by Casti et al. (2023).

A summary of recent studies using the partial safety format for the assessment of existing RC structures is provided in Table 3.8.

References	Structural Type	Variable Loads
Sykora et al. (2013)	Slab and pier	Traffic
Caspeele et al. (2013)	Beam and column	Wind, Imposed
Gino et al. (2020)	Box Girder Deck	Wind, Traffic
Lara et al. (2021)	Building Beam	Imposed
Orcesi et al. (2021)	Bridge deck	Wind, Traffic
Cosenza and Losanno (2021)	Orthotropic bridge deck	Wind, Traffic
Casti et al. (2024b)	Box girder deck	Traffic

Table 3.8: Partial safety format for the assessment of existing RC structures.

3.5.2.2 Global Safety Format

The assessment of existing structures may require the evaluation of the structural performance at the system level by exploiting Non-Linear Structural Analysis (NLSA). In this context, different studies propose the application of the GSF strategies (Allaix et al., 2013; fib, 2013; Pimentel et al., 2014; H. Zhang et al., 2014; H. Zhang et al., 2018).

The proposed methodology, which is consistent with the guidelines provided in the Swiss Standard for existing structures SIA 269 (SIA, 2011; Brühwiler et al., 2012) and the Eurocodes (CEN, 2005), relies on the application of a global safety factor to the overall resistance of the system. The exploitation of PSF associated with NLSA can lead to unreliable results (fib, 2016), especially when dealing with existing RC structures.

For this reason, global resistance methodologies are generally adopted (Blomfors et al., 2016; Slobbe et al., 2020). This safety format accounts for the mean values of material resistance and the nominal value of the geometry in comparison to to the characteristic values considered in the partial factor format. Pimentel et al. (2014) show that the GSF may be more accurate than the PSF, even at the member level.

The system reliability of different steel structures has been investigated by H. Zhang et al. (2014), H. Zhang et al. (2018) accounting for uncertainties in loads, resistances, and stiffness, as well as uncertainties in the initial geometry and imperfections of the structures. The research discusses the peculiarities, benefits, and drawbacks of these alternative methodologies to steel structure design, highlighting that partial factor methodologies might not be appropriate to ensure system reliabilities.

The estimation of the Coefficient of Variation (CoV) of global structural resistance associated with the aleatory uncertainty of the material properties V_R is a crucial step for the application of the GSF associated with NLSA (Castaldo et al., 2022), which may be performed using different methodologies, e.g., the Estimation of Coefficient of Variation (ECoV) method (Cervenka, 2013). One of the main assumptions concerning the ECoV methodology is related to the selection of a lognormal probability density function for resistance and the estimation of the coefficient of variation, being not always adequate for the analysis. Furthermore, selecting an appropriate value for model uncertainties is fundamental when dealing with NLSA (Kadlec and Červenka, 2016; Gino et al., 2021).

A discussion on the semi-probabilistic approach compliant with NLSA for the assessment of existing RC structures using different safety formats is presented in Castaldo et al. (2019). Methods for assessing uncertainties and estimating the coefficient of variation of the resistance of RC structures are also presented in Novák et al. (2023). In Gino et al. (2024), an evaluation of the design value of global structural resistance is proposed using NLSA according to the GSF, exploiting a novel strain-based methodology to account for the influence of aleatory uncertainties related to material properties on the global structural response.

3.5.2.3 Considerations on Deteriorating Structures

An important limitation common to the aforementioned studies regards the deterioration processes affecting RC structures which are assumed to be negligible.

An explicit formulation for the calibration of partial safety factors considering chloride-induced corrosion in RC structures is reported by Holicky et al. (2008). The research compares the partial safety factors obtained by accounting and neglecting deterioration for different values of the reliability target, highlighting how the reliability level over time is strongly influenced by deterioration processes and, consequently, the calibration

of safety factors. In this case, the limitation relies on the fact that the obtained results are significantly dependent on the model used. Consequently, a suitable and reliable corrosion modeling should be implemented, considering the impact of climate change on the initiation and propagation phases, as well as a more refined load modeling considering different ratios between permanent and variable loadings.

In Tanner et al. (2011), the uncertainties related to resistance models for corrosion-damaged RC beams are estimated. However, the results obtained are not exploitable for the direct calibration of partial safety factors, as more refined modeling should be devoted to characterizing the resistance of deteriorating structures. Further research related to model uncertainties of the corrosion-damaged RC structure is provided in Sykora et al. (2015).

The calibration of the safety factors for the assessment of anchorage capacity in existing RC structures under corrosion is addressed in Blomfors et al. (2019). In the study, the partial safety factors are calibrated for different levels of corrosion, considering the presence or absence of stirrups. The results obtained are verified using simulation-based techniques for several design situations. The discussed methodology may, in principle, be extended to the calibration of safety factors for existing structures subjected to chloride-induced or carbonate-induced corrosion. Nevertheless, further research is needed for the quantification of the sensitivity factors in deteriorating structures.

Eventually, different research groups propose the exploitation of Bayesian updating combined with field measurements to assess existing RC structures subjected to corrosion processes (Enright and Frangopol, 1999; Faroz et al., 2016; Jacinto et al., 2016; Liljefors and Köhler, 2023).

3.6 Semi-Probabilistic Assessment under Climate Change

Calibration of semi-probabilistic design formats has usually been performed under the assumption of a stationary climate. Nowadays, climate change is recognized as a concerning reality, as reported by the Intergovernmental Panel on Climate Change assessments (IPCC, 2022, 2023b), and its impact on structural demand and capacity is addressed in a large number of studies (Nasr et al., 2021; Mishra and Sadhu, 2023; Orcesi et al., 2022).

Moreover, climate change has a significant impact on the intensity and frequency of extreme events, and different researchers investigated this issue to assess the possible effect on new or existing structural systems in order to provide adaptation strategies with respect to extreme events, e.g. hurricanes (Bjarnadottir et al., 2011; Q. Li et al., 2016; J. Y. Lee and Ellingwood, 2017), tsunamis (Nazarnia et al., 2020; Sepúlveda et al.,

2021; Alhamid et al., 2022), and floods (Bhatkoti et al., 2016; Kim et al., 2017; Cea and Costabile, 2022). Additionally, the concept of return period is significantly related to the assumption of stationarity in structural codes, leading to the need to propose different formulations in the context of climate change (Rootzén and Katz, 2013). Nowadays, design standards are beginning to consider the impact of the changing climate in the calibration of semi-probabilistic methodologies for appropriately estimating structural safety and performance. Specifically, the impact of climate change on the reliability elements of the semi-probabilistic methodology with respect to structural demand and capacity is discussed in Sections 3.6.1 and 3.6.2, respectively.

3.6.1 Characteristic Structural Demand

Recent studies have proposed calibration strategies for the definition of structural demand explicitly considering climate change. Croce et al. (2019) propose a general procedure to assess the impact of climate change on climatic actions, based on the analysis of historical and future environmental projections. Furthermore, a framework for evaluating non-stationary characteristic values using climate model projections is discussed in Abrahamczyk and Uzair (2023). In the following, a general overview of the state of research for the standardization of structural demand is provided, and eventually the focus is directed at the European context.

In the United States, extreme wind and heat waves are analyzed for the Washington, DC area considering different airports by Lombardo and Ayyub (2015). A slight decrease in wind speed was observed over the last 50-70 years, while a significant increase was observed for the intensity and frequency of heat waves. The need for implementation in structural codes of the impact of future climate projections on these actions is highlighted.

Al-Rubaye et al. (2022) reviewed developments on the calibration of snow loads under climate change. A discussion on the necessity to consider non-stationarity for the definition of design standards with a focus on new climatic loading design maps is proposed by Ghosn and Ellingwood (2023), starting from a review of the current U.S. regulations. A simple scaling procedure is proposed to address the impact of climate change and applied in the case of wind loading.

Moreover, the committee on adaptation to a changing climate of the American Society of Civil Engineers has investigated the performance of the target structural performances in terms of resilience and sustainability under the effect of climate change and other hazards (ASCE, 2018).

An extensive review of available information on climate change to identify methodologies and tools that would help the civil engineering profession addressing the impacts of climate change on the life-cycle safety of structures and infrastructure facilities is also

available as the result of a SEI/ASCE special project (Biondini et al., 2025).

In the Canadian context, significant research on the evolution of the values of characteristic loadings due to climate change has been performed, particularly focusing on wind and snow actions. H. Hong et al. (2021) performed a reliability-based code calibration in the context of possible implementation in the National Building Code of Canada (NBCC), focusing on the definition of design values of wind and snow loads, as well as load factors. In the study, the stationary extremes derived from observed meteorological data and the non-stationary effects of climate change are considered. Based on the analysis performed and the results of the climate change modeling, the load scaling factors are calibrated for different regions in Canada. Despite the load factors being specifically computed for the Canadian environment and climate change significantly varying from region to region, the proposed calibration procedure may be exploited in other geographical contexts.

S. H. Li (2023) assessed the impact of climate change on structural reliability for Canada. The study provides a general methodology for the integration of non-stationarity in design values of loads, eventually focusing on wind speeds and ground snow loads.

In Pandey and Lounis (2023), a methodology is proposed to develop a stochastic load model that accounts for non-stationary changes in the frequency and intensity of loading events based on the use of the non-homogeneous Poisson process. An illustrative example is discussed to address the effect of non-stationary climate with respect to design percentiles, return period, and annual probability of failure, highlighting the influence of the change in climate and the need for a revision of the current standards.

European institutions already highlighted the need for a revised version of the current Eurocodes, specifically addressing the development of regulations for existing structures and an extension of the current scope of standards considering the impact of climate change (M/515, 2012; CEN, 2013). The Joint Research Center (JRC) of the European Union addressed the current and future impact of climate change on structures and infrastructures in Europe through different reports on thermal design (Athanasopoulou et al., 2020), snow load (Croce et al., 2016), river flood risk (Dottori et al., 2020), and coastal flood risk (Vousdoukas et al., 2020). Moreover, in the context of European Standardization, the work by Arnold and Kraus (2022) focused on the calibration of a semi-probabilistic code format considering the evolution of climate. In the mentioned research, the FORM methodology is extended to a non-stationary approach, deriving the reliability index and sensitivity factor for the sake of calibration. A practical application is presented involving a simply supported beam subjected to snow action. Eventually, it is highlighted that the uncertainties involved in climate projection and the selection of the time window may significantly influence the results.

In Table 3.9, different studies investigating the definition of characteristic and design

values of structural loadings under the impact of climate change are summarized, focusing on the European standardization context.

Research Proposal	Loading	Findings	Reference
General framework for assessing possible changes in characteristic values of climatic actions, focusing on extreme wind speed in North Western Europe. The impact on the natural variability of wind with respect to the definition of design velocity is also discussed	Wind	Climate change leads to a modification of -0.8 % and +2.3 % in the hourly mean wind speed with a 50-year return period.	Steenbergen et al. (2012).
Procedure for the derivation of ground snow load from daily temperature and precipitation; furthermore, the characteristic value of the snow load is deduced for future climate projections. Results are provided for different Italian regions.	Snow	Snow loads, under climate change scenarios, is generally expected to increase in the northern and eastern Italian regions, while the opposite trend is observed in western and southern regions.	Croce et al. (2016), Croce, Formichi, Landi, and Marsili (2018), and Croce, Formichi, Landi, Mercogliano, et al. (2018)
General methodology to evaluate the impact of climate change on climatic actions; the results are reported in terms of changes in characteristic values for Italy and Germany, considering different climate models and climate scenarios.	Temperature, precipitation, snow, and wind	Climate change is reported to have a significant impact on temperature, precipitation, and snow loadings while wind velocity is not particularly affected for the 2 considered regions.	Croce et al. (2019).
Research on ground snow load considering non-stationary extreme values models in the French context.	Snow	Return levels under climate change are observed to exceed the standards by 15 % on average for the French building code under a stationary assumption, although a historical decrease in snow load.	Le Roux et al. (2020).
Methodology for the definition of characteristic and design values of loadings considering non-stationarity, applying the time window approach.	Snow	Design and characteristic values of snow load are expected to decrease in time, for the case study considered, under climate change.	Arnold and Kraus (2022).

Research Proposal	Loading	Findings	Reference
Framework to evaluate the non-stationary characteristic values of structural loadings using climate observations and model projections.	Temperature	The non-stationary characteristic values of temperature are expected to increase in time due to climate change.	Abrahamczyk and Uzair (2023).
Framework for the elaboration of climate maps for thermal loading exploiting public datasets and harmonized methodologies. A case study for Italy is proposed.	Temperature	An increase in characteristic values of maximum temperature, as well as limited variations in spatial extent and magnitude of characteristic values of minimum temperature, are predicted considering climate.	Rianna et al. (2023).
Studies on the impact of climate change concerning the evolution of climatic loadings, specifically focusing on the definition of minimum and maximum uniform temperatures for the case of a cable-stayed viaduct located in France. The obtained results are compared with respect to the original design and Eurocode regulations.	Temperature	The characteristic values of maximum and minimum temperatures are expected to increase under climate change for the considered case study. The results show that the maximum and minimum uniform components of temperature loading are respectively underestimated and overestimated with respect to the original design and Eurocode regulations.	Casti et al. (2024a).

Table 3.9: Characteristic and design values of loadings considering climate change in the European standardization.

3.6.2 Characteristic Structural Capacity

Civil structures and infrastructures may be affected by several deterioration phenomena during their lifetime, leading to an evolution of their capacity. Specifically, in RC structures, these processes, coupled with aging, can adversely affect structural reliability (Biondini and Frangopol, 2016, 2018). In this context, climate change may have a severe impact on these deterioration processes, enhancing mechanical, physical, chemical, and biological mechanisms, causing material deterioration and consequently negatively influencing structural capacity over time. Different research groups have addressed this risk and the possible adaptation focusing on critical structures, i.e., bridges (Mondoro et al., 2018; Nasr et al., 2020; Nasr et al., 2021; Nava et al., 2023; Nava et al., 2024).

Focusing on RC structures, climate change is reported to have an impact on freeze-thaw cycles, which are connected to the physical deterioration of concrete (Meyer and Weigel, 2011). In Pakkala et al. (2014), this degradation mechanism is assessed in Finland, finding that the current Finnish regulations are sufficient to withstand the evolution in freeze-thaw cycles. It should be highlighted that the previous result is not globally valid, and a specific regional assessment should be performed to evaluate the micro-climatic trend in the analyzed location.

The evolution of the frequency and intensity of wildfires due to climate change (Lozano et al., 2017; Strydom and Savage, 2017) can also lead to the deterioration of the structural capacity of concrete.

Scour is observed to be one of the most common causes of bridge collapse (Briaud et al., 2014; Cook et al., 2015), affecting the structural capacity at the foundation level and the overall stability of the system. Extreme precipitation and wind events due to climate change are predicted to enhance scour rate and damage, significantly impacting the structural resistance of existing bridges (Khandel and Soliman, 2019; Yang and Frangopol, 2019; Nava et al., 2023).

Eventually, the more frequent exploitation of de-icing salt under climate change can also represent an indirect risk for reinforced concrete structures (Darwin et al., 2007; Nasr et al., 2021), being a possible source of chloride-induced corrosion.

Among the different deterioration processes affecting the capacity of RC structures, corrosion is recognized as one of the most critical (Tuutti, 1982; Bertolini et al., 2013), and the induced damage may be enhanced by climate change. Recent reports by the JRC assessed this issue at the European level (Raposo De M. Do N. E S. De Sotto Mayor et al., 2020; Dimova et al., 2024). Corrosion-induced processes can lead to different damages, such as a reduction in the steel cross-section and ductility primarily (Coronelli and Gambarova, 2004; Biondini and Vergani, 2015), but also to the possible spalling of the concrete cover and the deterioration of the bond between concrete and steel (Prieto et al.,

2016; Prieto et al., 2016). Furthermore, the initiation and propagation of corrosion in RC structures are particularly influenced by the evolution of environmental conditions during the lifetime of the structure; different researchers proposed methodologies to account for this evolution, especially with regard to the impact of changes in temperature and relative humidity (Saetta et al., 1993; DuraCrete, 2000; Andrade et al., 2002; Yoon et al., 2007; Guo et al., 2015). In Table 3.10, different studies addressing the impact of climate change on corrosion-induced processes and consequently on structural capacity, focusing on RC structures.

The evaluation of the characteristic and design values of the capacity of deteriorated existing RC structures under climate change is still an open issue due to the significant uncertainties involved and the lack of experimental data. For this reason, a full-probabilistic analysis is often recommended in these cases instead of the application of semi-probabilistic methodology. Further research should be devoted to address this research gap to provide practitioners with tools to assess existing aging structures under climate change using the semi-probabilistic approach.

Research Proposal	Environmental Parameters*	Findings	Reference
Probabilistic approach for the estimation of corrosion initiation and damage, i.e., loss in reinforcement area, for RC infrastructures subjected to chloride and carbonation-induced corrosion under climate change scenarios.	C_{CO_2}, T, and RH.	Carbonation and chlorides-induced risk may increase respectively by over 400 % and 15 % in the Australian temperate area by 2100.	Stewart et al. (2011).
Probabilistic methodology accounting for the impact of climate change on corrosion deterioration processes. The proposed approach is exploited for the assessment of the probability of failure of an RC bridge beam subjected to chloride-induced corrosion considering future climate scenarios.	T and RH	Climate change may reduce the failure time by up to 31 % or shorten the service life by up to 15 years for moderate levels of environmental aggressiveness.	Bastidas-Arteaga et al. (2013).
A study on the impact of climate change on the initiation and propagation of carbonate-induced corrosion. The application of the proposed assessment is performed for RC facades and balconies of the building.	C_{CO_2}, T, and p.	Corrosion initiation and propagation are predicted to be accelerated by the future evolution of temperature and precipitation in Finland.	Köliö et al. (2014).
Stochastic framework for the evaluations of the combined impact of chloride-induced corrosion and cyclic loading under climate change. The methodology is applied to study the performance of an RC bridge girder.	T, RH, and R.	The change in climate leads to reductions in the lifetime of the structure, ranging between 1.4 and 2.3 % neglecting fatigue. If cyclic loading is considered, the lifetime reduction may increase up to 7 %.	Bastidas-Arteaga (2018).
Evaluation of corrosion rate changes in 223 coastal areas in the U.S., assessing the impact of these changes on the service life of structures, and consequently evaluating direct economic losses over the period 2000-2100 under climate change scenarios.	T, RH, and v_s.	The service life of RC structures may decrease by 1.7-2.7 % under the climate change's most pessimistic scenario by the end of the 21st century.	Y. Zhang et al. (2022).

Research Proposal	Environmental Parameters*	Findings	Reference
Simulation-based framework for life-cycle structural reliability analysis under climate change scenarios. The approach is exploited for the evaluation of an RC bridge pier cross-section exposed to chloride-induced corrosion.	T and RH.	The impact of climate change leads to a larger reliability index β decay, approximately 20% and 30% for the most optimistic and pessimistic scenarios, with respect to the discard of climate change.	Nava et al. (2023).

*Atmospheric CO_2 concentration C_{CO_2}, Temperature T, Relative Humidity RH, Precipitation p, Duration of cold or dry season R, and Wind Speed v_s

Table 3.10: Impact of climate change on the capacity of RC structures under corrosion.

3.7 Research Gaps and Challenges in Semi-Probabilistic Assessment

This Chapter proposed a review of past research and recent developments in the field of semi-probabilistic assessment of existing RC structures, with emphasis on the impact of deterioration and climate change on the calibration of these methodologies.

Firstly, a background on code calibration, focusing on the different level of decision-making for the evaluation of structural performance is discussed in Section 3.1. The fundamental concepts and methodology of structural reliability analysis are reported in Section 3.2, highlighting the benefits and drawbacks of each strategy. In Section 3.3, the focus is devoted to reliability-based calibration of semi-probabilistic methodologies. Eventually, the semi-probabilistic assessment for the design of new structure, the assessment of existing structures considering deterioration and integrating the impact of climate change is analyzed in Sections 3.4, 3.5, and 3.6, respectively. In these Sections, the findings of several studies are summarized to report the state of the art of the semi-probabilistic assessment of existing aging structures under climate change. Three crucial aspects are reviewed:

- the definition of reliability target;
- the derivation of characteristic and design values of structural demand and capacity.
- the calibration of reliability elements of the code, such as safety factors.

The analysis highlighted the effort made in the last years to provide a reliable procedure for the evaluation of residual structural performance of existing structures to practitioners. This procedure is generally recognized coincident with the semi-probabilistic safety format, due to the simplicity and the replicability in the case of usual situations. A wide number of researchers underlined the need for the consideration of the changing climate in this methodology and several studies proposing frameworks for the incorporation of climate change impact are discussed and reviewed. The review highlighted the significant amount of research advances in these fields, but also research gaps and challenges to be dealt with to appropriately calibrate semi-probabilistic formats for the assessment of existing aging structures under climate change scenarios:

- the definition of the reliability target for existing structures still remains an open issue for the lack of coherence between the different values proposed in the literature, the deficit of data for the analytical formulations, and the difficulties in the standardization of different RC structures. Moreover, climate change and deterioration

may have an impact on the economic and human safety considerations at the base of the reliability target definition and this should be addressed in future studies.

- The derivation of the characteristic and design values for structural loadings accounting for climate change impact, e.g., non-stationarity, is currently being addressed by different research groups. Nevertheless, considering characteristic and design values of structural resistance under climate change, aging, and environmental aggressiveness additional efforts are necessary to achieve a more complete understanding of the phenomena.

  This is due to several factors such as the combination of the deep uncertainty of climate change with the one related to the environmental aggressiveness, as well as the local nature of the detrimental processes that may be active only in delimited portions of the analyzed structures. Moreover, the modeling of these phenomena is often a complex task and the employment of the proposed models need very high expertise. For this reason, the development of simplified and standardized methodologies, which may be used by practitioners, is a crucial step for the evaluation of aging existing structures subjected to detrimental processes under climate change.

- The calibration of safety factors tailored for the assessment of existing structures has been extensively investigated in the literature over the last decades considering both partial and global safety formats. The standardization of these semi-probabilistic methodologies has been proposed in different countries by national and international codes, even if further studies are needed for a wider exploitation in practice. The need for a refined characterization of the uncertainties affecting the existing structures as well as standardized prescriptions for dealing with significantly deteriorated structural elements are crucial aspects for future investigations. In conclusion, the changes in current and future climate are affecting the structural systems, and, in general, the built environment leading the hypothesis of stationarity assumed by several national and international standards to be questionable. Further developments are needed also along these lines of research in order to revise semi-probabilistic methodologies for the assessment of RC structures subjected to detrimental processes in a changing climate. Eventually, although some studies analyzed the non-stationary evolution of climate and its impact on environmental actions, more steps for the characterization of uncertainties and the definition of basic assumptions are needed for the consequent calibration of semi-probabilistic design codes.

Based on the discussed gaps and challenges, this thesis research focus on the definition of a methodology for the calibration of semi-probabilistic format focusing on the impact of deterioration and climate change on structural capacity.

Chapter 4

Structural Capacity Modeling under Deterioration

4.1 Reliability of Deteriorating Structures

The structural demand and capacity of deteriorating systems under climate change conditions generally evolve over time. In this case, the failure of a structural system may be described by a time-dependent limit state function $g(\mathbf{X}, t)$ as a function of the vector of stochastic parameters $\mathbf{X}$ and time t (Ditlevsen and Madsen, 1996; Melchers and Beck, 2018). Depending on the nature of these parameters, they are modeled as random variables (e.g., physical, model, and statistical uncertainties) or random processes (e.g., loads and environmental parameters randomly evolving evolving time). In this context, the time-dependent probability of a failure event $p_f(t)$ can be defined as:

$$p_f(t) = P[g(\mathbf{X}, t) \leq 0] \tag{4.1}$$

The time-variant probability of failure is generally used as a metric to describe the reliability of deteriorating structural systems (Sarveswaran and Roberts, 1999; Bastidas-Arteaga et al., 2009; Barone and Frangopol, 2014; Biondini and Frangopol, 2016). Although the estimation of $p_f(t)$ formally requires solving a time-variant reliability problem, which is inherently complex, in most practical applications the problem can be reformulated as a sequence of time-invariant reliability analyses by evaluating the limit state at discrete time instants.

In general, the underlying random variables or stochastic processes $\mathbf{X}$ associated with a structural system can be partitioned into those governing the structural capacity, denoted by $\mathbf{X}_R$, and those governing the structural demand, denoted by $\mathbf{X}_S$. The time-dependent structural capacity $R(\mathbf{X}_R(t))$ and demand $S(\mathbf{X}_S(t))$ are both influenced by the uncertain-

ties inherent in the basic random variables involved in their formulation. Consequently, the probability of failure for a time-variant reliability problem can be expressed as:

$$p_f(t) = P[R(\mathbf{X}_R(t)) \leq S(\mathbf{X}_S(t))] \tag{4.2}$$

Moreover, in the case of deteriorating structural systems under climate change, basic random variables may evolve not only in terms of their statistical parameters but also with respect to their probability distributions. In particular, capacity-related random variables may experience substantial changes due to progressive damage mechanisms. As deterioration accumulates, an initially uni-modal distribution may transition into a multi-modal form, or become inflated on certain thresholds, reflecting the development of damage. The latter description is generalizable to any type of structural material and deterioration process. Nevertheless, for the sake of this Thesis, the focus is devoted in the following Sections to RC subjected to corrosion.

Strategies for assessing the time-variant capacity of deteriorating structural systems under climate change are discussed in Sections 4.2. Eventually, a general overview of the deterioration phenomena that affect RC structures is provided in Section 4.3, while Section 4.4 is devoted to corrosion induced processes, with particular emphasis on the impact of climate change and its modeling.

4.2 Structural Capacity Modeling under Deterioration

Uncertainties are invariably present in practical engineering systems (Ang and Tang, 2007). These are commonly categorized into two main types: aleatory and epistemic uncertainties (Hoffman and Hammonds, 1994). Aleatory uncertainties represent the intrinsic natural variability in observable physical phenomena, whereas epistemic uncertainties are related to the limitations in accurately interpreting real physical processes due to inaccurate predictive models or a lack of empirical data. Moreover, in practical engineering problems related to analytical modeling and design, determining the nature of a specific set of uncertainties presents significant challenges (Der Kiureghian and Ditlevsen, 2009). These uncertainties may be related to material strength, manufacturing processes, random loads, deterioration mechanisms, and climate change, affecting the structural performance of an engineering system, such as reliability (Melchers and Beck, 2018) and robustness (X. Du and Chen, 2000). For these reasons, the assessment, analysis, and representation of uncertainties have become a critical issue for engineers to address.

Considering existing structures, the uncertainties that characterize their structural

capacity and demand may evolve over the designed lifetime. For instance, they can be reduced due to additional knowledge, such as that derived from testing on the materials and data concerning the loadings. Furthermore, for structures affected by deterioration mechanisms such as corrosion, the probability density function $f_R(t)$ that describes a generic resistance random variable R may be significantly impacted by the uncertainties inherent in the damage process.

Damage might not only influence the statistical moments of $f_R(t)$ but also the probability distribution function itself. For example, the material strength is typically represented by a Lognormal distribution at the initial time $f_R(t_0)$; after the occurrence of damage at time t_d, $f_R(t > t_d)$ may no longer follow a lognormal distribution. In cases of severe damage, the distribution transitions from a uni-modal to a multi-modal distribution or it becomes inflated at a specific value.

Climate change may exacerbate this phenomenon, thereby intensifying the consequences of the deterioration processes affecting RC structures. The probability distribution function $f_S(t)$ that describes climatic loadings may also be influenced by climate change, particularly in relation to its statistical moments, given the intrinsic non-stationarity of the process. This is highlighted in several studies (Cheng et al., 2014; Croce et al., 2019; Arnold and Kraus, 2022). In order to assess these phenomena and accurately evaluate the performance of structural systems over time, it is critical to characterize the temporal propagation of uncertainty. Considering a generic resistance random variable $R = g(\mathbf{X})$ as a function of n random variables $\mathbf{X} = [X_1, X_2, ..., X_n]$, the primary objective of probabilistic uncertainty propagation is to derive the statistical moments and probability distribution function of R, utilizing the distribution information of the input random variables $\mathbf{X}$. This can be performed using various methodologies that can be categorized into 4 groups (Z. Zhang et al., 2019):

- Sampling-based methods, including Monte Carlo simulation (Gao et al., 2018) , importance sampling (Mori and Kato, 2003), and adaptive sampling (Bucher, 1988);
- Most probable point (MPP)-based methods, such as FORM (Rackwitz and Fiessler, 1978) and SORM (Breitung, 1984);
- Surrogate model-based methods, such as those employing polynomial functions (Bucher and Bourgund, 1990), Kriging models (Echard et al., 2011), and polynomial chaos expansions (Xu et al., 2017);
- Moment-based methods (Zhao and Ono, 2001; S. H. Lee and Kwak, 2006).

While the aforementioned methods are effective for propagating uncertainty at specific time intervals, the continuous nature of deterioration in RC structures may be captured

through stochastic processes, such as Markov Chains or Gamma Processes (Shibata and Takeyama, 1977; Bastidas-Arteaga et al., 2010; Valor et al., 2013; W. Zhou et al., 2017).

Most of these methods are applicable to univariate distributed random variables. However, as mentioned above, the random variable may follow a multi-modal distribution , such as the structural fatigue stress of a steel bridge carrying both highway and railway traffic (Ni et al., 2012) or the structural resistance under damage mechanisms.

In order to address this issue, Z. Zhang et al. (2019) propose the combination of reliability methods, such as simulation, FORM, and SORM, with the statistical mixture model to describe the multi-modality of the random variable or to estimate the distribution of an unknown probability density function over time.

4.3 Deterioration Mechanisms in Reinforced Concrete Structure

Reinforced concrete structures, when exposed to aggressive environments, can be affected by different deterioration processes leading to an evolution in their structural capacity and demand over time. Extreme loadings, weathering, and the attack of aggressive agents can lead to the progressive deterioration of steel and concrete under various physical and chemical processes, as summarized in Table 4.1.

Among the environmental hazards affecting RC structures, corrosion is considered one of the most critical (Bertolini et al., 2013); for this reason, it is the subject of Section 4.4, with a particular focus on the impact of changes in climatic conditions. Nevertheless, to provide a comprehensive overview of the deterioration mechanisms affecting RC structures, the main physical and chemical damage processes are concisely outlined in the following.

4.3.1 Physical Deterioration

Physical damage is mainly related to the temperature variation that may occur in RC structures. The most common types of physical damage are thermal variations due to hydrating heat, freeze-thaw cycles, and fire damage.

Hydrating Heat. Damage in concrete can arise during the curing phase, as large temperature gradients are induced by hydrating chemical reactions. These may lead to the generation of tensile stresses and, subsequently, cracking of the concrete. The hydrating heat ranges between 380 KJ/kg and 500 KJ/kg for Portland cement, and this depends mainly on the amount of cement paste in the concrete mix design. This

Type of Deterioration	Causes	Deterioration Mechanism
Deterioration of concrete	*Mechanical*	Abrasion
		Erosion
		Impact
		Explosion
	Physical	Hydrating Heat
		Freeze-thaw
		Fire
	Structural	Overloading
		Settlement
		Cyclic loading
	Chemical	Alkali aggregate reactions
		Acid attack
		Sulfate attack
		Pure water attack
	Biological	Fouling
		Biogenic Attack
Corrosion of Reinforcement	*Corrosion*	Carbonation
		Chlorides
		Stray Current

Table 4.1: Main deterioration mechanisms in RC structures, based on Bertolini et al., 2013.

process may be especially relevant for massive structural elements, producing large temperature gradients between the shrinking external surfaces, cooled by the surrounding environment, and the expanding core subjected to more severe hydrating heat.

Freeze-Thaw Cycles. The water trapped in the concrete pore system may freeze at low temperatures, producing an increase in volume by about 9% and generating tensile stresses that can cause scaling, cracking, or spalling, or in the most severe scenarios, also complete delamination of the concrete cover. Pore water freezing is generally a gradual process, particularly influenced by the temperature gradient between the air and the concrete, occurring from the surface and moving towards the core of the concrete. Capillary pores may represent a favorable environment for freeze-thaw cycles,

as they rapidly saturate and can be subjected to large pressure, although the thermal conductivity of concrete is significantly low. Concrete resistance to freeze-thaw cycles can be improved through adequate curing and low ratios w/c, resulting in a reduction in the number of pores and their interconnection. In addition, air-entraining additives may be incorporated into the concrete mix to promote a uniform and interconnected system of microscopic air voids, allowing water to expand upon freezing without generating excessive tensile stresses within the material.

Fire Damage. Concrete is characterized by low thermal conductivity, involving good structural response to fire hazards. In general, the external part of RC members is the most exposed to fire, protecting the embedded reinforcing steel. However, significant damage may arise depending on the temperature history and the time of exposure to the fire. For temperatures greater than 30 °C, water is ejected from the pores and the hydration products decompose, leading concrete to shrink and aggregates to expand. The consequences may be various, from cracking to explosive delamination if the water trapped in the inner pores is prevented from reaching the surface and releasing the related pressure. Usually, concrete thermal properties are assumed to be independent of the state of stress (CEN, 2004a). However, in some cases, the occurrence of stress-related damage phenomena may lead to the coupling of heat transfer and spatial distribution of temperature with the structural response (Biondini and Nero, 2011).

4.3.2 Chemical Deterioration

Chemical damage is mainly related to the degradation of the material properties of concrete or the creation of tensile stresses due to expansive chemical reactions. The most severe types of chemical damage are due to sulfate attack and Alkali-Aggregate Reaction (AAR).

Sulfate Attack. The penetration of sulfates into concrete can lead to a reaction with calcium hydroxide, creating gypsum, which severely reduces the material strength at the macroscopic scale. Moreover, ettringite may result from the reaction between gypsum and aluminates. Ettringite is an expansive reaction product that may induce severe cracking, or in the worst scenario, disaggregation of concrete. This phenomenon is usually observed in underground RC structures in contact with water containing a high concentration of sulfate ions. Moreover, in cases of high relative humidity and low temperatures, thaumasite may be produced, which in the long term may lead to severe deterioration of concrete. Mix designs inducing low permeability of concrete are usually exploited to prevent sulfate attacks.

Alkali-Agregates Reaction. Cement paste is characterized by a highly alkaline pore solution in which cations Na^+ and K^+ are dissolved. These may react with silica (SiO_2) present in certain types of aggregates, producing an expansive gel if in contact with water. Cracks in concrete may form as a result of this expansion. The location of the reactive areas depends on the aggregates. Pozzolanic material and fly ashes can be added to the design mix to reduce the alkali content in the cement paste.

4.4 Corrosion of Reinforced Concrete Structures

Corrosion of RC structures is a complex phenomenon involving several mechanisms and uncertainty. These are related to the environmental conditions and material properties that influence the physical and chemical processes governing corrosion phases.

Considering the service-life of an RC structure subjected to corrosion-induced processes, two main phases are recognized, i.e., corrosion initiation and propagation, marked by the corrosion onset (Tuutti, 1982), as depicted in Figure 4.1. During the initiation phase, the reinforcement is still surrounded by the passive film, and corrosion has not yet started. Due to phenomena such as carbonate or chloride penetration, passivity is lost, leading to the onset of corrosion and the consequent propagation phase.

The model proposed by Tuutti (1982) and reported in Figure 4.1 assumes that the propagation phase immediately follows the initiation phase. In reality, this may be considered excessively conservative as it neglects several factors. For instance, Angst et al. (2022) suggest the incorporation of a transition period between the first depassivation of the film and the establishment of stable active corrosion. During this time, the steel may undergo several cycles of re-passivation, effectively delaying the onset of structural damage. Moreover, the model proposed in Figure 4.1 assumes a relatively constant pro-

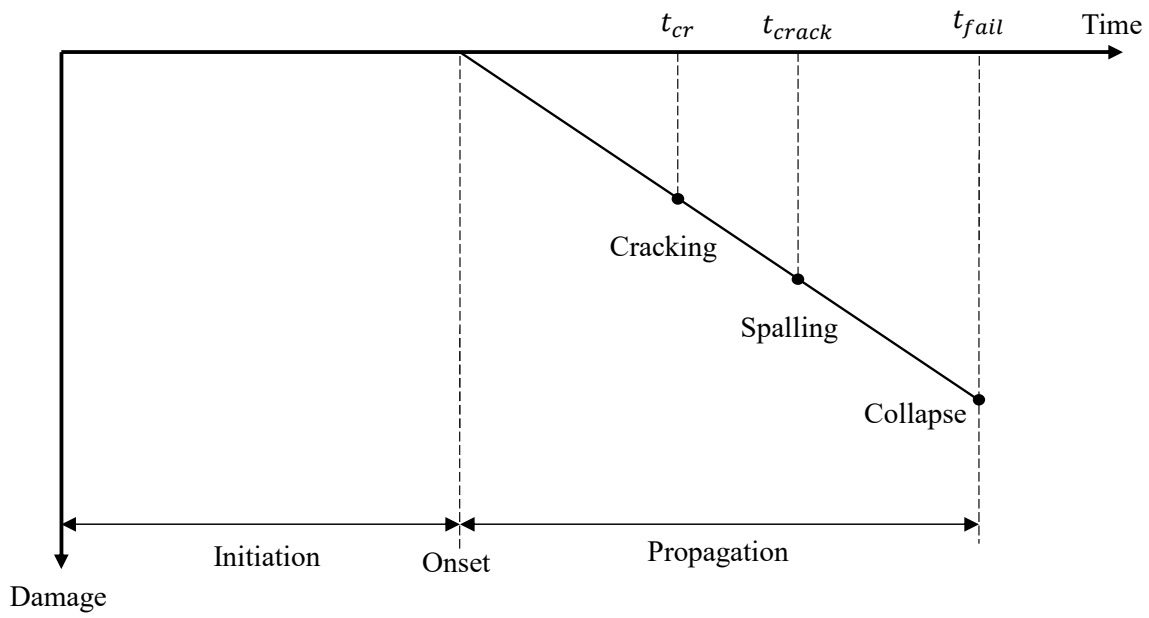

Figure 4.1: Phases of corrosion and damage propagation, adapted from Gjørv (2009a).

gression once initiation is reached. However, the propagation rate is often self-limiting due to the accumulation of corrosion products which may limit the diffusion, or due to a lack of sufficient oxygen and water content. In Melchers (2021) and Melchers and Li (2006), alternative models taking into account the time-variant nature of the corrosion propagation are discussed. Nevertheless, the model proposed by Tuutti, 1982 is often used due to its simplicity, also concerning the incorporation in engineering codes, and its ability to provide 'safe-side' estimations.

The duration of the initiation phase depends on designed quantities, such as the concrete cover, and on characteristics of environmental exposure, e.g., the concentration of aggressive agents and their diffusivity in concrete. The onset of the mechanism may also be influenced by any form of polarization of the reinforcement. After the breakdown of the protective layer, corrosion can propagate only if oxygen and water are present on the reinforcement surface.

Moreover, the corrosion rate can be influenced by environmental conditions. The initiation, onset, and propagation of corrosion can also be significantly influenced by local weather and climate conditions, mainly in the form of temperature and relative humidity. Consequently, climate change is expected to have an impact on corrosion.

The serviceability, safety, and performance of RC structures may be severely affected by corrosion processes due to the induced damage, such as the loss of the reinforcement cross section and cracking of the concrete cover, leading to spalling and, in the worst case scenario, to collapse. A schematic representation of the corrosion consequences is

reported in Figure 4.2.

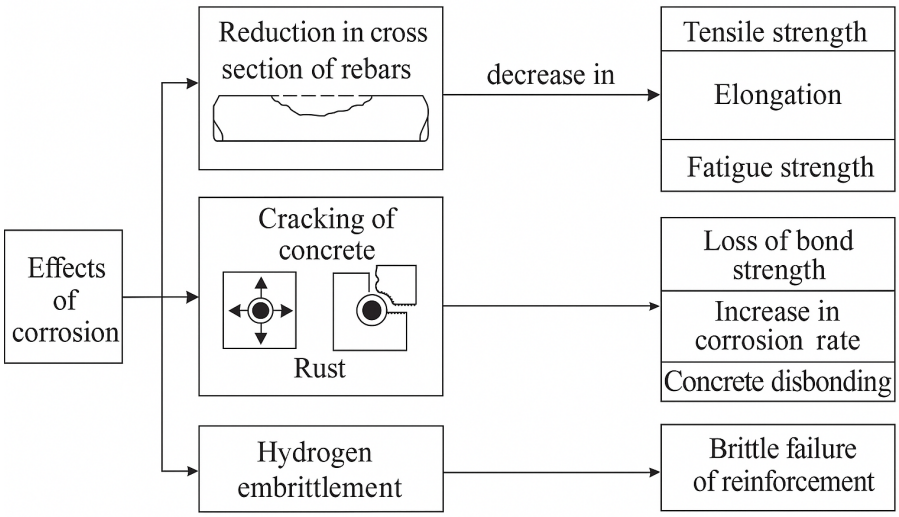

Figure 4.2: Corrosion consequences in RC structure, from Bertolini et al. (2013)

In the following sections, the different phases of corrosion and the induced damage in RC structures are discussed in detail, focusing mainly on chloride and carbonation-induced corrosion, as well as the impact of climate change on these deterioration phenomena.

4.4.1 Corrosion Initiation

The initiation phase describes the period before the onset of the corrosion phenomenon; it may be defined as the time that aggressive agents require to reach a certain concentration, i.e., the critical chloride concentration C_{cr} for chloride-induced corrosion, or penetrate at the level of reinforcement, for carbonation-induced corrosion.

In the early stage of the lifetime of RC structures, the concrete hydration products are characterized by a high pH, approximately equal to 12 or 13, and the alkaline environment surrounding the steel reinforcement bars leads to the development of a passive layer along their surface, preventing the occurrence of corrosion. Nonetheless, being concrete a porous and conductive material, external agents and electrical current can penetrate within its microstructure, interacting and undermining the mechanical properties of both concrete and steel. In this context, corrosion initiation in RC members consists of the ingress of carbon dioxide, chlorides, and other aggressive agents, leading to a decay of concrete pH below a pH of 11.5, and the consequent disruption of the protective film along reinforcement bars.

4.4.1.1 Chloride-Induced Corrosion

Chloride-induced corrosion is recognized as one of the main processes leading to the degradation of RC structures. The source of chloride ions in concrete may be internal, deriving from raw material or admixtures embedded in the concrete mix, or external, due to exposure to aggressive environments. Local depassivation of the protective film surrounding the steel bars is expected, leading to localized damage, if the chloride concentration on the reinforcement surface C_s is greater than or equal to the critical chloride concentration C_{cr}. The kinetics of penetration of chlorides in concrete should be assessed to properly evaluate the corrosion initiation time; this is influenced by several parameters related to the concrete design, such as the water-cement ratio w/c, the moisture content, the type of cement, as well as related to the surrounding environment, e.g., temperature T and relative humidity RH. Moreover, the initial chloride concentration, the critical concentration threshold, and the concrete cover also affect the duration of the initiation phase.

Migration of fluids and ions in concrete is governed mainly by four physical and chemical processes, i.e., diffusion, permeation, electrical migration, and capillary suction (Camnasio, 2013). In particular, the transport of chlorides in concrete is predominantly governed by diffusion due to concentration gradients. Although pure diffusion occurs only in saturated concrete, Fick's second law of diffusion is generally adopted to describe the ingress of chloride ions into concrete, also based on empirical evidence from in situ measurements in real marine and road structures exposed to deicing salts (Bertolini et al., 2013). Equation 4.3 is often used to assess chloride concentration C at a specific depth x and time t:

$$D_c \frac{\partial^2 C}{\partial x^2} = \frac{\partial C}{\partial t} \tag{4.3}$$

where D_c is the diffusion coefficient or diffusivity.

Theoretically, Equation 4.3 describes the kinetics of a non-stationary process, under the assumptions of mono-dimensional diffusion for an isotropic, homogeneous, and time invariant medium (Collepardi et al., 1972); nevertheless, empirical evidence reports a good approximation of the real chloride concentration with the estimated one using Equation 4.3.

The analytical solution of Equation 4.3 can be obtained in closed form:

$$C(x,t) = C_s \left[1 - \operatorname{erf}\left(\frac{x}{2\sqrt{D_c t}}\right)\right] \tag{4.4}$$

where $C(x,t)$ is the total chloride content at time t and at depth x with respect to the concrete surface, C_s is the chloride content on the surface, and D_c is the diffusion coefficient or diffusivity. The fib Bulletin N° 76 (fib, 2015) recommends the following

value of for the stochastic modeling of C_s considering different exposure classes (Table 4.2).

Exposure class	$C_{s,0}/C_{s,\Delta x}$ **[wt.-/b]**	
	Mean μ	CoV
XD1	$0.5 \leq \mu \leq 1.5$	0.75
XD2	$2.0 \leq \mu \leq 4.0$	0.75
XD3	$2.0 \leq \mu \leq 4.0$	0.75
XS1	$1.0 \leq \mu \leq 2.0$	0.45
XS2	$2.0 \leq \mu \leq 4.0$	0.25
XS3	$2.0 \leq \mu \leq 4.0$	0.45

Table 4.2: Surface chloride content for different exposure classes (fib, 2015).

Enforcing $C(x,t)$ equal to the critical corrosion content C_{cr} in Equation 4.4, the corrosion initiation time may be retrieved as:

$$t_{cr} = \frac{x^2}{4D_c}\left[\text{erf}^{-1}\left(1 - \frac{C_s}{C_{cr}}\right)\right]^{-2} \tag{4.5}$$

The critical corrosion content C_{cr} is generally affected by large uncertainties, and typical values range from 0.1% to 2.0% with respect to cement weight. In particular, several technical reports and standards (fib, 2006, 2015, 2023) recommend to model the critical concentration as a random variable following a bounded beta distribution between 0.2% and 2.0% and characterized by the mean value μ and standard deviation σ equal to 0.6% and 0.15%, respectively.

4.4.1.2 Carbonation-Induced Corrosion

The ingress of carbon dioxide CO_2 dispersed in the air and the reaction with alkaline constituents present in the concrete trigger carbonation-induced corrosion in RC structures. These are located in the pore liquid solution, principally in the form of sodium and potassium hydroxides, $NaOH$ and KOH respectively, as well as in solid hydration products, for example calcium hydroxide $Ca(OH)_2$ or calcium silicate hydrate $C-S-H$. Considering that $Ca(OH)_2$ reacts most promptly with CO_2 in aqueous solution, the chemical reaction may be described by Equation 4.6:

$$CO_2 + Ca(OH)_2 \rightarrow CaCO_3 + H_2O \tag{4.6}$$

where $CaCO_3$ and H_2O are the products of the reaction, i.e. calcium carbonate and water, respectively.

Carbonation starts on the surface of concrete and gradually develops towards the inner zones, leading to a decrease from normal pH values to values lower than 11.5, often approaching neutrality. Furthermore, carbonation can alter the binding capacity of cementitious materials with respect to chlorides. During this process, chlorides may become incorporated into calcium chloroaluminate hydrates, while those previously adsorbed or chemically bound to other hydrated phases may be released, increasing the concentration of free chlorides in the pore solution, and thereby enhancing its aggressiveness (Tuutti, 1982; Bertolini et al., 2013).

Finally, carbonation-induced corrosion begins when the alkalinity level at the steel reinforcement location is uniformly reduced to sufficiently low levels, allowing corrosion to occur if sufficient oxygen and water are present in the proximity of the bar (Heiyantuduwa et al., 2006).

Analytically, carbonation penetration may be described using Equation 4.7 (Bertolini et al., 2013):

$$x_c(t) = Kt^{\frac{1}{n}} \tag{4.7}$$

where $x_c(t)$ is the carbonation depth , K is the carbonation coefficient, and t is time. Generally, the exponent n is approximately considered equal to 2, and the penetration depth tends to show a parabolic profile over time. Several probabilistic formulations that explicitly account for environmental and material factors can be found in the literature (DuraCrete, 1998; fib, 2006; Y. Zhou et al., 2015).

The carbonation coefficient K can be considered an estimate of the carbonation rate; K is affected by both environmental factors, specifically humidity RH, temperature T, carbon dioxide concentration C_{CO_2}, and concrete related factors, such as alkalinity and permeability. The carbonation rate is also inversely proportional to the water-cement ratio w/c in a properly cured concrete (Skjolsvold, 1986; Page, 1992). Practically, an accurate prediction of K is complex because this parameter may vary over time and in space with respect to the structure considered (Stewart et al., 2002).

Several analytical models have been developed to adequately predict carbonation depth x_c and a complete review can be found in DuraCrete (1998). Yoon et al. (2007) recommend the model reported in Equation 4.8, assuming that carbonation penetration is governed by the diffusion process.

$$x_c(t) = \sqrt{\frac{2D_{CO_2}(t)}{a} C_{CO_2}(t) t} \left(\frac{t_0}{t}\right)^{n_m} \quad t \geq t_0 \tag{4.8}$$

In Equations 4.8, $D_{CO_2}(t)$ is the diffusion coefficient of CO_2 in concrete, $C_{CO_2}(t)$ is the time-dependent mass concentration of ambient CO_2, t_0 is the initial year of analysis, n_m

is the age factor for micro-climatic conditions associated with the frequency of wetting and drying cycles, equal to 0 for sheltered outdoor while 0.12 for unsheltered outdoor, and a is the amount of CO_2 needed for complete carbonation; a is related to the CO_2 binding capacity and may be computed according to Equation 4.9:

$$a = 0.75 \cdot C_e \cdot C_{a0} \cdot \alpha_H \cdot \frac{M_{CO_2}}{M_{Ca0}} \tag{4.9}$$

where C_e is the cement content, CaO is the CaO content in cement usually assumed equal to 0.65, M_{CaO} is the molar mass of CaO (56 g/mol), M_{CO_2} is the molar mass of CO_2 (44 g/mol), and α_H is the degree of hydration for Ordinary Portland Cement (OPC) after more than 400 days, which can be estimated using Equation 4.10.

$$\alpha_H = 1 - e^{-3.38w/c} \tag{4.10}$$

In equation 4.10, w/c is the water-cement ratio.

The diffusion coefficient $D_{CO_2}(t)$ is defined by Equation 4.11:

$$D_{CO_2}(t) = D_1 t^{-n_d} \tag{4.11}$$

where D_1 is the diffusion coefficient of CO_2 in concrete after one year, and n_d is the age factor.

Eventually, carbonation-induced corrosion starts at time t_{in}, defined as the time required for the carbonation front to reach a depth x_c equal to the one of the analyzed steel bar layer x.

4.4.1.3 Climate Change Impact on Corrosion Initiation

Chloride and carbonation-induced corrosion phenomena are significantly influenced by the evolution of environmental parameters. Climate change, by altering these parameters, may accelerate corrosion processes, thereby having a non-negligible impact on the structural safety over time. In this section, the impact of climate change is analyzed, first, with respect to chloride-induced corrosion, and second, considering carbonation-induced corrosion.

Chloride-induced Corrosion

The penetration of chlorides into concrete is governed by diffusion, as discussed in Section 4.4.1.1. Diffusion is influenced by several factors, among which are environmental parameters such as temperature T and relative humidity RH. In Equation 4.4, chloride diffusivity D_c is assumed to be constant and is defined with respect to the reference temperature T_{ref} and relative humidity RH_{ref} equal to 20 °C and 75%, respectively.

Saetta et al. (1993) propose a correction for the formulation of D_c to account for time-variant temperature T and pore relative humidity RH, as well as the effects of aging:

$$D_c(t) = D_{c,ref} \cdot F_T(t) \cdot F_{RH}(t) \cdot F_a(t) \tag{4.12}$$

where $D_{c,ref}$ is the reference chloride diffusion coefficient estimated at T_{ref} and RH_{ref}; the terms $F_T(t)$, $F_{RH}(t)$, and $F_a(t)$ represent correction functions accounting for the impacts of temperature, relative humidity, and the aging of concrete, respectively.

Higher temperatures increase the diffusion coefficient, which in turn reduces the initiation time, as reported by Hansson and Sørensen (1990). Experimental analysis have demonstrated that the temperature correction function $F_T(t)$ at time t can be analytically modeled using the Arrhenius law (Equation 4.13):

$$F_T(t) = exp\left[\frac{E_a}{R_g}\left(\frac{1}{T_{ref}} - \frac{1}{273 + T(t)}\right)\right] \tag{4.13}$$

where E_a represents the activation energy of the chloride diffusion process, R_g is the gas constant ($8.314 \cdot 10^3\ kJ/K \cdot mol$), T_{ref} denotes the reference temperature, which is typically assumed to be 293 K (20 °C), and $T(t)$ indicates the actual temperature at time t. As reported by Page et al. (1981), the values of the activation energy E_a for the chloride diffusion process in Portland cement pastes depend on the water-cement ratio w/c; for instance, E_a is equal to 41.8 kJ/mol, 44.6 kJ/mol, and 32.0 kJ/mol for w/c ratios of 0.4, 0.5, and 0.6, respectively.

Chloride diffusion can only occur in the presence of water within the capillary pores of concrete. Therefore, a decrease in relative humidity hinders the penetration of chlorides towards the reinforcement. The correction function $F_{RH}(t)$ is proposed to account for the modification in chloride diffusivity at time t with respect to relative humidity RH (Equation 4.14):

$$F_{RH}(t) = \left[1 + \frac{(1 - RH(t))^4}{(1 - RH_{ref})^4}\right]^{-1} \tag{4.14}$$

where RH_{ref} denotes the reference relative humidity, which is typically assumed to be 0.75. This value represents the threshold at which the diffusion coefficient is reduced to 0.5 (Bažant and Najjar, 1971).

Ultimately, chloride diffusivity decreases with the increase of hydration in concrete and, consequently, with aging. This phenomenon is represented by the correction function $F_a(t)$, which is described in Equation 4.15.

$$F_a(t) = \left(\frac{\tilde{t}}{t}\right)^a \tag{4.15}$$

Where $\tilde{t}$ represents a duration of 28 days, t denotes the actual time, and a indicates the aging factor.

The correction functions illustrated in Equations 4.13 and 4.14 allow the examination of the impacts of climate change on the diffusivity of chlorides in concrete. In figure 4.3 (a) and (b), the correction functions are represented for different values of temperature T and relative humidity RH, respectively. Additionally, the time variant diffusivity $D_c(t)$ normalized with respect to the reference diffusivity $D_{c,ref}$ is depicted in Figure 4.3 (c) for different combinations of T and RH.

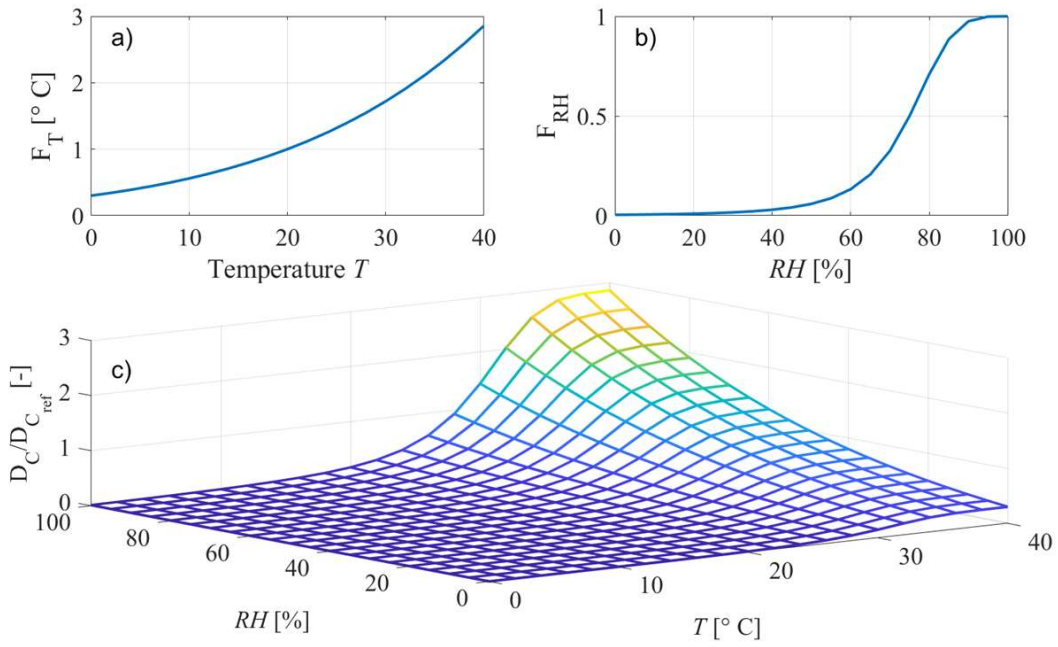

Figure 4.3: Impact of temperature and relative humidity on chloride diffusivity in concrete.

In conclusion, climate change, modifying the values of temperature T and relative humidity RH, may increase the diffusivity of chlorides in concrete, leading to a significant anticipation of the corrosion initiation time . Nava (2022) also highlights that this impact is more significant for increasing values of concrete cover.

The onset of chloride-induced corrosion occurs when the chloride concentration $C(x,t)$ at the level of reinforcing steel x equals the critical chloride content C_{cr}. Various studies have emphasized the significance of temperature evolution concerning C_{cr} (Hussain

et al., 1995; Gastaldi and Bertolini, 2014). According to Shirkhani et al. (2020), the chloride threshold value can be considered inversely proportional to the rates of corrosion reactions. Physically and chemically, the chloride threshold value is reduced due to the enhanced release of chloride ions from concrete at elevated temperatures, which occurs concurrently with accelerated corrosion reactions. Assuming that the two mechanisms are independent of each other, the evolution of $C_{cr}(t)$ with respect to temperature can be expressed according to Equation 4.16 (J. Zhang et al., 2018; Shirkhani et al., 2020):

$$C_{cr}(t) = C_{cr,ref} \cdot \exp\left[\frac{(E_{Cl\text{-}concr} + E_{Cl\text{-}steel})}{R_g}\left(\frac{1}{273 + T(t)} - \frac{1}{T_{ref}}\right)\right] \tag{4.16}$$

where $C_{cr,ref}$ is the chloride threshold value at the reference temperature $T_{ref} = 293$ K, R_g is the gas constant ($8.314 \cdot 103\ kJ/K \cdot mol$), $E_{Cl-concr}$ represents the activation energy for the release of free chlorides, $E_{Cl-steel}$ denotes the rebar activation energy, respectively, and $T(t)$ (in °C) is the actual temperature at the time t. The activation energy ($E_{Cl-concr} + E_{Cl-steel}$) can reach values of up to 48 kJ/mol when combining the mechanisms.

The above formulation is based on the assumption that the chloride threshold value decreases with increasing temperature, following the inverse of the Arrhenius law. This conclusion is drawn from a limited number of available studies. In this context, more fundamental investigations are necessary to understand the temperature dependence of the critical chloride concentration in RC structures. This understanding is crucial for more accurate predictions of the remaining lifetime in a changing climate (Shirkhani et al., 2020; Shirkhani et al., 2023).

Carbonation-induced Corrosion

The concentration of carbon dioxide in the atmosphere is one of the main parameters influencing carbonation-induced corrosion. According to IPCC (2023a), the concentration of carbon dioxide CO_2 is expected to increase over time, thereby leading to an increase in the carbonation rate. Ho and Lewis (1987) performed accelerated tests in the laboratory to assess the resistance of different types of concrete to carbonation. The research reported that seven days of exposure to an atmosphere containing 4 % of CO_2 resulted in the same level of carbonation penetration as that observed after a year of exposure to a normal atmosphere (values of CO_2 for the urban environment are around 0.1%). To accurately model the impact of CO_2 abundance, Stewart et al. (2002) and Stewart et al. (2011) propose a modification to Equation 4.8, taking into account the gradual increase of CO_2 concentration over time:

$$x_c(t) = \sqrt{\frac{2D_{CO_2}(t)}{a} k_{site} \int_{t_0}^{t} C_{CO_2}(t)dt} \left(\frac{t_0}{t}\right)^{n_m} \quad t \geq t_0 \tag{4.17}$$

where k_{site} accounts for the modified CO_2 levels in the considered site, which is equal to 1.15 for the urban area (Stewart et al., 2011), $D_{CO_2}(t)$ is the diffusion coefficient of CO_2 in concrete, $C_{CO_2}(t)$ is the time-dependent mass concentration of ambient CO_2, t_0 is the initial year of analysis, n_m is the age factor for micro-climatic conditions associated with the frequency of wetting and drying cycles, equal to 0 for sheltered outdoor while 0.12 for unsheltered outdoor, and a is the amount of CO_2 needed for complete carbonation.

Moreover, the carbonation penetration is influenced by the evolution of temperature and relative humidity in time. In general, assuming other conditions remain unchanged, the corrosion penetration rate increases with higher temperatures; on the other hand, relative humidity affects the penetration of CO_2 in concrete in a more complex manner. As a matter of fact, the diffusion of carbon dioxide within concrete is inhibited when the pores are saturated. However, the carbonation reaction may occur only in the presence of water. In fact, the carbonation penetration rate is maximized for relative humidity RH values ranging from 60 % to 70 % (Tuutti, 1982; Bertolini et al., 2013). Eventually, carbonation penetration is also influenced by wetting related parameters (Parrott, 1992).

The effect of temperature and relative humidity on the diffusion process can be accounted for by exploiting Equation 4.18:

$$D_{CO_2}(t) = D_{CO_2,ref}(t) \cdot F_T(t) \cdot F_{RH}(t) \tag{4.18}$$

where $D_{CO_2,ref}(t)$ is the carbon dioxide diffusion coefficient (Equation 4.11), while $F_T(t)$ and $F_{RH}(t)$ are correction functions that account for the dependence of time-variant diffusion $D_{CO_2}(t)$ on temperature and relative humidity, respectively.

The Model Code for Service Life Design (fib, 2006) proposes Equation 4.19 for the definition of $F_{RH}(t)$, while $F_T(t)$ is calculated using Equation 4.13, which was previously defined for the case of chloride-induced corrosion.

$$F_{RH}(t) = \begin{cases} 0 & \text{if } RH(t) \leq 0.25 \\ \left(\dfrac{1 - RH^{f_e}}{1 - RH_{ref}^{f_e}}\right)^{g_c} & \text{if } RH(t) > 0.25 \end{cases} \tag{4.19}$$

In Equation 4.19, RH_{ref} is the reference relative humidity, assumed to be equal to 0.65, while f_e and g_c are two constants, equal to 5.0 and 2.5, respectively. The factor F_{RH} exceeds one when the relative humidity is between 25% and 65%, and reduces to zero when it is equal to 100% (Figure 4.4 (b)). Moreover, the model reflects the experimental evidence that the penetration of CO_2 in concrete is negligible for values of RH lower than

or equal to 25 % (Richardson, 1988), while carbonation penetration tends to be highest for relative humidity of 50-70 % (Russell et al., 2001).

The correction functions illustrated in Equations 4.13 and 4.19 allow the examination of the impacts of climate change on the diffusivity of carbonate in concrete. In figure 4.4 (a) and (b), the correction functions are represented for different values of temperature T and relative humidity RH, respectively. Additionally, the time variant diffusivity $D_{CO_2}(t)$ normalized with respect to the reference diffusivity $D_{CO_2,ref}$ is depicted in Figure 4.4 (c) for different combinations of T and RH.

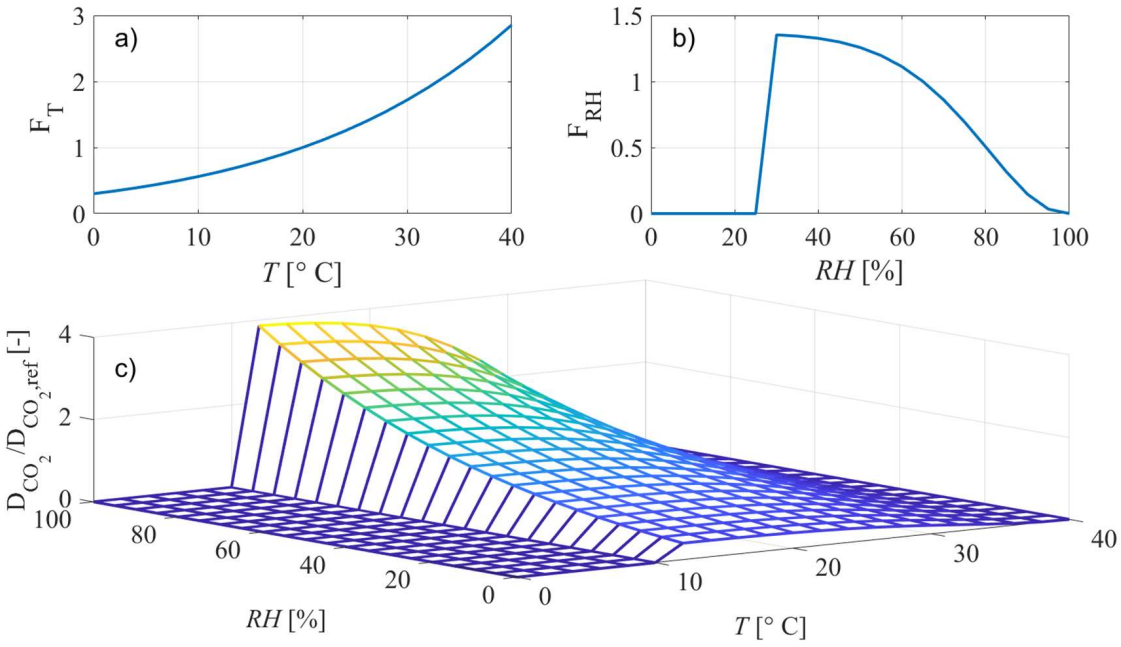

Figure 4.4: Impact of temperature and relative humidity on carbonate diffusivity in concrete.

Nava (2022) studied the effect of climate change on carbonation penetration, highlighting that the increase in carbon dioxide concentrations C_{CO_2} is the dominant parameter with respect to the reduction of the initiation time of carbonation-induced corrosion. On the other hand, relative humidity may enhance carbonate penetration only for values between 25 % and 65 %. Consequently, extreme RH values resulting from climate change may have a beneficial effect in terms of prolonging corrosion initiation.

4.4.2 Corrosion Propagation

Corrosion initiation is directly related to the depassivation of the embedded reinforcement. In the case of carbonation, this phenomenon occurs when the carbonation front x_c reaches the concrete cover c. Conversely, in the case of chloride-induced corrosion,

it is associated with the attainment of the critical chloride concentration C_{cr}. In addition, the presence of oxygen and water is necessary for the occurrence of corrosion; on the other hand, conditions of complete and permanent saturation of the concrete prevent oxygen from reaching the steel surface and, consequently, inhibit the corrosion process. The corrosion rate is typically described, according to Faraday's first law of electrochemical stoichiometry, defining the penetration rate dp_s/dt, expressed in mm/year, through Equation 4.20:

$$\frac{\partial p_s}{\partial t} = 0.0116 \cdot i_{corr}(t) R_f \quad \text{if } t \geq t_{cr} \tag{4.20}$$

where i_{corr} represents the corrosion electric current density, which is typically expressed in $\mu A/cm^2$, the value 0.0116 serves as the corrosion rate conversion factor, while R_f denotes the pitting factor, defined as the ratio of maximum corrosion penetration x_{max} to its average depth x (Equation 4.21).

$$R_f = \frac{x_{max}}{x} \tag{4.21}$$

Among the main parameters influencing the corrosion rate, concrete resistivity ρ plays a critical role (Andrade and Alonso, 2001; Morris et al., 2004), as illustrated in Figure 4.5. Moreover, resistivity is severely influenced by the pores water content (Gjørv, 2009b).

The definition of the corrosion current density i_{corr} is a complex task. A qualitative classification of i_{corr} is presented in Table 4.3.

Corrosion Rate	i_{corr} $[\mu A/cm^2]$
Negligible	< 0.1
Low	0.1 - 0.5
Moderate	0.5 - 1.0
High	> 1.0

Table 4.3: Classifications of corrosion rate severity (Somerville et al., 1995)

Moreover, in the literature, different empirical models are available, based on the correlation identified between the corrosion rate and other variables. A summary of these models is presented in Table 4.4.

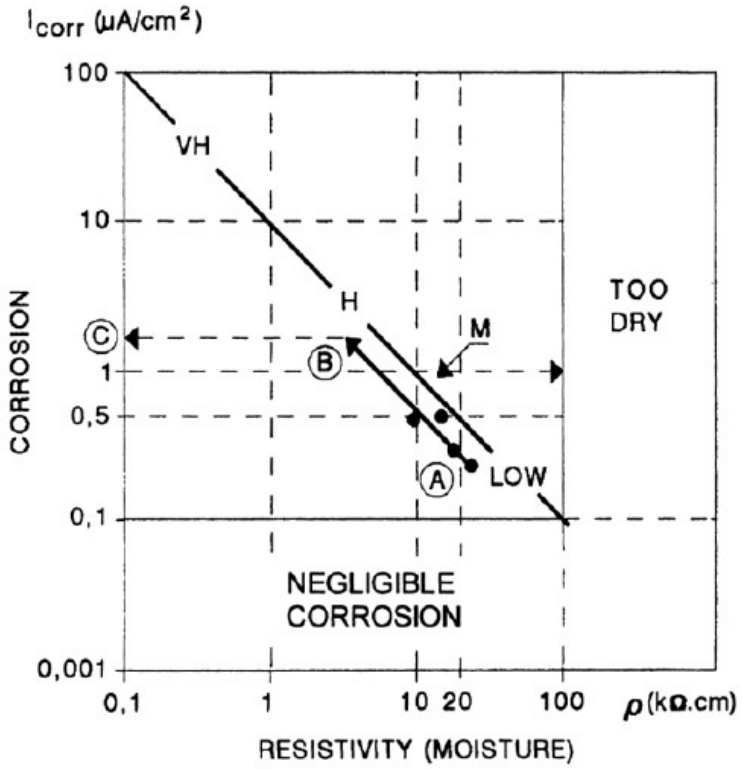

VH=very high, H=high, M=moderate

Figure 4.5: Influence of concrete resistivity on corrosion rate, from Andrade and Alonso (2001)

Table 4.4: Summary of Corrosion Rate Models, based on the review performed by Otieno et al. (2012) and Guo et al. (2015).

Reference	**Model**	**Variables**
Alonso et al. (1988)	$i_{\text{corr}} = \dfrac{100}{\rho_{\text{con}}}$ $[mA/m^2]$	ρ_{con} = concrete resistivity
Yalcyn and Ergun (1996)	$i_{\text{corr}}(t) = i_{\text{corr},0} e^{(-1.1\times10^{-3}t)}$ $[\mu A/cm^2]$	$i_{\text{corr},0} = 0.53\ \mu A/\text{cm}^2$; t = time (days) from corrosion initiation
T. Liu and Weyers (1998)	$i_{corr}(t) = 0.9259 \cdot exp[8.37 + 0.618 \cdot ln(1.69Cl) - 3034/T - 0.000105 \cdot R_c + 2.32t^{-0.215}]$ $[\mu A/cm^2]$	Cl = chloride concentration (kg/m^3); T = annual mean concrete temperature at the depth of the steel surface (Kelvin); R_c = ohmic resistance of the concrete cover (ohms); and t = time (years) after corrosion initiation
Stewart and Rosowsky (1998)	$i_{\text{corr}} = 1.5$ $[\mu A/\text{cm}^2]$	-
Ahmad and Bhattacharjee (2000)	$i_{\text{corr}} = 37.726 + 6.12\,C \cdot 2.231A^2B + 2.722\,B^2C^2$ $[nA/cm^2]$	$A = \frac{\text{cement content}(kg/m^3)-300}{50}$; $B = \frac{w/c-0.65}{0.075}$; $C = \frac{\%\text{CaCl}_2(\text{by weight of cement})-2.5}{1.25}$
DuraCrete (2000)	$i_{\text{corr}}(t) = \frac{104}{\rho(t)} \cdot F_{Cl} \cdot F_{\text{Galv}} \cdot F_{\text{oxide}} \cdot F_{O_2}$ where $\rho(t) = \rho_0 \cdot f_e \cdot f_t \cdot (\frac{t}{t_0})^n$ $[\mu A/cm^2]$	$F_{Cl}, F_{Galv}, F_{Oxide}, F_{O_2}$ = factors accounting for chloride content, galvanic effects, formation of oxides and aging on the corrosion rate, and availability of oxygen, respectively; $\rho(t)$ = actual resistivity at time t; ρ_0 = resistivity (Ωm) of the concrete measured by a compliance test at time t_0; n = factor accounting for aging; f_e, f_t = factor accounting for exposure and the resistivity test method.
Vu and Stewart (2000)	$i_{\text{corr}}(t) = i_{\text{corr},0} \cdot 0.85 \cdot t^{-0.29}$ $[\mu A/cm_2]$	$i_{\text{corr},0} = 37.8(1 - w/c)^{1.64}$; d_c = concrete cover depth (mm).
Qing Li (2004)	$i_{\text{corr}} = 0.3683 \cdot \ln(t) + 1.1305$ $[\mu A/cm^2]$	t = time (year) from corrosion initiation
Martı´nez and Andrade (2009)	$i_{\text{corr}} = \dfrac{B}{R_p}$ $[\mu A/\text{cm}^2]$	B = constant from anodic/cathodic Tafel slopes; R_p = polarization resistance in $\text{k}\Omega \cdot \text{cm}^2$
Guo et al. (2015)	$i_{corr} = i_{corr,0} \cdot f_{O_2} \cdot f_{mc} \cdot f_{res} \cdot f_{Cl} \cdot f_{w/c} \cdot f_{d_c} \cdot f_T$ $[\mu A/cm^2]$	f_{O_2} , f_{mc}, f_{res} , $f_{w/c}$, f_{d_c} , f_T , and f_{Cl} are the correction functions considering the influence of oxygen concentration, moisture content, concrete resistivity, water-cement ratio, concrete cover depth, temperature, and chloride concentration, respectively; $i_{corr,0}$ is the basic corrosion rate

* For reference environmental conditions ($RH_{ref} = 75\%$ and $T_{ref} = 20$ °C).

In the following discussion, the model proposed by Guo et al. (2015) is adopted. This model allows for consideration of the influence of concrete characteristics and environmental conditions on the evolution of the corrosion rate. Nevertheless, this model combine correction functions defined in different studies for the sake of accounting for all the influencing parameters. When using this model, particular attention should be devoted to the assumptions and the conditions used to define each correction function in the specific study (T. Liu and Weyers, 1998; Vu and Stewart, 2000; Pour-Ghaz et al., 2009; Balafas and Burgoyne, 2010).

In Section 4.4.2.1, 4.4.2.2, and 4.4.2.3, the corrosion rate is discussed with a focus on the peculiarities of chloride-induced corrosion, carbonation-induced corrosion, and the impact of climate change.

4.4.2.1 Chloride-Induced Corrosion

The rate of chloride corrosion is influenced by the availability of water and oxygen at the steel surface. Furthermore, the electrical resistivity of concrete is also a crucial factor, particularly when the ambient relative humidity is low. On the other hand, when relative humidity is high, oxygen availability becomes the controlling factor affecting the corrosion rate (Tuutti, 1982). Eventually, the chloride-induced corrosion rate is influenced by the variation of temperature and relative humidity over time (Section 4.4.2.3).

In DuraCrete (1998), the reference rate of carbonation-induced corrosion $i_{corr,0}$ is proposed to be modeled using a lognormal distribution, depending on various exposure scenarios (Table 4.5).

Exposure class	μ [μA/cm^2]	σ [μA/cm^2]
Cl1 - Wet-rarely dry	0.345	0.259
Cl2 - Cyclic wet-dry	2.586	1.724
Cl3 - Airborne sea water	2.586	1.724
Cl4 - Submerged*	-	-
Cl5 - Tidal Zone	6.035	3.448

*Not expected except for bad concrete or lower cover.

Table 4.5: Chloride-induced corrosion rates $i_{\text{corr},0}$ for various exposures (DuraCrete, 1998).

4.4.2.2 Carbonation-Induced Corrosion

The corrosion rate induced by carbonation is significantly influenced by exposure conditions and atmospheric factors (Raupach, 2006; Peng and Stewart, 2008). If oxygen and water are available in adequate quantities, the corrosion rate is governed by the resistivity of the concrete. The moisture content is one of the primary factors influencing the resistivity of carbonated concrete. Moreover, the microstructure of concrete and the factors that determine it, such as the type of cement, water-cement ratio, and curing conditions, are important parameters influencing the carbonation rate. The carbonation-induced corrosion rate is also influenced by variations in temperature and relative humidity. This particular impact is detailed in Section 4.4.2.3. The presence of chlorides in concrete, even in small quantities, may increase the corrosion rate for carbonation-induced corrosion (Lambert et al., 1991), as shown in Figure 4.6. In this context, Rincon et al. (2026) review key experimental and modeling research addressing the combined effects of carbonation and chloride penetration in concrete structures.

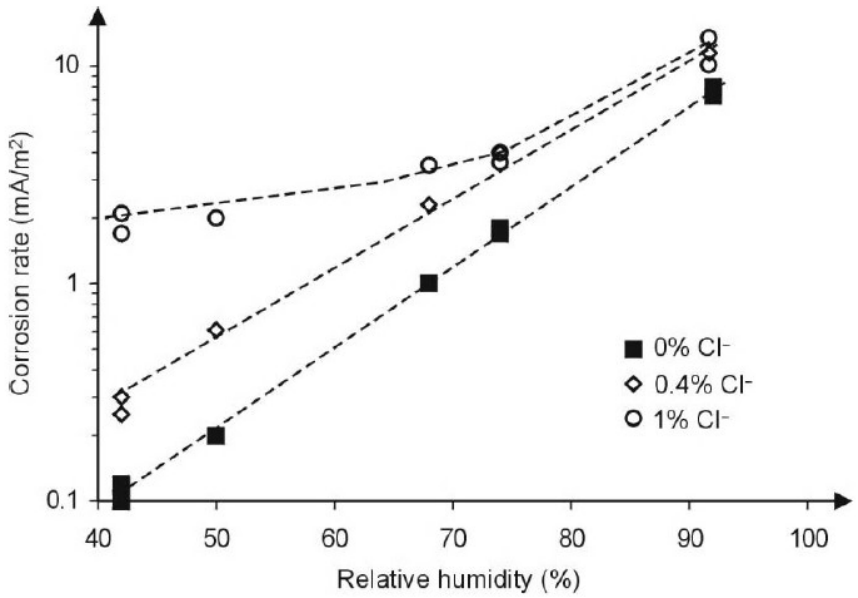

Figure 4.6: Corrosion rate in carbonated mortar, both for different chloride content and relative humidity, from Lambert et al. (1991)

A critical review of the corrosion rate in carbonate concrete is presented by Stefanoni et al. (2018).

In DuraCrete (1998), the reference carbonation-induced corrosion rate $i_{corr,0}$ is proposed to be modeled using a lognormal distribution, depending on various exposure scenarios (Table 4.6).

Exposure class	μ [μA/cm^2]	σ [μA/cm^2]
C1 - Dry	0.0	0.0
C2 - Wet rarely–dry (unsheltered)	0.345	0.259
C3 - Moderate humidity (sheltered)	0.172	0.086
C4 - Cyclic wet-dry (unsheltered)	0.431	0.259

Table 4.6: Carbonation-induced corrosion rates $i_{corr,0}$ for various exposures (DuraCrete, 1998).

4.4.2.3 Climate Change Impact on Corrosion Propagation

The rate of corrosion induced by chloride and carbonate is significantly influenced by the evolution of the surrounding environmental conditions, primarily relative humidity and temperature. This is related to the fact that concrete resistivity is impacted by the modifications in temperature and relative humidity (Gonzalez and Andrade, 1982). Values for the corrosion penetration rate, considering different exposure and environmental conditions, are represented in Table 4.7.

Penetration rate (µm/year)	**Concrete condition**	**Relative Humidity**	**Remarks**
≈ 1000	Heavily contaminated by chloride	95–98%	Very high penetration rate
≈ 100–300	Contaminated by chloride or carbonated concrete	90–95% (chloride) or 95–98% (carbonated)	Very high penetration rate
≈ 10–100	Contaminated by chloride or carbonated concrete	80–90% (chloride) or 90–95% (carbonated)	High-intermediate penetration rate
≈ 2–10	Contaminated by chloride or carbonated concrete	50–80% (chloride) or 70–90% (carbonated)	Low-intermediate penetration rate
≈ 0.1–2	Carbonated or contaminated by chloride saturated by water or dry	<50% (chloride) or <70% (carbonation)	Negligible penetration rate
<0.1	Non-carbonated and without chloride	/	Negligible penetration rate

Table 4.7: Corrosion penetration rate considering different exposure scenario, based on Andrade et al. (1988) and Bertolini et al. (2013)

According to Bertolini et al. (2013), the corrosion penetration rate for RC structures exposed to the atmosphere can vary from several tens of mm/year to localized values of 1 mm/year as the relative humidity increases from 70 % to 95 %, and the chloride content rises from 1 % by mass of cement to higher values. Moreover, the corrosion penetration rate can be considered negligible at low relative humidity values (lower than 40 %); experimental tests evidenced an exponential increase in the corrosion rate for RH ranging from 50% to 65%, followed by a plateau up to 85%, and a subsequent rapid decrease from 90% to complete saturation (Balafas and Burgoyne, 2010). Indeed, for very high relative humidity values, the rate at which oxygen reaches the surface of the reinforcement is typically low, leading to reduced propagation of corrosion. In order to analytically model this influence, the modification factor $f_{RH}(t)$ is defined according to equation 4.22:

$$f_{RH}(t) = e^{-6000(RH(t)-RH_{ref})^6} \tag{4.22}$$

where $RH(t)$ is the relative humidity at time t and RH_{ref} is the reference relative humidity assumed equal to 0.75.

Moreover, it is observed that a rise in temperature results in an increase of the corrosion rate (DuraCrete, 1998). In order to analytically model this influence, the modification factor $f_T(t)$ is defined according to equation 4.23:

$$f_T(t) = 1 + K_T(T(t) - T_{ref}) \tag{4.23}$$

where $T(t)$ is the temperature at time t, T_{ref} is the reference temperature, which is assumed to be equal to 20 °C, and K_T is a factor that takes values of 0.025 and 0.073, respectively, depending on whether the temperature is lower than or equal to or greater than T_{ref}. Equation 4.23 is closely correlated with the Arrhenius equation, at least for temperatures below 20 °C. However, it may be conservative for T (t) > 20 °C.

$$K_T = \begin{cases} 0.025 & \text{if } T \leq 20°C \\ \\ 0.073 & \text{if } T > 0.25 \end{cases} \tag{4.24}$$

In the case of carbonated concrete, the consideration of the impact of relative humidity and temperature on the corrosion rate may be considered analogous to that discussed for chloride induced corrosion.

The correction functions, illustrated in Equations 4.23 and 4.22, allow the incorporation of the impacts of climate change on the corrosion rate in concrete. In figure 4.7 (a) and (b), the correction functions are depicted for varying values of temperature T and relative humidity RH, respectively. Additionally, the time variant corrosion current

density $i_{corr}(t)$ normalized with respect to the reference value $i_{corr,ref}$ is represented in Figure 4.7 (c) for different combinations of T and RH.

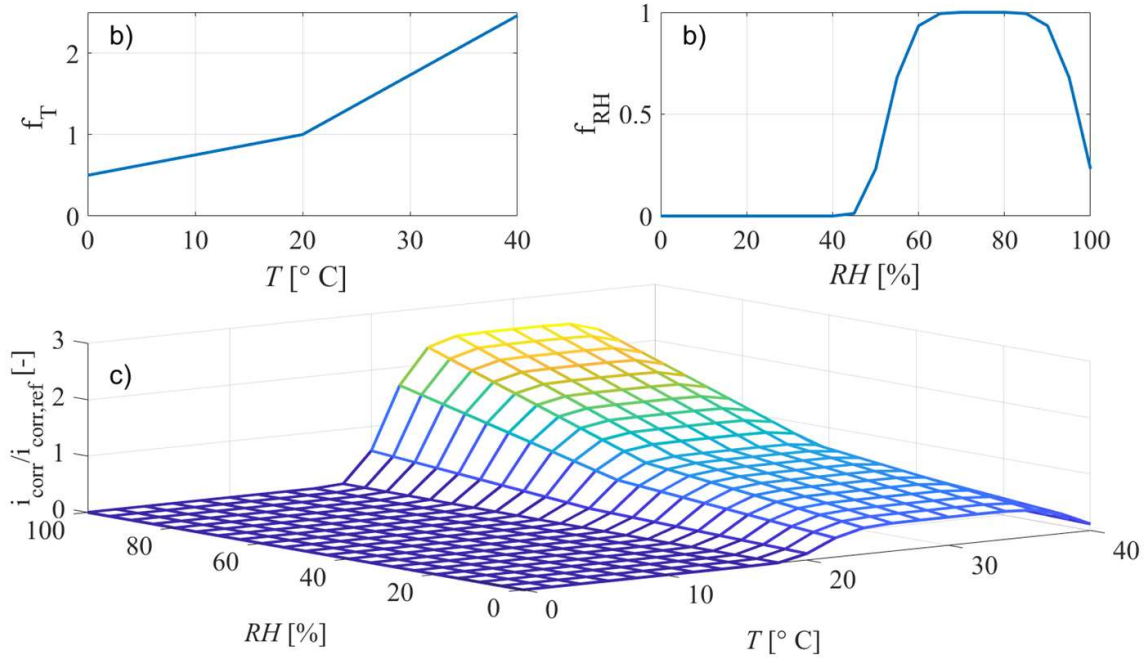

Figure 4.7: Impact of temperature and relative humidity on the corrosion rate.

4.4.3 Corrosion Damage

Damages induced by corrosion can significantly affect the aesthetic appearance, serviceability, safety, and structural performance of RC structures. The most critical consequence of corrosion is the reduction of the reinforcement area, leading to a significant loss of the structural capacity. Moreover, the formation of corrosion products, which can occupy a volume 2 to 6 times larger than the one of the undamaged bars, induces tensile stresses in the concrete cover area. This phenomenon can ultimately result in localized spalling and, in certain instances, to complete delamination of the concrete cover. In addition, a reduction in the bonding between the reinforcement and the concrete, along with a decrease in the steel ductility may also be observed as a consequence of corrosion.

However, corrosion affecting real RC structures is a highly uncertain phenomenon. Consequently, a mathematical description of the damages may be complex and not always feasible due to incomplete information regarding the initiation processes and propagation patterns of the deterioration. Due to this complexity and the lack of experimental data, a significant part of the uncertainty affecting the outcomes of time-dependent performance evaluation arises from the selection of appropriate deterioration models that are capable

of capturing the impact of environmental damage on structural capacity (Ellingwood, 2005; Biondini and Frangopol, 2016).

Several models have been developed to establish simple and realistic relationships between structural damage and progressive material degradation. The extent of structural deterioration can generally be quantified by a time-variant damage index $\delta(t)$, which is defined to range from 0 to 1. In particular, $\delta(t) = 0$ corresponds to the undamaged state, while $\delta(t) = 1$ corresponds to the full damage. Considering the penetration depth $p_s(t)$ and the initial diameter of the rebar ϕ_0, the penetration index δ may be defined as follows:

$$\delta(t) = \frac{p_s(t)}{\phi_0} \tag{4.25}$$

The following Sections discuss effective modeling strategies for defining the reduction of mechanical properties of steel and concrete in RC members exposed to corrosion.

4.4.3.1 Steel Mass Reduction

The most critical effect of corrosion in RC structures is the reduction of the resisting area of the steel reinforcement bars. In general, Equation 4.26 can be employed to model the damage of steel bars as the evolution of their area $A_s(t)$ (Biondini et al., 2004):

$$A_s(t) = [1 - \delta_s(t)]A_{s0} \tag{4.26}$$

where $A_{s0} = \pi\phi_0/4$ is the undamaged rebar area and $\delta_s(t)$ is the damage index. The definition of $\delta_s(t)$ depends on the type of corrosion and the environmental exposure.

For instance, in marine and industrial environments characterized by high concentrations of sulfates and chlorides, empirical evidence suggests considering a linear relationship between corrosion rate and chloride content (Y. P. Liu and Weyers, 1998; Thoft-Christensen, 1998; Bertolini et al., 2013). According to Biondini et al. (2004), the loss rate of steel reinforcement area $\partial\delta_s(t)/\partial t$, due to chloride-induced corrosion, can be defined in terms of a damage rate coefficient q_s and the time-variant chloride content $C(t)$ after the corrosion initiation :

$$\frac{\partial\delta_s}{\partial t} = q_s C(t) \tag{4.27}$$

Depending on the nature of the corrosion process, the damage index δ_s may be related to the penetration index δ through geometrical relationships, as graphically illustrated in Figure 4.8.

In carbonated concrete without relevant chloride content, corrosion is expected to occur uniformly along the lateral surface of the bar cross-section. As reported in Figure

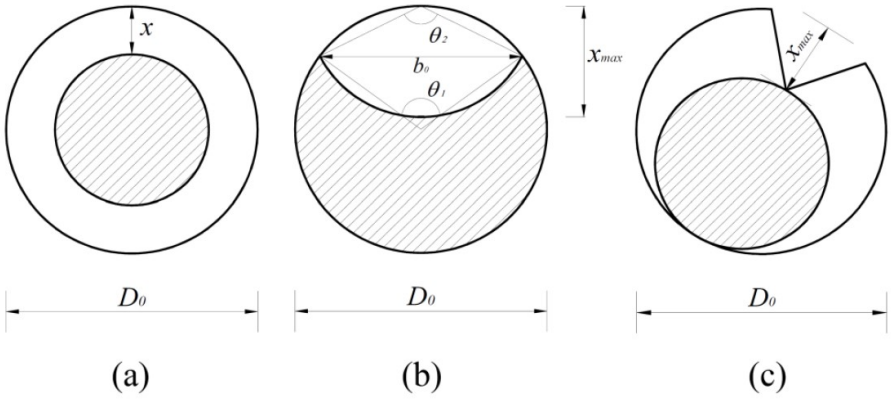

Figure 4.8: Cross-section reduction of steel reinforcement: (a) uniform corrosion; (b) pitting corrosion; (c) mixed corrosion, adapted from Val and Melchers (1997) and Biondini and Vergani (2015).

4.8 (a), the penetration depth is equal to $p_s = 2x$; consequently, the damage index δ_s is defined by Equation 4.28 (Biondini and Vergani, 2012, 2015):

$$\delta_s(t) = \delta(t)[2 - \delta(t)] \tag{4.28}$$

where $\delta(t)$ is the penetration index at time t. A model capable of accounting for one-sided or two-sided corrosion attack is proposed by Saetta et al. (1999).

On the other hand, localized corrosion occurs in the presence of chlorides, leading to the formation of irregular pits in the area of the steel rebar. The significance of the pits can be characterized through the pitting factor R_f (Equation 4.21). In cases of uniform corrosion, R_f is generally assumed to be equal to 1, as the maximum corrosion penetration is equal to the average corrosion penetration. Common values of R_f for chloride-induced corrosion are bounded between 4 and 8 for natural corrosion, whereas in the case of accelerated tests, R_f may vary between 5 and 13 (Gonzalez et al., 1995). Moreover, according to R. Zhang et al. (2010), the spatial distribution of pits is generally associated with the presence of defects in the passive film or at the interface between steel and concrete.

A hemispherical geometry is typically employed to describe the pits (Val and Melchers, 1997), under the assumption that the pitting area is characterized by a radius equal to x_{max} (Stewart and Al-Harthy, 2008; Biondini and Vergani, 2015), as illustrated in Figure 4.8 (b). Consequently, the damage index δ_s is defined by equation 4.29.

$$\delta_s = \begin{cases} \delta_{s1} + \delta_{s2} & \text{for } 0 \leq \delta \leq \dfrac{\sqrt{2}}{2} \\ 1 - \delta_{s1} + \delta_{s2} & \text{for } \dfrac{\sqrt{2}}{2} < \delta \leq 1 \end{cases} \tag{4.29}$$

Where:

$$\delta_{s1} = \frac{1}{2\pi}\left(\theta_1 - 2\beta\left|1 - 2\delta^2\right|\right) \tag{4.30}$$

$$\delta_{s2} = \frac{2\delta^2}{\pi}\left(\theta_2 - \beta\right) \tag{4.31}$$

$$\theta_1 = 2\arcsin\beta \tag{4.32}$$

$$\theta_2 = 2\arcsin\left(\frac{\beta}{2\delta}\right) \tag{4.33}$$

$$\beta = \frac{b_0}{D_0} = 2\delta\sqrt{1-\delta^2} \tag{4.34}$$

where θ_1, θ_2, b_0, and β are geometrical parameters related to the elliptical representation of pit formation. Additionally, δ_{s1} and δ_{s2} represent the components of the damage index that accounts for the formation of the pit. Eventually, δ_s is the damage index and δ represents the penetration index.

Moreover, it is possible to model the coupled action of localized and uniform corrosion, as depicted in Figure 4.8 (c), by exploiting Equation 4.28 and assuming a penetration depth of $p_s = x_{max}$. Nevertheless, this approach is reliable only for accelerated corrosion tests, while it is not recommended for natural corrosion processes (R. Zhang et al., 2010).

4.4.3.2 Steel Strength Reduction

The effect of corrosion on the properties of reinforcing steel, in terms of yielding strength $f_{sy}(t)$ and ultimate strength $f_{su}(t)$, is generally considered negligible. The empirical tests conducted by Y. G. Du et al. (2005) demonstrate a linear relationship between the variation of $f_{sy}(t)$ and $f_{su}(t)$ and the level of corrosion (Vergani, 2010), which may be modeled through Equations 4.35 and 4.36, respectively.

$$f_{sy}(t) = [1 - \delta_{f_s}(t)]f_{sy0} \tag{4.35}$$

$$f_{su}(t) = [1 - \delta_{f_s}(t)]f_{su0} \tag{4.36}$$

where f_{sy0} and f_{su0} represent the initial yielding strength and the ultimate strength, respectively. The damage index $\delta_{f_s}(t)$ can be defined using Equation 4.37:

$$\delta_{f_s}(t) = \beta \cdot \delta_{f_{s,u}}(t) \tag{4.37}$$

where β is a coefficient accounting for the type of corrosion, and $\delta_{f_{s,u}}(t)$ is a damage index assumed to be equal to $\delta_s(t)$, as defined in Equation 4.28.

The reduction in steel strength is primarily related to localized corrosion along the rebar. Theoretically, for a uniform corrosion damage along the bar, the strength of steel would remain unvaried (Vergani, 2010), assuming $\beta = 0$. Nevertheless, in Vergani (2010), a value of $\beta = 0.005$ is suggested to account for the effect of uniform corrosion on the strength of the rebars; considering localized corrosion, β may be assumed to be equal to 0.5.

4.4.3.3 Steel Ductility Reduction

Another important consequence of corrosion is the reduction in the ductility of steel bars, which may lead to brittle failure (Almusallam, 2001), as illustrated in Figure 4.9.

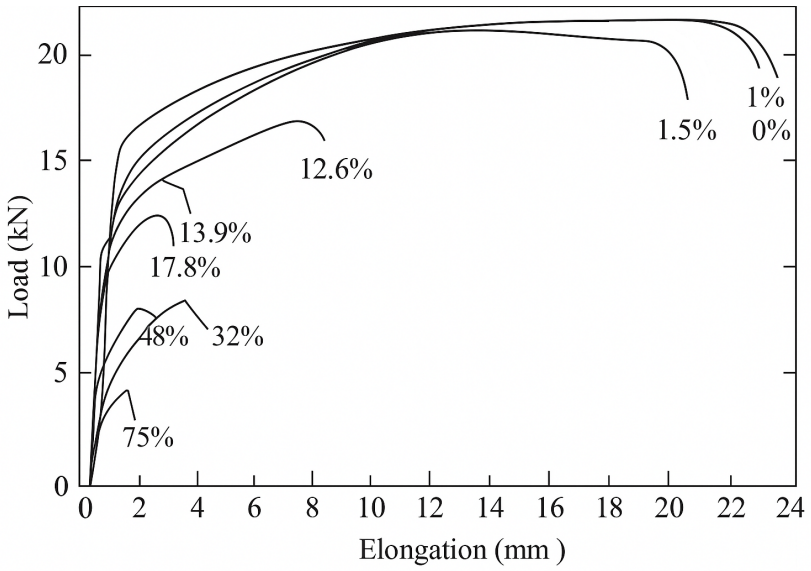

Figure 4.9: Reduction of steel ductility for different levels of corrosion, from Almusallam (2001).

In particular, empirical tests conducted by Apostolopoulos and Papadakis (2008) highlight the influence of steel mass loss in relation to the reduction of ductility induced by the corrosion process. This may be analytically defined by Equation 4.38, which relates the steel ultimate strain $\varepsilon_{su}(t)$ to the damage index $\delta_s(t)$ (Biondini and Vergani, 2012). Other models accounting for the reduction in ductility due to corrosion are available in

the literature, including those proposed by Coronelli and Gambarova (2004) and Stewart (2009).

$$\varepsilon_{su}(t) = \begin{cases} \varepsilon_{s0} & \text{for } 0 \leq \delta(t) \leq 0.016 \\ 0.1521 \cdot \varepsilon_{s0} \cdot \delta_s(t)^{-0.4583} & \text{for } 0.016 < \delta(t) \leq 1 \end{cases} \tag{4.38}$$

4.4.3.4 Concrete Cover Reduction

The consequences of corrosion in RC structures are not limited to the reinforcing steel. In particular, longitudinal cracks and cover spalling occur as a result of the formation of corrosion products. A critically reviews empirical, analytical and numerical models to predict the cracking time due to corrosion of reinforcing bars is reported by Jamali et al. (2013).

Different deterioration patterns may be recognized depending on the mechanical and geometric configuration of the steel bars in the member cross-section (Camnasio, 2013), as scaling, delamination, and corner effect (Figure 4.10).

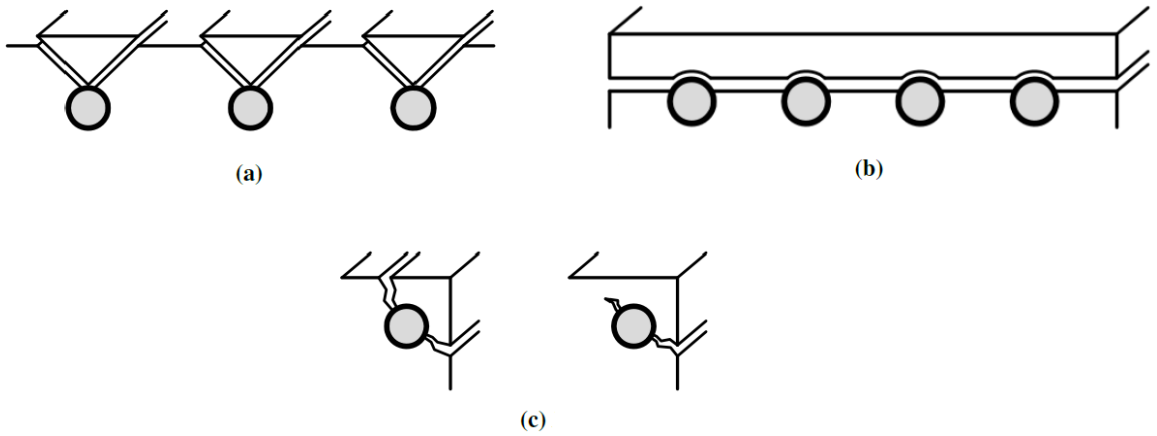

Figure 4.10: Damage patterns induced by corrosion cracks in RC structures (Vergani, 2010): (a) scaling, (b) delamination, (c) border effects.

The effects of this damage mechanism can be modeled by reducing the effective compression strength $f_c(t)$ of the concrete cover as a function of the damage index $\delta_s(t)$ (Coronelli and Gambarova, 2004):

$$f_c(t) = \frac{f_{c0}}{1 + \kappa \dfrac{\varepsilon_{\perp}(t)}{\varepsilon_{c0}}} \tag{4.39}$$

where f_{c0} is the strength of the undamaged concrete, κ is a coefficient related to the diameter and roughness of the rebars (0.1 for medium-diameter ribbed bars), ε_{c0} represents

the concrete strain at peak compressive stress, and $\varepsilon_{\perp}(t)$ is the average tensile strain in cracked concrete, measured at right angles to the direction of the applied stress.

The parameter $\varepsilon_{\perp}(t)$ may be evaluated as the ratio between the average mean crack opening $\omega(t)$ and the width of the undamaged cross-section (Equation 4.40):

$$\varepsilon_{\perp}(t) = \frac{\omega(t)}{b_i} = \frac{b_f(t) - b_i}{b_i} \tag{4.40}$$

where $b_f(t)$ and b_i are the width of the cracked and undamaged cross-section, respectively.

Vidal et al. (2004) propose the empirical relationship described in Equation 4.41 to model the average mean crack opening $\omega(t)$ for each bar in terms of the damage index:

$$\omega(t) = \kappa_{\omega}[\delta_s(t) - \delta_{s0}]A_{s0} \tag{4.41}$$

where κ_{ω} is considered equal to 0.0575 mm[1] , $\delta_s(t)$ is the time variant damage index, and A_{s0} is the undamaged area of the steel bar; additionally, δ_{s0} represents the amount of steel damage necessary for the initiation of cracking, evaluated using Equation 4.42 (Biondini and Vergani, 2012):

$$\delta_{s0} = 1 - \left[1 - \frac{R_f}{\phi_0}\left(7.53 + 9.32\frac{c}{\phi_0}\right)10^{-3}\right]^2 \tag{4.42}$$

where R_f represents the pitting factor, ϕ_0 denotes the diameter of the undamaged steel bar, and c is the concrete cover.

Assuming that the critical width leading to spalling is equal to 1 mm, the effective compression strength $f_c(t)$ of the concrete cover can be characterized as follows:

$$f_c(t) = \begin{cases} \dfrac{f_{c0}}{1+\kappa\dfrac{\varepsilon_{\perp}(t)}{\varepsilon_{c0}}} & \text{if } 0 \leq \omega(t) < 1 \text{ mm} \\ 0 & \text{if } \omega(t) \geq 1 \text{ mm} \end{cases} \tag{4.43}$$

where f_{c0} is the strength of the undamaged concrete, κ is a coefficient related to the diameter and roughness of the rebars (0.1 for medium-diameter ribbed bars), ε_{c0} represents the concrete strain at peak compressive stress, and $\varepsilon_{\perp}(t)$ is the average tensile strain in cracked concrete, measured at right angles to the direction of the applied stress.

In Equation 4.44, the damage index $\delta_{Ac}(t)$ accounts for the reduction in the area of the concrete cover, where a value of 1 represents complete spalling, and a value of 0 indicates an undamaged concrete cover:

$$\delta_{Ac}(t) = 1 - \frac{f_c(t)}{f_{c0}} \tag{4.44}$$

Eventually, the reduction of concrete cover area over time $A_c(t)$ can be modeled according to Equation 4.45 proposed by Biondini et al. (2004):

$$A_c(t) = [1 - \delta_{Ac}] \cdot A_{c0} \tag{4.45}$$

where A_{c0} is the undamaged concrete cover area.

4.4.3.5 Steel-Concrete Bond Reduction

The degradation of the steel-concrete interface is a mechanical consequence of corrosion; as corrosion products accumulate at the interface, they initially increase the bond strength through enhanced surface roughness and internal confinement pressure. However, once the expansion exceeds the tensile capacity of the concrete cover, longitudinal cracking occurs, leading to a rapid reduction in adherence due to the loss of confinement and the effect of the oxide layer (Cabrera, 1996).

Several empirical and analytical models are proposed in the literature to quantify the bond strength loss $f_b(t)$ due to corrosion (Bhargava et al., 2007; Berto et al., 2008; Prieto et al., 2016; Y.-Z. Wu et al., 2016; Lin, Zhao, Feng, et al., 2019; Lin, Zhao, Ozbolt, et al., 2019).

4.5 Remarks on Corrosion Modeling

Section 4.4 is developed to discuss the basic concepts related to corrosion processes in RC structures and the consequent induced damages. The equations and models proposed are consequently instrumental to the definition of the methodology and the case study presented in Chapter 5, considering a complete overview and review of this subject out of the scope of the Thesis. Nevertheless, some insights on the limitations of the models discussed as well as the description of more advanced models are outlined in this Section.

Angst (2018) summarizes the societal, economic, technological, and educational challenges related to corrosion of steel in concrete, and presents a state-of-the-art of the most relevant issues in the field. Moreover, an overview of the probabilistic modeling of corrosion processes affecting RC structures and their structural implications, including the historical perspective and current state-of-the-art, is provided by Val et al. (2025).

Chloride-induced Corrosion

The penetration of chlorides in concrete is usually assumed to be governed by diffusion (Bertolini et al., 2013). As discussed in Section 4.4.1.1, the second law of Fick (Equation 4.3) can be used to model this phenomena, and it can be solved analytically (Equation 4.4)

under the assumptions of mono-dimensional diffusion for an isotropic, homogeneous, and time invariant medium. This formulation is very useful in a practical sense, considering implementation in structural standards, and is observed to provide good approximation of the reality (Bertolini et al., 2013). However, this approximation may lead to a certain error and therefore more advanced models are proposed. For instance, a comprehensive model coupling the effects of convection, chloride binding, concrete aging, temperature and relative humidity is reported by Bastidas-Arteaga et al. (2010). The study focus on the assessment of the influence of weather conditions and global warming on chloride ingress into concrete based on the formulation of four partial differential equations describing chloride ingress, moisture and heat diffusion, and oxygen transport (Martın-Pérez et al., 2001).

A coupled thermo-hydro-chemical model for predicting chloride penetration into concrete accounting for realistic weather conditions is proposed by Nguyen et al., 2017. The described numerical model considers multiple factors affecting chloride ingress such as diffusion, convection, chloride binding, ionic interaction, and concrete aging, while also proposing simplifications to reduce the computational cost.

Cherif et al. (2022) discussed a multispecies transfer model, based on Nernst-Planck equation, considering the thermodynamic equilibria induced by the dissolution/precipitation phenomena of the solid matrix compounds. The proposed model simulates chloride transfer conditions considering real exposure to seawater.

In addition, Equation 4.4 defines mono-dimensional kinetics of chlorides in concrete, leading to a further approximation in case of non-uniform chloride front. In order to improve this aspect, Biondini et al. (2004) and Nava et al. (2025) propose a cellular automata technique for the modeling of bi-dimensional of chlorides in concrete.

Eventually, corrosion initiation is often determined exploiting the concept of critical chloride content. Angst et al. (2022) concludes that this concept presents a major barrier for developing reliable corrosion forecast models, since, in reality, corrosion in reinforced concrete is a continuous process rarely separable into uncoupled, sequential phases. Consequently, the authors propose a multi-scale and multi-disciplinary approach to combine the scientific and practical contributions from materials science, corrosion science, cement/concrete research, and structural engineering in order to quantify the time- and space-variant corrosion rate from the moment steel is placed in concrete until it reaches the end of the service life.

Carbonation-induced Corrosion

The penetration of carbon dioxide into concrete is usually modeled by Fick's 1st law of diffusion. Considering the mono-dimensional case, the depth of carbonation may be

described by Equation 4.7 (Papadakis et al., 1991; Bertolini et al., 2013). The advantage of this model is the simplicity in the application, grouping all the unknown in the carbonation coefficient. However, using Equation 4.7, the consideration of the factors influencing the carbonation depth in concrete is difficult. In order to overcome this limitation, new mathematical models have been developed to consider temperature, relative humidity, carbon dioxide concentration, aggregate, curing time, and external loads, as the one proposed in Equation 4.8. A more complete overview of the existing prediction models for concrete carbonation depth is discussed by Wang et al. (2024).

Saetta and Vitaliani (2004) proposed a carbonation model coupling the transport of heat-moisture-CO_2, defining five governing differential equations. These equations allow to incorporate the impact of relative humidity, absolute temperature , the concentration of carbon dioxide, the relative calcium carbonate and relative hydration period. A modification of this carbonation model is proposed by Shi et al. (2021) based on the adjustment of parameters and introduction of a novel equation to evaluate the stress damage effect.

Corrosion Rate

Corrosion rate is a critical parameter controlling corrosion propagation and damage in RC structures. If possible, the corrosion rate should be measured and monitored on-site in terms of the corrosion current density i_{corr}. In the cases of unavailability of these measurement, empirical models can be used to estimate corrosion rate. Several models define the corrosion rate through functions of i_{corr} considering the influence of different parameters, as reported in Section 4.4.2. Nevertheless, a significant lack of consensus persists in the literature regarding the most reliable formulation for predicting corrosion rates across diverse environmental scenarios. Otieno et al. (2012) present a critical review of some of the available corrosion rate prediction models focusing mainly on chloride-induced corrosion, highlighting the need of the explicit incorporation of factors such as cover cracking, concrete resistivity, concrete quality and cover depth into the models. Moreover, the study underline the need of model validation using both field and laboratory data to develop reliable corrosion rate prediction models. Moreover, the inherent variability of corrosion rate and the factors influencing should be accounted using probabilistic methods.

Eventually, a review summarizing the state-of-the-art, reporting corrosion rate data for a broad range of cement types, water-cement ratios, and environmental conditions is provided by Stefanoni et al. (2018); the study analyses correlations between the corrosion rate and its main influencing parameters.

Corrosion Damage

Consequences of corrosion propagation are discussed in Section 4.4.3. The models proposed for the assessment of steel mass, steel ductility, and concrete cover reduction are based limiting assumptions. For instance, the steel mass reduction is modeled through simplified geometrical model that may lead to approximated results, as well as the empirical model presented for steel ductility, which is based on a limited amount of data. Moreover, the concrete cover cracking and eventual deterioration is modeled indirectly through the concrete strength, losing the direct physical connection.

More advanced models are available in the literature. A three-dimensional cross-correlation empirical model coupled with onsite non-destructive testing results is proposed by Villain et al. (2012) to perform a durability diagnosis of RC structure exposed to marine environment. Ožbolt et al. (2012) present a 3D chemo-hygrothermo-mechanical model for concrete, accounting for the interaction between non-mechanical influences (distribution of temperature, humidity, oxygen, chloride and rust) and mechanical properties of concrete. Numerical studies demonstrated that the model is able to realistically predict corrosion of reinforcement and its consequences for durability of RC structures (Ožbolt et al., 2011). A 3D time-dependent numerical model developed to simulate localized corrosion in both circumferential and longitudinal directions, incorporating effects of non-uniform corrosion-induced cracking, is discussed by Bui and Tan (2023). The study reports that once a vertical crack propagates through the concrete cover, the corroded area spreads faster, current densities substantially increases, and the shape of corroded depth becomes more rounded.

Chapter 5

Semi-Probabilistic Assessment of Existing Structure under Climate Change-induced Deterioration

5.1 Existing Aging Structure under Climate Change

Civil structures are continuously exposed to environmental actions that evolve throughout their service life. These variations may significantly affect deterioration mechanisms, thereby impacting structural capacity over time. On the other hand, changes in climatic actions, such as wind, snow, precipitation, and extreme weather events, influence the structural demand. As a result, accurately assessing the long-term performance of structures considering the evolution in climatic conditions is essential for developing robust design guidelines, maintenance planning, and repairing strategies for both new and existing infrastructure.

Full-probabilistic approaches represent the current state-of-the-art for analyzing time-variant structural performance, as they enable comprehensive modeling of uncertainties and degradation processes. However, these methods are computationally demanding and require advanced expertise, limiting their widespread applicability in practical engineering contexts. Consequently, there is a growing need to calibrate efficient semi-probabilistic formats specifically tailored for evaluating existing structures subjected to climate change-induced deterioration.

The goal of this Thesis is to contribute to the ongoing effort by proposing a methodological groundwork for the calibration of semi-probabilistic formats considering time-variant reliability, deterioration, and climate change. A general framework is introduced in Section 5.1.1, followed by the description of an analytical methodology that incorporates both deterioration and climate change influences in Section 5.1.2. Finally, the

proposed methodology is applied to a case study, where its advantages and limitations are critically examined concerning key influencing parameters (Section 5.2).

5.1.1 Proposed Framework

A framework for the semi-probabilistic assessment of existing aging structures under climate change is presented in Figure 5.1.

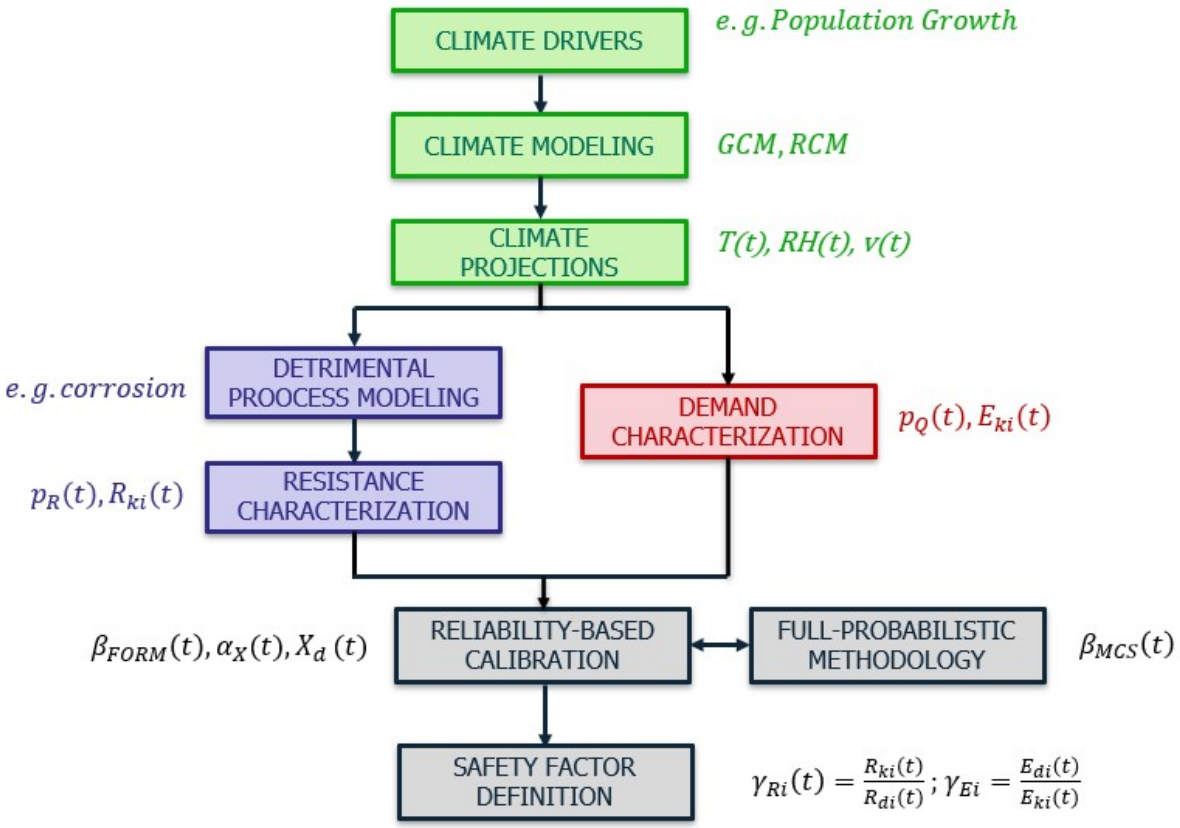

Figure 5.1: Calibration of semi-probabilistic format for the assessment of existing aging structures under climate change.

Four main research areas are explored and interrelated for this purpose: climate change modeling, characterization of structural capacity under environmental aggressiveness, characterization of structural demand, and reliability-based calibration.

Appropriate modeling of climate future projections is fundamental for estimating the impact of environmental aggressiveness and characterizing the resultant damages. Several climate projections are provided by the scientific community, depending on the climate models and the climate change scenarios used; the SSPs, current reference scenarios, are based on assumptions regarding the future evolution of climate change drivers, such

as demographic and economic growth, policy, governance, technological development, availability of natural resources, culture, and lifestyle, as well as mitigation and adaptation strategies. Based on the SSP of interest, climate models are employed to obtain climate projections for specific environmental parameters in accordance with the objectives of the analysis, e.g., temperature, relative humidity, wind speed, and surface PH.

The evolution of environmental parameters, such as temperature and relative humidity, may greatly influence deterioration processes, including corrosion. Consequently, a proper future estimation of these parameters is fundamental for accurately assessing the deterioration process in question and, as a result, the structural capacity.

Moreover, future projections of climatic loadings, such as wind speed, snow and rain abundance, maximum and minimum temperature, are also expected to have an impact on structural demand.

In this context, the reliability elements of the semi-probabilistic approach are characterized by taking into account the non-stationarity of the processes involved, as well as the time variability that is intrinsic to the problem.

The proposed framework is defined to be generalizable accounting for different climate models, deterioration processes, structural types and materials. Nevertheless, in the following, the focus will be devoted to RC structures subjected to chloride-induced corrosion under climate change.

5.1.2 Analytical Methodology

The framework described in Section 5.1.1 aims to derive the reliability elements of the semi-probabilistic methodology, such as safety factors γ_X, nominal values X_k, and design values X_d, for structures subjected to deterioration processes under climate change. To achieve this result, two methodologies are proposed and eventually compared with those reported in the literature.

Different approaches for calibrating safety factors, characteristic values, and design values are defined in the literature. In principle, the values recommended in the standards are derived by solving a reliability-based optimization problem (Section 3.3.2), which can be summarized by the flowchart depicted in Figure 5.2.

The "traditional" methodology is based on the assumption of stationarity and the absence of significant damage in the structural systems. In this context, the variables associated with structural demand E_i, capacity R_j, reliability level β, and ultimately the safety factors $\boldsymbol{\gamma}$ are considered constant over time.

However, when structural systems are subjected to environmental aggressiveness, the assumption of time-invariant resistance may be misleading, as the damage can result in a decrease in resistance parameters over time $R_j(t)$. Moreover, environmental parameters

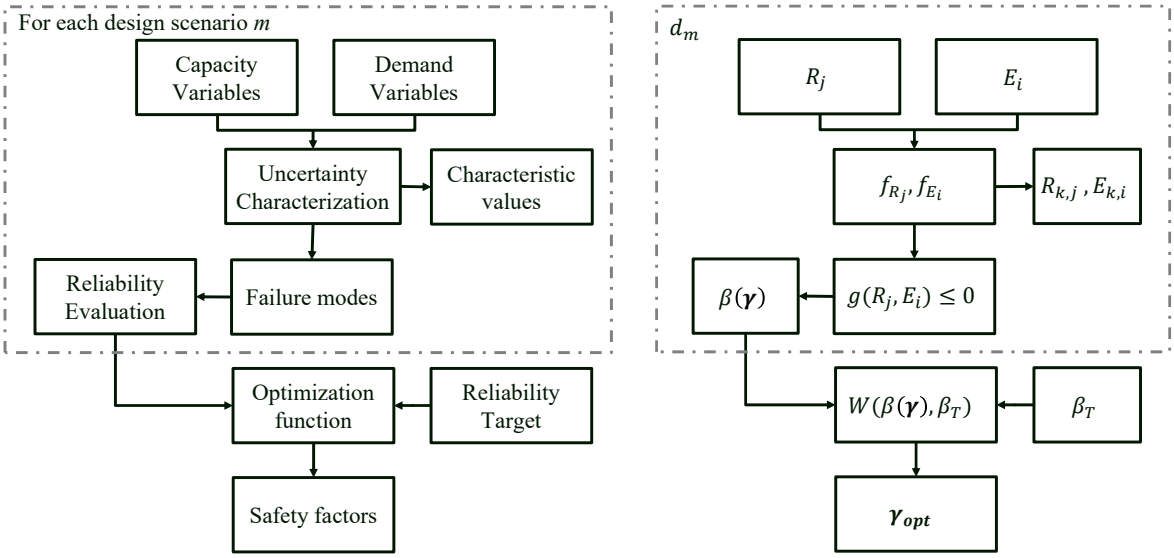

Figure 5.2: "Traditional" calibration of safety factors by solving the reliability-based optimization problem.

projections in a changing climate $\eta_k(t)$ may impact the evolution of both climatic loadings, influencing the structural demand $E_i(t)$, and environmental aggressiveness $\delta_j(t)$, and consequently the structural capacity $R_j(t)$. Due to the time-variant nature of the problem, the probabilistic distributions $f_{E_i}(t)$ and $f_{R_j}(t)$, the limit state function $g(R_j(t), E_i(t))$, and the reliability index $\beta(\boldsymbol{\gamma}(t))$ for the considered design scenario d_m evolve over time. The limit state function presented in Equation 3.21 may be modified as:

$$g(\mathbf{z}(t)) = R_d(\mathbf{z}(t)) - E_d(\mathbf{z}(t)) > 0 \tag{5.1}$$

where $g(\mathbf{z}(t))$ is the time-variant limit state function, R_d is the design resistance, E_d is the design demand, $\mathbf{z}(t)$ is the vector of the design parameters at time t.

Eventually, the optimal safety factors $\gamma_{\mathbf{opt}}(t)$ are calculated by fixing a specific reliability target and solving the optimization problem for different design scenarios d_m over time. The methodology described above is represented in Figure 5.3.

The elements of the codes can also be defined using the Design Value Method (Section 3.3.3), which is illustrated by the flowchart presented in Figure 5.4. In the traditional DVM, safety factors may be determined by the evaluation of the characteristic and design values of the resistance and demand variables.

In the proposed methodology, the impact of climate change and environmental aggressiveness is accounted for in the definition of the safety factors $\gamma(t)$, through the characterization of uncertainty over time $f_{R_j}(t)$ and $f_{E_i}(t)$, and the consequent definition of the characteristic and design values, as depicted in Figure 5.5. The methodology depicted

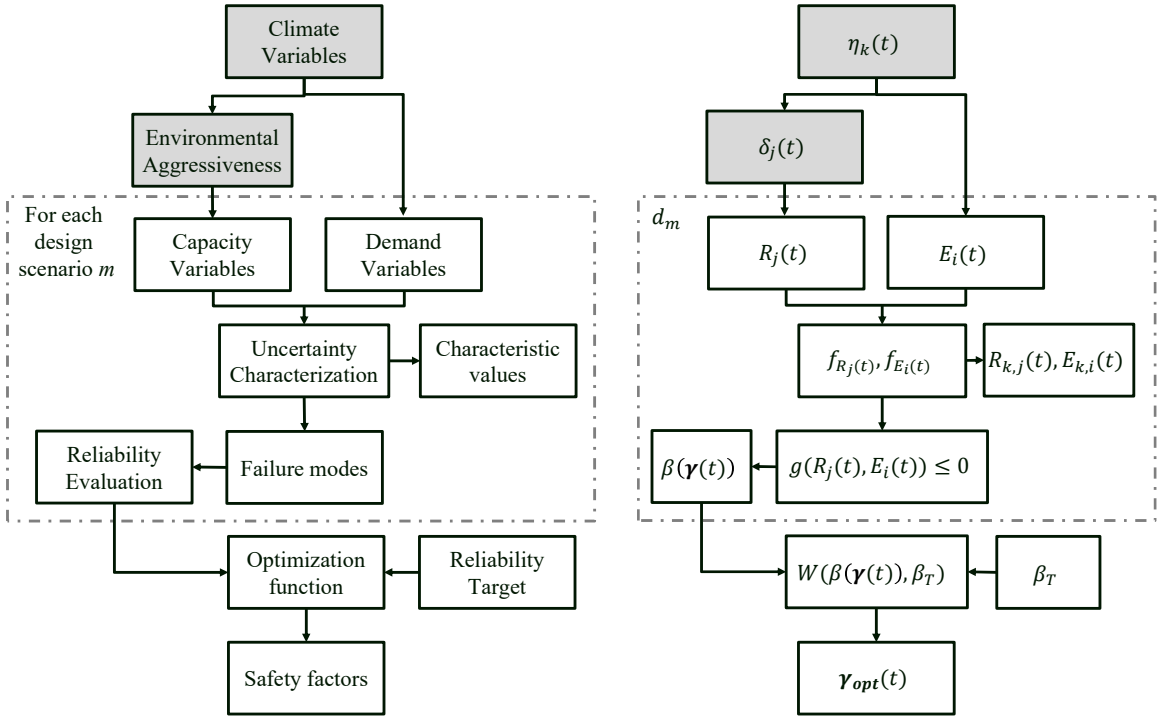

Figure 5.3: Proposed methodology for calibration of safety factors by solving the reliability-based optimization problem.

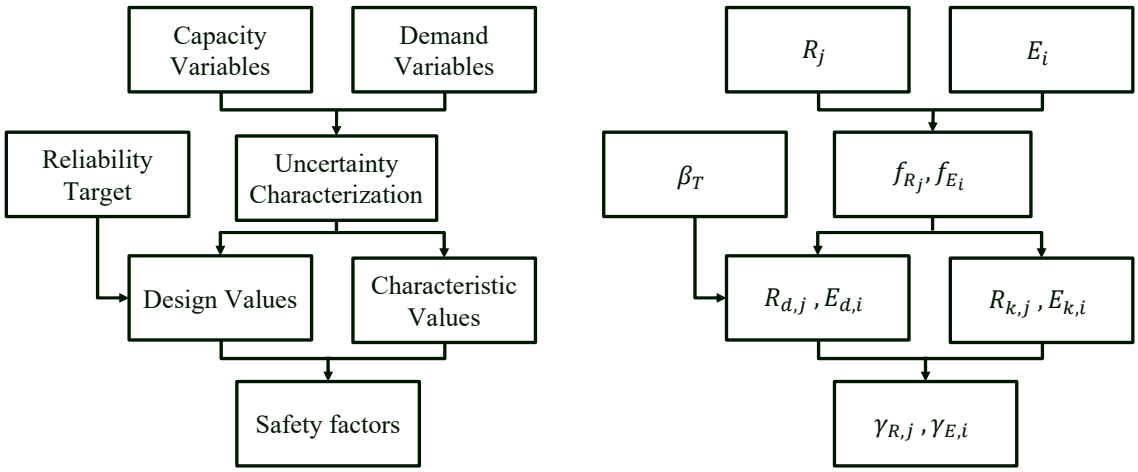

Figure 5.4: "Traditional" methodology for the determination of safety factors by using the design value method.

may be used both for the Partial Safety Format (Section 3.4.1) and the Global Safety Format (Section 3.4.2) of the semi-probabilistic methodology.

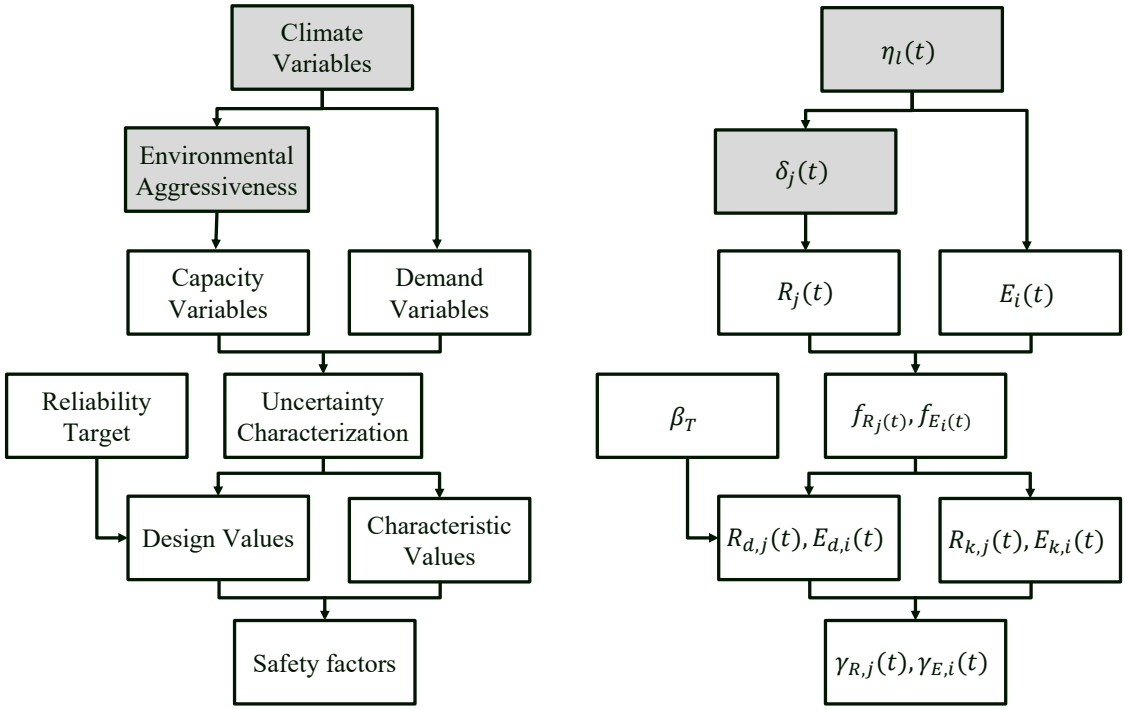

Figure 5.5: Proposed methodology for the determination of safety factors by using the design value method.

In the following, the proposed methodology is detailed for the definition of the reliability elements of the PSF and the GSF using the DVM tailored for the assessment of existing RC structures under climate change-induced corrosion.

PSF for existing RC structures under climate change-induced corrosion

The partial safety factors for aging structures under climate change are expected to vary over time; they may be redefined by the equations 5.2, 5.4, and 5.3:

$$\gamma_{m,i}(t) = \frac{X_{k,i}(t)}{X_{d,i}(t)} = \frac{F_{X_i}(t)^{-1}(q_R)}{F_{X_i}(t)^{-1}[\Phi(-\alpha_R \beta_T)]} \tag{5.2}$$

$$\gamma_{q,i}(t) = \frac{Q_{d,i}(t)}{Q_{k,i}(t)} = \frac{F_{Q_i}^{-1}(t)[\Phi(-\alpha_E \beta_T)]}{F_{Q_i}(t)^{-1}(q_Q)} \tag{5.3}$$

$$\gamma_{g,i} = \frac{G_{d,i}}{G_{k,i}} = \frac{F_{G_i}^{-1}[\Phi(-\alpha_E \beta_T)]}{F_{G_i}^{-1}(q_G)} \tag{5.4}$$

where $\gamma_{m,i}(t)$, $\gamma_{q,i}(t)$, and $\gamma_{g,i}$ are the safety factors for materials, variable loadings, and permanent loadings, respectively; $X_{k,i}(t)$, $Q_{k,i}(t)$, and $G_{k,i}$ are the characteristic

values and $X_{d,i}(t)$, $Q_{d,i}(t)$, and $G_{d,i}$ are the design values of the random variable $X_i(t)$, $Q_i(t)$, and G_i, respectively; $F^{-1}(t)$ is the time-variant inverse CDF; Φ^{-1} is the inverse standard normal CDF; β_T is the reliability target, α_R and α_E are the sensitivity factors for capacity and demand; q_R, q_Q, and q_G is generally assumed to be equal to the 5th percentile, 98th percentile, and 50th percentile, respectively (JCSS, 2001). The main modification in these definitions involves the estimation of the time-variant CDF $F^{-1}(t)$ of the random variables of material strength and variable loading, while it is assumed that the permanent loading remains constant over time.

Considering the material properties, characteristic and design values can be reformulated as a function of a reference value $X_{k,i,ref}$ and $X_{d,i,ref}$, which is defined as the initial stationary value, and a correction function $\zeta(t)$, considering the time-variant modifications, as shown in Equations 5.5 and 5.6, respectively.

$$X_{k,i}(t) = X_{k,i,ref} \cdot \zeta_{k,i}(t) \tag{5.5}$$

$$X_{d,i}(t) = X_{d,i,ref} \cdot \zeta_{d,i}(t) \tag{5.6}$$

where $\zeta_{k,i}(t)$ and $\zeta_{d,i}(t)$ are correction functions accounting for the impact of climate change-induced deterioration on the characteristic and design values, respectively. Eventually, the partial safety factors for material properties are defined analogously as a function of the initial reference partial factor $\gamma_{m,i,ref}$, multiplied by the correction functions accounting for time-variant modifications.

$$\gamma_{m,i}(t) = \gamma_{m,i,ref} \cdot \kappa_{m,i}(t) \tag{5.7}$$

Analogously, characteristic and design values for climatic loadings can be reformulated as a function of the reference stationary values $Q_{k,i,ref}$ and $Q_{d,i,ref}$ and correction functions accounting for the impact of climate change $\lambda_{k,i,CC}(t)$ and $\lambda_{d,i,CC}(t)$, as described in Equations 5.8 and 5.9, respectively.

$$Q_{k,i}(t) = Q_{k,i,ref} \cdot \lambda_{k,i,CC}(t) \tag{5.8}$$

$$Q_{d,i}(t) = Q_{d,i,ref} \cdot \lambda_{d,i,CC}(t) \tag{5.9}$$

Eventually, the partial safety factors are defined by considering the reference partial factor $\gamma_{q,i,ref}$, which is multiplied by a correction function that accounts for the impact of climate change $\kappa_{q,i,CC}(t)$.

$$\gamma_{q,i}(t) = \gamma_{q,i,ref} \cdot \kappa_{q,i,CC}(t) \tag{5.10}$$

Nevertheless, the predominant type of damage caused by corrosion in RC structures is the reduction of the steel mass. Moreover, the spalling damage should be also considered reducing the concrete cover area A_c. These aspects lead to the proposition of the introduction of two additional partial safety factors, $\gamma_{As,l}$ and γ_{Ac}, following the same philosophy applied for material strength:

$$\gamma_{As,l}(t) = \frac{A_{sk,l}(t)}{A_{sd,l}(t)} = \frac{F_{A_{s,l}}(t)^{-1}(q_R)}{F_{A_{s,l}}(t)^{-1}[\Phi(-\alpha_R\beta_T)]} \tag{5.11}$$

$$\gamma_{Ac}(t) = \frac{A_{ck}(t)}{A_{cd}(t)} = \frac{F_{A_c}(t)^{-1}(q_R)}{F_{A_c}(t)^{-1}[\Phi(-\alpha_R\beta_T)]} \tag{5.12}$$

where $\gamma_{As,l}(t)$ and $\gamma_{Ac}(t)$ are the time-variant partial safety factors for the area of the l-th steel bar and the concrete cover, respectively; $A_{sk,l}(t)$ and $A_{ck}(t)$ denote the characteristic values, while $A_{sd,l}(t)$ and $A_{cd}(t)$ represent the design values, respectively. Additionally, $F_{A_{s,l}}(t)^{-1}$ and $F_{A_c}(t)^{-1}$ denote the inverse CDF for the steel area and concrete cover, q_R indicates the 5th percentile, Φ^{-1} is the inverse standard normal CDF, α_R is the sensitivity factor, and β_T represents the reliability target.

GSF for RC structures under climate change-induced corrosion

Similarly to the proposal for the PSF, the global safety factor is expected to vary over time in case of aging structures under climate change. This factor may be redefined based on Equation 3.31 as follows:

$$\gamma_R(t) = \frac{R_m(t)}{R_d(t)} = \frac{R(x_{m,i}(t), a_{nom})}{F_R^{-1}(t)[\Phi(-\alpha_R\beta_T)]} \tag{5.13}$$

where $\gamma_R(t)$ is the time-variant global safety factors for the overall structural capacity R, $R_m(t)$ denotes the mean value, $R_d(t)$ represents the design value, $F_R^{-1}(t)$ is the inverse CDF, q_R indicates the 5th percentile, Φ^{-1} is the inverse standard normal CDF, α_R is the sensitivity factor, β_T represents the reliability target; moreover, $x_{m,i}(t)$ are the mean values of the material properties affecting the overall capacity, and a_{nom} are the nominal geometric parameters. The main modification in these definitions pertains to the estimation of the time-variant mean global resistance value $R_m(t)$ and the CDF $F_R^{-1}(t)$ of the global resistance over time.

The mean and design values can be reformulated as functions of reference values for the considered structure $R_{m,ref}$ and $R_{d,ref}$, along with a correction function $\rho(t)$, accounting

for the time variant modifications, as shown in Equations 5.14 and 5.15, respectively:

$$R_m(t) = R_{m,ref} \cdot \rho_m(t) \tag{5.14}$$

$$R_d(t) = R_{d,ref} \cdot \rho_d(t) \tag{5.15}$$

where $\rho_{m,i}(t)$ and $\rho_{d,i}(t)$ are correction functions for the mean and design values, respectively. Eventually, the global resistance safety factors can also be defined by considering the reference global factor for the structure in question $\gamma_{R,ref}$, multiplied by a correction function $\kappa_r(t)$ that accounts for the time variant modifications induced by deterioration and climate change.

$$\gamma_R(t) = \gamma_{R,ref} \cdot \kappa_r(t) \tag{5.16}$$

5.2 Semi-probabilistic Assessment of a RC beam under climate change-induced corrosion

5.2.1 Case Study Description

The statically indeterminate RC beam shown in Figure 5.6 is analyzed. The rectangular cross-section of the beam (Figure 5.7) is subjected to chloride attack at the extrados and intrados, assuming a uniform chloride surface concentration C_s. The upper and lower layers of longitudinal reinforcement are characterized by 4Φ16 steel bars, which have a net concrete cover of $c = 35$ mm. The deterministic geometrical variables are summarized in Table 5.1. The evolution of temperature T and relative humidity RH is considered in time due to climate change, while structural demand is assumed to be constant in time. The flexural response of the structure is evaluated by means of the ultimate bending moment $M_R(t)$.

Geometrical Parameter	Value [m]
Beam Length L	5
Cross-Section Height h	0.5
Cross-Section Width b	0.3

Table 5.1: Geometrical characteristics of the clamped-hinged beam.

A life-cycle reliability assessment is conducted to determine the reliability elements of the semi-probabilistic approach in accordance with the methodology illustrated in Figure

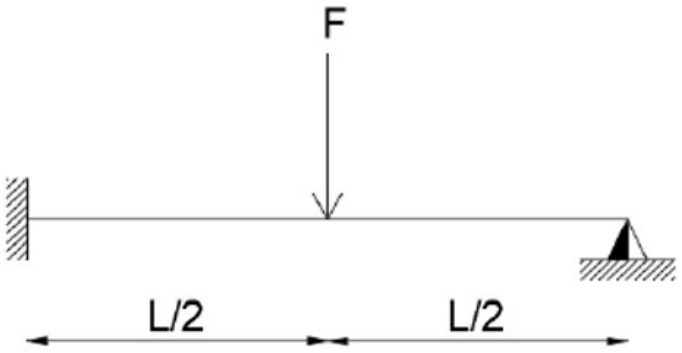

Figure 5.6: Static scheme of the clamped-hinged RC beam.

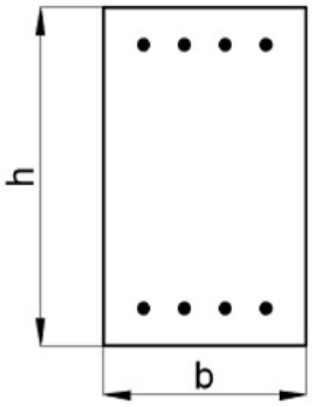

Figure 5.7: Cross-section of the clamped-hinged RC beam.

5.5. In order to characterize the uncertainty evolution of the resisting variables over time due to corrosion and climate, simulation based techniques are used, i.e., Crude Monte Carlo simulation.

In the following, the different aspects of the assessment are detailed to provide a general overview of the proposed methodology. A parametric study is conducted to evaluate the impact of the format (PSF and GSF), spatial scale, and exposure aggressiveness on the semi-probabilistic analysis (Section 5.2.2). Eventually, the obtained results are reported and discussed.

Uncertainty Definition

The fundamental random variables related to the environmental deterioration process, the mechanical properties of the material, the geometry, and the loading conditions are presented in Table 5.2, which summarizes the types of probabilistic distributions and

their corresponding statistical descriptors. The variables involved in the deterioration process include the surface concentration C_s, the reference concrete diffusivity $D_{c,ref}$, the aging parameter a, the reference critical concentration $C_{cr,ref}$, the reference current density $i_{corr,ref}$, and the pitting factor R_f. The initial concrete strength f_{c0} and the steel yielding strength f_{sy0} account for material uncertainty, while geometric uncertainty is addressed through the concrete cover c and the initial steel bar diameter ϕ_0. Ultimately, the variability of structural demand is modeled by the concentrated load F applied at the mid-span. For the sake of simplicity, statistical independence between variables is assumed.

Climate Change Modeling

As evidenced in previous Sections, structural performance is influenced, among other factors, by the evolution of surrounding environmental conditions. In the case of corrosion-induced damage, the variation in temperature and relative humidity is particularly significant.

For the sake of this analysis, the reference period is set to be from year 2000 to year 2100 (100 years); temperature and relative humidity projections are retrieved from the data available in the Climate Change Knowledge Portal (WorldBankGroup, 2025) for multiple SSPs, based on the Sixth phase of the Coupled Model Intercomparison Project (CMIPs6, Eyring et al., 2016). To account for the uncertainties inherent in climate projections, the projections considered are derived from a multi-model ensemble approach to reduce the dependency on any single model and provide a more robust estimate of future climate conditions (Section 2.3.3). Ensemble statistics, such as the median, the 10th percentile, and the 90th percentile, allow for the quantification of model spread and scenario uncertainty, which is essential for probabilistic assessments of climate impacts. The data are retrieved at a yearly temporal scale. Moreover, the projections are derived for spatially aggregated units in France for national and sub-national (regional) entities, which are considered appropriate for the sake of code standardization where more refined data may be difficult to incorporate. For these spatial aggregations, both a shapefile and latitudinal weighting are applied. The spatial variability of temperature and relative humidity in France under different climate change scenarios is depicted in Figures 5.8 and 5.9.

Specifically, in this study, $T(t)$ and $RH(t)$ represent the evolution of the annual average mean surface air temperature and relative humidity in time. These parameters are retrieved as their median value, 10th percentile, and 90th percentile for climate scenario SSP1-2.6 and SSP5-8.5. Eventually, an additional scenario is considered in which the influence of climate change is neglected, denoted as No Climate Change (NCC); the

Random Variable	Distribution	Mean	Std Dev	Bounds
Chloride Surface Concentration C_s [wt.%/cem] (fib, 2006, 2015)	Truncated Normal	1.5	0.45 $\cdot\mu$	$C_s \geq 0$
Chloride Critical Concentration $C_{cr,ref}$ [m^2/year] (fib, 2015)	Beta	0.6	0.15	$0.2 \leq C_{cr} \leq 2$
Diffusivity Coefficient $D_{c,ref}$ [m^2/year] (fib, 2006, 2015)	Truncated Normal	15.8	0.2 $\cdot\mu$	$D_c \geq 0$
Aging Factor a [-] (fib, 2006, 2015; Gahlen, 2000)	Beta	0.30	0.12	$0 \leq a \leq 1$
Corrosion rate $i_{corr,ref}$ [μ/cm^2] (DuraCrete, 1998)	Lognormal	2.586	1.724	$i_{corr} \geq 0$
Pitting R_f [-] (Rodriguez et al., 1997; Stewart and Al-Harthy, 2008)	Lognormal	4.0	0.15	$R_f \geq 0$
Concrete compressive Strength f_{c0} [MPa] (JCSS, 2001)	Lognormal	30	0.15 $\cdot\mu$	$f_{c0} \geq 0$
Steel Yielding Strength f_{sy0} [MPa] (JCSS, 2001)	Lognormal	1.1 $\cdot$ 450	0.05 $\cdot\mu$	$f_{sy0} \geq 0$
Concrete Cover c [m] (fib, 2006)	Truncated Normal	0.035	0.2$\cdot\mu$	$c \geq 0$
Steel bar diameter ϕ_0 [m] (JCSS, 2001)	Truncated Normal	0.016	0.02$\cdot\mu$	$\phi_0 \geq 0$
Concentrated Loading F [kN] (JCSS, 2001)	Lognormal	100	0.2 $\cdot\mu$	$F \geq 0$

Table 5.2: Statistical characteristics of the considered random variables.

NCC scenario implies a stationary temperature and relative humidity, respectively equal to $T(t_0)$ and $RH(t_0)$ over the entire reference period. This scenario is defined to observe the impact of the deterioration mechanism on the evolution of structural reliability, excluding the influence of climate change.

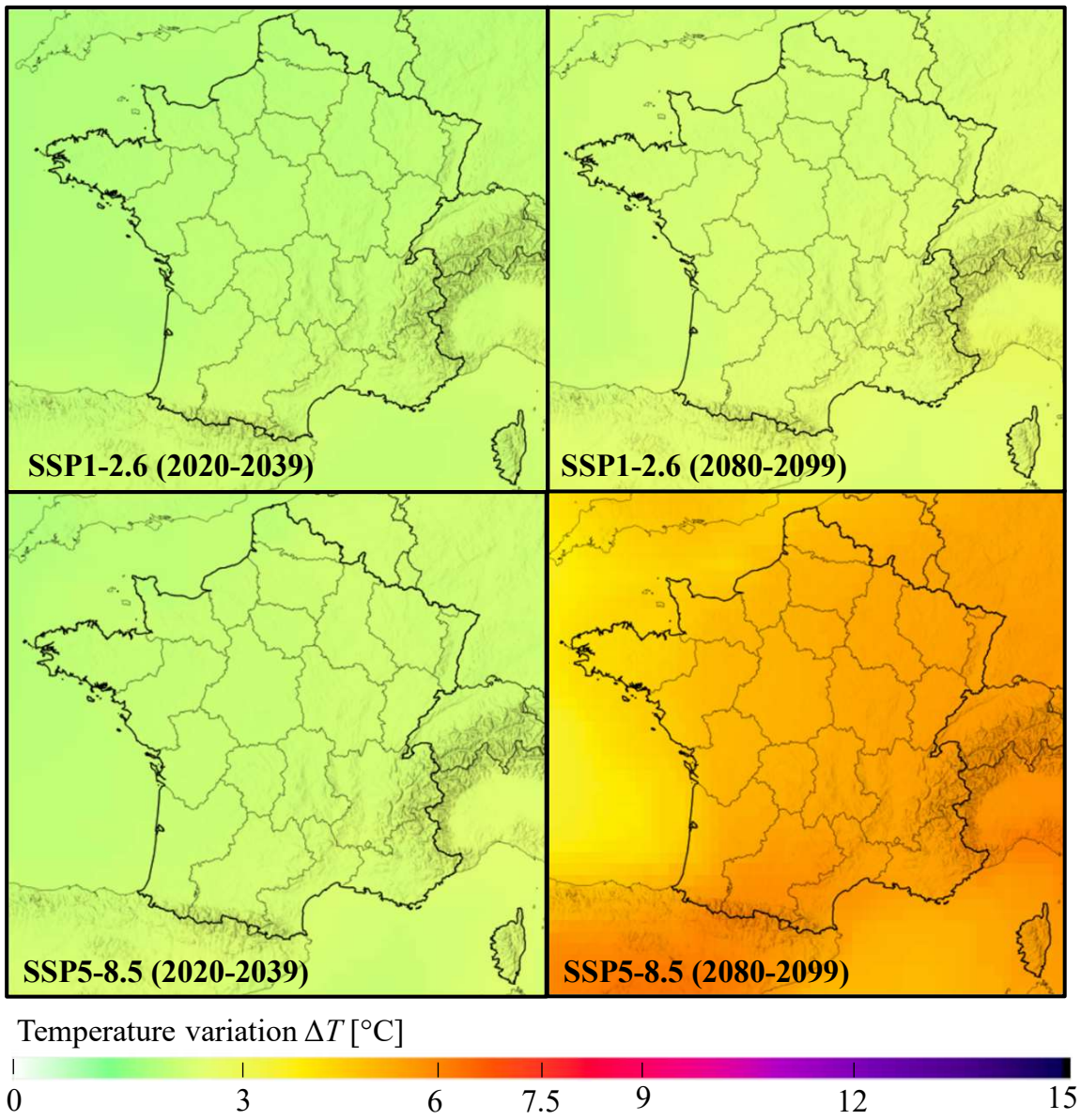

Figure 5.8: Variation in average mean surface air temperature in France for different climate change scenarios (WorldBankGroup, 2025).

Corrosion Damage Modeling

The corrosion process is modeled by assuming that the kinetics of chloride ions in concrete are governed by diffusion, utilizing a model based on the one-dimensional solution of Fick's law (DuraCrete, 2000; Stewart et al., 2011), as depicted in Equation 5.17:

$$C(x,t) = C_s \cdot \left[1 - \text{erf}\left(\frac{x}{2\sqrt{D_c(t) \cdot t}}\right)\right] \tag{5.17}$$

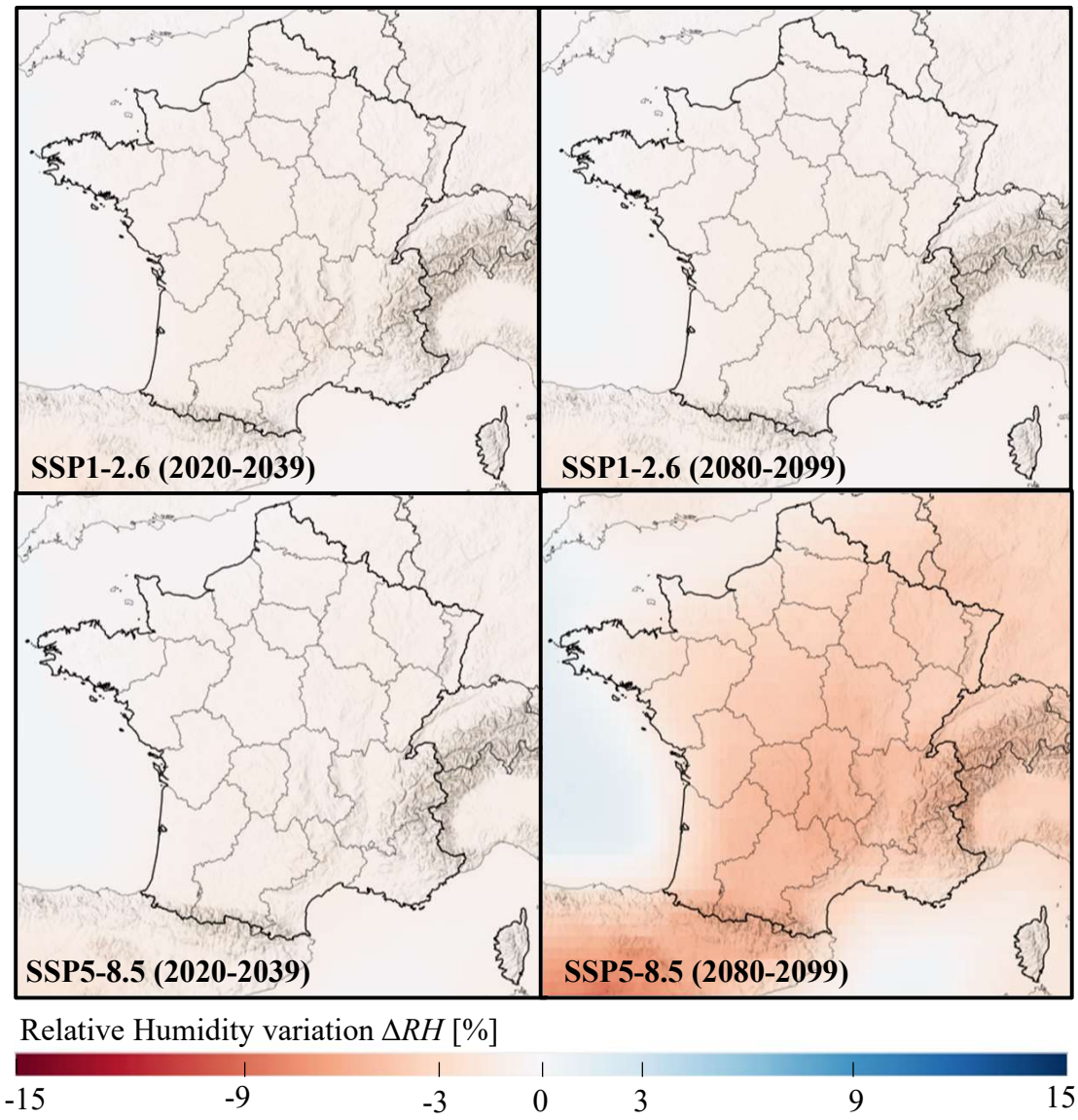

Figure 5.9: Variation in relative humidity in France for different climate change scenarios (WorldBankGroup, 2025).

where $C(x,t)$ is the total chloride content at time t and at depth x with respect to the concrete surface, C_s is the chloride content on the surface, and $D_c(t)$ is the diffusivity of the chlorides.

$D_c(t)$ is considered as a function of aging, temperature, and relative humidity (Equation 5.18):

$$D_c(t) = D_{c,ref} \cdot exp\left[\frac{E_a}{R_g}\left(\frac{1}{T_{ref}} - \frac{1}{273+T(t)}\right)\right] \cdot \left[1 + \frac{(1-RH(t))^4}{(1-RH_{ref})^4}\right]^{-1} \cdot \left(\frac{\tilde{t}}{t}\right)^a \quad (5.18)$$

where $D_{c,ref}$ is the reference chloride diffusivity, E_a is the activation energy of the chloride diffusion process, R_g is the gas constant, T_{ref} is the reference temperature (293 K = 20 °C), $T(t)$ is the actual temperature at time t, $RH_{ref} = 0.75$ is the reference relative humidity, $RH(t)$ is the actual relative humidity at time t, $\tilde{t}$ is equal to 28 days, t is the actual time and a is the aging factor.

The onset of corrosion is assumed to occur at time $t = t_{cr}$, when the chloride concentration $C(x,t)$, at a depth $x = c$ (i.e., concrete cover), reaches the critical chloride content $C_{cr}(t)$.

$$C(x,t) = C_{cr}(t) \quad \text{for} \quad t = t_{cr} \tag{5.19}$$

The critical chloride content $C_{cr}(t)$ is defined by equation 4.16, reported in the following for the sake of completeness, depending on the value of temperature $T(t)$ (J. Zhang et al., 2018; Shirkhani et al., 2020):

$$C_{cr}(t) = C_{cr,ref} \cdot \exp\left[\frac{(E_{Cl\text{-}concr} + E_{Cl\text{-}steel})}{R_g}\left(\frac{1}{273 + T(t)} - \frac{1}{T_{ref}}\right)\right] \tag{5.20}$$

where $C_{cr,ref}$ is the chloride threshold value at the reference temperature $T_{ref} = 293$ K, R_g is the gas constant ($8.314 \cdot 103\ kJ/K \cdot mol$), $E_{Cl-concr}$ represents the activation energy for the release of free chlorides, $E_{Cl-steel}$ denotes the rebar activation energy, respectively, and $T(t)$ (in °C) is the actual temperature at the time t. The activation energy ($E_{Cl-concr} + E_{Cl-steel}$) can reach values of up to 48 kJ/mol when combining the mechanisms.

After initiation, chloride-induced corrosion propagates into the reinforcement with a rate proportional to the electrical current density $i_{corr}(t)$. The penetration rate is calculated using Equation 5.21, while $i_{corr}(t)$ is defined by Equation 5.22.

$$\frac{\partial p_s}{\partial t} = 0.0116 \cdot i_{corr}(t) R_f \quad \text{if } t \geq t_{cr} \tag{5.21}$$

In Equation 5.21, the value 0.0116 serves as the corrosion rate conversion factor, while R_f denotes the pitting factor.

$$i_{corr}(t) = i_{corr,ref} \cdot [1 + K_T(T(t) - T_{ref})] \cdot e^{-6000(RH(t) - RH_{ref})^6} \cdot 0.85(t - t_{cr})^{-0.29} \tag{5.22}$$

In Equation 5.22, $i_{corr,ref}$ is the reference corrosion rate, $T(t)$ is the temperature at time t, $T_{ref} = 20$ °C is the reference temperature, K_T is a factor equal to 0.025 and 0.073 when $T(t) > T_{ref}$, respectively. Additionally, $RH(t)$ is the relative humidity at time t, $RH_{ref} = 0.75$ is the reference relative humidity, and t_{cr} is the onset time for the

propagation phase.

The dimensionless corrosion penetration index $\delta \in [0;\ 1]$ is obtained by integrating the penetration rate in time and normalizing it with respect to the undamaged diameter of the bar ϕ_0, as shown in Equation 5.23:

$$\delta(t) = \frac{\int_{t_{cr}}^{t} p_s \cdot dt}{\phi_0} \quad \text{for} \quad t > t_{cr} \tag{5.23}$$

Once the penetration index is defined, the damage related to chloride-induced corrosion is modeled as described in Section 4.4.3, considering reduction of steel mass, strength, and ductility, as well as concrete cover.

In figures 5.10, 5.11 and 5.12, the evolution of the empirical CDF and PDF for the steel bar area, the yielding strength, and the concrete cover area are represented to show the effect of corrosion.

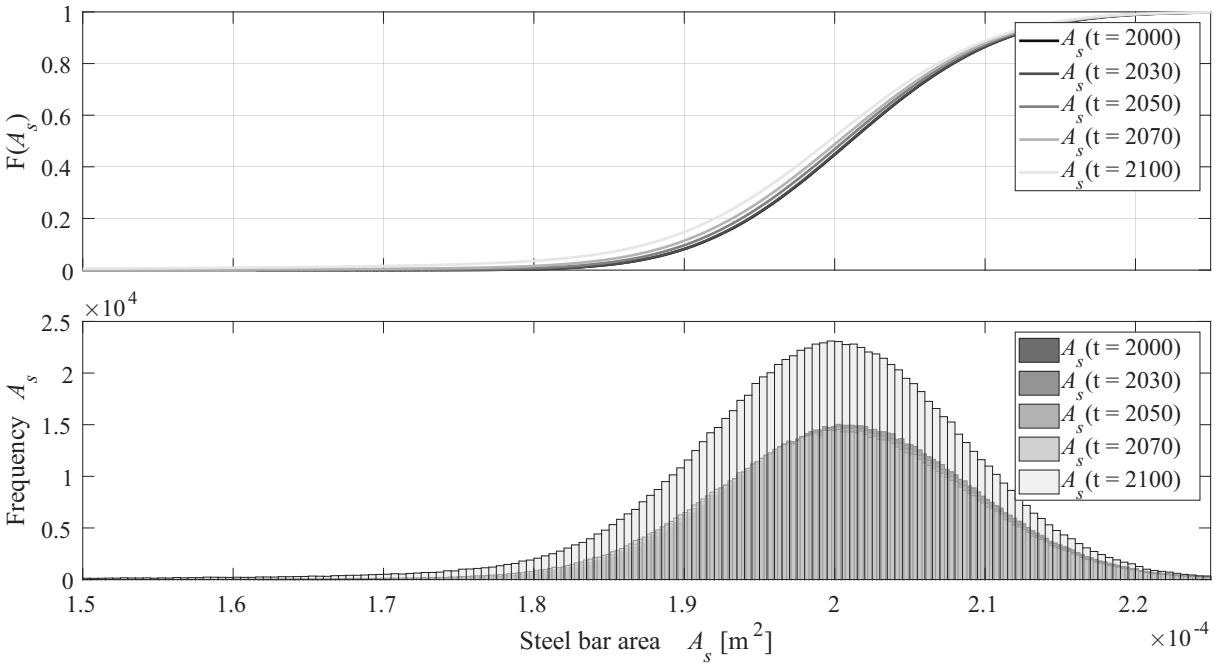

Figure 5.10: Evolution of the empirical CDF and PDF of the steel area due to corrosion.

Particularly of interest is the effect on the concrete cover, which transitions from a unimodal distribution initially to a zero-inflated distribution over time due to the cracking and eventual spalling of the concrete cover Figures 5.12 .

Structural Analysis

Defined the time-variant evolution of the parameters influencing the structural capacity under chloride induced corrosion, the ultimate resisting bending moment $M_R(t)$ is selected as the resisting variable to be evaluated. $M_R(t)$ is estimated analytically assessing the

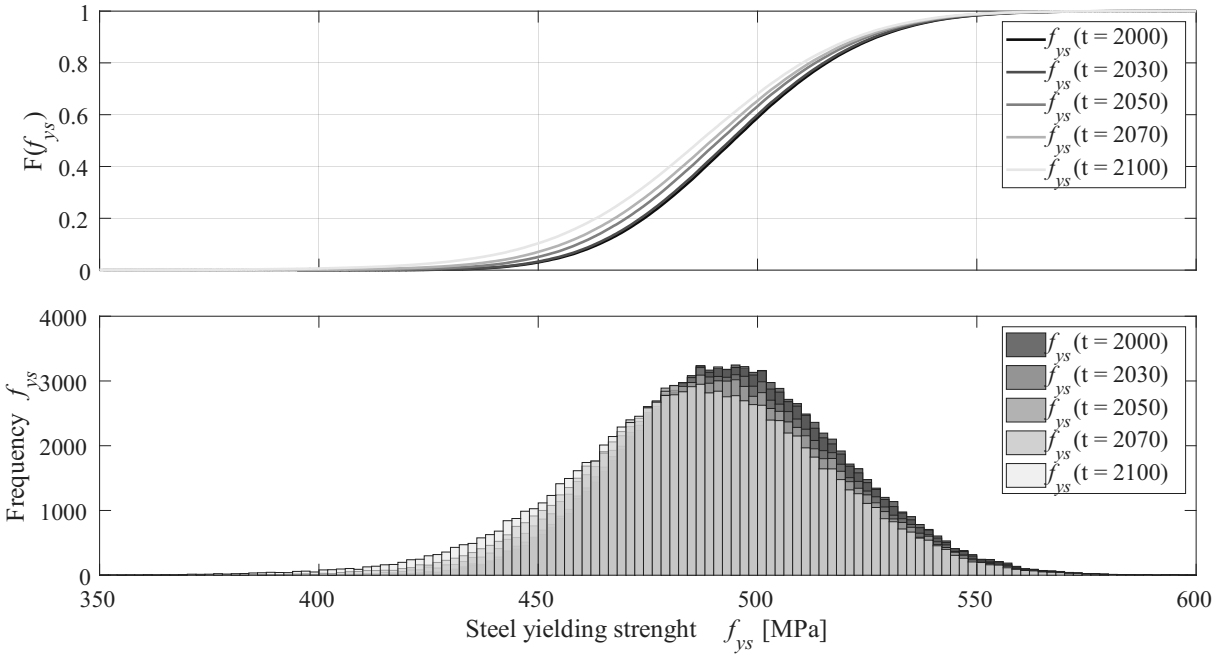

Figure 5.11: Evolution of the empirical CDF and PDF of the steel yielding strength due to corrosion.

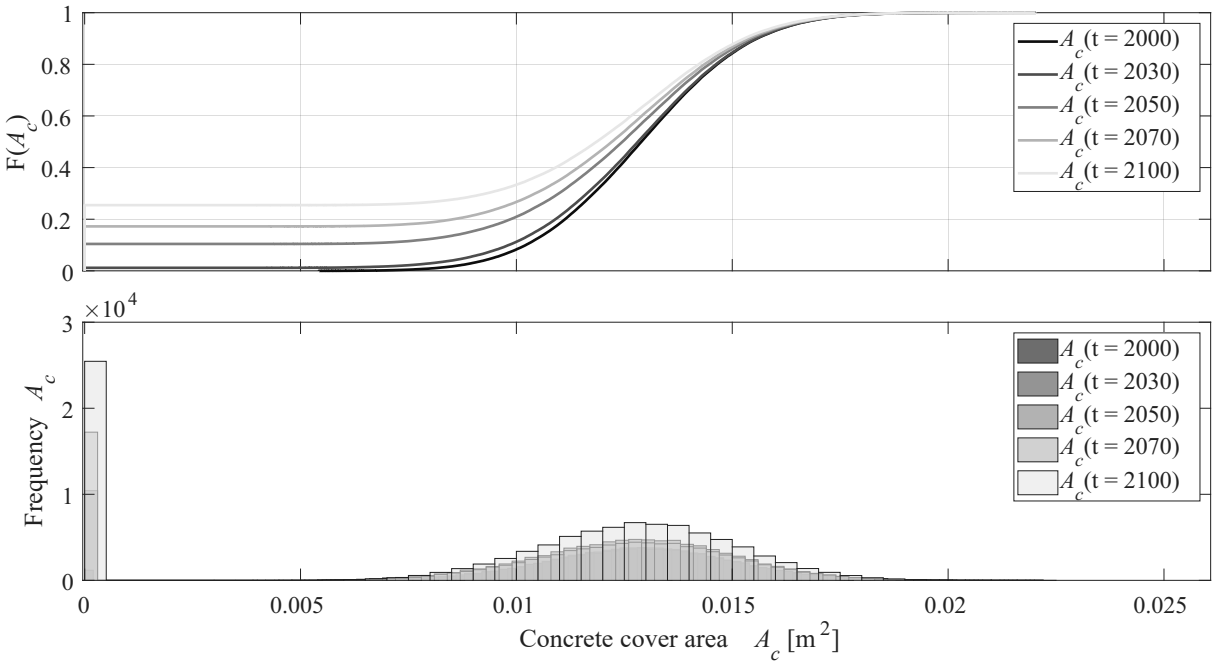

Figure 5.12: Evolution of the empirical CDF and PDF of the concrete cover area due to corrosion.

translational and rotational equilibrium, under the assumptions that the cross section remains planar following bending, there is no relative slippage between the reinforcement and the concrete, zero-tensile strength, and the steel demonstrates elastic-perfectly plastic behavior. Assuming that the bottom and top part of the concrete cross-section are

in tension and compression due to bending, respectively, the horizontal and rotational equilibrium is deduced by Figure 5.13.

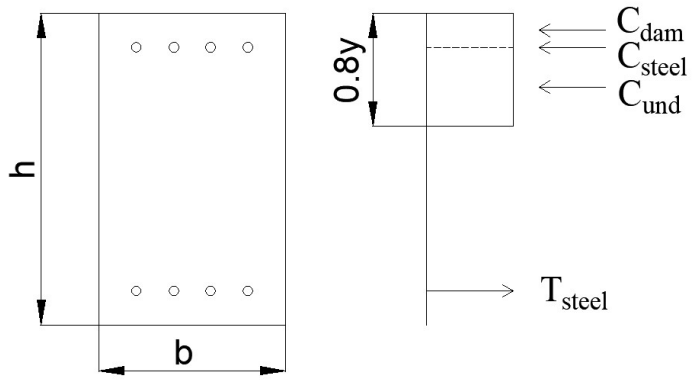

Figure 5.13: Internal forces in the damaged RC section under bending.

The internal forces $C_{steel}(t)$ and $T_{steel}(t)$ correspond to the contributions of steel in compression and tension , respectively. These parameters vary over time due to corrosion-induced reduction of steel mass, strength, and ductility as reported in Equations 5.24 and 5.25:

$$C_{steel}(t) = \sum_{j=1}^{J} \cdot A_{s,j}(t) \cdot f_{ys,j}(t) \tag{5.24}$$

$$T_{steel}(t) = \sum_{i=1}^{I} \cdot A_{s,i}(t) \cdot f_{ys,i}(t) \tag{5.25}$$

where J and I are the number of rebars in the compressed and tensioned reinforcement layer, $A_{s,j}(t)$ and $A_{s,i}(t)$ are the steel area of the individual i-th and j-th bars, and $f_{ys,j}(t)$ and $f_{ys,i}(t)$ are the steel yielding strength at time t.

The internal force due to concrete in compression C_{concr} is divided into 2 components: a time-variant component $C_{dam}(t)$ for the concrete cover (Equation 5.26), which is affected by cracking and eventual spalling due to corrosion, and a time-invariant C_{und} for the core (Equation 5.27):

$$C_{dam}(t) = f_c \cdot A_c(t) \tag{5.26}$$

$$C_{und} = f_c \cdot b \cdot (0.8y - d') \tag{5.27}$$

where f_c is the concrete compressive strength, $A_c(t)$ concrete cover area at time t,

b is the width of the cross-section, y is depth of the neutral axis, and $d' = (c + \phi_0/2)$ is the distance accounting for the concrete cover depth c and half of the rebar diameter ϕ_0.

Eventually, $M_R(t)$ is assessed based on the rotational equilibrium of the internal forces. The variation of its empirical CDF and PDF is illustrated in Figure 5.14.

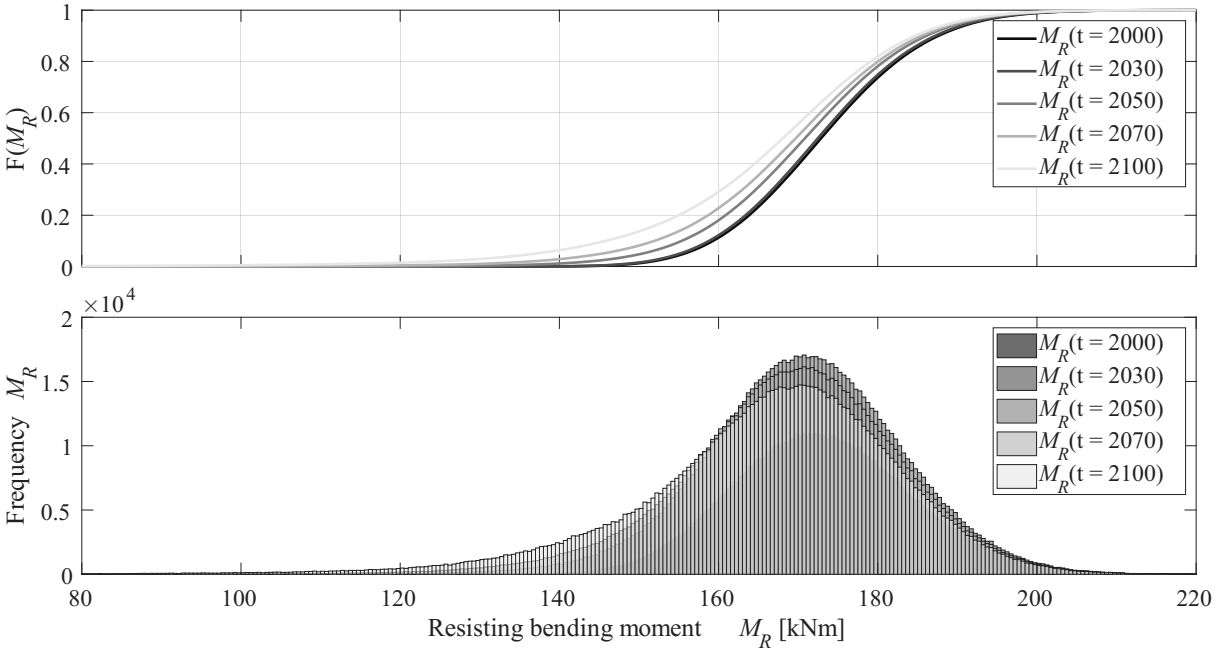

Figure 5.14: Evolution of the empirical CDF and PDF of the resisting bending moment due to corrosion.

Reliability Elements Definition

Knowing the time-variant evolution of the probability distributions of the resisting parameters, it is possible to estimate their characteristic values $X_{k,i}(t)$ based on the empirical percentiles (Figure 5.15), according to the following equation:

$$X_{k,i}(t) = F_{X_i}^{-1}(t)(q_R) \tag{5.28}$$

where q_R is the empirical 5th-percentile, and $F_{X_i}(t)$ is the inverse of the empirical CDF of the generic resisting variable $X_i(t)$ evaluated through simulation-based techniques. Concerning the GSF, the empirical mean value of $M_{Rm}(t)$ is numerically estimated from the simulated population.

The design values $X_{d,i}(t)$ are defined according to Equation 5.29:

$$X_{d,i}(t) = F_{X_i}^{-1}(t)[\Phi(-\alpha_R \beta_T)] \tag{5.29}$$

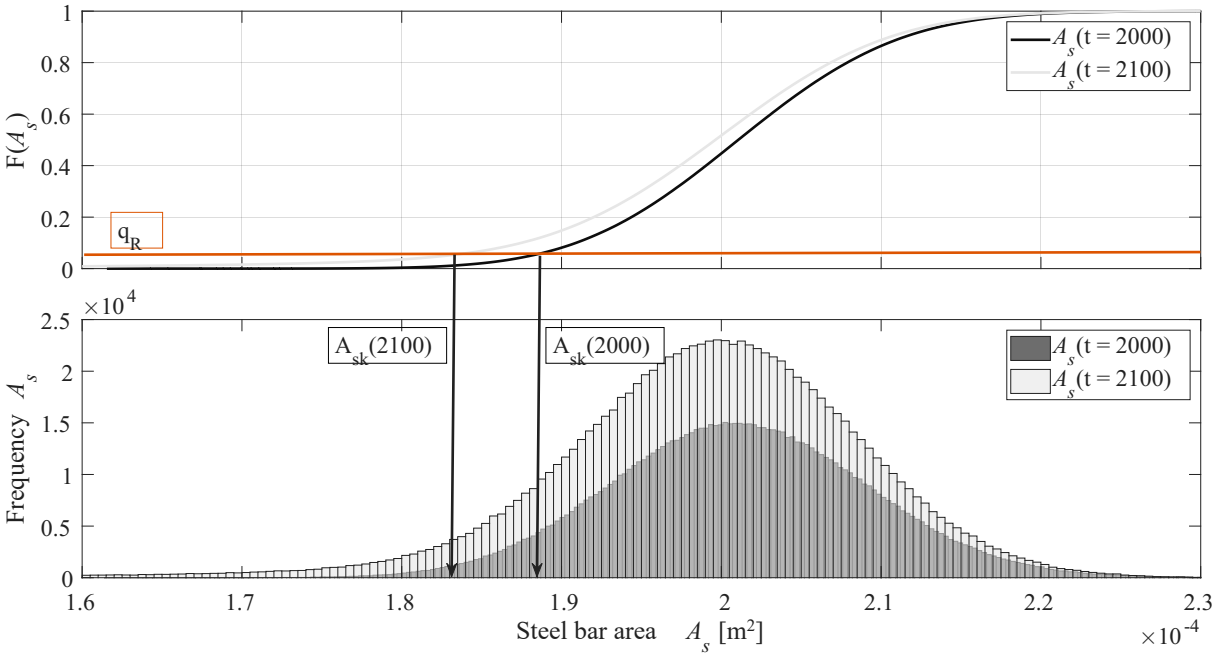

Figure 5.15: Determination of characteristic values for steel area.

where Φ^{-1} is the inverse standard normal CDF, α_R is the sensitivity factor for the resistance, and β_T denotes the reliability target. For the purposes of this analysis, the 1-year reliability target is selected from Table 3.2 to reflect small cost of safety measures and small consequences of failure, i.e., $\beta_{T,1y} = 4.2$. Assuming that the lifetime of the structure t_T is 100 years, the value of β_T is calculated as follows:

$$\beta_T = \Phi^{-1}(\Phi(\beta_{T,1y})^{t_T}) \tag{5.30}$$

Consequently , $\beta_T = 3.0$ is defined for the structure under consideration.

Eventually, the time-variant safety factors for the PSF and GSF are evaluated using Equations 5.31 and 5.32, respectively:

$$\gamma_{m,i}(t) = \frac{X_{k,i}(t)}{X_{d,i}(t)} \tag{5.31}$$

$$\gamma_R = \frac{R_m(t)}{R_d(t)} \tag{5.32}$$

where $\gamma_{m,i}(t)$, $X_{k,i}(t)$, and $X_{d,i}(t)$ are the partial safety factor, the characteristic value, and the design value for the i-th material property; $\gamma_R(t)$, $R_m(t)$, and $R_d(t)$ are the global safety factor, the mean value, and the design value for the overall bending resistance.

Reliability Analysis

The random outcomes for the analysis are reproduced using simulation-based techniques, i.e., Monte Carlo simulation, leading to the evaluation of the time-variant ultimate resisting bending moment $M_R(t)$. In this context, the collapse multiplier $\Theta(t)$ can be defined using limit analysis theory, under the assumption that the beam cross-section exhibits perfectly plastic behavior, as follows:

$$\Theta(t) = \frac{3M_R(t)}{FL} \tag{5.33}$$

where F is the concentrated loading at mid-span, and L is the length of the beam.

Consequently, the probability of failure $p_f(t)$ is defined in accordance with Equation 5.34.

$$p_f(t) = P[\Theta(t) \leq 1] \tag{5.34}$$

If both $M_R(t)$ and F are modeled as statistically independent lognormal Random Variable (RV)s, $p_f(t)$ and, consequently the reliability index $\beta(t)$, could be estimated in close form (Biondini, 2008). Nevertheless, this is generally not verified in realistic case studies.

Taking into account the marginal distributions f_F and $f_{M_R}(t)$, the reliability index $\beta(t)$ can be estimated based on the generation of n_{MCS} samples in accordance with Equation 5.35:

$$\bar{p}_f(t) = \frac{1}{n_{MCS}} \sum_{j=1}^{n_{MCS}} I\left[\frac{3m_{u,j}(t)}{f_j L} \leq 1\right] = \frac{1}{n_{MCS}} \sum_{j=1}^{n_{MCS}} I\left[\theta_j(t) \leq 1\right] \tag{5.35}$$

where $m_{R,i}(t)$ are the time-variant sample of the ultimate moment, f_i are the sample of the concentrated force, L is the length of the beam, n_{MCS} is the number of simulations, and I is an indicator function taking the sample of the collapse multiplier $\theta_j(t) \leq 1$ while in the other cases $I = 0$.

Since the accuracy of this approach is significantly influenced by the number of simulations n_{MCS}, the convergence of the investigated variables, namely the characteristic and design values, is illustrated in Figures 5.16 - 5.19. The characteristic and design values of the different resisting variables converge to a stable result for $n_{MCS} \geq 10^4$.

The time of achievement of three different limit states is also studied, defining:

- t_{cr} represents the critical time, i.e., the initiation of corrosion;

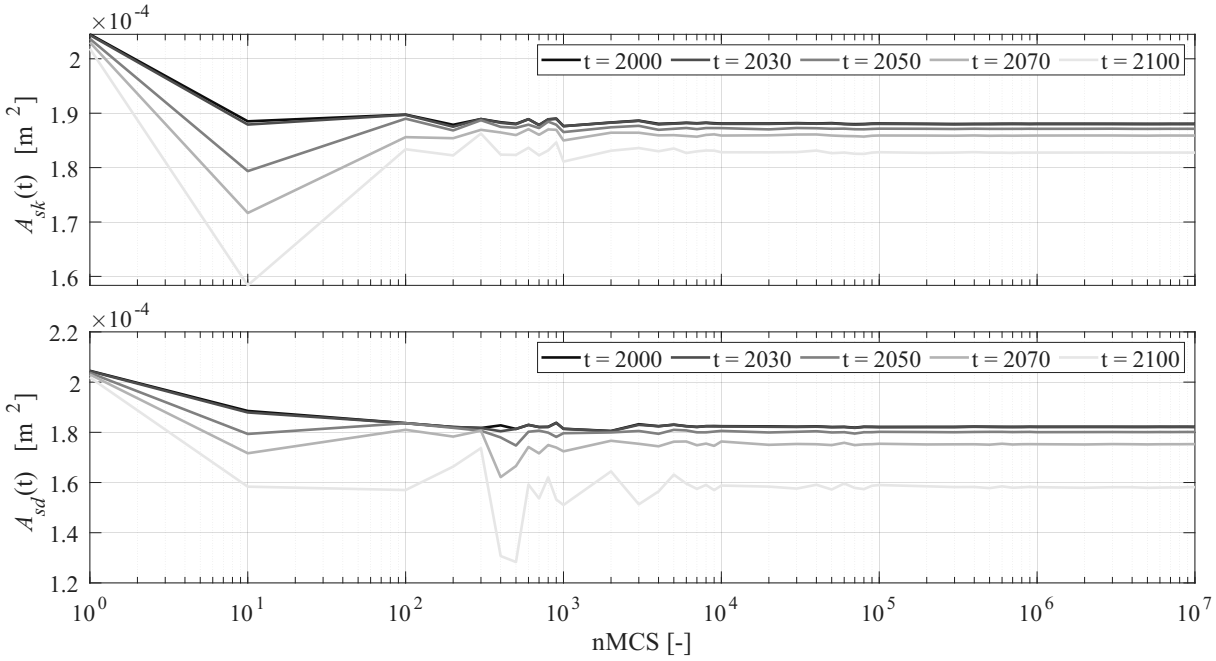

Figure 5.16: Variation of the characteristic and design values of steel area with sample size.

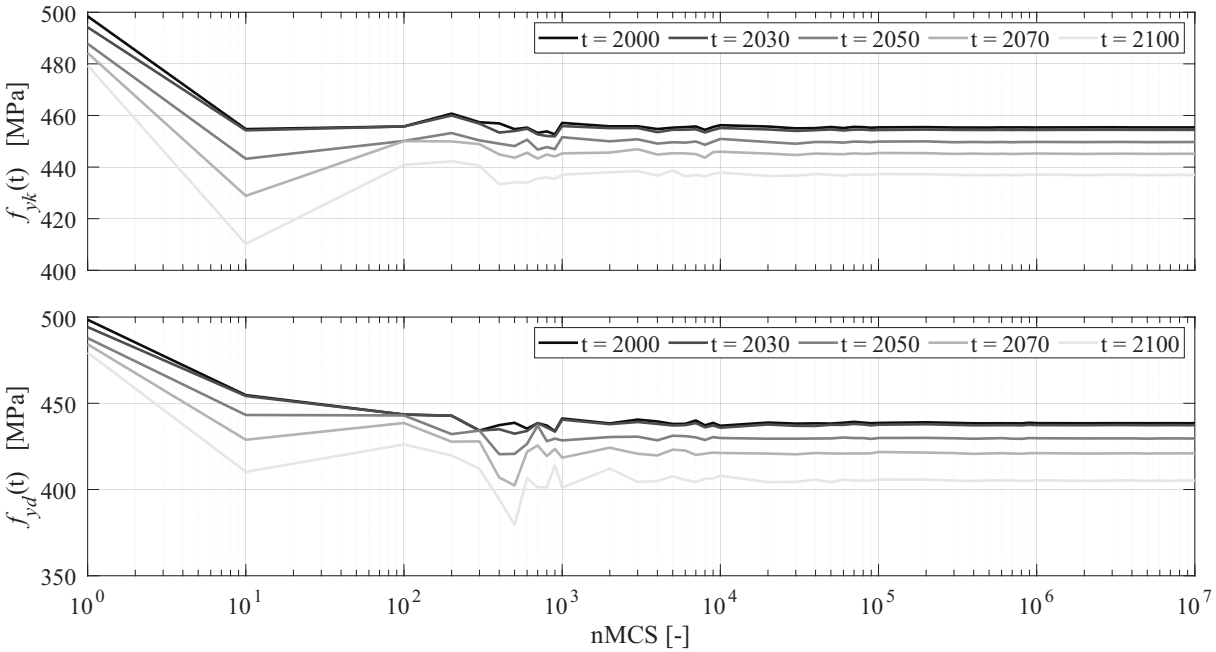

Figure 5.17: Variation of the characteristic and design values of steel yielding strength with sample size.

- t_{crack} is the cracking time, i.e., the emergence of the first crack;
- t_{fail} is the failure time, i.e., the occurrence of collapse.

The evolution of the empirical CDF of t_{cr}, t_{crack}, and t_{fail} is investigated for different

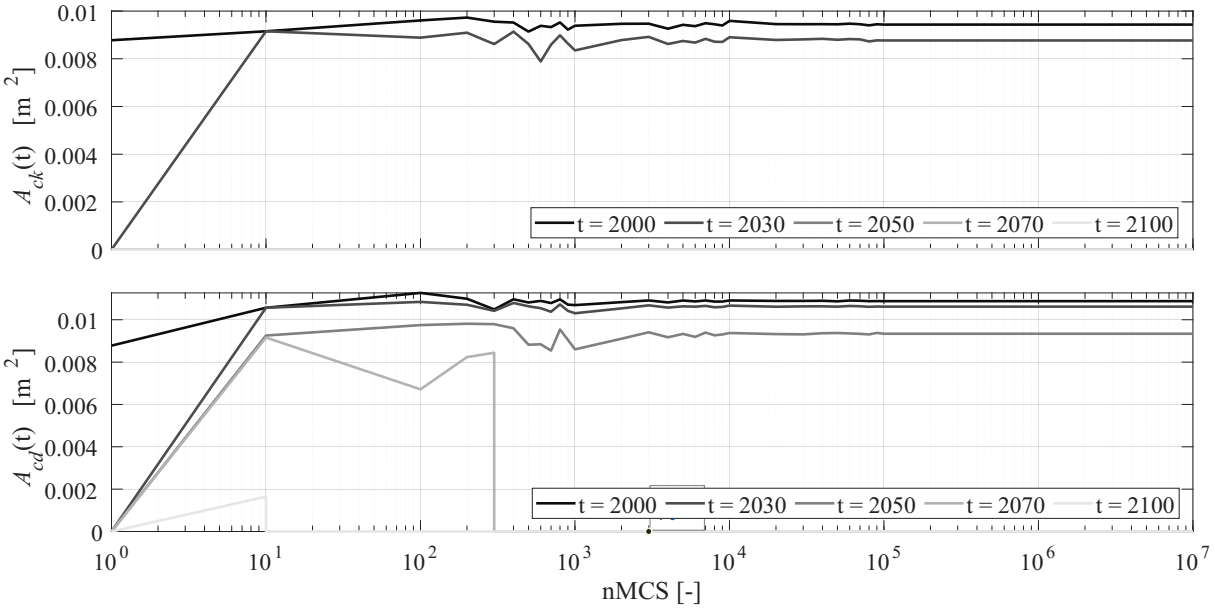

Figure 5.18: Variation of the characteristic and design values of concrete cover area with sample size.

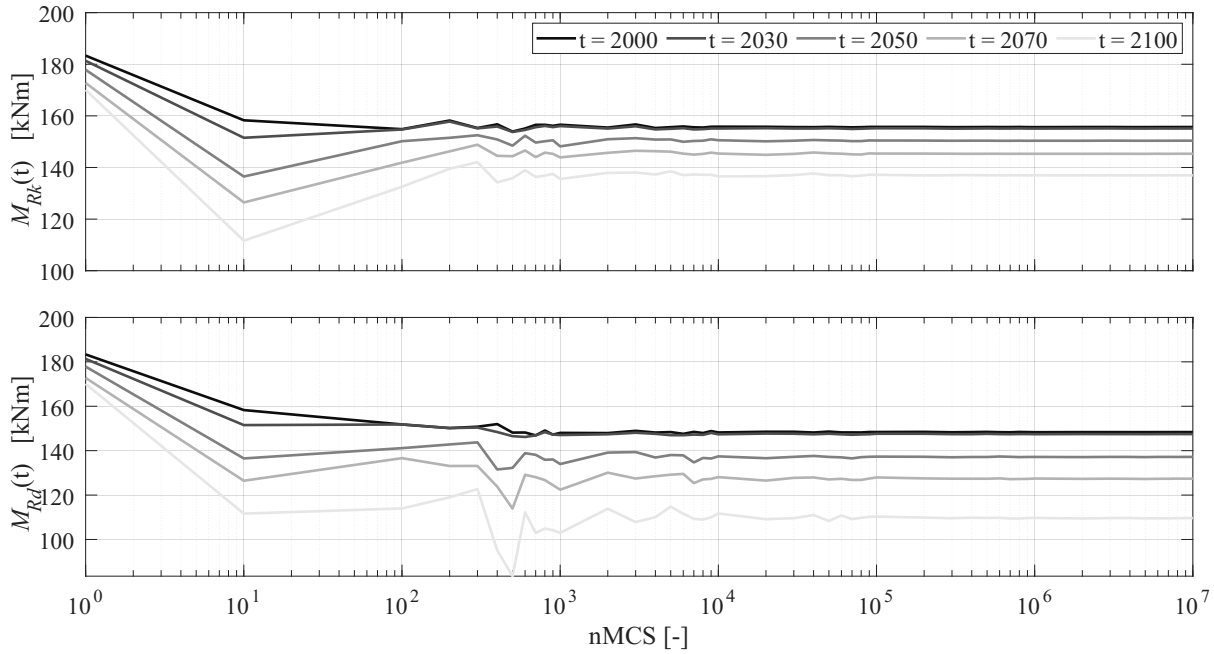

Figure 5.19: Variation of the characteristic and design values of ultimate bending moment with sample size.

sample sizes n_{MCS}, as illustrated in Figures 5.20 and 5.21. For these limit states, it is possible to observe the convergence of the results for $n_{MCS} \geq 10^5$.

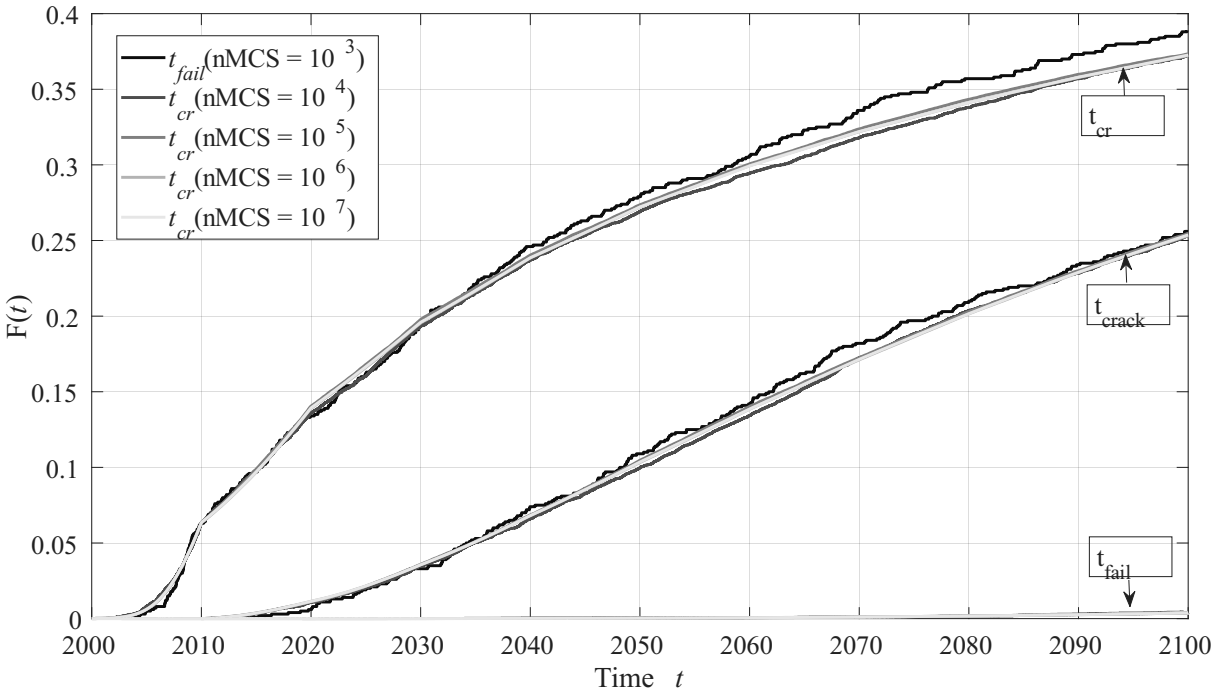

Figure 5.20: Variation of empirical CDF for the critical, cracking, and failure time with sample size.

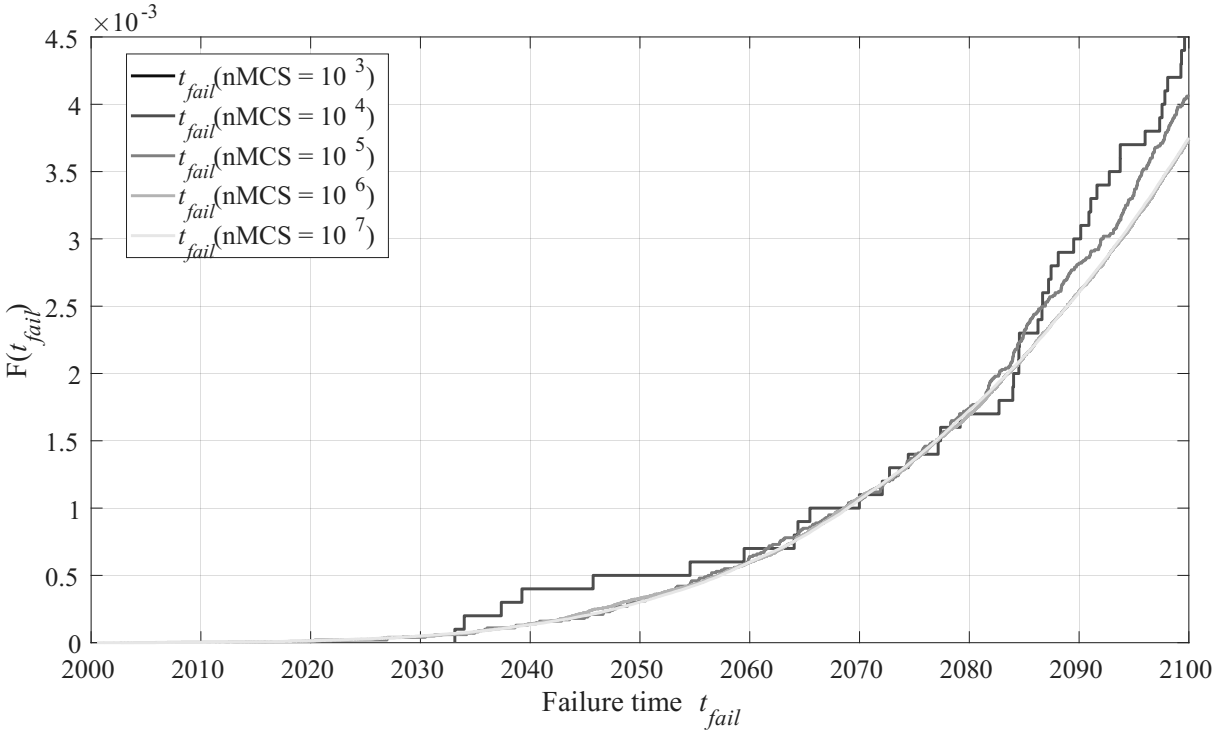

Figure 5.21: Detail of the variation of empirical CDF failure time with sample size.

Eventually, Figure 5.22 shows the value of the reliability index β for different sample sizes every 20 years.

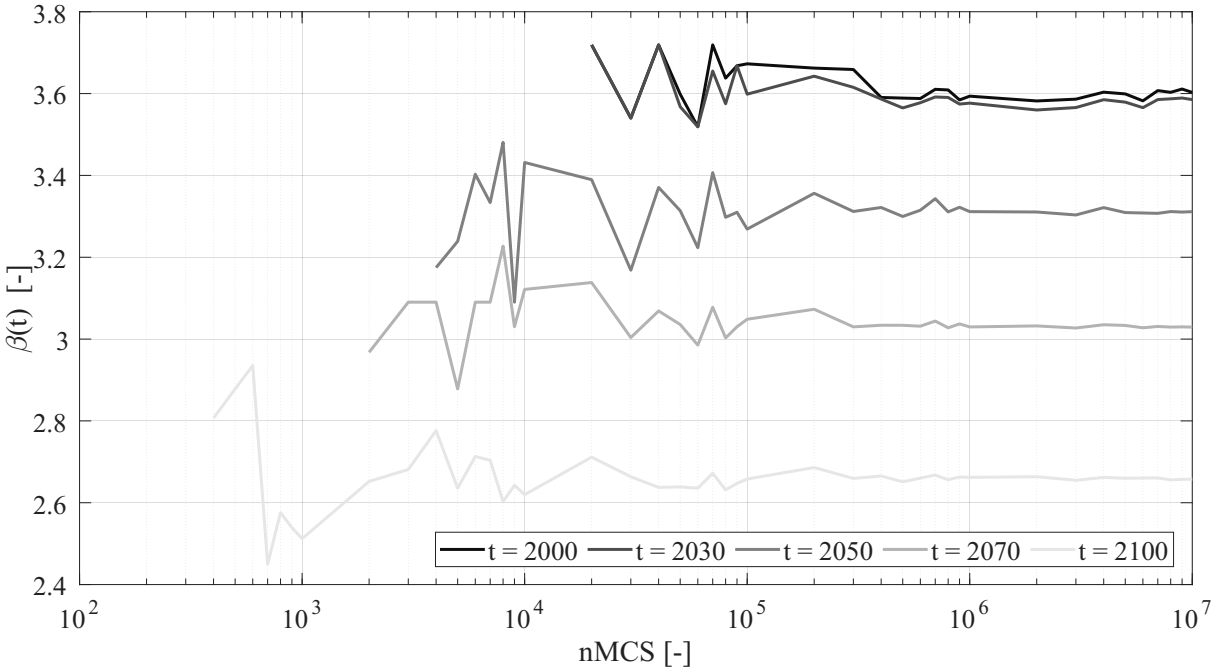

Figure 5.22: Variation of the reliability index with sample size.

The study of the convergence highlights that the number of simulations required for a reliable estimation of characteristic and design values, as well as for the limit state times, can be assumed to be equal to $nMCS = 10^5$; however, the reliability index may be accurately estimated only for $nMCS = 10^6$.

5.2.2 Results and Discussion

The results of the analysis are presented in this Section. First, the reference case study is assessed according to the procedures and parameters outlined in Section 5.2.1 for both the PSF and GSF. In addition, a parametric study is proposed to evaluate the influence of various factors concerning the definition of the reliability elements of the semi-probabilistic methodology. Two different aspects are studied:

- spatial scale of the analysis: climate projections for five distinct French regions are compared with those acquired at the national scale, underlining the importance of selecting an appropriate spatial scale based on the specific scope of the assessment;
- level of environmental aggressiveness: four distinct scenarios in terms of environmental aggressiveness are examined to evaluate the significance of an accurate representation of the aggressiveness scenarios.

The analysis varies the selected parameters to quantify their individual effects on the quantities of interest referring to the reference case study (section **??**) for comparison.

5.2.2.1 Reference Study

Based on the procedure and variables described in 5.2.1, the reference case study is analyzed. Climate change is assessed by projecting the average mean surface air temperature and relative humidity in France, at the national scale, for the NCC, SSP1-2.6 and SSP5-8.5 scenarios (Figures 5.23 and 5.24, respectively). The NCC scenario underlines the impact of corrosion on the investigated variables; SSP1-2.6 and SSP5-8.5 highlight the impact of both "optimistic" and "pessimistic" narratives of climate change on corrosion and, consequently, on the variables under investigation. Eventually, a life-cycle reliability analysis is conducted to obtain the time-variant reliability index (Figure 5.25).

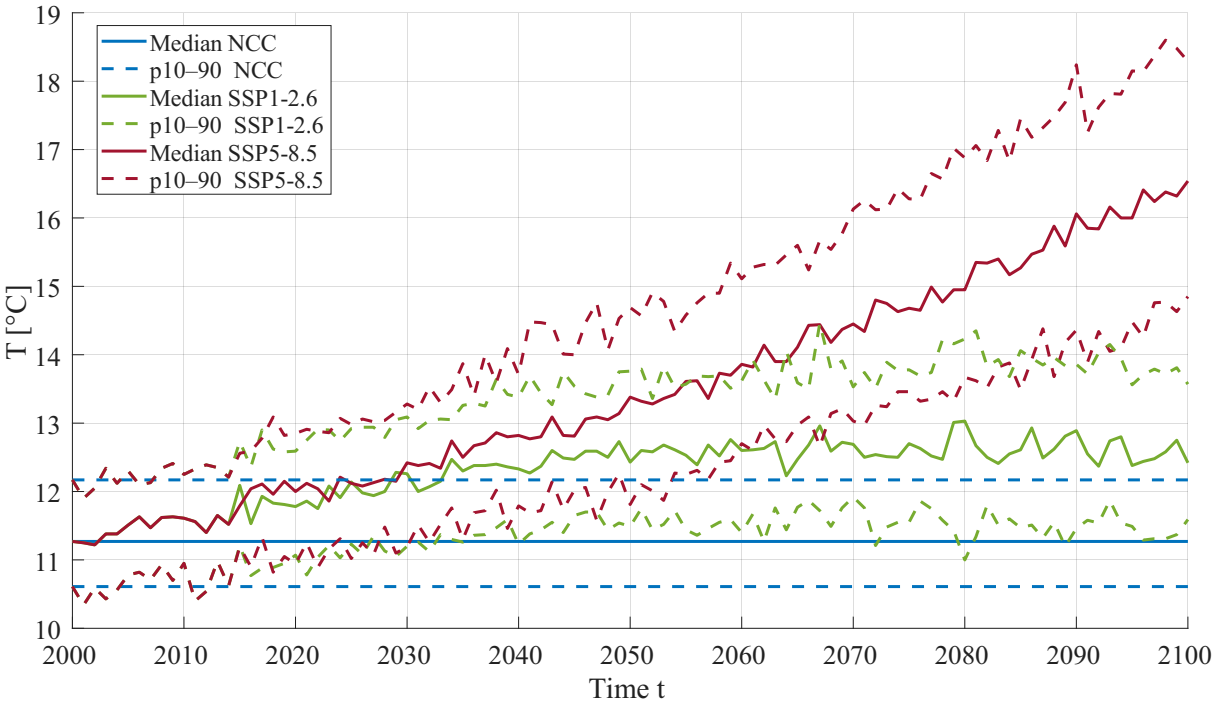

Figure 5.23: Scenarios for projected mean surface air temperature in France for the 2000-2100 period.

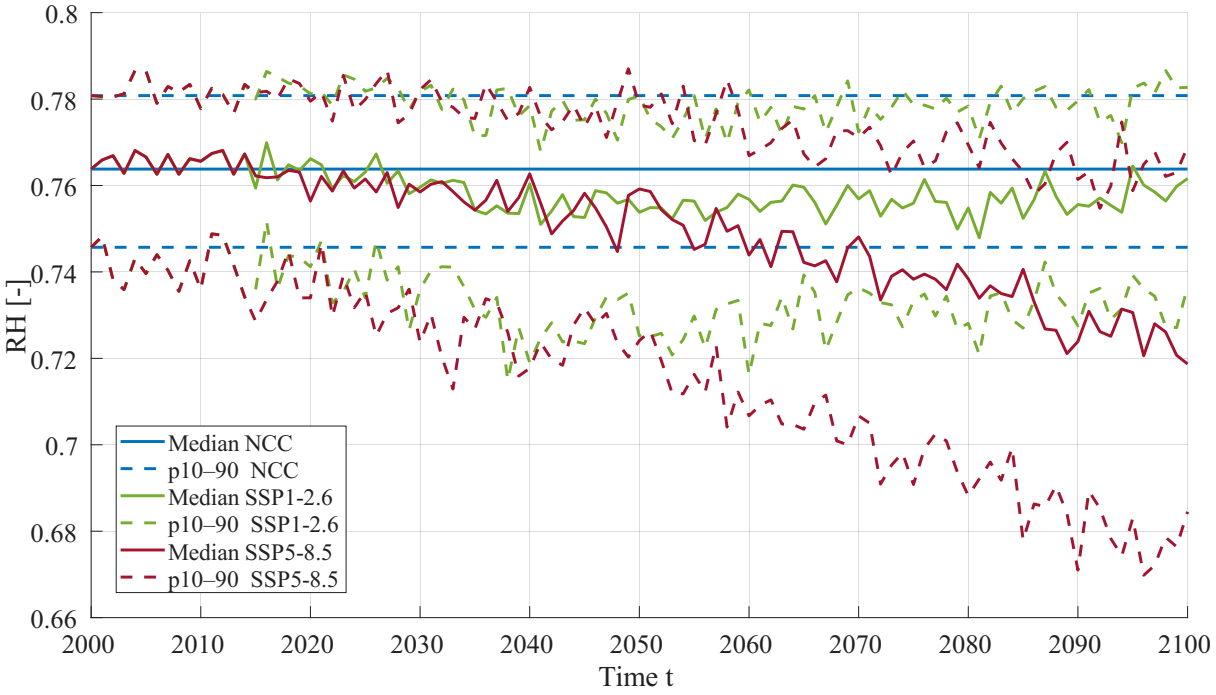

Figure 5.24: Scenarios for projected relative humidity in France for the 2000-2100 period.

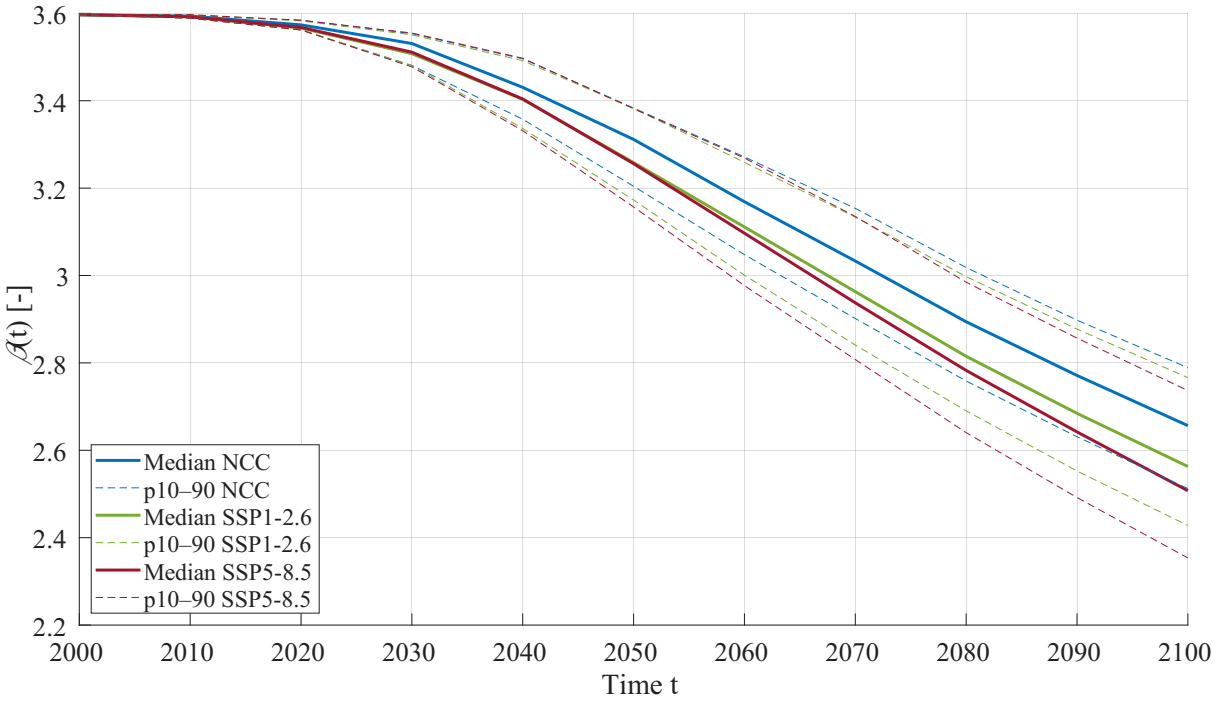

Figure 5.25: Evolution of the reliability index for different climate change scenarios.

Partial Safety Format

The PSF is firstly utilized to evaluate the structural bending capacity (Section 3.4.1). The evolution of the characteristic values of the steel reinforcement area, yielding strength, and concrete cover area as well as their respective correction functions for different climatic scenarios are illustrated in Figures 5.26 - 5.28. It can be observed that:

- for the NCC scenario where climate conditions are assumed to be stationary, corrosion leads to a decrease in all examined resisting variables. In particular, a smooth decrease can be observed in the steel area and yielding strength, while A_{ck} and A_{cd} exhibit a sudden drop due to the spalling of the concrete cover;
- climate change exacerbates this decline, as illustrated in the Figures. The decrease is more pronounced for the climate scenario SSP5-8.5, while it is milder for SSP1-2.6, as expected;
- The dashed lines in the Figures provide simplified information on climate change uncertainty , representing the values computed considering the projections of T and RH at the 10th and 90th percentiles. These show the increase of the uncertainties linked to climate change projections in time.

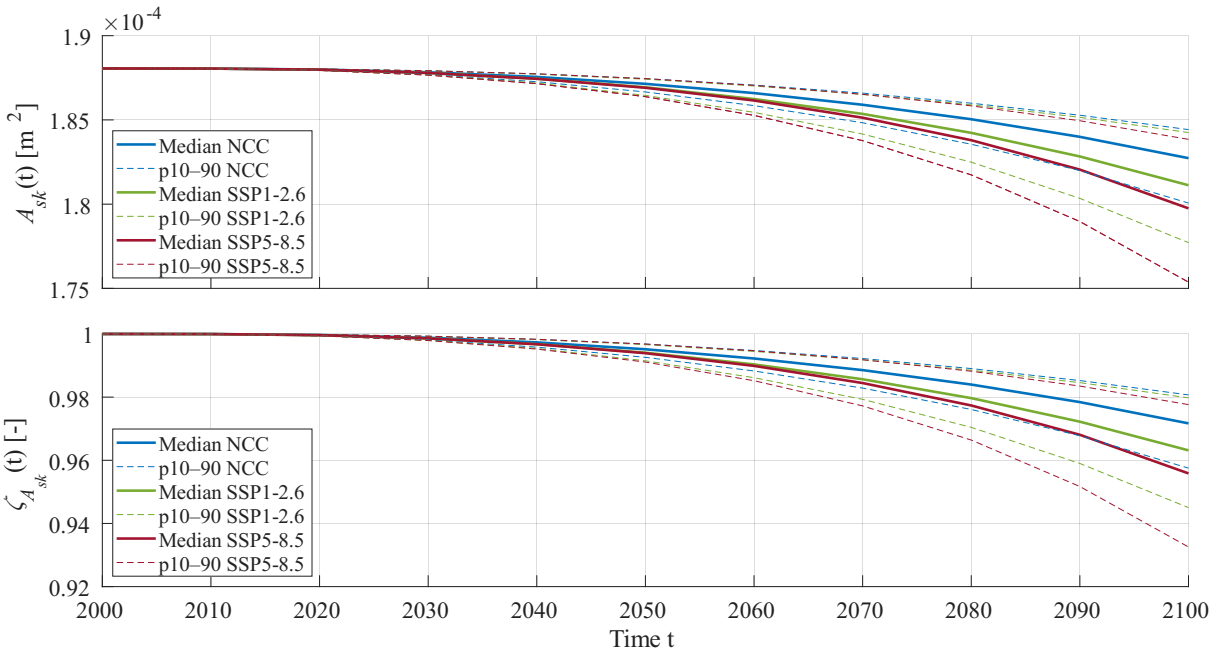

Figure 5.26: Evolution of the characteristic value (top) and the correction function (bottom) of the steel area for different climate change scenarios

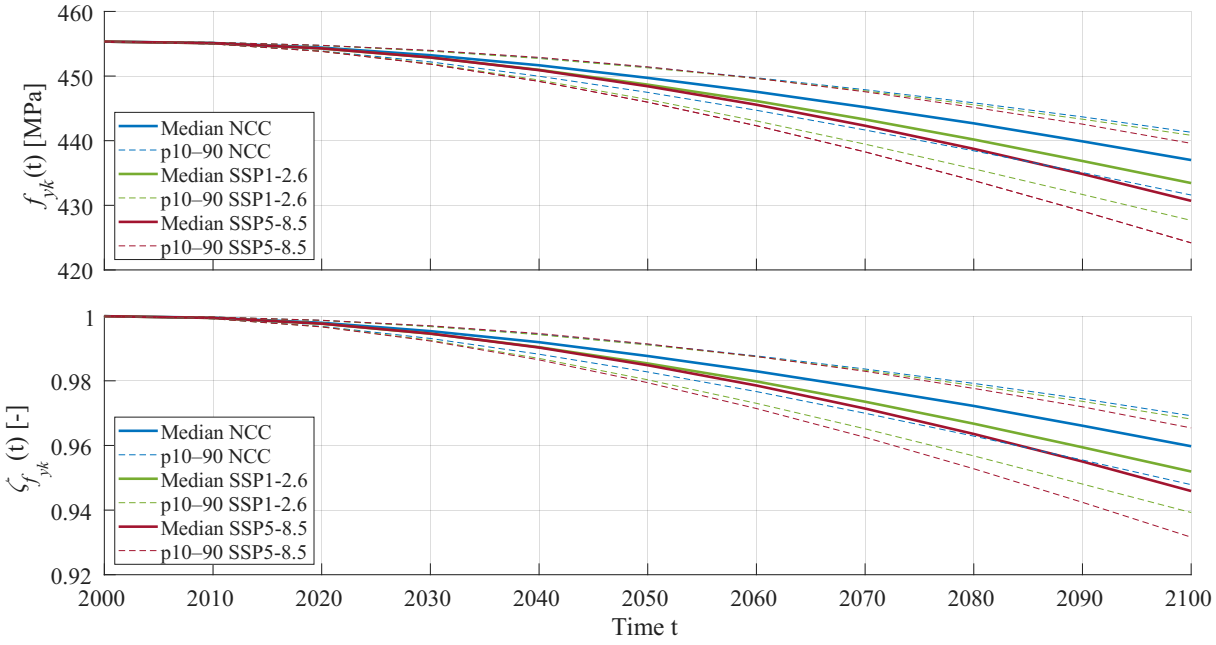

Figure 5.27: Evolution of the characteristic value (top) and the correction function (bottom) of the steel yielding strength for different climate change scenarios

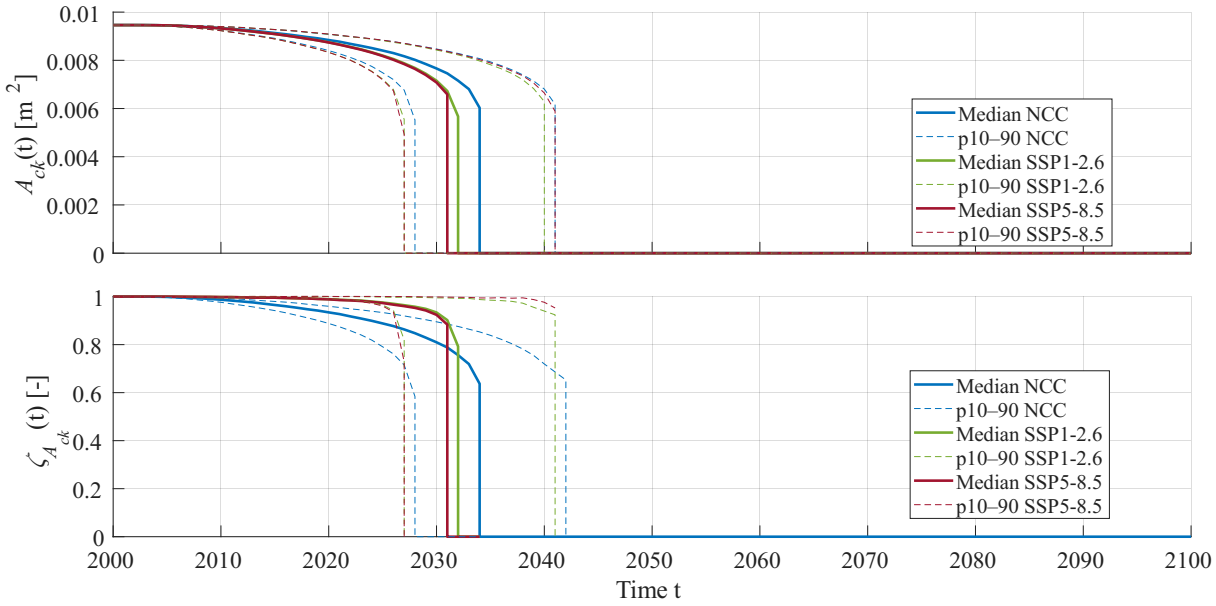

Figure 5.28: Evolution of the characteristic value (top) and the correction function (bottom) of the concrete cover area for different climate change scenarios.

Figures 5.29 - 5.31 show the evolution of the design values and the corresponding correction functions for the resisting parameters investigated for different climatic scenarios. The previous discussion provided for the results depicted in Figures 5.26 - 5.28 holds also for these ones. In addition, the design values are computed by assuming the resisting variable non-dominant ($\alpha_R = 0.32$) and dominant ($\alpha_R = 0.8$), as shown in the left and right side of the Figures, respectively. It can be observed that the decrease for the dominant case is much more significant than those for the non-dominant scenario. This is due to the fact that the dominant design values are located further in the tail of the distribution, which are more influenced by the corrosion process.

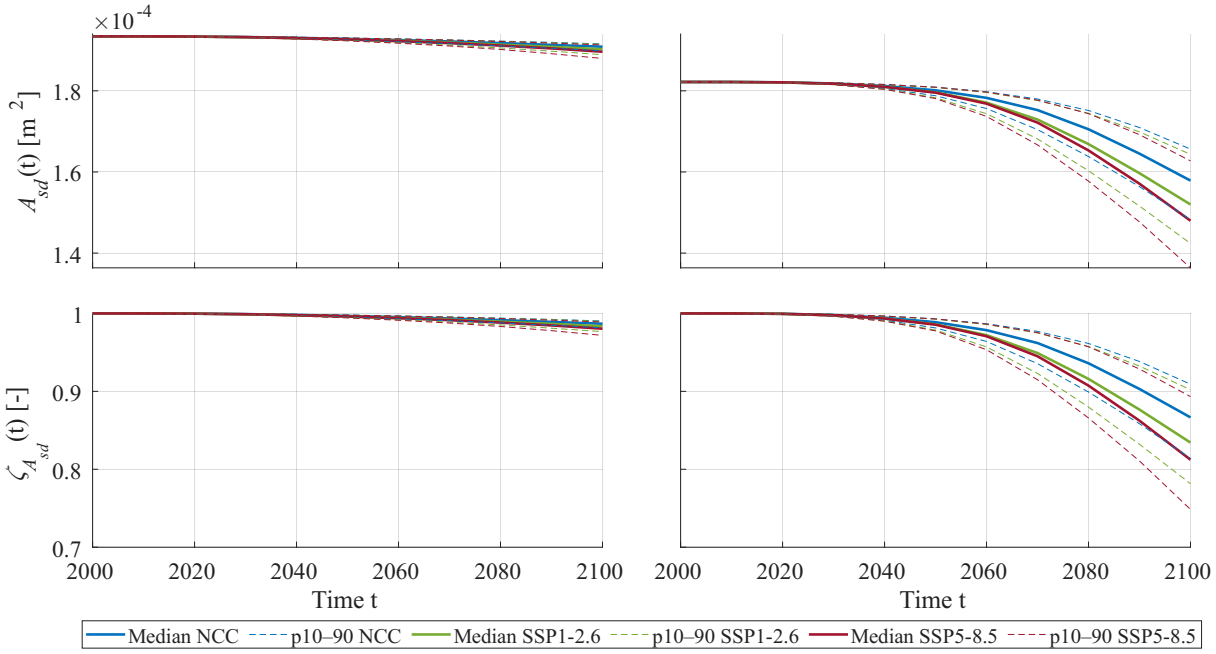

Figure 5.29: Evolution of the design value (top) and the correction function (bottom) of the steel area for different climate change scenarios (non-dominant case on the left side and dominant case on the right side).

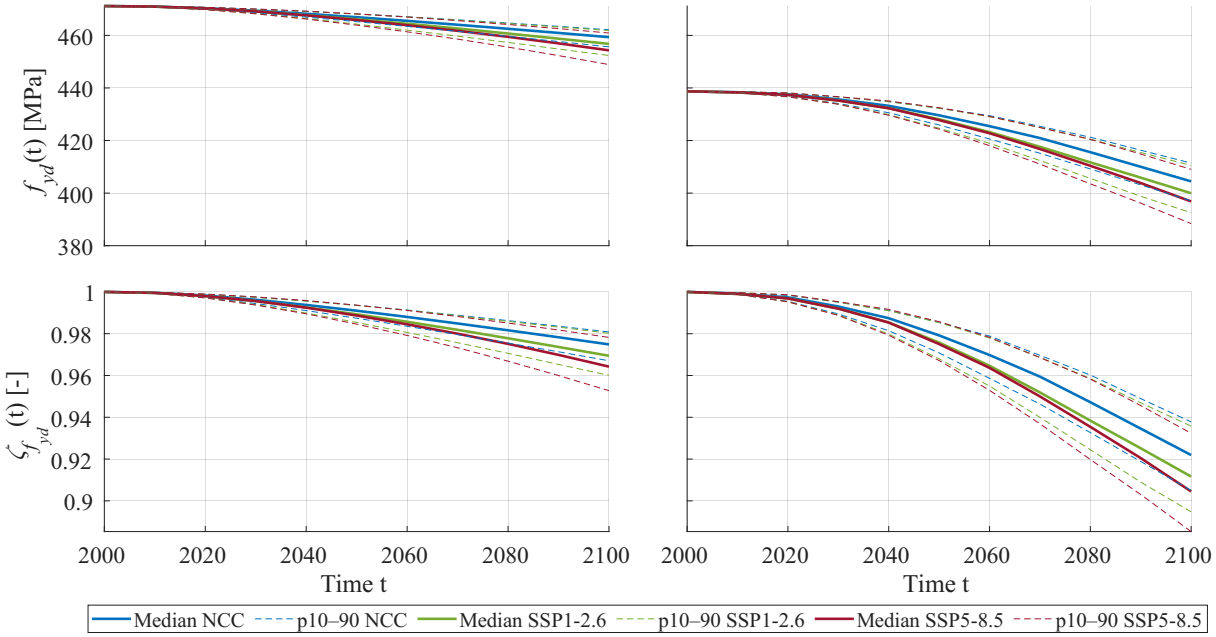

Figure 5.30: Evolution of the design value (top) and the correction function (bottom) of the steel yielding strength for different climate change scenarios (non-dominant case on the left side and dominant case on the right side).

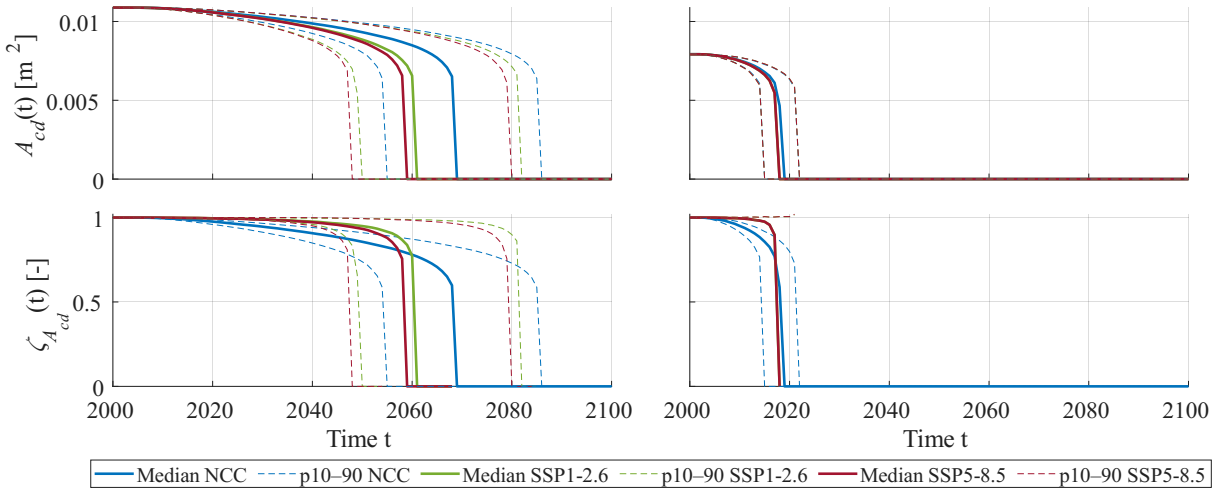

Figure 5.31: Evolution of the design value (top) and the correction function (bottom) of the concrete cover area for different climate change scenarios (non-dominant case on the left side and dominant case on the right side).

The partial safety factors for the steel reinforcement area, yielding strength, and concrete cover area are represented in Figures 5.32, 5.33, and 5.34, respectively. In the non-dominant case, the design values are greater than the characteristic values, resulting in partial safety factors smaller than 1 following a decreasing trend. On the other hand, considering the dominant case, the design values is smaller than the characteristic values, leading to partial safety factors greater than 1 following an increasing pattern over time. For a partial safety factor lower than 1, it is generally assumed the value of 1 for safety considerations. The partial safety factor γ_{Ac} (Figure 5.34) is definable only for characteristic values A_{ck} greater than zero, i.e., prior to the occurrence of spalling of the concrete cover.

The increases over time of the partial safety factors is the result of a larger spread of uncertainty due to corrosion-induced damage. In addition, this increase is exacerbated by climate change, which compounds the effects of corrosion.

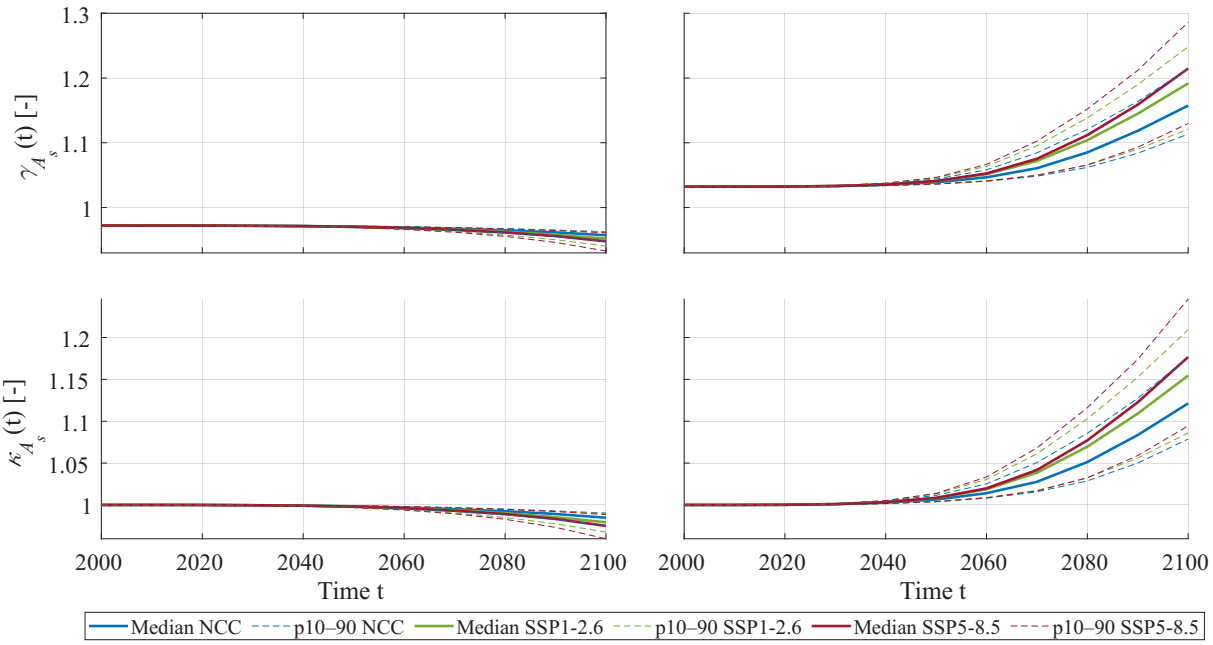

Figure 5.32: Evolution of the partial safety factor (top) and the correction function (bottom) of the steel area for different climate change scenarios (non-dominant case on the left side and dominant case on the right side).

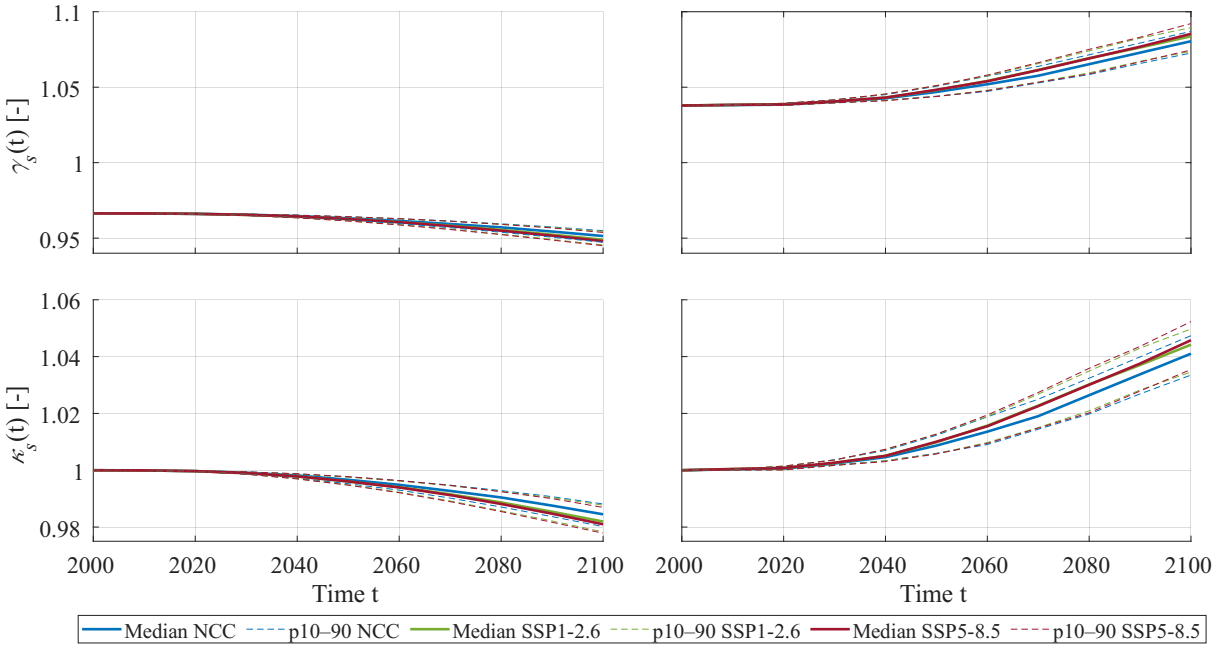

Figure 5.33: Evolution of the partial safety factor (top) and the correction function (bottom) of the steel yielding strength for different climate change scenarios (non-dominant case on the left side and dominant case on the right side).

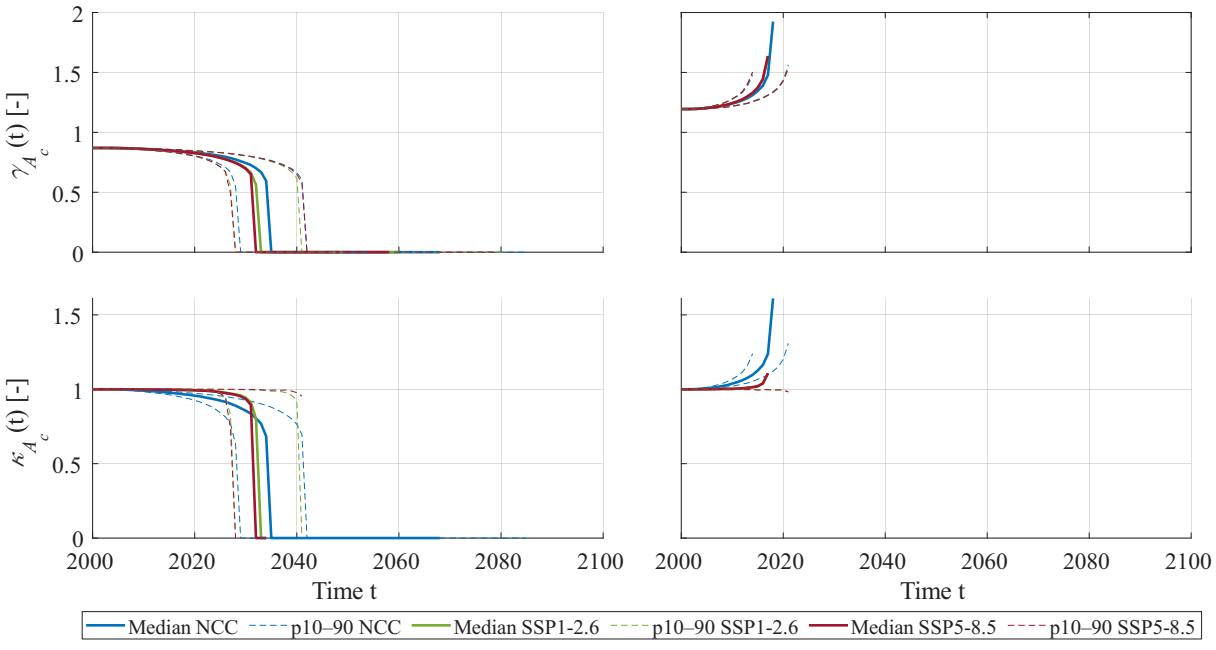

Figure 5.34: Evolution of the partial safety factor (top) and the correction function (bottom) of the concrete cover area for different climate change scenarios (non-dominant case on the left side and dominant case on the right side).

Given $A_{sd}(t)$, $f_{yd}(t)$, $A_{cd}(t)$, and f_{cd}, the design value of the ultimate bending moment $M_{rd}(t)$ may be defined as a function of the individual design values of the variables contributing to the overall bending resistance. $M_{rd}(t)$ is evaluated considering the:

- the Reference Partial Safety Format (PSF_{ref}): the design values are considered only for yielding strength $f_y(t)$ and the concrete compressive strength f_c, while the nominal values of steel area and concrete cover are defined through their mean values $A_{s,m}(t)$ and $A_{c,m}(t)$; moreover, two scenarios are analyzed:
  - all resisting variable non-dominant $\alpha_{f_y} = \alpha_{f_c} = 0.32$;
  - all resisting variable dominant $\alpha_{f_y} = \alpha_{f_c} = 0.8$;
- the Modified Partial Safety Format (PSF_{mod}): the design values are considered for $f_y(t)$, $A_s(t)$, f_c, and $A_c(t)$; moreover, two scenarios are analyzed:
  - all resisting variable non-dominant $\alpha_{f_y} = \alpha_{A_s} = \alpha_{f_c} = \alpha_{A_c} = 0.32$;
  - all resisting variable dominant $\alpha_{f_y} = \alpha_{A_s} = \alpha_{f_c} = \alpha_{A_c} = 0.8$.

The results are reported in Figure 5.35. It is observed that PSF_{ref} leads to greater values of $M_{rd}(t)$ over time due to the consideration of mean values for the reduction of the steel area and concrete cover, rather than their design values. The reference strategy PSF_{ref} is also inadequate for capturing the spalling of the concrete cover. Moreover, considering non-dominant the different resisting variables, $M_{rd}(t)$ show a less significant decrease with respect to the dominant case for both PSF_{ref} and PSF_{mod}.

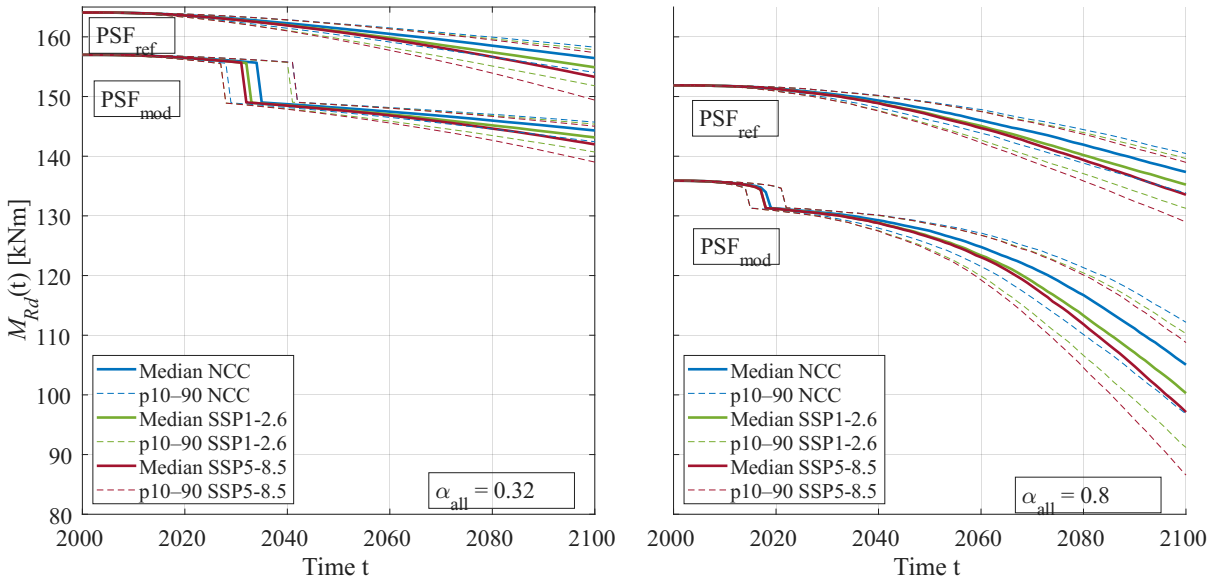

Figure 5.35: Comparison between the reference and modified PSF for different climate change scenarios (non-dominant case on the left side and dominant case on the right side).

Global Safety Format

The structural capacity of the RC beam under consideration may also be evaluated using the global safety format (Section 3.4.2). The global resistance is assumed to be described by the ultimate bending moment M_R.

The evolution of the mean value M_{Rm} and the corresponding correction function ρ_{Rm} for various climatic scenarios is illustrated in Figures 5.36. Analogously to the pattern observed for the PSF, corrosion results in a decrease in M_{rm} over time (NCC scenario). Climate change exacerbates this decrease, contingent upon the considered scenario, with smaller and greater enhancements for SSP1-2.6 and SSP5-8.5, respectively. The dashed lines provide simplified information regarding the uncertainty associated with climate change projections. They represent the mean value calculated based on the projections of environmental variables at the 10th and 90th percentiles.

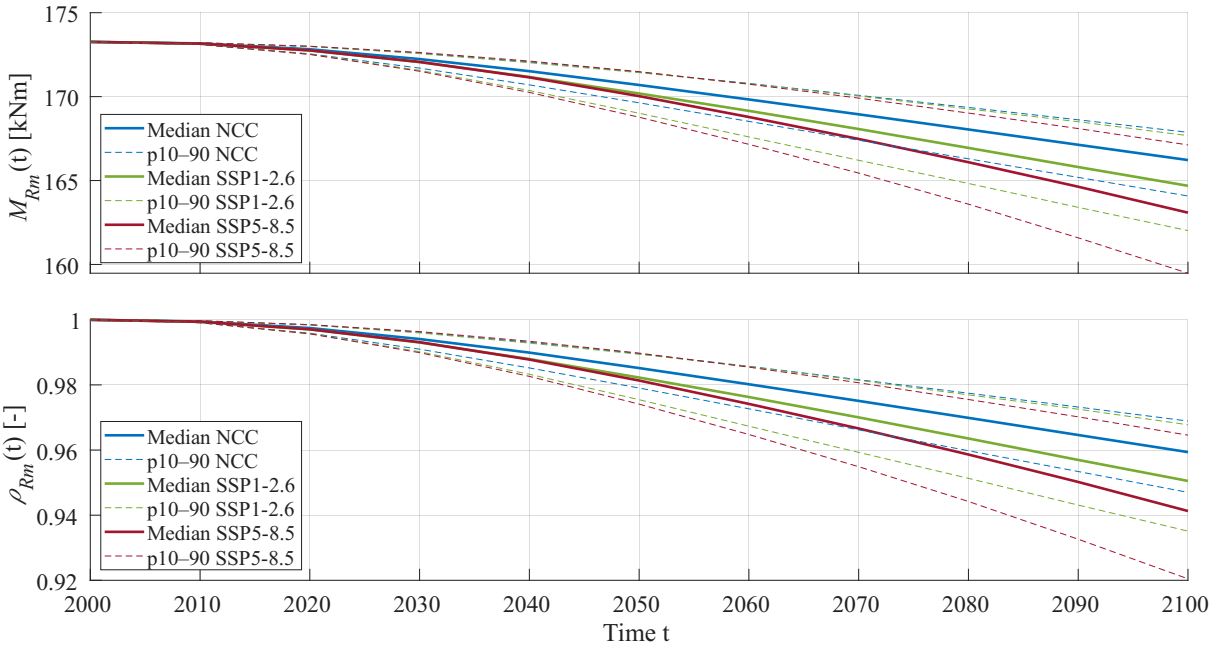

Figure 5.36: Evolution of the mean value (top) and the correction function (bottom) of the ultimate bending moment for different climate change scenarios.

A decreasing trend is also observed for the design value M_{Rd}, assuming dominant variable ($\alpha_R = 0.8$), as shown in Figure 5.37. The decrease of M_{Rd} is more significant than the one of M_{Rm}, since the design value lays further in the tail and consequently it is more impacted by the corrosion process.

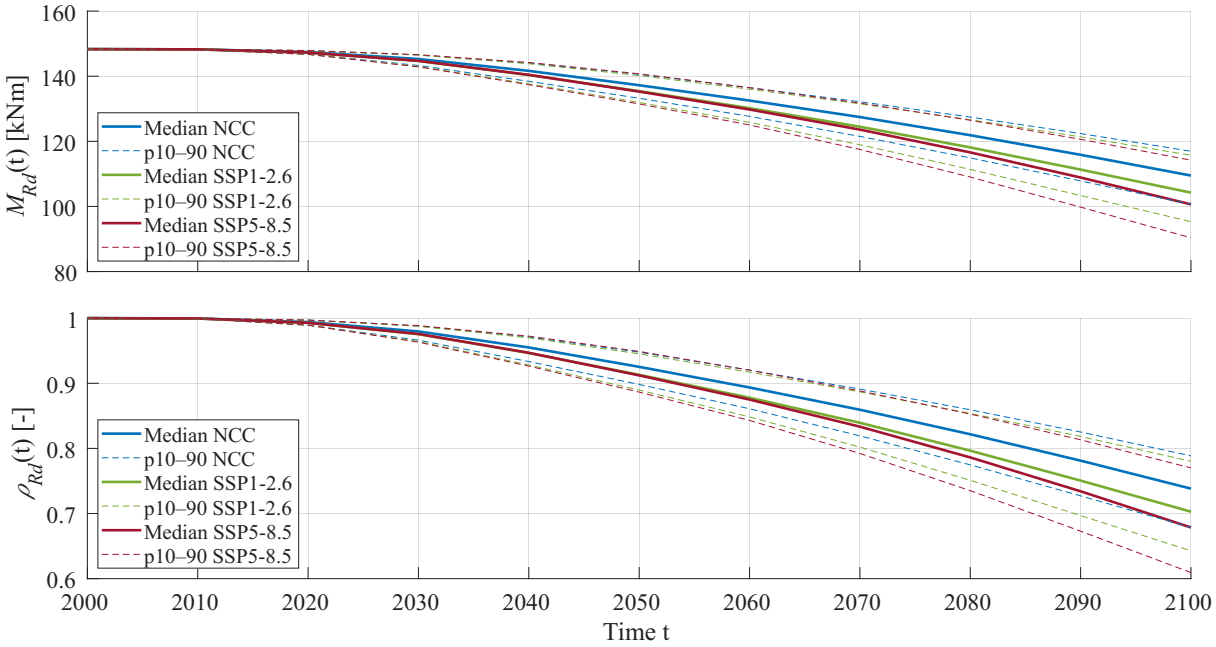

Figure 5.37: Evolution of the design value (top) and the correction function (bottom) of the ultimate bending moment for different climate change scenarios.

The global safety factor γ_R for the ultimate bending moment is represented in Figure 5.38. It is possible to observe that γ_R increases over time, resulting from a larger spread of uncertainty due to corrosion-induced damage. Moreover, this increase is exacerbated by climate change, which compounds the effects of corrosion.

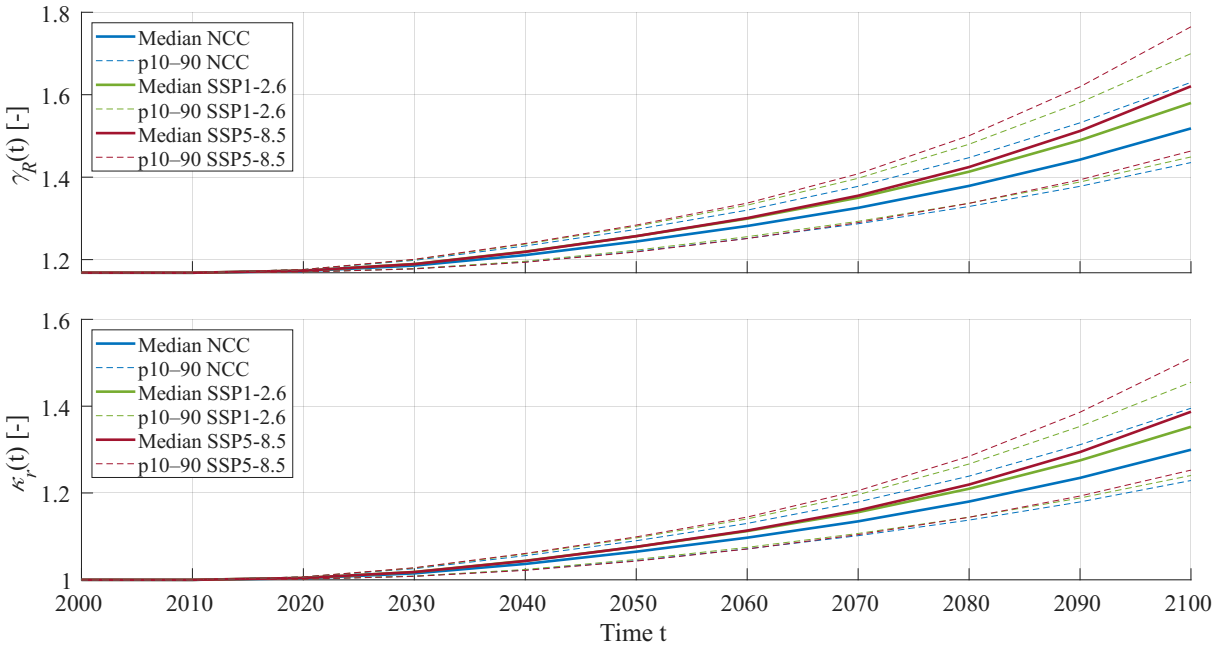

Figure 5.38: Evolution of the global safety factor (top) and the correction function (bottom) of the ultimate bending moment for different climate change scenarios.

The GSF is capable of integrating all the uncertainties related to climate change-induced corrosion into a single global safety factor, being particularly practical in the context of semi-probabilistic assessments. Indeed, this format may reduce the complexity of the incorporation of multiple partial safety factors as well as providing more accurate estimation of the overall resistance. A comparison between the PSF and the GSF is discussed in the following.

Comparison between Partial and Global Safety Format

The peculiarities of the applied PSF and GSF are discussed in relation to the design value of the ultimate bending moment. For this purpose, M_{Rd} is using in the following formats:

- Case 1: Global Safety Format (GSF), assuming:
  - dominant $\alpha_{M_R} = 0.8$;
- Case 2: Modified Partial Safety Format (PSF_{mod}), assuming:
  - non-dominant $\alpha_{f_y} = \alpha_{f_c} = \alpha_{A_c} = 0.32$ and dominant $\alpha_{A_s} = 0.8$;
- Case 3: Reference Partial Safety Format (PSF_{ref}), assuming:
  - non-dominant $\alpha_{f_c} = 0.32$ and dominant $\alpha_{f_y} = 0.8$.

The results are shown in Figure 5.39, where GSF is compared with the PSF_{mod} (left side of the Figure) and PSF_{ref} (right side of the Figure).

It is observed that M_{Rd} obtained for PSF_{mod} is very close to the one estimated with GSF at the initial time. After the loss of the concrete cover, the results start to diverge, each decreasing at different rates. Considering PSF_{ref}, M_{Rd} is overestimated even at the initial time with a slower decrease respect to both PSF_{mod} and GSF due to the incorporation of the steel area and concrete cover area as mean values, and consequently unable to represent the effect of corrosion at failure. The M_{Rd} obtained with GSF does not exhibit any sudden drop, since it directly models the ultimate bending moment integrating all the different damages involved and then evaluate M_{Rd}. The result obtained by GSF represents the resistance through the actual combination of uncertainty, while the PSF account for the individual uncertainties of the resisting parameters contributing to the global resistance. For this reason, the GSF is recommended for the semi-probabilistic assessment of RC structures under climate change-induced corrosion.

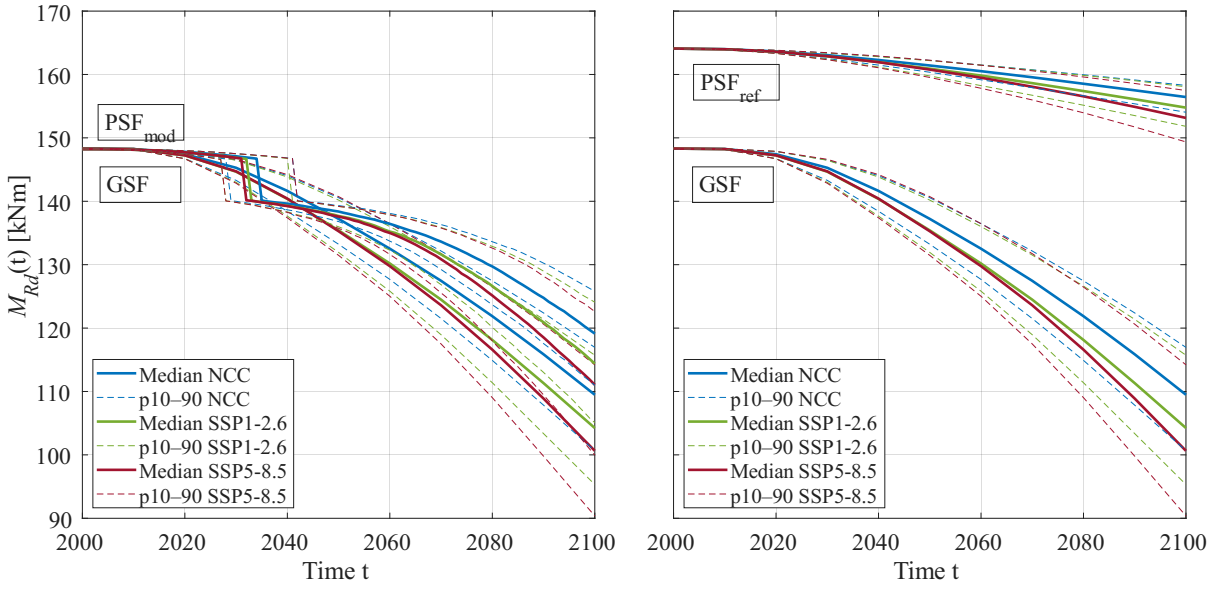

Figure 5.39: Evolution of the design value of the ultimate bending moment for different semi-probabilistic formats (PSF_{mod} - GSF on the left side and PSF_{ref} - GSF on the right side).

5.2.2.2 Impact of Space Variability

The reference study presents results that are applicable at the national scale in France. However, climatic data depend on local surrounding conditions and may vary significantly from a region to another. For this reason, regional climate models typically have a finer spatial resolution, such as grid-sizes of approximately 50 km or even 12 km (Jacob, Petersen, Eggert, Alias, Christensen, et al., 2014), thereby allowing for a detailed analysis at the local scale.

In the standards for civil engineering, a compromise between variability and applicability is achieved through the definition of a limited number of sub-national entities that reflect similar climatic conditions across the national territory. For example, in the context of metropolitan France, the national annexes of the Eurocodes delineate 8 regions concerning the characteristic value of snow load (CEN, 2007), 4 regions pertaining to basic wind speed (CEN, 2008), and provide maximum and minimum temperature values for 96 departments (CEN, 2004b). The same concept can be applied considering that chloride-induced corrosion is significantly influenced by surrounding environmental conditions. For the sake of this analysis, the 5 main climate groups in France are considered (Météo France, 2025), and for each of them a representative administrative region is evaluated:

- Oceanic Climate: Poitou-Charentes region (Figure 5.40);
- Altered Oceanic Climate: Ile-de-France region (Figure 5.41);

- Semi-continental Climate: Alsace region (Figure 5.42);

- Mountain Climate: Rhone-Alpes region (Figure 5.43);

- Mediterranean Climate: Corse region (Figure 5.44).

The data are retrieved from the Climate Change Knowledge Portal (WorldBankGroup, 2025) for the selected regions. In Figures 5.40 - 5.44, the regional projections are compared with the national projections regarding mean surface air temperature T and relative humidity RH.

From these projections, it can be observed that T ranges between 8 °C and 20 °C, while RH varies between 68% and 80% for all the different regions. The highest and lowest temperatures are recorded in Corse and Rhone-Alpes, respectively; Ile-de-France exhibits a very similar temperature evolution respect to the one observed for France. In addition, the highest and lowest relative humidity is expected in Ile-de-France and Rhone-Alpes, respectively; Poitou-Charentes and Alsace exhibit a relative humidity evolution similar to the one at the national scale.

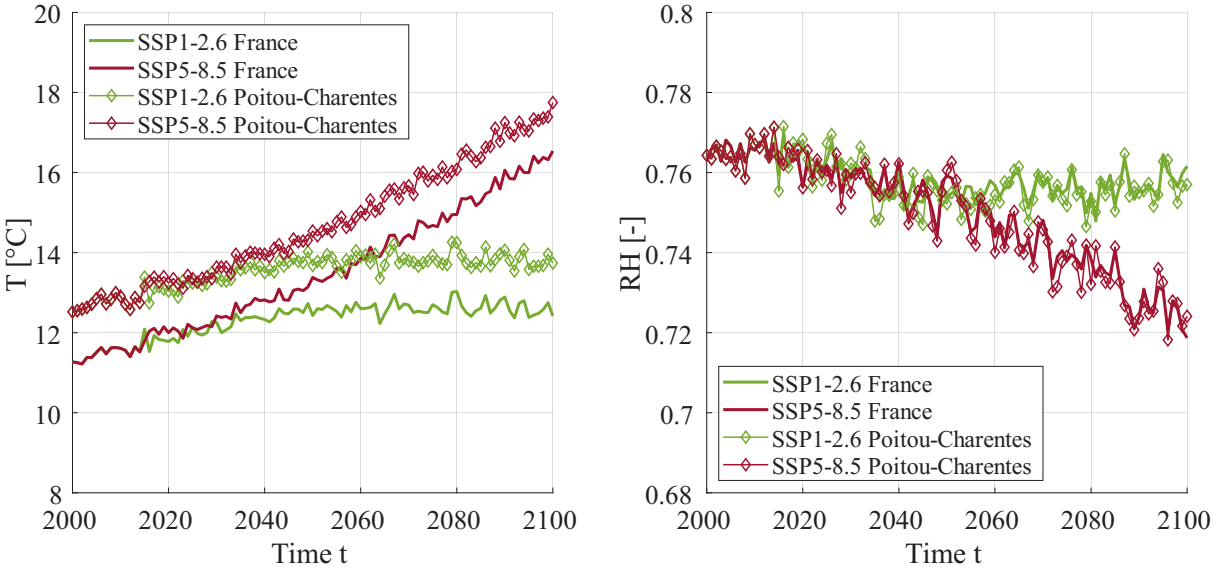

Figure 5.40: Projected temperature and relative humidity in Poitou-Charentes VS France.

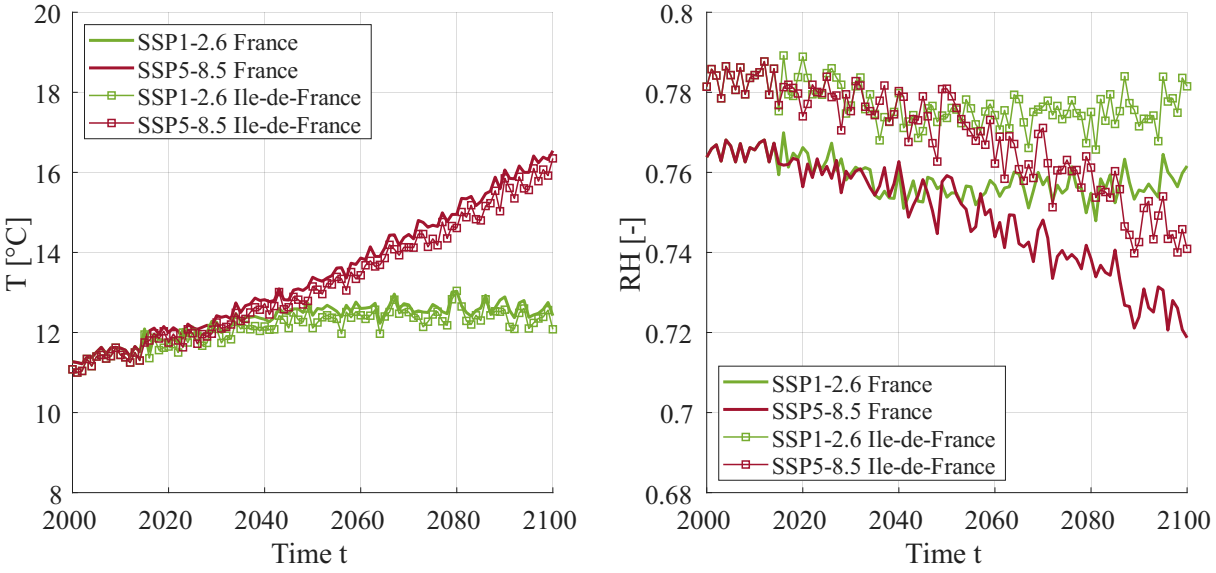

Figure 5.41: Projected temperature and relative humidity in Ile-de-France VS France.

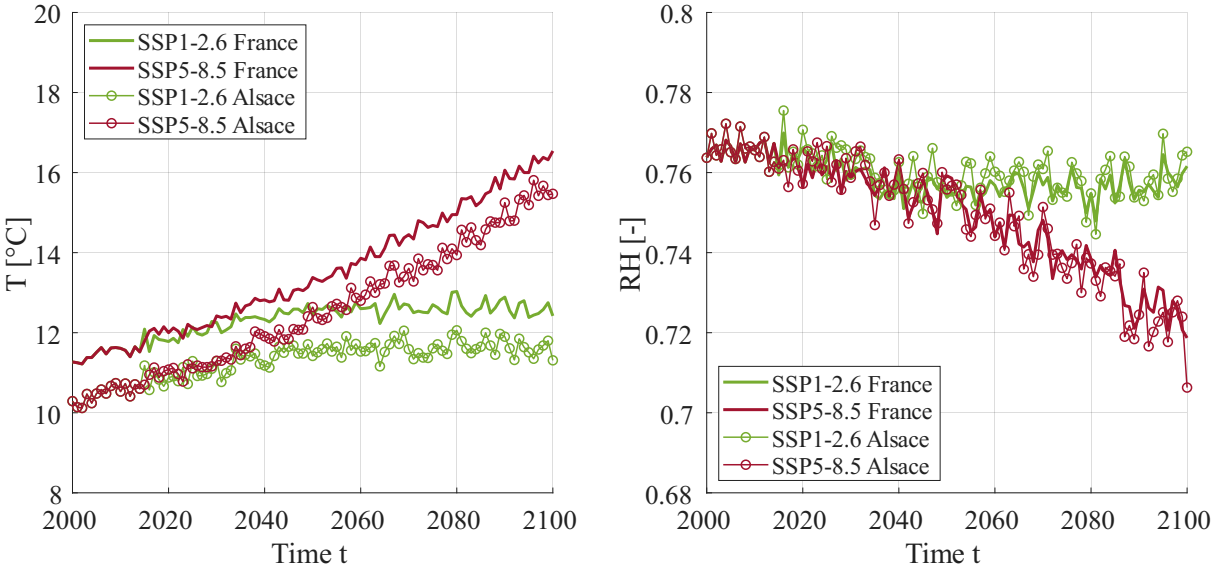

Figure 5.42: Projected temperature and relative humidity in Alsace VS France.

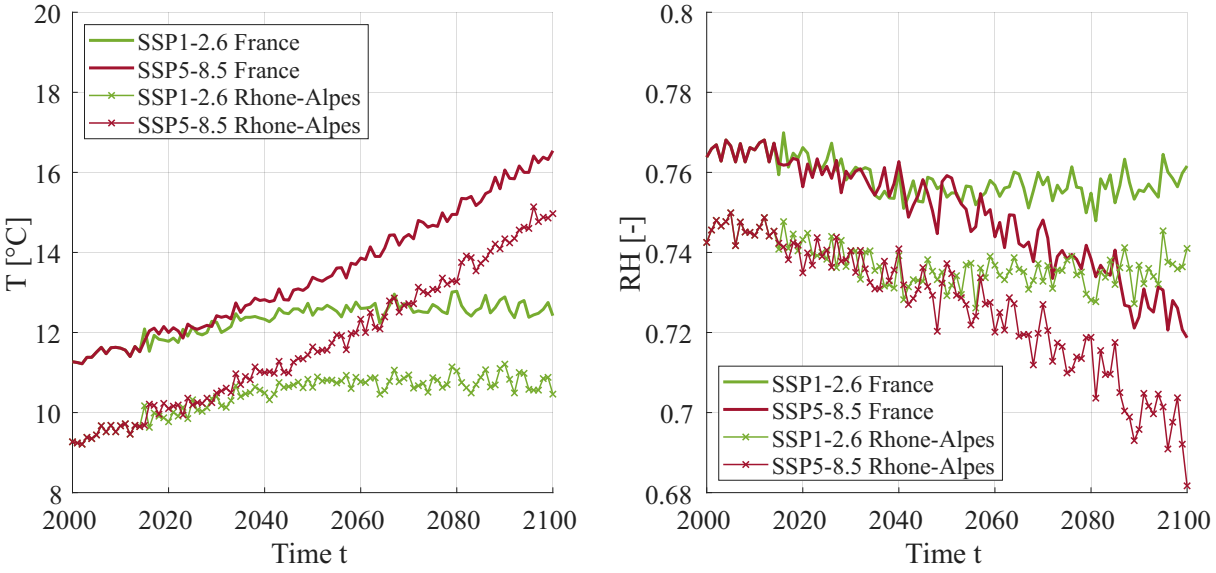

Figure 5.43: Projected temperature and relative humidity in Rhone-Alpes VS France.

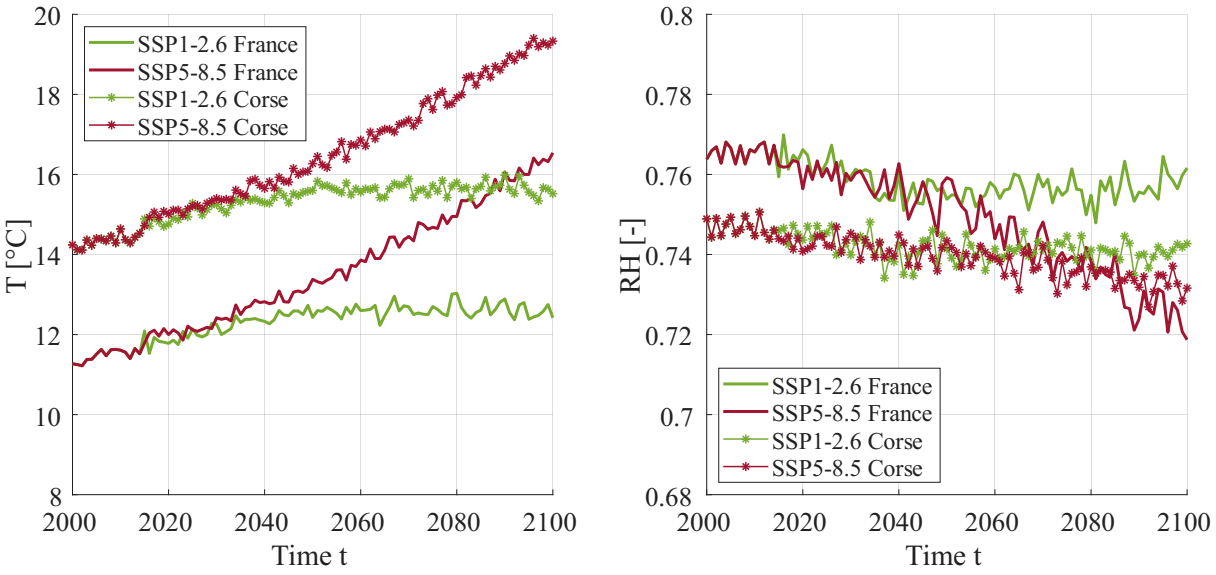

Figure 5.44: Projected temperature and relative humidity in Corse VS France.

A life-cycle reliability analysis is performed to retrieve the time-variant reliability index assuming the RC beam located in the different regions (Figure 5.45). The Figure shows the impact of the local on the beam reliability. Depending on the region, corrosion initiation may be faster or slower and propagation may be more or less severe. For the considered cases, the most favorable environmental conditions for corrosion are reported for Corse (Mediterranean climate), leading to the largest decrease in the reliability index, while the opposite is predicted in Rhone-Alpes (mountain climate).

The evolution of the mean value $M_{Rm}(t)$ and the design value $M_{Rd}(t)$ of the ultimate bending moment is shown in Figure 5.46. For the sake of graphical clarity, only the

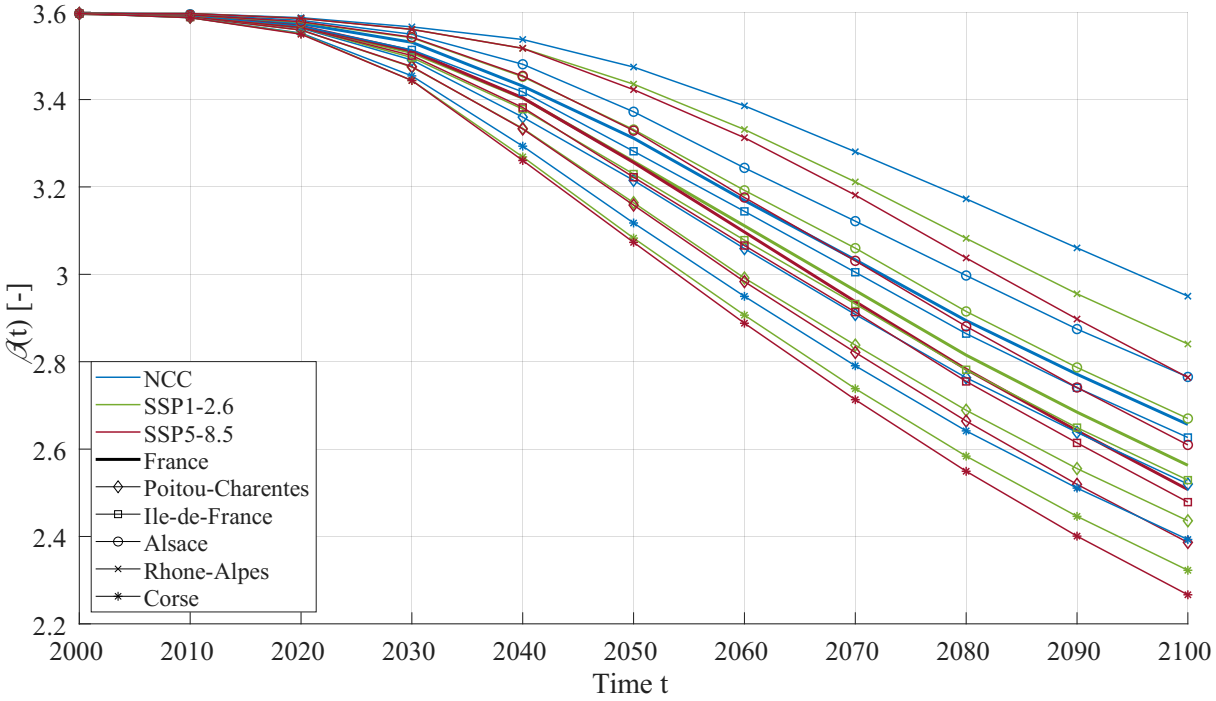

Figure 5.45: Evolution of the reliability index of the aging RC beam under climate change for different French regions.

reference case and the extreme regional cases (Corse and Rhone-Alpes) are represented. The decrease in $M_{Rm}(t)$ and $M_{Rd}(t)$ is more significant in Corse due to the environmental conditions that are more prone to corrosion, while the opposite is observed for Rhone-Alpes. This decrease is exacerbated by climatic evolution, the severity of which depends on the selected climate change trajectory. The correction functions for the mean value ρ_{Rm} and design value ρ_{Rd} are shown in Figure 5.47.

Eventually, the global safety factor γ_R and the correction function κ_r are represented in Figure 5.48. γ_R increases over time more significantly for Corse due to the more favorable conditions for corrosion, as discussed previously. In addition, this increase is intensified by climate change. The values of the correction functions of the mean value and safety factor are compared in Table 5.3 considering different scenarios of climate change, the regional climate, and the time. The design values may be computed using the data reported in the Table 5.3 and the equations defined in Section 5.1.2.

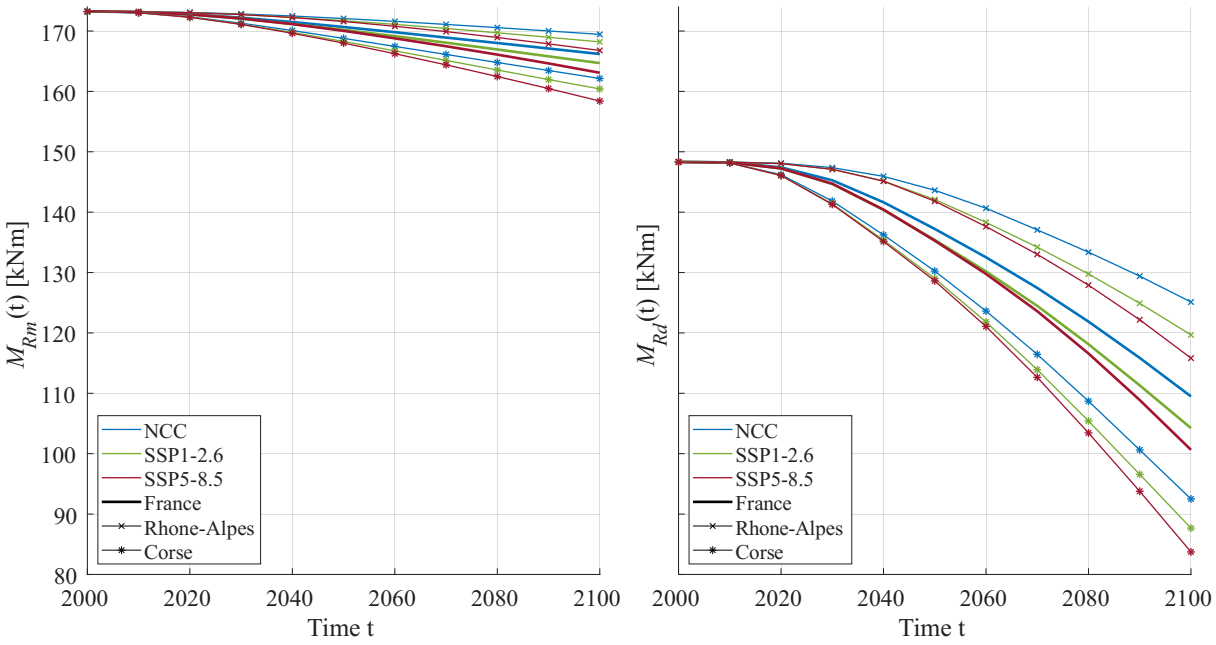

Figure 5.46: Evolution of the mean value (left side) and the design value (right side) of the ultimate bending moment for selected French climates.

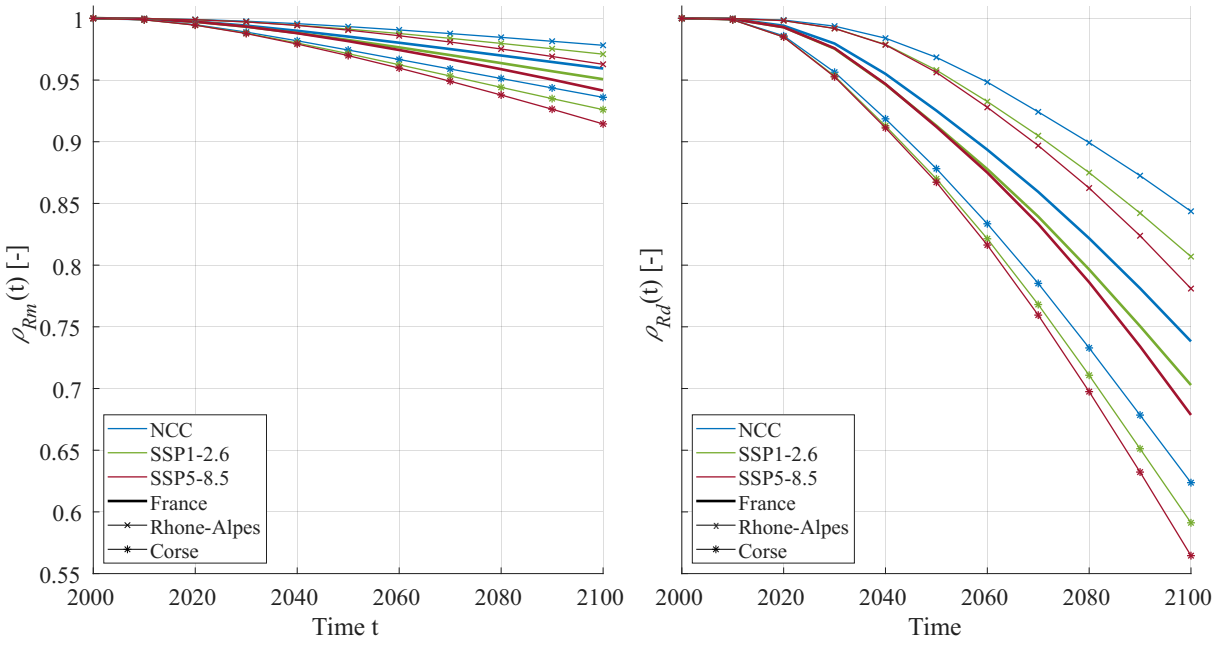

Figure 5.47: Evolution of the correction functions for the mean value (left side) and for the design value (right side) of the ultimate bending moment under climate change for selected French climates.

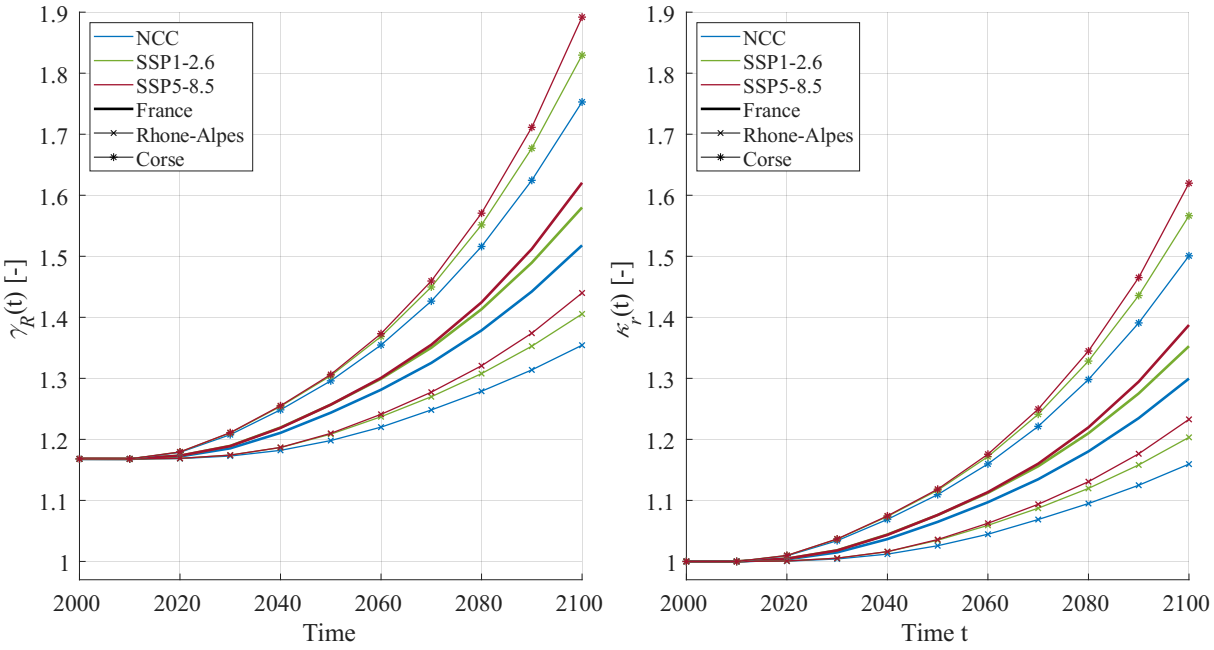

Figure 5.48: Evolution of the safety factor and correction function of the ultimate bending moment for selected French climates.

Parameter	Region	Climate	t = 2000	t = 2020	t = 2040	t = 2060	t = 2080	t = 2100
$\rho_{\mathrm{Rm,det}}$	Poitou–Charentes	Oceanic	1.00	1.00	0.99	0.97	0.96	0.95
	Ile-de-France	Altered oceanic	1.00	1.00	0.99	0.98	0.97	0.96
	Alsace	Semi-continental	1.00	1.00	0.99	0.98	0.98	0.97
	Rhone–Alpes	Mountain	1.00	1.00	1.00	0.99	0.98	0.98
	Corse	Mediterranean	1.00	0.99	0.98	0.97	0.95	0.94
$\rho_{\mathrm{Rm,det_{SSP1}}}$	Poitou–Charentes	Oceanic	1.00	1.00	1.00	1.00	0.99	0.99
	Ile-de-France	Altered oceanic	1.00	1.00	1.00	1.00	0.99	0.99
	Alsace	Semi-continental	1.00	1.00	1.00	1.00	0.99	0.99
	Rhone–Alpes	Mountain	1.00	1.00	1.00	1.00	1.00	0.99
	Corse	Mediterranean	1.00	1.00	1.00	1.00	0.99	0.99
$\rho_{\mathrm{Rm,det_{SSP5}}}$	Poitou–Charentes	Oceanic	1.00	1.00	1.00	0.99	0.99	0.98
	Ile-de-France	Altered oceanic	1.00	1.00	1.00	0.99	0.99	0.98
	Alsace	Semi-continental	1.00	1.00	1.00	0.99	0.99	0.98
	Rhone–Alpes	Mountain	1.00	1.00	1.00	1.00	0.99	0.98
	Corse	Mediterranean	1.00	1.00	1.00	0.99	0.99	0.98
$\kappa_{\mathrm{r,det}}$	Poitou–Charentes	Oceanic	1.00	1.01	1.05	1.13	1.23	1.39
	Ile-de-France	Altered oceanic	1.00	1.00	1.04	1.10	1.19	1.31
	Alsace	Semi-continental	1.00	1.00	1.03	1.08	1.15	1.24
	Rhone–Alpes	Mountain	1.00	1.00	1.01	1.04	1.09	1.16
	Corse	Mediterranean	1.00	1.01	1.07	1.16	1.30	1.50
$\kappa_{\mathrm{r,det_{SSP1}}}$	Poitou–Charentes	Oceanic	1.00	1.00	1.01	1.02	1.03	1.05
	Ile-de-France	Altered oceanic	1.00	1.00	1.01	1.02	1.03	1.05
	Alsace	Semi-continental	1.00	1.00	1.01	1.01	1.02	1.03
	Rhone–Alpes	Mountain	1.00	1.00	1.00	1.01	1.02	1.04
	Corse	Mediterranean	1.00	1.00	1.01	1.01	1.02	1.04
$\kappa_{\mathrm{r,det_{SSP5}}}$	Poitou–Charentes	Oceanic	1.00	1.00	1.01	1.02	1.04	1.07
	Ile-de-France	Altered oceanic	1.00	1.00	1.01	1.02	1.03	1.06
	Alsace	Semi-continental	1.00	1.00	1.01	1.01	1.03	1.06
	Rhone–Alpes	Mountain	1.00	1.00	1.00	1.02	1.03	1.06
	Corse	Mediterranean	1.00	1.00	1.01	1.01	1.04	1.08

Table 5.3: Comparison of the correction functions for selected regions under different climate scenarios.

Both correction functions for NCC scenarios $\rho_{rm,det}$ and $\rho_{rd,det}$ are based on the assumption of a stationary climate, in which corrosion is not influenced by temporal changes in environmental parameters. Normalizing the resistance obtained considering the climate change scenario $M_{Rdet_{cc}}$ by the one neglecting climate change $M_{Rdet,ref}$ of the reference case study, it is possible to isolate the effect of climate change from the corrosion one (Figures 5.49 and 5.50).

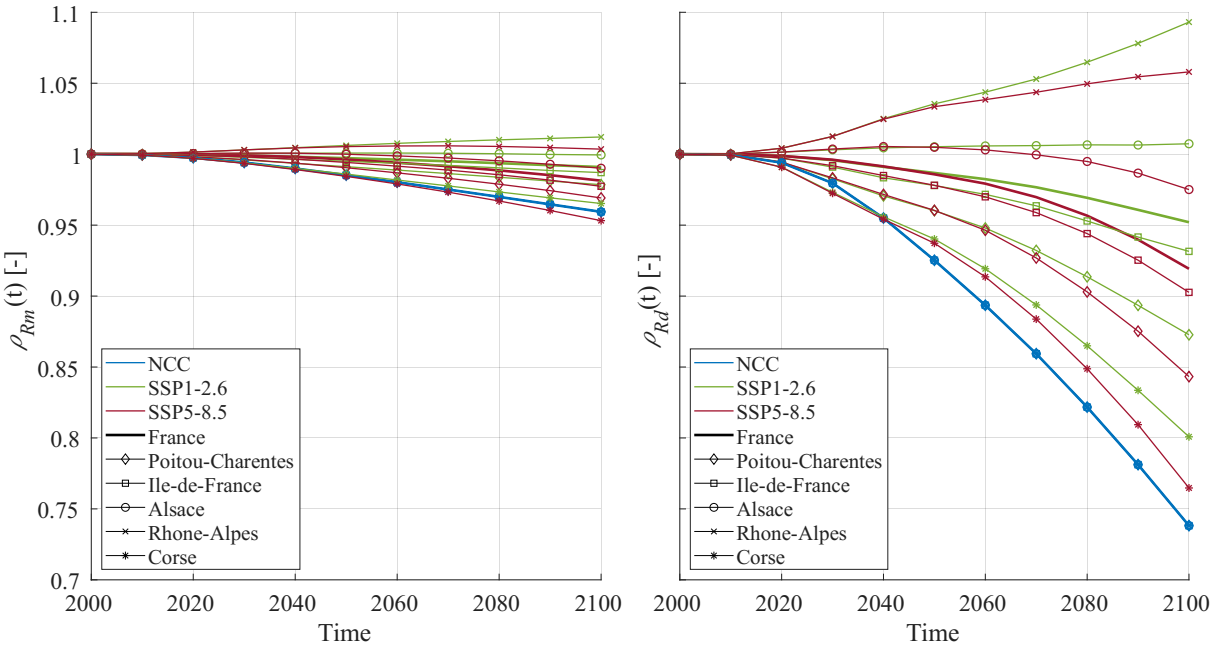

Figure 5.49: Evolution of the normalized correction function for the mean values (left side) and for the design values (right side) of the ultimate bending moment for selected French climates.

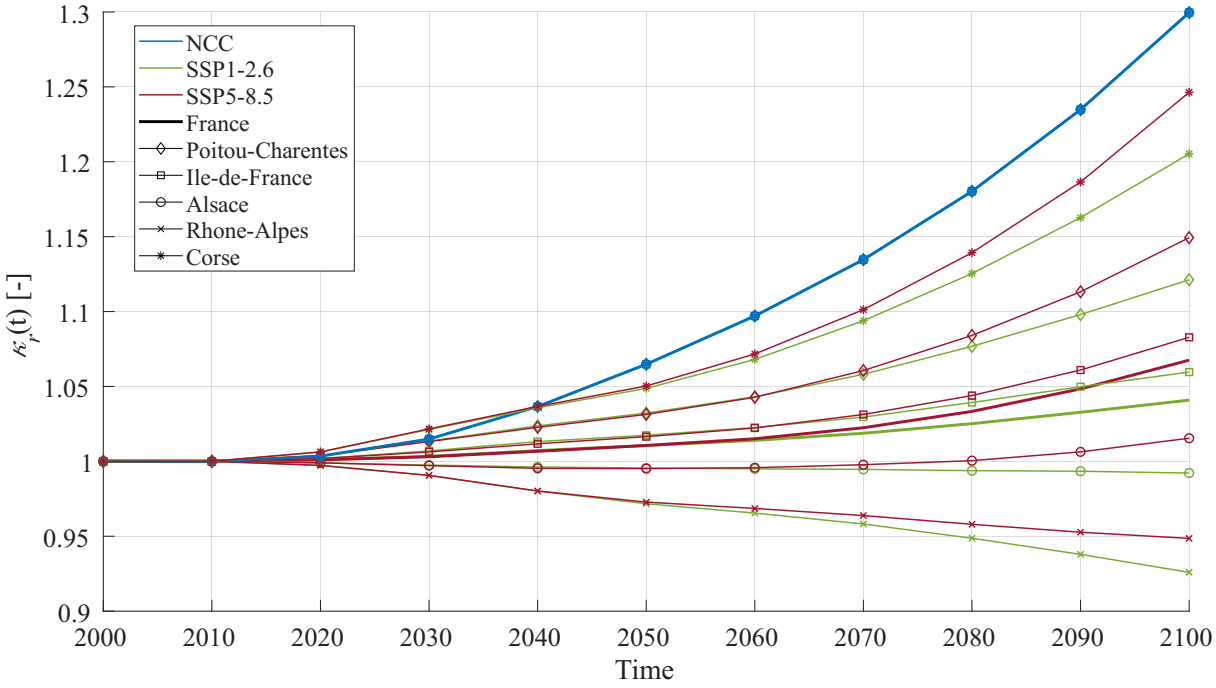

Figure 5.50: Evolution of the normalized correction function for the the safety factors of the ultimate bending moment for selected French climates.

The results of this analysis underscore the critical necessity of utilizing regional and local environmental projections to obtain reliable reliability elements of the semi-probabilistic methodology. A primary evidence is that corrosion-induced damage is highly sensitive to localized environmental variables; consequently, national-level spatial aggregates often fail to capture the unique micro-climates and site-specific conditions inherent to a actual location of the structure.

It is important to clarify that the comparison presented between national and regional assessments serves the specific purpose of highlighting the sensitivity of the results to spatial scale. In practice, a clear distinction must be maintained between national scale, which is useful for broad policy-making and general overviews, regional scale, which provides the necessary resolution for standard engineering design, and local/micro-scale, which is recommended for strategic or high-value structures, as environmental stressors can exhibit significant gradients even within a single region.

Furthermore, this study applies an equal surface chloride concentration C_s across both national and regional scales. While this assumption is physically unrealistic, given the high stochastic variability of chloride concentration across different locations, it is adopted as a controlled variable to decouple the impact of climatic spatial scales from chloride abundance.

5.2.2.3 Impact of Corrosion Aggressiveness

The reference study is analyzed for different corrosion aggressiveness scenarios. In the case of chloride-induced corrosion, Eurocode (CEN, 2005) defines 6 exposure classes distinguishing between different sources of chlorides, as reported in Table 5.4.

Corrosion induced by chlorides		
XD1	Moderate humidity	Concrete surfaces exposed to airborne chlorides
XD2	Wet, rarely dry	Swimming pools Concrete components exposed to industrial waters containing chlorides
XD3	Cyclic wet and dry	Parts of bridges exposed to spray containing chlorides Pavements Car park slabs
Corrosion induced by chlorides from sea water		
XS1	Exposed to airborne salt but not in direct contact with sea water	Structures near to or on the coast
XS2	Permanently submerged	Parts of marine structures
XS3	Tidal, splash and spray zones	Parts of marine structures

Table 5.4: Exposure classes related to corrosion induced by chlorides according to CEN (2005).

Based on this table, four environmental aggressiveness scenarios are selected for the analysis and modeled according to the values proposed in the Tables 4.2 and 4.5. The selected scenarios are reported in Table 5.5.

A life-cycle reliability analysis is performed to retrieve the time-variant reliability index assuming that the RC beam is subjected to the 4 different environmental aggressiveness conditions. The Figure illustrates how the structural reliability of the RC beam, and consequently the probability of failure, is influenced by the environmental aggressiveness. For the considered cases, the least severe scenario is XD2-Cl1 because the wet environment limits the corrosion rate to a very low value. In contrast, the most severe scenario is XD3-Cl2, characterized by both the highest initial chloride concentration and corrosion rate.

The evolution of the mean value $M_{Rm}(t)$ and the design value $M_{Rd}(t)$ of the resisting bending moment is shown in Figure 5.52. The decrease in $M_{Rm}(t)$ and $M_{Rd}(t)$ is more significant for the scenario XD3-Cl2 due to severe aggressiveness, while the opposite is observed for XD2-Cl1. Climate change exacerbates this reduction, with the magnitude of the impact contingent upon the specific climatic projection considered. The correction functions for the mean value ρ_{Rm} and design value ρ_{Rd} are shown in Figure 5.53.

Aggressiveness Level	C_s [wt.%/cem] (fib, 2015)	$i_{corr,ref}$ [µA/cm^2] (DuraCrete, 1998)
XD1-Cl2	XD1	Cyclic wet-dry
	$\mu = 1$ $\sigma = 0.75 \cdot \mu$	$\mu = 2.586$ $\sigma = 1.724$
XD2-Cl1	XD2	Wet rarely-dry
	$\mu = 3$ $\sigma = 0.75 \cdot \mu$	$\mu = 0.345$ $\sigma = 0.259$
XD3-Cl2	XD3	Cyclic wet-dry
	$\mu = 3$ $\sigma = 0.75 \cdot \mu$	$\mu = 2.586$ $\sigma = 1.724$
XS1-Cl2	XS1	Cyclic wet-dry
	$\mu = 1.5$ $\sigma = 0.45 \cdot \mu$	$\mu = 2.586$ $\sigma = 1.724$

Table 5.5: Selected corrosion aggressiveness scenarios.

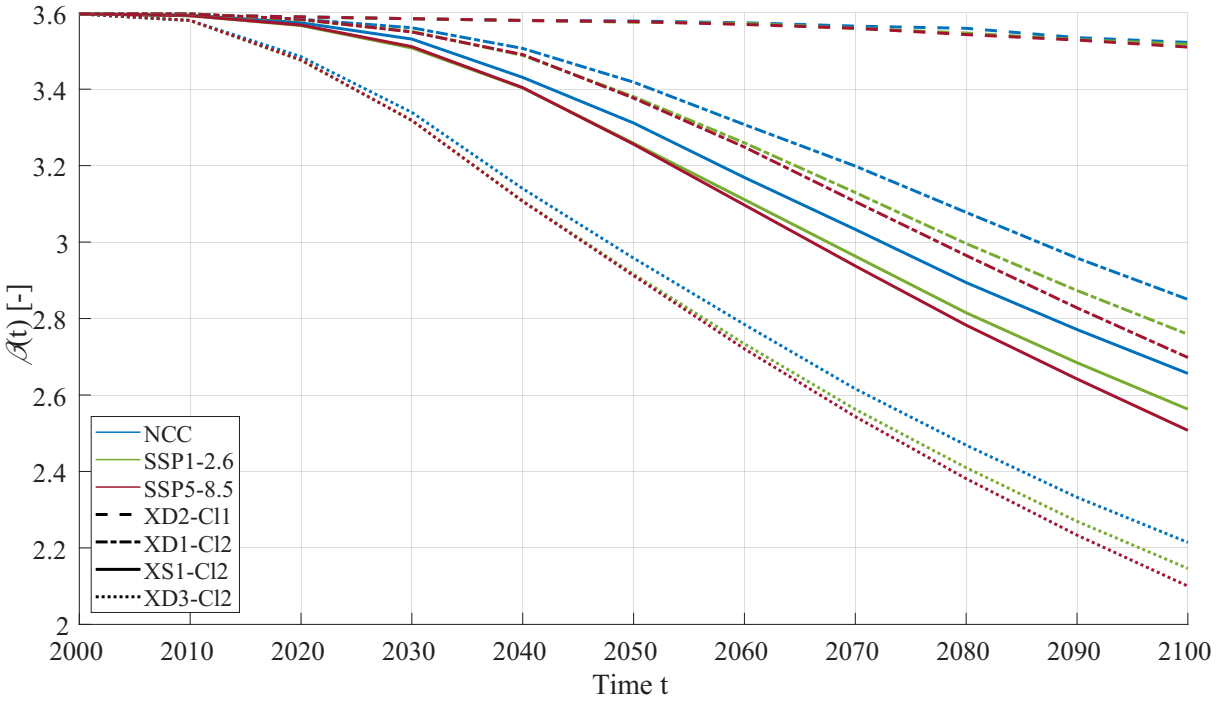

Figure 5.51: Evolution of the reliability index of the aging RC beam for the selected corrosion scenarios.

Eventually, the global safety factor γ_R and the correction function κ_r for the ultimate bending moment are represented in Figure 5.54. It is possible to observe that γ_R increases over time more significantly for the scenario $XD3 - Cl2$ as expected for the reasons discusses previously. In addition, this increase is intensified by climate change.

The values of the correction functions of the mean value and the safety factor are

reported over time in Table 5.6 for corrosion aggressiveness scenarios and climate change scenarios. The safety factor may be computed using the value in the Table 5.6 and the equations defined in Section 5.1.2.

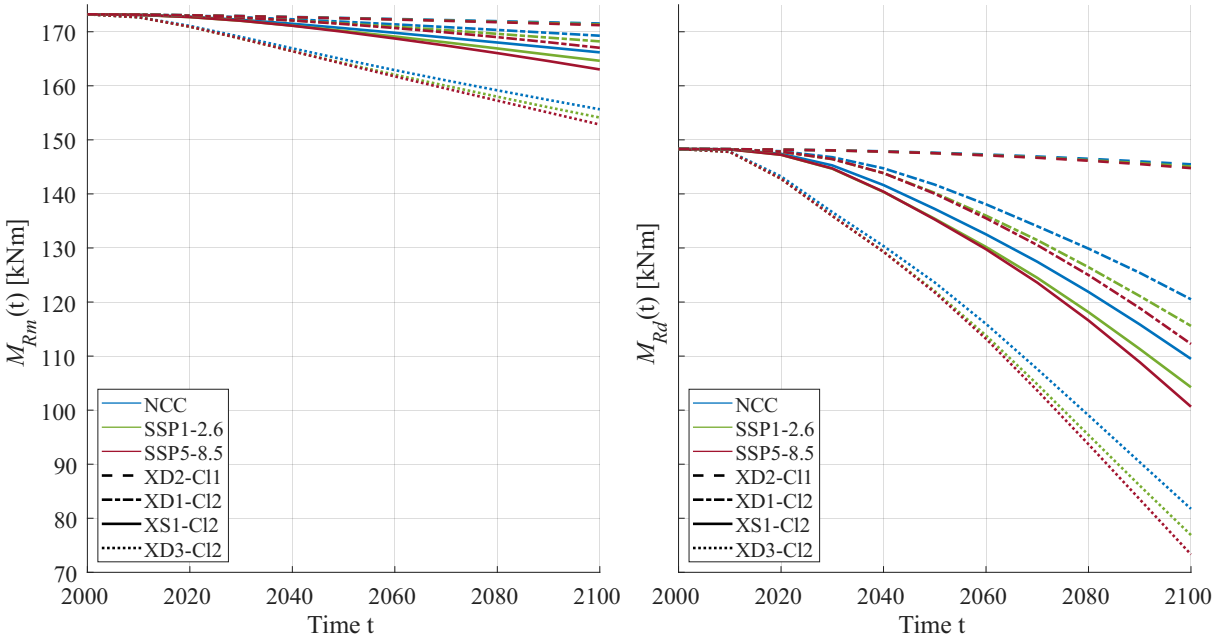

Figure 5.52: Evolution of the mean value (left side) and the design value (right side) of the ultimate bending moment for the selected environmental aggressiveness scenarios.

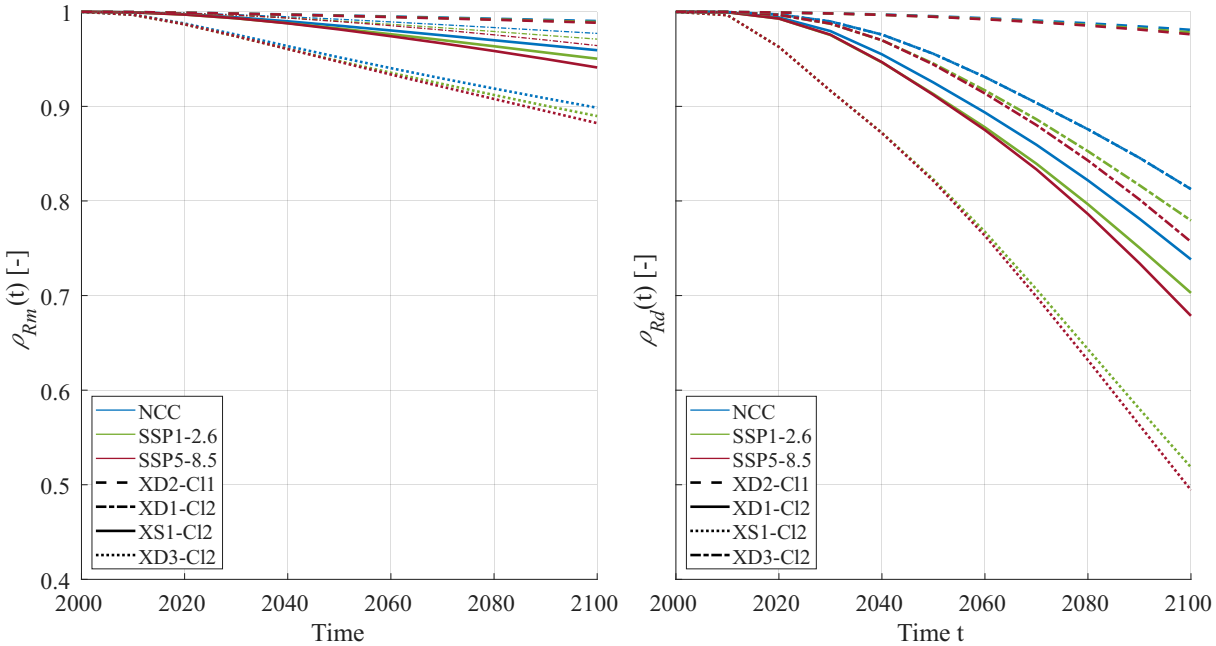

Figure 5.53: Evolution of the correction function for mean values (left side) and design values (right side) of the ultimate bending moment for the selected environmental aggressiveness scenarios.

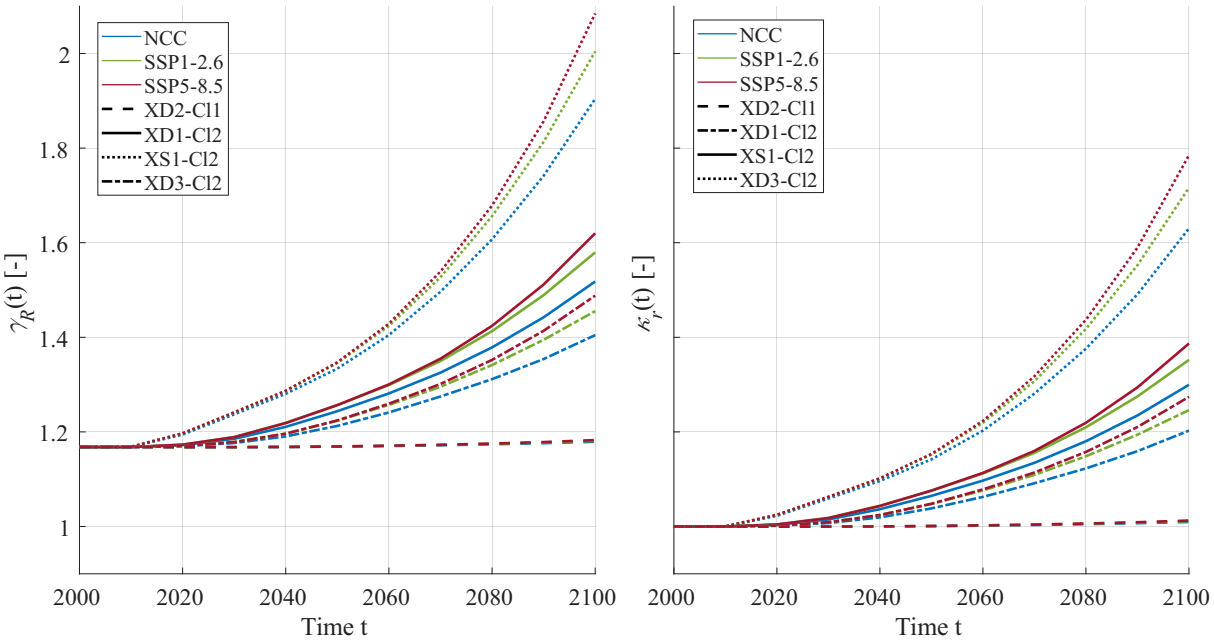

Figure 5.54: Evolution of the safety factor (left side) and correction function (right side) of the ultimate bending moment the selected environmental aggressiveness scenarios.

Parameter	**Aggressiveness Scenario**	$t = 2000$	$t = 2020$	$t = 2040$	$t = 2060$	$t = 2080$	$t = 2100$
$\rho_{Rm,\mathrm{det}}$	XS1-CI2	1.00	1.00	0.99	0.98	0.97	0.96
	XD1-CI2	1.00	1.00	0.99	0.99	0.98	0.98
	XD2-CI1	1.00	1.00	1.00	1.00	0.99	0.99
	XD3-CI2	1.00	0.99	0.96	0.94	0.92	0.90
$\rho_{Rm,det_{SSP1}}$	XS1-CI2	1.00	1.00	0.99	0.98	0.96	0.95
	XD1-CI2	1.00	1.00	1.00	0.99	0.99	0.97
	XD2-CI1	1.00	1.00	1.00	1.00	0.99	0.99
	XD3-CI2	1.00	0.99	0.96	0.94	0.91	0.89
$\rho_{Rm,det_{SSP5}}$	XS1-CI2	1.00	1.00	0.99	0.97	0.96	0.94
	XD1-CI2	1.00	1.00	0.99	0.99	0.99	0.96
	XD2-CI1	1.00	1.00	1.00	1.00	1.00	0.99
	XD3-CI2	1.00	0.99	0.96	0.93	0.91	0.88
$\kappa_{r,\mathrm{det}}$	XS1-CI2	1.00	1.04	1.10	1.18	1.30	1.34
	XD1-CI2	1.00	1.02	1.06	1.12	1.20	1.30
	XD2-CI1	1.00	1.02	1.10	1.20	1.38	1.63
	XD3-CI2	1.00	1.01	1.00	1.00	1.00	1.00
$\kappa_{r,det_{SSP1}}$	XS1-CI2	1.00	1.00	1.02	1.08	1.15	1.25
	XD1-CI2	1.00	1.00	1.01	1.02	1.04	1.06
	XD2-CI1	1.00	1.00	1.00	0.99	0.99	0.93
	XD3-CI2	1.00	1.01	1.04	1.07	1.13	1.21
$\kappa_{r,det_{SSP5}}$	XS1-CI2	1.00	1.00	1.02	1.08	1.15	1.27
	XD1-CI2	1.00	1.00	1.01	1.02	1.04	1.08
	XD2-CI1	1.00	1.00	1.00	0.98	0.97	0.96
	XD3-CI2	1.00	1.01	1.04	1.07	1.14	1.25

Table 5.6: Comparison of the correction functions for selected environmental aggressiveness scenarios and climate scenarios.

By normalizing the resistance obtained under climate change scenario $M_{Rdet_{cc}}$ against the one retrieved neglecting the impact of climate change $M_{Rdet,ref}$, it is possible to isolate the effects of corrosion from those attributable to climate change (Figures 5.55 and 5.56).

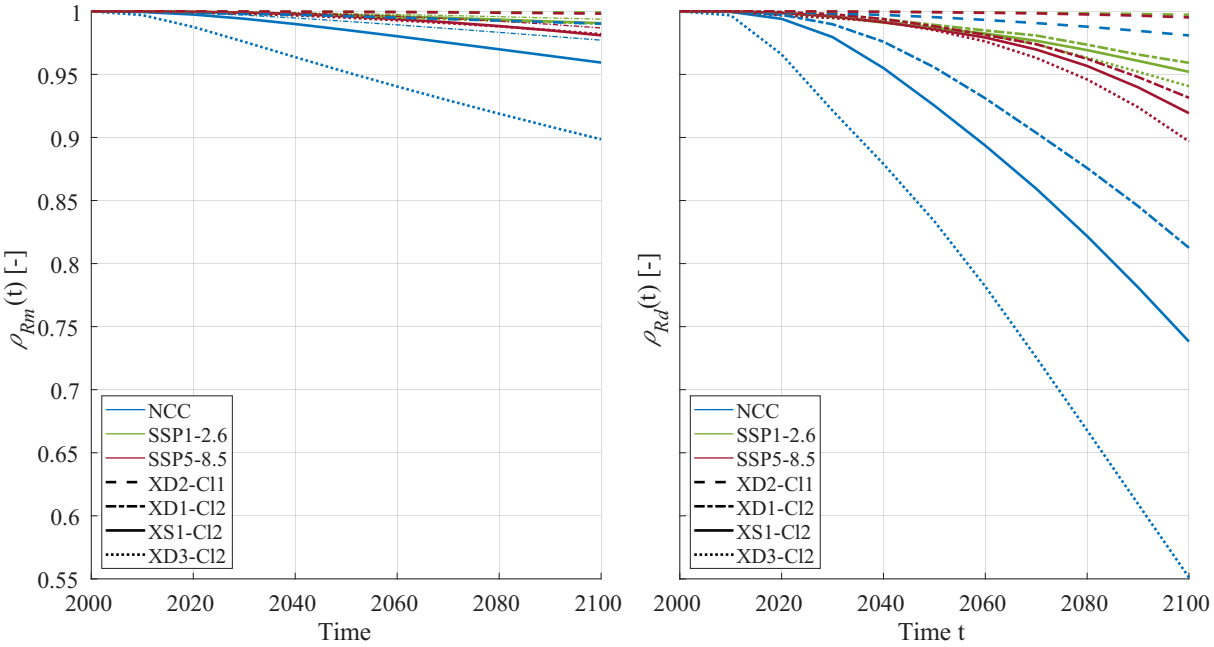

Figure 5.55: Evolution of the normalized correction function for the mean values (left side) and for the design values (right side) of the ultimate bending moment for selected environmental aggressiveness scenarios.

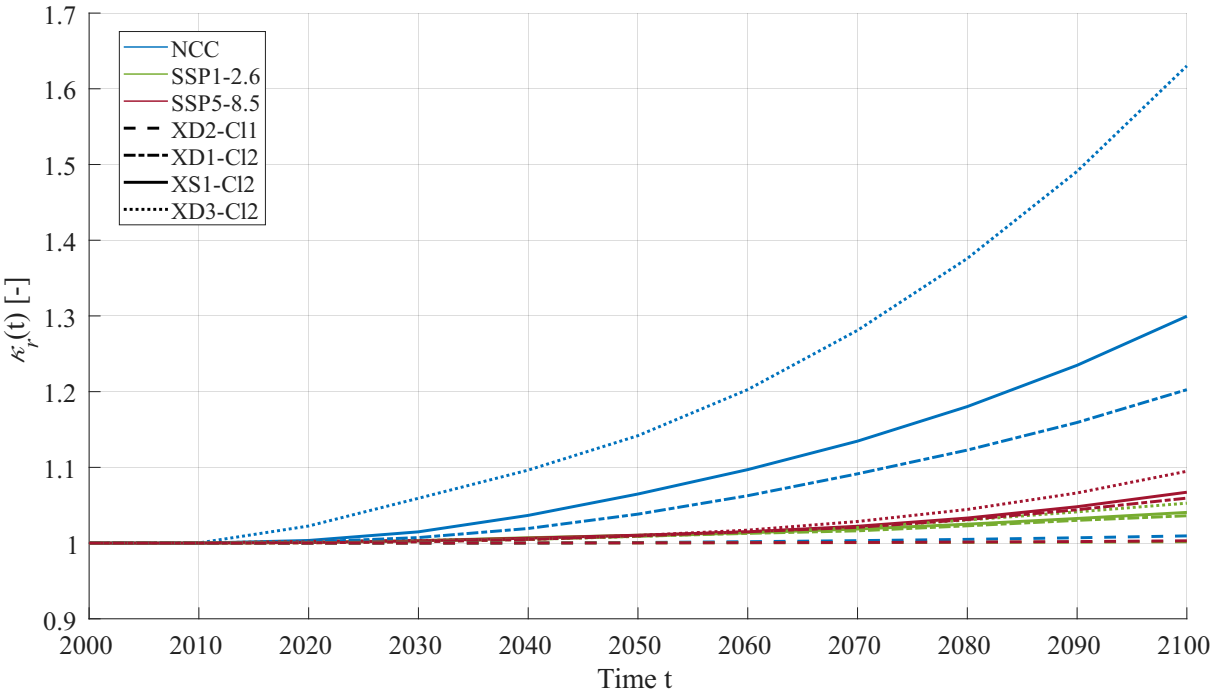

Figure 5.56: Evolution of the normalized correction function for the the safety factors of the ultimate bending moment for environmental aggressiveness scenarios.

Nevertheless, in Figures 5.55 and 5.56, the results indicate the impossibility of completely segregating the effects of climate change and corrosion using this simplified normalization, underlining the need for additional research to study this aspect.

The results of this analysis underscore the need of characterizing and selecting correctly the environmental aggressiveness to obtain reliable reliability elements of the semi-probabilistic methodology. A primary evidence is that corrosion-induced damage is highly dependent on the exposure scenario and, consequently, on the actual location of the structure. Furthermore, in this study, a uniform concrete cover c is maintained across all exposure scenarios. While this assumption deviates from standard design practices, where more aggressive environments typically necessitate increased cover depths, it is adopted here as a controlled variable. This methodological choice is instrumental to isolate the impact of different deterioration rate from any change in structural geometry.

5.3 Closing Remarks and Practical Implications

This chapter proposed a generalized framework for the semi-probabilistic assessment of existing structures subjected to climate-induced deterioration. While the framework is designed for broad applicability across diverse structural systems and environmental stressors, its efficacy is demonstrated through a specialized application to RC structures subjected to chloride-induced corrosion. This specific degradation represents one of the most critical processes affecting structural safety within the context of a changing climate.

The application of the framework to a representative case study revealed significant discrepancies between standard assessment protocols and the proposed tailored methodologies. The traditional time-invariant semi-probabilistic approach, typically optimized for new or undamaged structures, is observed to significantly misestimate reliability elements when applied to deteriorating assets. This often results in an overestimation of structural safety. Considering the different formats:

- Partial Safety Format (PSF): the analysis indicates that the reference PSF is not designed to accommodate corrosion effects, such as the reduction in the effective cross-sectional area of reinforcement A_s. For this reason, a modified PSF is proposed, introducing time variant design values for the corroded steel area and residual concrete cover; nevertheless, this increases computational complexity through the requirement of additional safety factors.

- Global Resistance Format (GSF): conversely, the GSF allows for the holistic integration of uncertainties related to corrosion into a single safety factor γ_R for the overall

resistance. Given the inherent advantages of the GSF in capturing system-level behavior, this study suggests it as the more appropriate format for incorporating correctly uncertainties of corrosion-induced damage.

The results demonstrate that the PSF format tends to yield overestimated values of design resistance compared to the GSF approach.

The impact of climate change is reported to impact significantly corrosion-induced damage and consequently structural performance, though its effects are highly location-specific:

- climate change projections across various regions in France indicate a general acceleration of corrosion-induced damage. However, the magnitude of this enhancement is strictly location-dependent. Different results may be retrieved in other geographic regions;

- the findings emphasize that reliable reliability elements cannot be derived from national aggregates; instead, local or regional environmental projections are required combined with appropriate aggressiveness scenarios to capture the high spatial variability of both environmental parameters and chlorides abundance.

In general, this thesis represent a first step for the exploitation of semi-probabilistic assessment of existing structure under climate-change induced damage; even if significant further research is needed to face all the challenges related to this proposal, the following remarks are proposed for practical implementation:

- assessment of deteriorating structures under climate change must utilize specifically calibrated reliability elements, avoiding severe overestimation of residual capacity and structural safety;

- engineering assessments must account for the high spatial variability of environmental aggressiveness and climate change projections;

- the definition of target reliability values should be reconsidered for existing, deteriorating structures under climate change to balance safety, economic viability, and environmental sustainability;

- to facilitate practical application, the development of regional maps providing the correction functions for climate change-induced deterioration is recommended to assist practitioners in site-specific assessments;

- semi-probabilistic models should, whenever possible, be supplemented by in-situ experimental campaigns, e.g., corrosion rate monitoring and material characterization, to reduce epistemic uncertainty and refine the reliability assessment.

Chapter 6

Conclusions and Future Perspectives

The assessment of the residual performance of existing structures is a critical issue, as a significant portion of the built environment is approaching or exceeding its originally designed service life. In contrast to the design of new structures, the evaluation of existing systems involves a broader spectrum of uncertainties, which may be reduced if additional information is available. These include uncertainties related to the current condition of the structure, the remaining lifetime under consideration, and the target reliability.

Time-dependent aging and deterioration processes can progressively reduce structural capacity, potentially compromising safety and serviceability. Moreover, climate change may exacerbate these detrimental processes by modifying the environmental conditions that affect both structural capacity, modifying the severity of the deterioration process, and structural demand by influencing the magnitude of climatic loadings as well as the intensity and frequency of natural hazards. Addressing these phenomena typically requires the application of full-probabilistic methodologies. However, these approaches are time-consuming and may necessitate substantial knowledge and expertise for numerical implementation. For this reason, the development of semi-probabilistic methodologies that incorporate the effects of climate change and deterioration into structural assessment, supported by appropriate calibration and validation, is nowadays of the essence.

This thesis proposes a mathematical framework for the calibration of semi-probabilistic formats addressing climate change-induced deterioration of existing structures. The proposed approach is based on reliability theory and focuses on the calibration under non-stationary conditions. The influence of deterioration and climate change on the reliability elements of the semi-probabilistic methodology, such as nominal values, design values, and safety factors, is addressed through the definition of correction functions that appropriately scale the corresponding reference values.

6.1 Conclusions

This thesis proposes a methodology for the assessment of existing structures under climate change-induced deterioration. In order to achieve this, a review of basic concepts and novel research for calibration of semi-probabilistic formats is provided in Chapter 3. Particular attention is devoted to the assessment of existing structures and the impact of climate change and deterioration on structural capacity for its incorporation into the semi-probabilistic approach, highlighting this as a critical research gap.

Fundamental concepts of climate change in the context of civil engineering are discussed in Chapter 2. The current state-of-the-art for climate change scenarios and modeling is presented, highlighting the challenges involved in the definition of future projections of environmental parameters also in terms of uncertainties. The main civil engineering risk reported to be impacted by climate change are also described, underlining its influence on the evolution of deterioration processes in RC structures.

Chapter 4 depicts an overview of these mechanisms, focusing on corrosion and how it is impacted by climate change. Instrumental formulations for the sake of Thesis are analyzed and an summary of more recent and advanced methodology is also discussed. The probabilistic modeling of structural capacity under climate change-induced deterioration is also addressed highlighting the main challenges in the perspective of normalization.

Eventually, the proposed methodology for the semi-probabilistic assessment of existing structures under climate change-induced corrosion is presented in Chapter 5 and applied for the assessment of the structural capacity and reliability of a RC beam exposed to chloride-induced corrosion under climate change. This analysis illustrates both the capabilities and the limitations of the proposed methodology, evaluating the impact of climate change and corrosion on the reliability elements of semi-probabilistic formats. Climate change is integrated in the assessment by analyzing temperature and relative humidity across different scenarios, utilizing the median, 10th and 90th percentiles to account for uncertainties evolution in time. The structural deterioration is represented through corrosion-induced damages, which included steel mass loss, reduction in steel ductility, yielding strength, and concrete cover area, neglecting and considering the impact of climate change on deterioration. The reliability elements of the semi-probabilistic format were derived using the design value method combined with simulation-based techniques.

The main findings of this research can be summarized as follows:

- both nominal and design values of the structural capacity decrease over time due to deterioration induced by corrosion. The reduction in the design values is more pronounced because they are related to a smaller percentile with respect to the nominal values. This leads the design value representing extreme values in the tails

of the distributions, which are more sensitive to deterioration.

- The safety factors increase over time due to the larger spread in uncertainties; in this context, the assumption of constant nominal values, design values, and safety factors throughout the lifetime of the structure could lead to an underestimation of the actual probability of failure and result in an unsafe assessment of the considered structure.

- Climate change is projected to exacerbate the corrosion induced processes in France, thereby amplifying the reduction in nominal and design values and the increase in safety factors. The severity of these enhancement depends on the selected climate scenario; this results might be different in other regions where the change in relative humidity could actually moderate the corrosion aggressiveness.

- The spatial resolution of climate projections significantly affects the results. National-scale projections are not fully representative of regional climate behavior and may lead to misestimate the reliability elements of the semi-probabilistic methodology, and consequently the safety of the considered structure;

- The definition of reliability elements is highly dependent on the assumed environmental aggressiveness, demonstrating the sensitivity of semi-probabilistic formats to the specific exposure.

Safety factors obtained through both the PSF and the GSF are evaluated. The comparison highlights that:

- the GSF may be more appropriate for incorporating climate change-induced corrosion effects into a single safety factor, as it directly captures the global uncertainty in resistance. In contrast, the PSF addresses individual uncertainties separately, which may introduce approximations and, in this case, lead to an overestimation of structural performance.

- The conventional PSF formulation consists of the definition of design values only for concrete and steel strength, leading to an overestimation of the bending resistance and, consequently, structural safety; indeed, the nominal value of steel and concrete cover area are not able to reflect the impact of corrosion damage at failure.

- For this reason, a modified PSF extending the definition of design values to the steel area and of the concrete cover area is proposed. This strategy improves the estimate of the design bending moment and aligns the results more closely with the estimation retrieved by the GSF. Nevertheless, this approach continues to overestimate the resistance due to the individual consideration of uncertainties.

The provided results utilize the DVM, thereby limiting the applicability of the correction functions to the specific case study examined. Moreover, the uncertainty of climate change is considered in a simplistic way, exploiting the projection connected to the extreme percentiles without performing a real propagation of uncertainty. The impact of climate change has been analyzed on structural capacity and demand separately; however, while in real-world scenarios, the influence is simultaneous, potentially resulting in an increase in climatic structural demand and a decrease in structural capacity.

In conclusion, this thesis establishes a foundation for integrating climate change effects and deterioration mechanisms into semi-probabilistic assessment and for future standardization, supporting tailored evaluation and design of structural and infrastructural systems under future environmental conditions.

6.2 Future Perspectives

The proposed framework presents several opportunities for improvement and extension:

- based on the proposed methodology, the calibration of semi-probabilistic reliability elements need to be achieved through the solution of a time-dependent optimization problem in order to contribute to the future revision of civil engineering standards.
- Probabilistic density estimators, such as Gaussian Mixture Models (GMM), could be employed to assess the evolution of the PDF of the resisting variables in the context of climate change-induced deterioration. GMM could also be integrated with FORM to estimate the reliability of the investigated systems (Z. Zhang et al., 2019) to improve the accuracy and efficiency of reliability-based calibration.
- The definition of a reliability target for existing structures remains an open issue due to the lack of coherence among the different values proposed in the literature, the insufficient data for analytical formulations, and the challenges associated with standardizing different RC structures. Moreover, climate change may impact the economic and human safety considerations underlying the calibration of reliability targets, and this should be addressed in future studies.
- The use of fixed percentiles to define characteristic values may be questionable under deterioration and non-stationary climate effects, requiring further investigation devoted to this subject.
- The integration of more advanced corrosion models capable of capturing the actual kinetics of chlorides is necessary. In particular, approaches based on non-stationary

cellular automata exhibit significant potential for simulating chloride ingress and corrosion under varying temperature and humidity conditions (Nava et al., 2025).

- This Thesis primarily focuses on corrosion-induced deterioration. Future work could incorporate additional time-dependent mechanisms, such as alkali–silica reaction, fatigue, freeze–thaw damage, scour, or combined deterioration scenarios, thereby enabling a more comprehensive assessment of aging structures.

Advancing in these research directions could support the development of robust and reliable strategies for assessing reinforced concrete infrastructure, thereby ensuring structural safety and serviceability in an increasingly uncertain and evolving climate.

Bibliography

[1] AASHTO. (2020). *Lrfd bridge design specifications, 5th ed. with interims*. American Association of State Highway; Transportation Officials.

[2] Abrahamczyk, L., & Uzair, A. (2023). On the use of climate models for estimating the non-stationary characteristic values of climatic actions in civil engineering practice. *Frontiers in Built Environment*, *9*. https://doi.org/10.3389/fbuil.2023.1108328

[3] Adem, A., Melesse, A., Tilahun, S., Setegn, S., Ayana, E., Worqlul, A., & Assefa, T. (2014). Climate change projections in the upper gilgel abay river catchment, blue nile basin ethiopia. In A. Melesse, W. Abtew, & S. Setegn (Eds.), *Nile river basin*. Springer. https://doi.org/10.1007/978-3-319-02720-3_19

[4] AghaKouchak, A., Chiang, F., Huning, L. S., Love, C. A., Mallakpour, I., Mazdiyasni, O., Moftakhari, H., Papalexiou, S. M., Ragno, E., & Sadegh, M. (2020). Climate extremes and compound hazards in a warming world. *Annual review of earth and planetary sciences*, *48*(1), 519–548.

[5] Ahmad, S., & Bhattacharjee, B. (2000). Empirical modelling of indicators of chloride-induced rebar corrosion. *Journal of Structural Engineering*, *27*(3), 195–207.

[6] Alam, M., Schmidt, F., Orcesi, A., Ientile, S., & Lavergne, F. (2023). Sensitivity analysis of adjusted partial factors for the assessment of an existing reinforced concrete bridge. In F. Biondini & D. M. Frangopol (Eds.), *Proceedings of the 14th International Conference on Application of Statistics and Probability in Civil Engineering (ICASP14), Dublin, Ireland, July 9-13, 2023*. Trinity's Access to Research Archive. https://doi.org/http://hdl.handle.net/2262/103361

[7] Alhamid, A. K., Akiyama, M., Aoki, K., Koshimura, S., & Frangopol, D. M. (2022). Stochastic renewal process model of time-variant tsunami hazard assessment under nonstationary effects of sea-level rise due to climate change. *Structural Safety*, *99*, 102263. https://doi.org/10.1016/j.strusafe.2022.102263

[8] Allaix, D. L., Carbone, V. I., & Mancini, G. (2013). Global safety format for nonlinear analysis of reinforced concrete structures. *Structural Concrete*, *14*(1), 29–42. https://doi.org/10.1002/suco.201200017

[9] Allen, D. E. (1975). Limit States Design—A Probabilistic Study. *Canadian Journal of Civil Engineering*, *2*(1), 36–49. https://doi.org/10.1139/l75-004

[10] Almusallam, A. A. (2001). Effect of degree of corrosion on the properties of reinforcing steel bars. *Construction and building materials*, *15*(8), 361–368. https://doi.org/10.1016/S0950-0618(01)00009-5

[11] Alonso, C., Andrade, C., & González, J. (1988). Relation between resistivity and corrosion rate of reinforcements in carbonated mortar made with several cement types. *Cement and concrete research*, *18*(5), 687–698. https://doi.org/10.1016/0008-8846(88)90091-9

[12] Al-Rubaye, S., Maguire, M., & Bean, B. (2022). Design Ground Snow Loads: Historical Perspective and State of the Art. *Journal of Structural Engineering*, *148*(6), 03122001. https://doi.org/10.1061/(ASCE)ST.1943-541X.0003339

[13] Andrade, C., Alonso, C., & Sarrı´a, J. (2002). Corrosion rate evolution in concrete structures exposed to the atmosphere. *Cement and concrete composites*, *24*(1), 55–64. https://doi.org/10.1016/S0958-9465(01)00026-9

[14] Andrade, C., & Alonso, C. (2001). On-site measurements of corrosion rate of reinforcements. *Construction and building materials*, *15*(2-3), 141–145. https://doi.org/10.1016/S0950-0618(00)00063-5

[15] Andrade, C., Alonso, M. C., & Gonzales, J. A. (1988). An initial effort to use the corrosion rate measurements for estimating rebar durability. *Symposium on Corrosion Rate of Reinforcement in Concrete*, 29.

[16] Andrady, A. L., Hamid, H. S., & Torikai, A. (2003). Effects of climate change and uv-b on materials. *Photochemical & Photobiological Sciences*, *2*(1), 68–72. https://doi.org/10.1039/b211085g

[17] Ang, A. H.-S., & Tang, W. H. (2007). *Probability concepts in engineering: Emphasis on applications to civil and environmental engineering* (2nd, Vol. 1). Wiley.

[18] Angst, U. M. (2018). Challenges and opportunities in corrosion of steel in concrete. *Materials and structures*, *51*(1), 4. https://doi.org/10.1617/s11527-017-1131-6

[19] Angst, U. M., Isgor, O. B., Hansson, C. M., Sagüés, A., & Geiker, M. R. (2022). Beyond the chloride threshold concept for predicting corrosion of steel in concrete. *Applied Physics Reviews*, *9*(1), 011321. https://doi.org/10.1063/5.0076320

[20] Anyala, M., Odoki, J., & Baker, C. J. (2011). Assessment of the impact of climate change on road maintenance. *2nd International Conference on Advances in Engineering and Technology (AET2011)*, 457–463.

[21] Apostolopoulos, C. A., & Papadakis, V. (2008). Consequences of steel corrosion on the ductility properties of reinforcement bar. *Construction and Building Materials*, *22*(12), 2316–2324. https://doi.org/10.1016/j.conbuildmat.2007.10.006

[22] Arnell, N. W., & Gosling, S. N. (2013). The impacts of climate change on river flow regimes at the global scale. *Journal of Hydrology*, *486*, 351–364. https://doi.org/10.1016/j.jhydrol.2013.02.010

[23] Arnold, R., & Kraus, M. (2022). On the nonstationary identification of climate-influenced loads for the semi-probabilistic approach using measured and projected data. *Cogent Engineering*, *9*(1), 2143061. https://doi.org/10.1080/23311916.2022.2143061

[24] AS. (2017). *AS 5100.7 - Bridge Design, Part 7: Bridge assessment*. Standards Australia.

[25] ASCE. (1999). Life-cycle cost analysis for bridges. In D. M. Frangopol (Ed.), *Bridge safety and reliability* (pp. 210–236).

[26] ASCE. (2018). *Climate-resilient infrastructure: Adaptive design and risk management, committee on adaptation to a changing climate, manual of practice 140*. American Society of Civil Engineers.

[27] ASCE. (2022). *Minimum Design Loads and Associated Criteria for Buildings and Other Structures (ASCE/SEI 7-22)*. American Society of Civil Engineers.

[28] ASCE. (2025). *2025 report card for america's infrastructure*. American Society of Civil Engineers.

[29] Ascione, C., & Valdano, E. (2025). How floods may affect the spatial spread of respiratory pathogens: The case of emilia-romagna, italy in may 2023. *EPJ Data Science*, *14*(1), 43. https://doi.org/10.1140/epjds/s13688-025-00560-y

[30] Athanasopoulou, A., M., R. D. M. D. N. E. S. D. S. M., Dimova, S., Guido, R., Mercogliano, P., Villani, V., Croce, P., Landi, F., Formichi, P., & Markova, J. (2020). *Thermal design of structures and the changing climate*. Joint Research Center. https://publications.jrc.ec.europa.eu/repository/handle/JRC121351

[31] Au, S.-K., & Beck, J. L. (2001). Estimation of small failure probabilities in high dimensions by subset simulation. *Probabilistic engineering mechanics*, *16*(4), 263–277.

[32] Balafas, I., & Burgoyne, C. (2010). Environmental effects on cover cracking due to corrosion. *Cement and Concrete Research*, *40*(9), 1429–1440. https://doi.org/10.1016/j.cemconres.2010.05.003

[33] Baravalle, M., & Köhler, J. (2017). A framework for estimating the implicit safety level of existing design codes. *Proceedings of the 12th International Conference on Structural Safety and Reliability (ICOSSAR2017), TU Wien, Vienna, August 6-10, 2017*.

[34] Baravalle, M., & Köhler, J. (2019). A risk-based approach for calibration of design codes. *Structural Safety*, *78*, 63–75. https://doi.org/10.1016/j.strusafe.2018.12.003

[35] Baravalle, M. (2017). *Risk and reliability based calibration of structural design codes: Principles and applications* (Doctoral dissertation). NTNU.

[36] Baravalle, M., & Köhler, J. (2016). Risk and Reliability Based Calibration of Design Codes for Submerged Floating Tunnels. *Procedia Engineering*, *166*, 247–254. https://doi.org/10.1016/j.proeng.2016.11.547

[37] Barone, G., & Frangopol, D. M. (2014). Reliability, risk and lifetime distributions as performance indicators for life-cycle maintenance of deteriorating structures. *Reliability Engineering & System Safety*, *123*, 21–37. https://doi.org/10.1016/j.ress.2013.09.013

[38] Bastidas-Arteaga, E. (2018). Reliability of Reinforced Concrete Structures Subjected to Corrosion-Fatigue and Climate Change. *International Journal of Concrete Structures and Materials*, *12*(1), 10. https://doi.org/10.1186/s40069-018-0235-x

[39] Bastidas-Arteaga, E., Bressolette, P., Chateauneuf, A., & Sánchez-Silva, M. (2009). Probabilistic lifetime assessment of rc structures under coupled corrosion–fatigue deterioration processes. *Structural safety*, *31*(1), 84–96. https://doi.org/10.1016/j.strusafe.2008.04.001

[40] Bastidas-Arteaga, E., Chateauneuf, A., Sánchez-Silva, M., Bressolette, P., & Schoefs, F. (2010). Influence of weather and global warming in chloride ingress into concrete: A stochastic approach. *Structural Safety*, *32*(4), 238–249. https://doi.org/10.1016/j.strusafe.2010.03.002

[41] Bastidas-Arteaga, E., Schoefs, F., Stewart, M. G., & Wang, X. (2013). Influence of global warming on durability of corroding RC structures: A probabilistic approach. *Engineering Structures*, *51*, 259–266. https://doi.org/10.1016/j.engstruct.2013.01.006

[42] Bastidas-Arteaga, E., & Stewart, M. G. (2015). Damage risks and economic assessment of climate adaptation strategies for design of new concrete structures subject to chloride-induced corrosion. *Structural Safety*, *52*, 40–53. https://doi.org/10.1016/j.strusafe.2014.10.005

[43] Bastidas-Arteaga, E., & Stewart, M. G. (2016). Economic assessment of climate adaptation strategies for existing reinforced concrete structures subjected to chloride-induced corrosion. *Structure and Infrastructure Engineering*, *12*(4), 432–449. https://doi.org/10.1080/15732479.2015.1020499

[44] Bažant, Z. P., & Najjar, L. (1971). Drying of concrete as a nonlinear diffusion problem. *Cement and concrete research*, *1*(5), 461–473.

[45] Beck, M. W., Losada, I. J., Menéndez, P., Reguero, B. G., Dı´az-Simal, P., & Fernández, F. (2018). The global flood protection savings provided by coral reefs. *Nature communications*, *9*(1), 2186. https://doi.org/10.1038/s41467-018-04568-z

[46] Belin, B. (2022). *Rapport d'information au Sénat n° 669 (in French)*. Sénat. https://www.senat.fr/rap/r21-669/r21-669.html

[47] Berggren, K., Olofsson, M., Viklander, M., Svensson, G., & Gustafsson, A.-M. (2012). Hydraulic impacts on urban drainage systems due to changes in rainfall caused by climatic change. *Journal of Hydrologic Engineering*, *17*(1), 92–98. https://doi.org/10.1061/(ASCE)HE.1943-5584.0000406

[48] Berggren, K., Packman, J., Ashley, R., & Viklander, M. (2014). Climate changed rainfalls for urban drainage capacity assessment. *Urban Water Journal*, *11*(7), 543–556. https://doi.org/10.1080/1573062X.2013.851709

[49] Berto, L., Simioni, P., & Saetta, A. (2008). Numerical modelling of bond behaviour in rc structures affected by reinforcement corrosion. *Engineering Structures*, *30*(5), 1375–1385. https://doi.org/10.1016/j.engstruct.2007.08.003

[50] Bertolini, L., Elsener, B., Pedeferri, P., Redaelli, E., & Polder, R. B. (2013). *Corrosion of steel in concrete: Prevention, diagnosis, repair*. John Wiley & Sons.

[51] Bhargava, K., Ghosh, A., Mori, Y., & Ramanujam, S. (2007). Corrosion-induced bond strength degradation in reinforced concrete—analytical and empirical models. *Nuclear Engineering and Design*, *237*(11), 1140–1157. https://doi.org/10.1016/j.nucengdes.2007.01.010

[52] Bhatkoti, R., Moglen, G. E., Murray-Tuite, P. M., & Triantis, K. P. (2016). Changes to Bridge Flood Risk under Climate Change. *Journal of Hydrologic Engineering*, *21*(12), 04016045. https://doi.org/10.1061/(ASCE)HE.1943-5584.0001448

[53] Biondini, F., Lounis, Z., & Ghosn, M. (Eds.). (2025). *Effect of climate change on life-cycle performance of structures and infrastructure systems: Safety, reliability and risk*. American Society of Civil Engineers, ASCE Press, Reston, VA, USA. https://doi.org/10.1061/9780784485804

[54] Biondini, F. (2008). Use of simulation in structural reliability. *Structures Congress 2008: Crossing Borders*, 1–8.

[55] Biondini, F., Bontempi, F., Frangopol, D. M., & Malerba, P. G. (2004). Cellular automata approach to durability analysis of concrete structures in aggressive environments. *Journal of Structural Engineering*, *130*(11), 1724–1737. https://doi.org/10.1061/(ASCE)0733-9445(2004)130:11(1724)

[56] Biondini, F., & Frangopol, D. M. (2016). Life-cycle performance of deteriorating structural systems under uncertainty. *Journal of Structural Engineering*, *142*(9), F4016001.

[57] Biondini, F., & Frangopol, D. M. (2018). Life-cycle performance of civil structure and infrastructure systems: Survey. *Journal of Structural Engineering*, *144*(1), 06017008. https://doi.org/10.1061/(ASCE)ST.1943-541X.0001923

[58] Biondini, F., & Nero, A. (2011). Cellular finite beam element for nonlinear analysis of concrete structures under fire. *Journal of Structural Engineering*, *137*(5), 543–558. https://doi.org/10.1061/(ASCE)ST.1943-541X.0000307

[59] Biondini, F., & Vergani, M. (2012). Damage modeling and nonlinear analysis of concrete bridges under corrosion. In F. Biondini & D. M. Frangopol (Eds.), *Proceedings of the sixth international conference on bridge maintenance, safety and management (iabmas 2012)* (pp. 949–957). CRC Press.

[60] Biondini, F., & Vergani, M. (2015). Deteriorating beam finite element for nonlinear analysis of concrete structures under corrosion. *Structure and Infrastructure Engineering*, *11*(4), 519–532. https://doi.org/10.1080/15732479.2014.951863

[61] Bjarnadottir, S., Li, Y., & Stewart, M. G. (2011). A probabilistic-based framework for impact and adaptation assessment of climate change on hurricane damage risks and costs. *Structural Safety*, *33*(3), 173–185. https://doi.org/10.1016/j.strusafe.2011.02.003

[62] Blomfors, M., Engen, M., & Plos, M. (2016). Evaluation of safety formats for nonlinear finite element analyses of statically indeterminate concrete structures subjected to different load paths. *Structural Concrete*, *17*(1), 44–51. https://doi.org/10.1002/suco.201500059

[63] Blomfors, M., Ivanov, O. L., Honfi´, D., & Engen, M. (2019). Partial safety factors for the anchorage capacity of corroded reinforcement bars in concrete. *Engineering Structures*, *181*, 579–588. https://doi.org/10.1016/j.engstruct.2018.12.011

[64] Bonan, G. B. (2008). Forests and climate change: Forcings, feedbacks, and the climate benefits of forests. *Science*, *320*, 1444–1449. https://doi.org/10.1126/science.1155121

[65] Boucher, O., Randall, D., Artaxo, P., Bretherton, C., Feingold, G., Forster, P., Kerminen, V.-M., Kondo, Y., Liao, H., Lohmann, U., et al. (2013). Clouds and aerosols. In *Climate change 2013: The physical science basis. Contribution of working group I to the fifth assessment report of the intergovernmental panel on climate change* (pp. 571–657). Cambridge University Press.

[66] Bradfield, R., Wright, G., Burt, G., Cairns, G., & Van Der Heijden, K. (2005). The origins and evolution of scenario techniques in long range business planning. *Futures*, *37*(8), 795–812.

[67] Breitung, K. (1984). Asymptotic approximations for multinormal integrals. *Journal of Engineering Mechanics*, *110*(3), 357–366. https://doi.org/10.1061/(ASCE)0733-9399(1984)110:3(357)

[68] Briaud, J.-L., Gardoni, P., & Yao, C. (2014). Statistical, Risk, and Reliability Analyses of Bridge Scour. *Journal of Geotechnical and Geoenvironmental Engineering*, *140*(2), 04013011. https://doi.org/10.1061/(ASCE)GT.1943-5606.0000989

[69] Brühwiler, E., Vogel, T., Lang, T., & Lüchinger, P. (2012). Swiss Standards for Existing Structures. *Structural Engineering International*, *22*(2), 275–280. https://doi.org/10.2749/101686612X13291382991209

[70] Bucher, C. G. (1988). Adaptive sampling—an iterative fast monte carlo procedure. *Structural safety*, *5*(2), 119–126. https://doi.org/10.1016/0167-4730(88)90020-3

[71] Bucher, C. G., & Bourgund, U. (1990). A fast and efficient response surface approach for structural reliability problems. *Structural safety*, *7*(1), 57–66. https://doi.org/10.1016/0167-4730(90)90012-E

[72] Bui, H. T., & Tan, K. H. (2023). Time-dependent nonuniform numerical model of corrosion process and consequent corrosion-induced concrete cracking under chloride attack. *Structures*, *52*, 332–347. https://doi.org/10.1016/j.istruc.2023.03.113

[73] Burkhardt, U., & Kärcher, B. (2011). Global radiative forcing from contrail cirrus. *Nature climate change*, *1*(1), 54–58.

[74] Cabrera, J. G. (1996). Deterioration of concrete due to reinforcement corrosion. *Cement and Concrete Composites*, *18*(1), 47–59.

[75] Camnasio, E. (2013). *Lifetime performance and seismic resilience of concrete structures exposed to corrosion* (PhD thesis) [Supervisor: Fabio Biondini. XXV cycle]. Politecnico di Milano, Department of Civil, Environmental Engineering, Doctoral School in Structural, Seismic, and Geotechnical Engineering. Milan, Italy.

[76] Carvalho, D., Rocha, A., Gómez-Gesteira, M., & Santos, C. S. (2017). Potential impacts of climate change on european wind energy resource under the cmip5 future climate projections. *Renewable Energy*, *101*, 29–40. https://doi.org/10.1016/j.renene.2016.08.036

[77] Caspeele, R., & Taerwe, L. (2012). Updating partial factors for material properties of existing structures in a eurocode framework using bayesian statistics. In A. Grall & C. Guedes Soares (Eds.), *Advances in Safety, Reliability and Risk Management: Proceedings of the European Safety and Reliability Conference (ESREL 2011), Troyes, France, Septemeber 18-22, 2011* (pp. 311–314). CRC Press.

[78] Caspeele, R., Sykora, M., Allaix, D. L., & Steenbergen, R. D. J. M. (2013). The Design Value Method and Adjusted Partial Factor Approach for Existing Structures. *Structural Engineering International*, *23*(4), 386–393. https://doi.org/10.2749/101686613X13627347100194

[79] Caspeele, R., & Taerwe, L. (2014). Influence of concrete strength estimation on the structural safety assessment of existing structures. *Construction and Building Materials*, *62*, 77–84. https://doi.org/10.1016/j.conbuildmat.2014.03.033

[80] Castaldo, P., Gino, D., & Mancini, G. (2019). Safety formats for non-linear finite element analysis of reinforced concrete structures: Discussion, comparison and proposals. *Engineering Structures*, *193*, 136–153. https://doi.org/10.1016/j.engstruct.2019.05.029

[81] Castaldo, P., Gino, D., Marano, G. C., & Mancini, G. (2022). Aleatory uncertainties with global resistance safety factors for non-linear analyses of slender reinforced concrete columns. *Engineering Structures*, *255*, 113920. https://doi.org/10.1016/j.engstruct.2022.113920

[82] Casti, L., Schmidt, F., Biondini, F., & Makhoul, N. (2023). Semi-probabilistic methods for the assessment of existing concrete structures: An overview. In F. Biondini & D. M. Frangopol (Eds.), *Life-Cycle of Structures and Infrastructure Systems: Proceedings of the Eighth International Symposium on Life-Cycle Civil Engineering (IALCCE 2023), Milan, Italy, July 2-6, 2023* (pp. 3872–3879). CRC Press. https://doi.org/10.1201/9781003323020-475

[83] Casti, L., Schmidt, F., Biondini, F., Makhoul, N., & Pittet, R. (2024a). Climate change effects on characteristic values of temperature loadings. In J. A. O. Barros, V. M. C. F. Cunha, H. S. Sousa, J. C. Matos, & J. M. Sena-Cruz (Eds.), *Proceedings of the 4th fib International Conference on Concrete Sustainability (ICCS2024), Sep 2024, Guimarães, Portugal* (pp. 112–119). Springer. https://doi.org/10.1007/978-3-031-80672-8_14

[84] Casti, L., Schmidt, F., Biondini, F., Makhoul, N., & Pittet, R. (2024b). Comparison of partial factor methods for existing concrete structures: Application to a cable-stayed bridge. *Proceedings of the 12th International Conference on Bridge Maintenance, Safety and Management (IABMAS 2024), CRC Press/Balkema, London.*

[85] Cea, L., & Costabile, P. (2022). Flood Risk in Urban Areas: Modelling, Management and Adaptation to Climate Change. A Review. *Hydrology*, *9*(3), 50. https://doi.org/10.3390/hydrology9030050

[86] CEB. (1976). *First Order Reliability Concepts for Design Codes. CEB Bulletin No. 112*. Comité European du Béton. Paris, France.

[87] CEN. (2002). *EN 1990: Basis of structural design*. European Committee for Standardization. Brussels, Belgium.

[88] CEN. (2004a). *EN 1992-1-2: Design of Concrete Structures – Part 1-2: General Rules – Structural Fire Design*. European Committee for Standardization. Brussels, Belgium.

[89] CEN. (2004b). *NF EN 1991-1-5/NA: Eurocode 1 – Actions on Structures, Part 1-5: General Actions – Thermal Actions. National Annex* (Standard). European Committee for Standardization. Brussels, Belgium.

[90] CEN. (2005). *EN 1992-2: Eurocode 2: Design of Concrete Structures — Concrete Bridges — Design and Detailing Rules* (Standard). European Committee for Standardization. Brussels, Belgium.

[91] CEN. (2007). *NF EN 1991-1-3/NA. Eurocode 1 — Actions on structures — Part 1-3: General actions — Snow loads — National annex to NF EN 1991-1-3:2004* (Standard). European Committee for Standardization. Brussels, Belgium.

[92] CEN. (2008). *NF EN 1991-1-4/NA. Eurocode 1: Actions on structures — Part 1-4: General actions — Wind actions — National Annex to NF EN 1991-1-4:2005* (Standard). European Committee for Standardization. Brussels, Belgium.

[93] CEN. (2013). *TC250 - Response to Mandate M/515—Towards a Second-Generation of Eurocodes*. European Committee for Standardization. Brussels, Belgium.

[94] CEN. (2020). *TS17440: Technical Specification - Assessment and Retrofitting of Existing Structures*. European Committee for Standardization. Brussels, Belgium.

[95] CEN. (2024). *prEN 1990-2 – Basis of assessment and retrofitting of existing structures: general rules and actions*. European Committee for Standardization. Brussels, Belgium.

[96] Cerema. (2024). *Etat des ponts communaux en france* (tech. rep.). Cerema (in French). France.

[97] Cervenka, V. (2013). Reliability-based non-linear analysis according to fib model code 2010. *Structural Concrete*, *14*(1), 19–28. https://doi.org/10.1002/suco.201200022

[98] Chaize, P., & Dagbert, M. (2019). *Sécurité des ponts : Éviter un drame. rapport d'information au sénat n° 609 (in french)*. Sénat. https://www.senat.fr/rap/r18-609/r18-6091.pdf

[99] Chen, X., & Lind, N. (1982). Fast probability integration by three-parameter normal tail approximation. *Structural safety*, *1*(4), 269–276.

[100] Cheng, L., AghaKouchak, A., Gilleland, E., & Katz, R. W. (2014). Non-stationary extreme value analysis in a changing climate. *Climatic Change*, *127*(2), 353–369. https://doi.org/10.1007/s10584-014-1254-5

[101] Cherif, R., Hamami, A. E. A., Aıt-Mokhtar, A., & Bosschaerts, W. (2022). Thermodynamic equilibria-based modelling of reactive chloride transport in blended cementitious materials. *Cement and Concrete Research*, *156*, 106770. https://doi.org/10.1016/j.cemconres.2022.106770

[102] Christiane, L. (2009). *Monte carlo and quasi-monte carlo sampling*. Springer.

[103] Ciabatta, L., Camici, S., Brocca, L., Ponziani, F., Stelluti, M., Berni, N., & Moramarco, T. (2016). Assessing the impact of climate-change scenarios on landslide occurrence in umbria region, italy. *Journal of Hydrology*, *541*, 285–295. https://doi.org/10.1016/j.jhydrol.2016.02.007

[104] Ciais, P., Sabine, C., Bala, G., Bopp, L., Brovkin, V., Canadell, J., Chhabra, A., DeFries, R., Galloway, J., Heimann, M., Jones, C., Le Quéré, C., Myneni, R., Piao, S., & Thornton, P. (2013). Carbon and other biogeochemical cycles. In T. Stocker, D. Qin, G.-K. Plattner, M. Tignor, S. Allen, J. Boschung, A. Nauels, Y. Xia, V. Bex, & P. Midgley (Eds.), *Climate change 2013: The physical science basis. contribution of working group i to the fifth assessment report of the intergovernmental panel on climate change*. Cambridge University Press.

[105] Clarke, B., Otto, F., Stuart-Smith, R., & Harrington, L. (2022). Extreme weather impacts of climate change: An attribution perspective. *Environmental Research: Climate*, *1*(1), 012001.

[106] Claussen, M., Mysak, L., Weaver, A., Crucifix, M., Fichefet, T., Loutre, M.-F., Weber, S., Alcamo, J., Alexeev, V., Berger, A., et al. (2002). Earth system models of intermediate complexity: Closing the gap in the spectrum of climate system models. *Climate dynamics*, *18*(7), 579–586.

[107] Collepardi, M., Marcialis, A., & Turriziani, R. (1972). Penetration of chloride ions into cement pastes and concretes. *Journal of the American Ceramic Society*, *55*(10), 534–535.

[108] Collins, B. D., & Stock, G. M. (2016). Rockfall triggering by cyclic thermal stressing of exfoliation fractures. *Nature Geoscience*, *9*(5), 395–400. https://doi.org/10.1038/ngeo2686

[109] Cook, W., Barr, P. J., & Halling, M. W. (2015). Bridge Failure Rate. *Journal of Performance of Constructed Facilities*, *29*(3), 04014080. https://doi.org/10.1061/(ASCE)CF.1943-5509.0000571

[110] Cooley, D. (2012). Return periods and return levels under climate change. In A. AghaKouchak, D. Easterling, K. Hsu, S. Schubert, & S. Sorooshian (Eds.), *Extremes in a changing climate: Detection, analysis and uncertainty* (pp. 97–114). Springer. https://doi.org/10.1007/978-94-007-4479-0_4

[111] Cornell, C. A. (1969a). A probability-based structural code. *Journal of the American Concrete Institute*, *66*(12), 974–985.

[112] Cornell, C. A. (1969b). Structual safety specification based on second-moment reliability analysis. *IABSE Report: On Concepts of Safety of Structures and Methods of Design, Zurich, IABSE, London*, 235–246.

[113] Coronelli, D., & Gambarova, P. (2004). Structural Assessment of Corroded Reinforced Concrete Beams: Modeling Guidelines. *Journal of Structural Engineering*, *130*(8), 1214–1224. https://doi.org/10.1061/(ASCE)0733-9445(2004)130:8(1214)

[114] Cosenza, E., & Losanno, D. (2021). Assessment of existing reinforced-concrete bridges under road-traffic loads according to the new Italian guidelines. *Structural Concrete*, *22*(5), 2868–2881. https://doi.org/10.1002/suco.202100147

[115] Croce, P., Formichi, P., Landi, F., Mercogliano, P., Bucchignani, P., Dosio, A., & Dimova, S. (2016). *Towards new european snow load map: Support to policies and standards for sustainable construction*. Joint Research Center. https://publications.jrc.ec.europa.eu/repository/handle/JRC103265

[116] Croce, P., Formichi, P., & Landi, F. (2019). Climate Change: Impacts on Climatic Actions and Structural Reliability. *Applied Sciences*, *9*(24), 5416. https://doi.org/10.3390/app9245416

[117] Croce, P., Formichi, P., Landi, F., & Marsili, F. (2018). Climate change: Impact on snow loads on structures. *Cold Regions Science and Technology*, *150*, 35–50. https://doi.org/10.1016/j.coldregions.2017.10.009

[118] Croce, P., Formichi, P., Landi, F., Mercogliano, P., Bucchignani, E., Dosio, A., & Dimova, S. (2018). The snow load in Europe and the climate change. *Climate Risk Management*, *20*, 138–154. https://doi.org/10.1016/j.crm.2018.03.001

[119] CSA. (1974). *Standards for the Design of Cold-Formted Steel Members in Buildings, CSA S-137*. Canadian Standards Association.

[120] ČSN. (2019). *ČSN 73 0038 - Assessment and verification of existing structures - Supplementary guidance (in Czech)*. ÚNM Publishing.

[121] Cui, W., & Caracoglia, L. (2016). Exploring hurricane wind speed along us atlantic coast in warming climate and effects on predictions of structural damage and intervention costs. *Engineering Structures*, *122*, 209–225. https://doi.org/10.1016/j.engstruct.2016.05.003

[122] Darwin, D., Browning, J., Gong, L., & Hughes, S. R. (2007). *Effects of deicers on concrete deterioration*. University of Kansas Center for Research, Inc.

[123] Davy, R., Gnatiuk, N., Pettersson, L., & Bobylev, L. (2018). Climate change impacts on wind energy potential in the european domain with a focus on the black sea. *Renewable and sustainable energy reviews*, *81*, 1652–1659. https://doi.org/10.1016/j.rser.2017.05.253

[124] Der Kiureghian, A., & Ditlevsen, O. (2009). Aleatory or epistemic? does it matter? *Structural safety*, *31*(2), 105–112. https://doi.org/10.1016/j.strusafe.2008.06.020

[125] Der Kiureghian, A., Lin, H.-Z., & Hwang, S.-J. (1987). Second-order reliability approximations. *Journal of Engineering mechanics*, *113*(8), 1208–1225.

[126] Diamantidis, D., & Bazzurro, P. (2007). Safety acceptance criteria for existing structures. In M. H. Faber (Ed.), *Special workshop on risk acceptance and risk communication*. Elsevier.

[127] Dimova, S., Polo López, C., Sousa, M., Rianna, G., Bastidas-Arteaga, E., Nogal, M., Gervásio, H., Martorana, E., Reder, A., & Athanasopoulou, A. (2024). *Impact of climate change on the corrosion of the european reinforced concrete building stock*. Joint Research Center. https://data.europa.eu/doi/10.2760/016004

[128] Ditlevsen, O. (1997). Structural reliability codes for probabilistic design — a debate paper based on elementary reliability and decision analysis concepts. *Structural Safety*, *19*(3), 253–270. https://doi.org/10.1016/S0167-4730(97)00009-X

[129] Ditlevsen, O. (1979). Generalized second moment reliability index. *Journal of Structural Mechanics*, *7*(4), 435–451.

[130] Ditlevsen, O., & Madsen, H. O. (1996). *Structural reliability methods* (Vol. 178). Citeseer.

[131] Dottori, F., Mentaschi, L., Bianchi, A., Alfieri, L., & Feyen, L. (2020). *Adapting to rising river flood risk in the eu under climate change*. Joint Research Center. https://publications.jrc.ec.europa.eu/repository/handle/JRC118425

[132] Du, X., & Chen, W. (2000). Towards a better understanding of modeling feasibility robustness in engineering design. *J. Mech. Des.*, *122*(4), 385–394. https://doi.org/10.1115/1.1290247

[133] Du, Y. G., Clark, L. A., & Chan, A. H. C. (2005). Effect of corrosion on ductility of reinforcing bars. *Magazine of Concrete Research*, *57*(7), 407–419. https://doi.org/10.1680/macr.2005.57.7.407

[134] DuraCrete. (1998). *Modelling of degradation. DuraCrete—probabilistic performance based durability design of concrete structures*. EU—brite EuRam III. Contract BRPR-CT95-0132. Project BE95-1347/R4-5.

[135] DuraCrete. (2000). *Probabilistic performance based durability design of concrete structures (contract brpr-ct95-0132, project be95-1347. document be95-1347/r17)*.

[136] Echard, B., Gayton, N., & Lemaire, M. (2011). Ak-mcs: An active learning reliability method combining kriging and monte carlo simulation. *Structural safety*, *33*(2), 145–154. https://doi.org/10.1016/j.strusafe.2011.01.002

[137] Ellingwood, B. R. (2005). Risk-informed condition assessment of civil infrastructure: State of practice and research issues. *Structure and infrastructure engineering*, *1*(1), 7–18. https://doi.org/10.1080/15732470412331289341

[138] Ellingwood, B. R., Galambos, T. V., MacGregor, J. G., & Cornell, C. A. (1980). *Development of a probability based load criterion for American National Standard*

A58: Building code requirements for minimum design loads in buildings and other structures (Vol. 577). Department of Commerce, National Bureau of Standards.

[139] Enright, M. P., & Frangopol, D. M. (1999). Condition Prediction of Deteriorating Concrete Bridges Using Bayesian Updating. *Journal of Structural Engineering*, *125*(10), 1118–1125. https://doi.org/10.1061/(ASCE)0733-9445(1999)125:10(1118)

[140] Eyring, V., Bony, S., Meehl, G. A., Senior, C. A., Stevens, B., Stouffer, R. J., & Taylor, K. E. (2016). Overview of the coupled model intercomparison project phase 6 (cmip6) experimental design and organization. *Geoscientific Model Development*, *9*(5), 1937–1958.

[141] Faber, M. H., & Sørensen, J. D. (2003). Reliability-based code calibration: The jcss approach. In A. Der Kiureghian, S. Madanat, & J. M. Pestana (Eds.), *Applications of statistics and probability in civil engineering: Proceedings of the 9th international conference on applications of statistics and probability in civil engineering* (pp. 927–935).

[142] Faber, M. H., & Virguez Rodriguez, E. A. (2011). Supporting decisions on global health and life safety investments. *Applications of Statistics and Probability in Civil Engineering: Proceedings of the 11th international conference on applications of statistics and probability in civil engineering*, 434–443.

[143] Fahey, D., Doherty, S., Hibbard, K. A., Romanou, A., & Taylor, P. (2017). *Physical drivers of climate change*. Publications, Agencies; Staff of the U.S. Department of Commerce. 591. https://doi.org/http://digitalcommons.unl.edu/usdeptcommercepub/591

[144] Faroz, S. A., Pujari, N. N., & Ghosh, S. (2016). Reliability of a corroded RC beam based on Bayesian updating of the corrosion model. *Engineering Structures*, *126*, 457–468. https://doi.org/10.1016/j.engstruct.2016.08.003

[145] fib. (2006). *Bulletin no. 34: Model code for service life design*. International Federation for Structural Concrete. https://doi.org/doi.org/10.35789/fib.BULL.0034

[146] fib. (2013). *Model code for concrete structures 2010*. International Federation for Structural Concrete.

[147] fib. (2015). *Bulletin no. 76: Benchmarking of deemed-to-satisfy provisions in standards: Durability of reinforced concrete structures exposed to chlorides*. International Federation for Structural Concrete.

[148] fib. (2016). *Bulletin n°80: Partial factor methods for existing concrete structures*. International Federation for Structural Concrete.

[149] fib. (2023). *Model code for concrete structures (2020)*. International Federation for Structural Concrete.

[150] Fiessler, B., Neumann, H.-J., & Rackwitz, R. (1979). Quadratic limit states in structural reliability. *Journal of the Engineering Mechanics Division*, *105*(4), 661–676.

[151] Fischer, K., Bernardo, C., & Faber, M. H. (2012). Deriving target reliabilities from the lqi. *LQI Symposium, DTU Denmark, August 2013 (Paper Presentation)*.

[152] Flato, G. M. (2011). Earth system models: An overview. *Wiley Interdisciplinary Reviews: Climate Change*, *2*(6), 783–800.

[153] Flint, M. M., Fringer, O., Billington, S. L., Freyberg, D., & Diffenbaugh, N. S. (2017). Historical analysis of hydraulic bridge collapses in the continental united states. *Journal of infrastructure systems*, *23*(3), 04017005. https://doi.org/10.1061/(ASCE)IS.1943-555X.0000354

[154] Fowler, H. J., Blenkinsop, S., & Tebaldi, C. (2007). Linking climate change modelling to impacts studies: Recent advances in downscaling techniques for hydrological modelling. *International Journal of Climatology*, *27*(12), 1547–1578. https://doi.org/10.1002/joc.1556

[155] Fuentes, U., & Heimann, D. (2000). An improved statistical-dynamical downscaling scheme and its application to the alpine precipitation climatology. *Theoretical and Applied Climatology*, *65*(3), 119–135.

[156] Fujino, J., Nair, R., Kainuma, M., Masuif, T., & Matsuokan, Y. (2006). Multi-gas mitigation analysis on stabilization scenarios using aim global model. *The Energy Journal*, *27*(3_suppl), 343–354.

[157] Gahlen, G. (2000). *"Probability-Based service life design of reinforced concrete structures - Reliability studies for prevention of reinforced corrosion"*. DAdStb Helf 510, (in German).

[158] Galambos, T. V., Ellingwood, B., MacGregor, J. G., & Cornell, C. A. (1982). Probability Based Load Criteria: Assessment of Current Design Practice. *Journal of the Structural Division*, *108*(5), 959–977. https://doi.org/10.1061/JSDEAG.0005958

[159] Gao, W., Wu, D., Gao, K., Chen, X., & Tin-Loi, F. (2018). Structural reliability analysis with imprecise random and interval fields. *Applied Mathematical Modelling*, *55*, 49–67. https://doi.org/10.1016/j.apm.2017.10.029

[160] Gastaldi, M., & Bertolini, L. (2014). Effect of temperature on the corrosion behaviour of low-nickel duplex stainless steel bars in concrete. *Cement and Concrete Research*, *56*, 52–60. https://doi.org/10.1016/j.cemconres.2013.11.004

[161] Gayton, N., Mohamed, A., Sorensen, J. D., Pendola, M., & Lemaire, M. (2004). Calibration methods for reliability-based design codes. *Structural Safety*, *26*(1), 91–121. https://doi.org/10.1016/S0167-4730(03)00024-9

[162] Geymayer, H. G. (1970). *The effect of temperature on creep of concrete: A literature review* (Technical Report). U.S. Department of the Interior, Bureau of Reclamation.

[163] Ghosn, M., Frangopol, D. M., McAllister, T. P., Shah, M., Diniz, S. M. C., Ellingwood, B. R., Manuel, L., Biondini, F., Catbas, N., Strauss, A., & Zhao, X. L. (2016). Reliability-Based Performance Indicators for Structural Members. *Journal of Structural Engineering*, *142*(9), F4016002. https://doi.org/10.1061/(ASCE)ST.1943-541X.0001546

[164] Ghosn, M., & Ellingwood, B. R. (2023). Risk-informed design and safety assessment of structures in a changing climate: A review of U.S. practice and a path forward. *Structure and Infrastructure Engineering*, 1–15. https://doi.org/10.1080/15732479.2023.2265334

[165] Gino, D., Castaldo, P., Bertagnoli, G., Giordano, L., & Mancini, G. (2020). Partial factor methods for existing structures according to fib bulletin 80: Assessment of an existing prestressed concrete bridge. *Structural Concrete*, *21*(1), 15–31. https://doi.org/10.1002/suco.201900231

[166] Gino, D., Castaldo, P., Giordano, L., & Mancini, G. (2021). Model uncertainty in non-linear numerical analyses of slender reinforced concrete members. *Structural concrete*, *22*(2), 845–870. https://doi.org/10.1002/suco.202000600

[167] Gino, D., Miceli, E., Castaldo, P., Recupero, A., & Mancini, G. (2024). Strain-based method for assessment of global resistance safety factors for NLNAs of reinforced concrete structures. *Engineering Structures*, *304*, 117625. https://doi.org/10.1016/j.engstruct.2024.117625

[168] Giorgi, F., & Gutowski Jr, W. J. (2015). Regional dynamical downscaling and the cordex initiative. *Annual review of environment and resources*, *40*(1), 467–490. https://doi.org/10.1146/annurev-environ-102014-021217

[169] Giorgi, F., Jones, C., Asrar, G. R., et al. (2006). Addressing climate information needs at the regional level: The cordex framework. *World Meteorological Organization (WMO) Bulletin*, *58*(3), 175–183.

[170] Gjørv, O. E. (2009a). *Durability design of concrete structures in severe environments*. Taylor & Francis Group.

[171] Gjørv, O. E. (2009b). *Durability design of concrete structures in severe environments*. Taylor & Francis.

[172] Gonzalez, J., & Andrade, C. (1982). Effect of carbonation, chlorides and relative ambient humidity on the corrosion of galvanized rebars embedded in concrete. *British Corrosion Journal*, *17*(1), 21–28. https://doi.org/10.1179/000705982798274589

[173] Gonzalez, J., Andrade, C., Alonso, C., & Feliu, S. (1995). Comparison of rates of general corrosion and maximum pitting penetration on concrete embedded steel reinforcement. *Cement and concrete research*, *25*(2), 257–264. https://doi.org/10.1016/0008-8846(95)00006-2

[174] Gregory, P. J., Ingram, J. S., & Brklacich, M. (2005). Climate change and food security. *Philosophical Transactions of the Royal Society B: Biological Sciences*, *360*(1463), 2139–2148. https://doi.org/10.1098/rstb.2005.1745

[175] Gudipudi, P. P., Underwood, B. S., & Zalghout, A. (2017). Impact of climate change on pavement structural performance in the united states. *Transportation Research Part D: Transport and Environment*, *57*, 172–184. https://doi.org/10.1016/j.trd.2017.09.022

[176] Guo, Y., Trejo, D., & Yim, S. (2015). New model for estimating the time-variant seismic performance of corroding rc bridge columns. *Journal of Structural Engineering (United States)*, *141*(6). https://doi.org/10.1061/(ASCE)ST.1943-541X.0001145

[177] Guyennon, N., Romano, E., Portoghese, I., Salerno, F., Calmanti, S., Petrangeli, A., Tartari, G., & Copetti, D. (2013). Benefits from using combined dynamical-statistical downscaling approaches–lessons from a case study in the mediterranean region. *Hydrology and Earth System Sciences*, *17*(2), 705–720.

[178] Habeeb, B., Bastidas-Arteaga, E., & Liberge, E. (2024). A stochastic framework considering uncertainties of scouring on the stability of bridges. *13èmes Journées de Fiabilité des Matériaux et des Structures (JFMS 2024)*.

[179] Haldar, A., & Mahadevan, S. (2000). *Probability, reliability and statistical methods in engineering design*. John Wiley & Sons.

[180] Hansson, C. M., & Sørensen, B. (1990). The threshold concentration of chloride in concrete for the initiation of reinforcement corrosion. *Corrosion rates of steel in concrete*, 3–16.

[181] Harris, C., Arenson, L. U., Christiansen, H. H., Etzelmüller, B., Frauenfelder, R., Gruber, S., Haeberli, W., Hauck, C., Hoelzle, M., Humlum, O., et al. (2009). Permafrost and climate in europe: Monitoring and modelling thermal, geomorphological and geotechnical responses. *Earth-Science Reviews*, *92*(3-4), 117–171. https://doi.org/10.1016/j.earscirev.2008.12.002

[182] Hasofer, A. M., & Lind, N. C. (1974). Exact and invariant second-moment code format. *Journal of the Engineering Mechanics division*, *100*(1), 111–121.

[183] Hegglin, M., Plummer, D., Shepherd, T., Scinocca, J., Anderson, J., Froidevaux, L., Funke, B., Hurst, D., Rozanov, A., Urban, J., et al. (2014). Vertical structure

of stratospheric water vapour trends derived from merged satellite data. *Nature Geoscience*, *7*(10), 768–776.

[184] Heiyantuduwa, R., Alexander, M., & Mackechnie, J. (2006). Performance of a penetrating corrosion inhibitor in concrete affected by carbonation-induced corrosion. *Journal of materials in civil engineering*, *18*(6), 842–850. https://doi.org/10.1061/(ASCE)0899-1561(2006)18:6(842)

[185] Held, I. M. (2005). The gap between simulation and understanding in climate modeling. *Bulletin of the American Meteorological Society*, *86*(11), 1609–1614. https://doi.org/10.1175/BAMS-86-11-1609

[186] Henderson, J., & Blockley, D. (1982). Logical analysis of assumptions in code calibration. *Structural Safety*, *1*(2), 123–140.

[187] Hijioka, Y., Matsuoka, Y., Nishimoto, H., Masui, M., & Kainuma, M. (2008). Global ghg emission scenarios under gic; concentration stabilization targets. *J. Glob. Environ. Eng*, *13*, 97–108.

[188] Hintermaier, A., & Lin, N. (2024). An investigation of climate change effects on design wind speeds along the us east and gulf coasts. *Journal of Structural Engineering*, *150*(9), 04024123. https://doi.org/10.1061/JSENDH.STENG-11899

[189] Ho, D., & Lewis, R. (1987). Carbonation of concrete and its prediction. *Cement and Concrete Research*, *17*(3), 489–504.

[190] Hoffman, F. O., & Hammonds, J. S. (1994). Propagation of uncertainty in risk assessments: The need to distinguish between uncertainty due to lack of knowledge and uncertainty due to variability. *Risk analysis*, *14*(5), 707–712. https://doi.org/10.1111/j.1539-6924.1994.tb00281.x

[191] Holicky, M., Markova, J., & Sykora, M. (2008). Partial factors for assessment of existing reinforced concrete bridges. In C.-A. Graubner, H. Schmidt, & D. Proske (Eds.), *Proceedings of the 6th international probabilistic workshop, weimar, germany, november 5-6, 2014* (pp. 117–131). Technische Universität Darmstadt.

[192] Holicky, M., & Sykora, M. (2011). Conventional probabilistic models for calibration of codes. *Applications of Statistics and Probability in Civil Engineering: Proceedings of the 11th international conference on applications of statistics and probability in civil engineering*, 969–976.

[193] Hong, H., Tang, Q., Yang, S., Cui, X., Cannon, A., Lounis, Z., & Irwin, P. (2021). Calibration of the design wind load and snow load considering the historical climate statistics and climate change effects. *Structural Safety*, *93*, 102135. https://doi.org/10.1016/j.strusafe.2021.102135

[194] Hong, J.-H., Chiew, Y.-M., Lu, J.-Y., Lai, J.-S., & Lin, Y.-B. (2012). Houfeng bridge failure in taiwan. *Journal of Hydraulic Engineering*, *138*(2), 186–198. https://doi.org/10.1061/(ASCE)HY.1943-7900.0000430

[195] Houghton, H. G., & Radford, W. H. (1938). On the measurement of drop size and liquid water content in fogs and clouds. *Papers in Physical Oceanography and Meteorology*, *6*(4), 1–31.

[196] Hultén, C., Andersson-Sköld, Y., Ottosson, E., Edstam, T., & Johansson, Å. (2007). Case studies of landslide risk due to climate change in sweden. proceedings of the international conference on landslides and climate change. In R. McInnes, J. Jakeways, H. Fairbank, & E. Mathie (Eds.), *Landslides and climate change: Challenges and solutions* (pp. 149–157). Taylor & Francis.

[197] Hussain, S., Al-Musallam, A., Al-Gahtani, A., et al. (1995). Factors affecting threshold chloride for reinforcement corrosion in concrete. *Cement and Concrete Research*, *25*(7), 1543–1555. https://doi.org/10.1016/0008-8846(95)00148-6

[198] IPCC. (1990). Response strategies working group. In J. T. Houghton, G. J. Jenkins, & J. J. Ephraums (Eds.), *Climate change: The ipcc scientific assessment* (pp. 329–341). Cambridge University Press.

[199] IPCC. (1992). Emissions scenarios for ipcc: An update. In J. T. Houghton, B. A. Callander, & S. K. Varney (Eds.), *Climate change 1992: The supplementary report to the ipcc scientific assessment* (pp. 69–95). Cambridge University Press.

[200] IPCC. (2000). *Special Report on Emissions Scenarios: A Special Report of Working Group III of the Intergovernmental Panel on Climate Change*. Cambridge University Press.

[201] IPCC. (2007). *Climate Change 2007: Synthesis Report. Contribution of Working Groups I, II and III to the Fourth Assessment Report of the Intergovernmental Panel on Climate Change* (R. Pachauri & A. Reisinger, Eds.). Cambridge University Press.

[202] IPCC. (2013). *Climate Change 2013: The Physical Science Basis. Contribution of Working Group I to the Fifth Assessment Report of the Intergovernmental Panel on Climate Change* (T. Stocker, D. Qin, G.-K. Plattner, M. Tignor, S. Allen, J. Boschung, A. Nauels, Y. Xia, V. Bex, & P. Midgley, Eds.). Cambridge University Press. https://doi.org/10.59327/IPCC/AR6-9789291691647

[203] IPCC. (2022). *Climate Change 2022: Impacts, Adaptation and Vulnerability. Contribution of Working Group II to the Sixth Assessment Report of the Intergovernmental Panel on Climate Change*. Intergovernmental Panel on Climate Change.

[204] IPCC. (2023a). *Climate Change 2021 – The Physical Science Basis: Working Group I Contribution to the Sixth Assessment Report of the Intergovernmental Panel on Climate Change*. Cambridge University Press.

[205] IPCC. (2023b). *Climate Change 2023: Synthesis Report. Contribution of Working Groups I, II and III to the Sixth Assessment Report of the Intergovernmental Panel on Climate Change*. Intergovernmental Panel on Climate Change.

[206] ISO2394. (2015). *General principles on reliability for structures*. International Organization for Standardization.

[207] Jacinto, L., Neves, L. C., & Santos, L. O. (2016). Bayesian assessment of an existing bridge: A case study. *Structure and Infrastructure Engineering*, *12*(1), 61–77. https://doi.org/10.1080/15732479.2014.995105

[208] Jacob, D., Petersen, J., Eggert, B., Alias, A., Christensen, O., Bouwer, L., Braun, A., Colette, A., Déqué, M., Georgievski, G., Georgopoulou, E., Gobiet, A., Menut, L., Nikulin, G., Haensler, A., Hempelmann, N., Jones, C., Keuler, K., Kovats, S., ... Yiou, P. (2014). Euro-cordex: New high-resolution climate change projections for european impact research. *Regional Environmental Change*, *14*(2), 563–578. https://doi.org/10.1007/s10113-013-0499-2

[209] Jacob, D., Petersen, J., Eggert, B., Alias, A., Christensen, O. B., Bouwer, L. M., Braun, A., Colette, A., Déqué, M., Georgievski, G., Georgopoulou, E., Gobiet, A., Menut, L., Nikulin, G., Haensler, A., Hempelmann, N., Jones, C., Keuler, K., Kovats, S., ... Yiou, P. (2014). EURO-CORDEX: New high-resolution climate change projections for European impact research. *Regional Environmental Change*, *14*(2), 563–578. https://doi.org/10.1007/s10113-013-0499-2

[210] Jamali, A., Angst, U., Adey, B., & Elsener, B. (2013). Modeling of corrosion-induced concrete cover cracking: A critical analysis. *Construction and Building Materials*, *42*, 225–237. https://doi.org/10.1016/j.conbuildmat.2013.01.019

[211] JCSS. (2001). *Probabilistic model code*. Joint Committee on Structural Safety.

[212] JCSS. (2008). *Risk assessment in engineering - principles, system representation & risk criteria* (M. H. Faber, Ed.). Joint Committee on Structural Safety. https://www.jcss-lc.org/publications/raie/01_jcss_riskassessment.pdf

[213] Kadlec, L., & Červenka, V. (2016). Model uncertainties of fem nonlinear analyses of concrete structures. *Solid State Phenomena*, *249*, 197–202. https://doi.org/10.4028/www.scientific.net/SSP.249.197

[214] Kallias, A. N., & Imam, B. (2016). Probabilistic assessment of local scour in bridge piers under changing environmental conditions. *Structure and Infrastructure Engineering*, *12*(9), 1228–1241. https://doi.org/10.1080/15732479.2015.1102295

[215] Karl, T. R., Melillo, J. M., Peterson, T. C., & Hassol, S. J. (2009). Global climate change impacts in the united states. *Global climate change impacts in the United States*.

[216] Kawai, H., Koshiro, T., Endo, H., Arakawa, O., & Hagihara, Y. (2016). Changes in marine fog in a warmer climate. *Atmospheric Science Letters*, *17*(10), 548–555. https://doi.org/10.1002/asl.691

[217] Kerr, G. H., DeGaetano, A. T., Stoof, C. R., & Ward, D. (2018). Climate change effects on wildland fire risk in the northeastern and great lakes states predicted by a downscaled multi-model ensemble. *Theoretical and Applied Climatology*, *131*(1), 625–639. https://doi.org/10.1007/s00704-016-1994-4

[218] Khandel, O., & Soliman, M. (2019). Integrated Framework for Quantifying the Effect of Climate Change on the Risk of Bridge Failure Due to Floods and Flood-Induced Scour. *Journal of Bridge Engineering*, *24*(9), 04019090. https://doi.org/10.1061/(ASCE)BE.1943-5592.0001473

[219] Kiehl, J. T., & Trenberth, K. E. (1997). Earth's annual global mean energy budget. *Bulletin of the American meteorological society*, *78*(2), 197–208. https://doi.org/doi.org/10.1175/1520-0477(1997)078⟨0197:EAGMEB⟩2.0.CO;2

[220] Kim, Y., Eisenberg, D. A., Bondank, E. N., Chester, M. V., Mascaro, G., & Underwood, B. S. (2017). Fail-safe and safe-to-fail adaptation: Decision-making for urban flooding under climate change. *Climatic Change*, *145*, 397–412. https://doi.org/10.1007/s10584-017-2090-1

[221] Knutti, R., Furrer, R., Tebaldi, C., Cermak, J., & Meehl, G. A. (2010). Challenges in combining projections from multiple climate models. *Journal of Climate*, *23*(10), 2739–2758. https://doi.org/10.1175/2009JCLI3361.1

[222] Köhler, J., Sørensen, J. D., & Baravalle, M. (2019). Calibration of existing semi-probabilistic design codes. *Proceedings of the 13th International Conference on Applications of Statistics and Probability in Civil Engineering (ICASP2019), Seoul, South Korea, May 26-30, 2019*.

[223] Köhler, J., & Baravalle, M. (2019). Risk-based decision making and the calibration of structural design codes – prospects and challenges. *Civil Engineering and Environmental Systems*, *36*(1), 55–72. https://doi.org/10.1080/10286608.2019.1615477

[224] Köliö, A., Pakkala, T. A., Lahdensivu, J., & Kiviste, M. (2014). Durability demands related to carbonation induced corrosion for Finnish concrete buildings in changing climate. *Engineering Structures*, *62-63*, 42–52. https://doi.org/10.1016/j.engstruct.2014.01.032

[225] König, G., & Hosser, D. (1982). The simplified level ii method and its application on the derivation of safety elements for level i. *CEB bulletin*, *147*.

[226] Kovarik, J.-B. (2024). *Working with uncertainties in the design of civil engineering structures: How to accommodate reliability and economy* (Thèse de doctorat). Université Paris-Est. France.

[227] Kriegler, E., O'Neill, B. C., Hallegatte, S., Kram, T., Lempert, R. J., Moss, R. H., & Wilbanks, T. (2012). The need for and use of socio-economic scenarios for climate change analysis: A new approach based on shared socio-economic pathways. *Global Environmental Change*, *22*(4), 807–822.

[228] Kumar, P., & Imam, B. (2013). Footprints of air pollution and changing environment on the sustainability of built infrastructure. *Science of the total environment*, *444*, 85–101. https://doi.org/10.1016/j.scitotenv.2012.11.056

[229] Lambert, P., Page, C., & Vassie, P. (1991). Investigations of reinforcement corrosion. 2. electrochemical monitoring of steel in chloride-contaminated concrete. *Materials and Structures*, *24*(5), 351–358. https://doi.org/10.1007/BF02472068

[230] Lara, C., Tanner, P., Zanuy, C., & Hingorani, R. (2021). Reliability Verification of Existing RC Structures Using Partial Factors Approaches and Site-Specific Data. *Applied Sciences*, *11*(4), 1653. https://doi.org/10.3390/app11041653

[231] Le Roux, E., Evin, G., Eckert, N., Blanchet, J., & Morin, S. (2020). Non-stationary extreme value analysis of ground snow loads in the French Alps: A comparison with building standards. *Natural Hazards and Earth System Sciences*, *20*(11), 2961–2977. https://doi.org/10.5194/nhess-20-2961-2020

[232] Lean, J. (1997). The sun's variable radiation and its relevance for earth. *Annual review of Astronomy and Astrophysics*, *35*(1), 33–67.

[233] Lee, J. Y., & Ellingwood, B. R. (2017). A decision model for intergenerational life-cycle risk assessment of civil infrastructure exposed to hurricanes under climate change. *Reliability Engineering & System Safety*, *159*, 100–107. https://doi.org/10.1016/j.ress.2016.10.022

[234] Lee, S. H., & Kwak, B. M. (2006). Response surface augmented moment method for efficient reliability analysis. *Structural safety*, *28*(3), 261–272. https://doi.org/10.1016/j.strusafe.2005.08.003

[235] Lenner, R., Keuser, M., & Sỳkora, M. (2014). Safety concept and partial factors for bridge assessment under military loading. *Advances in Military Technology*, *9*(2), 5–20.

[236] Lenner, R., & Sykora, M. (2017). Partial factors for imposed loads in areas for storage and industrial use. *Structure and Infrastructure Engineering*, *13*(11), 1425–1436. https://doi.org/10.1080/15732479.2017.1285328

[237] Lenner, R., & Sýkora, M. (2016). Partial factors for loads due to special vehicles on road bridges. *Engineering Structures*, *106*, 137–146. https://doi.org/10.1016/j.engstruct.2015.10.024

[238] Lenner, R., Viljoen, C., & van Nierop, S. (2019). A comparative study of target reliability index derivation for reinforced concrete structures governed by service-

ability limit state. *Structural Concrete*, *20*(2), 670–677. https://doi.org/10.1002/suco.201800202

[239] Li, G., & Cheng, G. (2001). Optimal decision for the target value of performance-based structural system reliability. *Structural and Multidisciplinary Optimization*, *22*(4), 261–267.

[240] Li, Q., Wang, C., & Zhang, H. (2016). A probabilistic framework for hurricane damage assessment considering non-stationarity and correlation in hurricane actions. *Structural Safety*, *59*, 108–117. https://doi.org/10.1016/j.strusafe.2016.01.001

[241] Li, S. H. (2023). Effect of nonstationary extreme wind speeds and ground snow loads on the structural reliability in a future Canadian changing climate. *Structural Safety*, *101*, 102296. https://doi.org/10.1016/j.strusafe.2022.102296

[242] Liljefors, F., & Köhler, J. (2023). Decision support and structural assessment of a corroding reinforced concrete bridge considering new information. *Structure and Infrastructure Engineering*, *0*(0), 1–16. https://doi.org/10.1080/15732479.2023.2271962

[243] Lin, H., Zhao, Y., Feng, P., Ye, H., Ozbolt, J., Jiang, C., & Yang, J.-Q. (2019). State-of-the-art review on the bond properties of corroded reinforcing steel bar. *Construction and Building Materials*, *213*, 216–233. https://doi.org/10.1016/j.conbuildmat.2019.04.077

[244] Lin, H., Zhao, Y., Ozbolt, J., Feng, P., Jiang, C., & Eligehausen, R. (2019). Analytical model for the bond stress-slip relationship of deformed bars in normal strength concrete. *Construction and Building Materials*, *198*, 570–586. https://doi.org/10.1016/j.conbuildmat.2018.11.258

[245] Lind, N. (1977). Reliability based structural codes, practical calibration. In H. I. (Ed.), *Safety of structures under dynamic loading* (pp. 149–160). Norwegian Institute of Technology;

[246] Liu, L., Yang, D. Y., & Frangopol, D. M. (2021). Determining target reliability index of structures based on cost optimization and acceptance criteria for fatality risk. *ASCE-ASME Journal of Risk and Uncertainty in Engineering Systems, Part A: Civil Engineering*, *7*(2), 04021013. https://doi.org/10.1061/AJRUA6.0001127

[247] Liu, P. L., & Der Kiureghian, A. (1991). Optimization algorithms for structural reliability. *Structural safety*, *9*(3), 161–177.

[248] Liu, T., & Weyers, R. (1998). Modeling the dynamic corrosion process in chloride contaminated concrete structures. *Cement and Concrete research*, *28*(3), 365–379. https://doi.org/10.1016/S0008-8846(98)00259-2

[249] Liu, Y. P., & Weyers, R. E. (1998). Modeling the time-to-corrosion cracking in chloride contaminated reinforced concrete structures. *ACI Materials Journal*, *95*(6), 675–681.

[250] Lombardo, F. T., & Ayyub, B. M. (2015). Analysis of Washington, DC, Wind and Temperature Extremes with Examination of Climate Change for Engineering Applications. *ASCE-ASME Journal of Risk and Uncertainty in Engineering Systems, Part A: Civil Engineering*, *1*(1), 04014005. https://doi.org/10.1061/AJRUA6.0000812

[251] Lozano, O. M., Salis, M., Ager, A. A., Arca, B., Alcasena, F. J., Monteiro, A. T., Finney, M. A., Del Giudice, L., Scoccimarro, E., & Spano, D. (2017). Assessing Climate Change Impacts on Wildfire Exposure in Mediterranean Areas. *Risk Analysis*, *37*(10), 1898–1916. https://doi.org/10.1111/risa.12739

[252] Luechinger, P., Fischer, J., Chrysostomou, C., Dieteren, G., Landon, F., Leivestad, S., Malakatas, N., Mancini, G., Markova, J., Matthews, S., Nolan, T., Nuti, C., Osmani, E., Ronnow, G., Schnell, J., & Tanner, P. (2015). *New european technical rules for the assessment and retrofitting of existing structures*. JRC. https://publications.jrc.ec.europa.eu/repository/handle/JRC94918

[253] M/515, C. (2012). *Mandate for amending existing eurocodes and extending the scope of structural eurocodes*. European Committee for Standardization.

[254] Madsen, H. O., Krenk, S., & Lind, N. C. (2006). *Methods of structural safety*. Dover Publications.

[255] Mallick, R. B., Jacobs, J. M., Miller, B. J., Daniel, J. S., & Kirshen, P. (2018). Understanding the impact of climate change on pavements with cmip5, system dynamics and simulation. *International Journal of Pavement Engineering*, *19*(8), 697–705. https://doi.org/10.1080/10298436.2016.1199880

[256] Marchau, V. A. W. J., Walker, W. E., Bloemen, P. J. T. M., & Popper, S. W. (2019). Introduction. In V. A. W. J. Marchau, W. E. Walker, P. J. T. M. Bloemen, & S. W. Popper (Eds.), *Decision making under deep uncertainty: From theory to practice* (pp. 1–22). Springer. https://doi.org/10.1007/978-3-030-05252-2_1

[257] Martı´nez, I., & Andrade, C. (2009). Examples of reinforcement corrosion monitoring by embedded sensors in concrete structures. *Cement and Concrete Composites*, *31*(8), 545–554. https://doi.org/10.1016/j.cemconcomp.2009.05.007

[258] Martın-Pérez, B., Pantazopoulou, S. J., & Thomas, M. (2001). Numerical solution of mass transport equations in concrete structures. *Computers & Structures*, *79*(13), 1251–1264. https://doi.org/10.1016/S0045-7949(01)00018-9

[259] Matthews, S., Bigaj-van Vliet, A., Walraven, J., Mancini, G., & Dieteren, G. (2018). Fib Model Code 2020: Towards a general code for both new and exist-

ing concrete structures. *Structural Concrete*, *19*(4), 969–979. https://doi.org/10.1002/suco.201700198

[260] Melchers, R. E. (1989). Importance sampling in structural systems. *Structural safety*, *6*(1), 3–10.

[261] Melchers, R. E. (2021). Experience-based physico-chemical models for long-term reinforcement corrosion. *Corrosion and Materials Degradation*, *2*(1), 100–119. https://doi.org/10.3390/cmd2010006

[262] Melchers, R. E., & Beck, A. T. (2018). *Structural reliability analysis and prediction*. John wiley & sons.

[263] Melchers, R. E., & Li, C. Q. (2006). Phenomenological modeling of reinforcement corrosion in marine environments. *ACI Materials Journal*, *103*(1), 25.

[264] Météo France. (2025). Le climat en france hexagonale et corse [Accessed: 11-18-2025].

[265] Meyer, M. D., et al. (2008). Design standards for us transportation infrastructure: The implications of climate change. *Transportation Resilience and Vulnerability Collection*. https://rosap.ntl.bts.gov/view/dot/17365/dot_17365_DS1.pdf

[266] Meyer, M. D., & Weigel, B. (2011). Climate change and transportation engineering: Preparing for a sustainable future. *Journal of Transportation Engineering*, *137*(6), 393–403. https://doi.org/10.1061/(ASCE)TE.1943-5436.0000108

[267] Mishra, V., & Sadhu, A. (2023). Towards the effect of climate change in structural loads of urban infrastructure: A review. *Sustainable Cities and Society*, *89*, 104352. https://doi.org/10.1016/j.scs.2022.104352

[268] Misra, A. K. (2014). Climate change and challenges of water and food security. *International Journal of Sustainable Built Environment*, *3*(1), 153–165. https://doi.org/10.1016/j.ijsbe.2014.04.006

[269] Mondoro, A., Frangopol, D. M., & Liu, L. (2018). Bridge Adaptation and Management under Climate Change Uncertainties: A Review. *Natural Hazards Review*, *19*(1), 04017023. https://doi.org/10.1061/(ASCE)NH.1527-6996.0000270

[270] Mori, Y., & Kato, T. (2003). Multinormal integrals by importance sampling for series system reliability. *Structural Safety*, *25*(4), 363–378. https://doi.org/10.1016/S0167-4730(03)00015-8

[271] Morris, W., Vico, A., & Vázquez, M. (2004). Chloride induced corrosion of reinforcing steel evaluated by concrete resistivity measurements. *Electrochimica acta*, *49*(25), 4447–4453. https://doi.org/10.1016/j.electacta.2004.05.001

[272] Moss, R. H., Babiker, M., Brinkman, S., Calvo, E., Carter, T., Edmonds, J., Elgizouli, I., Emori, S., Erda, L., Hibbard, K., Jones, R., Kainuma, M., Kelleher, J., Lamarque, J. F., Manning, M., Matthews, B., Meehl, J., Meyer, L., Mitchell, J., ...

Zurek, M. (2008). *Towards new scenarios for analysis of emissions, climate change, impacts, and response strategies*. Cambridge University Press.

[273] Moss, R. H., Edmonds, J. A., Hibbard, K. A., Manning, M. R., Rose, S. K., Van Vuuren, D. P., Carter, T. R., Emori, S., Kainuma, M., Kram, T., et al. (2010). The next generation of scenarios for climate change research and assessment. *Nature*, *463*(7282), 747–756.

[274] Mudd, L., Wang, Y., Letchford, C., & Rosowsky, D. (2014a). Assessing climate change impact on the us east coast hurricane hazard: Temperature, frequency, and track. *Natural Hazards Review*, *15*(3), 04014001. https://doi.org/10.1061/(ASCE)NH.1527-6996.0000128

[275] Mudd, L., Wang, Y., Letchford, C., & Rosowsky, D. (2014b). Hurricane wind hazard assessment for a rapidly warming climate scenario. *Journal of Wind Engineering and Industrial Aerodynamics*, *133*, 242–249. https://doi.org/10.1016/j.jweia.2014.07.005

[276] Nasr, A., Björnsson, I., Honfi, D., Larsson Ivanov, O., Johansson, J., & Kjellström, E. (2021). A review of the potential impacts of climate change on the safety and performance of bridges. *Sustainable and Resilient Infrastructure*, *6*(3-4), 192–212. https://doi.org/10.1080/23789689.2019.1593003

[277] Nasr, A., Kjellström, E., Björnsson, I., Honfi, D., Ivanov, O. L., & Johansson, J. (2020). Bridges in a changing climate: A study of the potential impacts of climate change on bridges and their possible adaptations. *Structure and Infrastructure Engineering*, *16*(4), 738–749. https://doi.org/10.1080/15732479.2019.1670215

[278] Nath, S. K., Srivastava, N., Ghatak, C., Adhikari, M. D., Ghosh, A., & Sinha Ray, S. (2018). Earthquake induced liquefaction hazard, probability and risk assessment in the city of kolkata, india: Its historical perspective and deterministic scenario. *Journal of Seismology*, *22*(1), 35–68. https://doi.org/10.1007/s10950-017-9691-z

[279] Nathwani, J. S., Lind, N. C., & Pandey, M. D. (1997). *Affordable safety by choice: The life quality method*. University of Waterloo.

[280] Nava, G. V. (2022). *Effect of climate change on life-cycle reliability of concrete structures under corrosion* (Master's thesis). Politecnico di Milano. Milan, Italy.

[281] Nava, G. V., Capacci, L., Biondini, F., & Casti, L. (2023). Life-cycle structural reliability of rc bridge piers under corrosion in a changing climate. In F. Biondini & D. M. Frangopol (Eds.), *Life-Cycle of Structures and Infrastructure Systems: Proceedings of the Eighth International Symposium on Life-Cycle Civil Engineering (IALCCE 2023), Milan, Italy, July 2-6, 2023* (pp. 1625–1633). CRC Press. https://doi.org/10.1201/9781003323020-200

[282] Nava, G. V., D'Iorio, A., & Biondini, F. (2025). Nonstationary cellular automata for life-cycle assessment of concrete bridges under corrosion and climate change [(under publication)]. *Structure and Infrastructure Engineering*.

[283] Nava, G., D'Iorio, A., & Biondini, F. (2024). Cellular automata damage models incorporating climate change effects for life-cycle assessment of concrete bridges. In J. S. Jensen, D. M. Frangopol, & J. W. Schmidt (Eds.), *Bridge Maintenance, Safety, Management, Digitalization and Sustainability: Life-Cycle of Structures and Infrastructure Systems: Proceedings of the 12th International Conference on Bridge Maintenance, Safety, and Management (IABMAS 2024), Copenhagen, Denmark, June 24-28, 2024* (pp. 2755–2763). CRC Press. https://doi.org/10.1201/9781003483755-327

[284] Nazarnia, H., Nazarnia, M., Sarmasti, H., & Wills, W. O. (2020). A Systematic Review of Civil and Environmental Infrastructures for Coastal Adaptation to Sea Level Rise. *Civil Engineering Journal*, *6*(7), 1375–1399. https://doi.org/10.28991/cej-2020-03091555

[285] NEN. (2020). *NEN 8700. Assessment of existing structures in case of reconstruction and disapproval - Basic Rules (in Dutch)*. Royal Netherlands Standardization Institute.

[286] Nguyen, P. T., Bastidas-Arteaga, E., Amiri, O., & El Soueidy, C.-P. (2017). An efficient chloride ingress model for long-term lifetime assessment of reinforced concrete structures under realistic climate and exposure conditions. *International Journal of Concrete Structures and Materials*, *11*(2), 199–213. https://doi.org/10.1007/s40069-017-0185-8

[287] Ni, Y., Ye, X., & Ko, J. (2012). Modeling of stress spectrum using long-term monitoring data and finite mixture distributions. *Journal of Engineering Mechanics*, *138*(2), 175–183. https://doi.org/10.1061/(ASCE)EM.1943-7889.0000313

[288] NOAA. (2026). *Climate modeling*. Retrieved March 3, 2026, from https://www.gfdl.noaa.gov/climate-modeling/

[289] Novák, L., Červenka, J., Červenka, V., Novák, D., & Sỳkora, M. (2023). Comparison of advanced semi-probabilistic methods for design and assessment of concrete structures. *Structural Concrete*, *24*(1), 771–787. https://doi.org/10.1002/suco.202200179

[290] Nowak, A. S., & Lind, N. C. (1979). Practical code calibration procedures. *Canadian Journal of Civil Engineering*, *6*(1), 112–119.

[291] O'Neill, B. C., Kriegler, E., Ebi, K. L., Kemp-Benedict, E., Riahi, K., Rothman, D. S., Van Ruijven, B. J., Van Vuuren, D. P., Birkmann, J., Kok, K., et al. (2017).

The roads ahead: Narratives for shared socioeconomic pathways describing world futures in the 21st century. *Global environmental change*, *42*, 169–180.

[292] O'Neill, B. C., Kriegler, E., Riahi, K., Ebi, K. L., Hallegatte, S., Carter, T. R., Mathur, R., & Van Vuuren, D. P. (2014). A new scenario framework for climate change research: The concept of shared socioeconomic pathways. *Climatic change*, *122*(3), 387–400.

[293] O'Neill, B. C., Tebaldi, C., van Vuuren, D. P., Eyring, V., Friedlingstein, P., Hurtt, G., Knutti, R., Kriegler, E., Lamarque, J.-F., Lowe, J., Meehl, G. A., Moss, R., Riahi, K., & Sanderson, B. M. (2016). The Scenario Model Intercomparison Project (ScenarioMIP) for CMIP6. *Geoscientific Model Development*, *9*(9), 3461–3482. https://doi.org/10.5194/gmd-9-3461-2016

[294] Orcesi, A., Boros, V., Kušter Marić, M., Mandić Ivanković, A., Sýkora, M., Caspeele, J., R. ajd Köhler, O'Connor, A., Schmidt, F., Di Bernardo, S., & Makhoul, N. (2021). Bridge case studies on the assignment of partial safety factors for the assessment of existing structures. *Proceedings of the 18th International Probabilistic Workshop (IPW2021), University of Minho, Guimarães, Portugal, May 12-14, 2021*, 205–218. https://doi.org/10.1007/978-3-030-73616-3_15

[295] Orcesi, A., Diamantidis, D., O'Connor, A., Palmisano, F., Sykora, M., Boros, V., Caspeele, R., Chateauneuf, A., Mandić Ivanković, A., Lenner, R., et al. (2023). Investigating partial factors for the assessment of existing reinforced concrete bridges. *Structural engineering international*, *34*(1), 55–70. https://doi.org/10.1080/10168664.2023.2204115

[296] Orcesi, A., O'Connor Prof., A., Diamantidis Prof, D., Sykora Dr, M., Wu Dr, T., Akiyama Prof., M., Alhamid, A. K., Schmidt Dr, F., Pregnolato Dr, M., Li Prof., Y., Salarieh, B., Salman Prof, A. M., Bastidas-Arteaga Prof, E., Markogiannaki Dr, O., & Schoefs Prof., F. (2022). Investigating the Effects of Climate Change on Structural Actions. *Structural Engineering International*, *32*(4), 563–576. https://doi.org/10.1080/10168664.2022.2098894

[297] Otieno, M., Beushausen, H., & Alexander, M. (2012). Prediction of corrosion rate in reinforced concrete structures–a critical review and preliminary results. *Materials and Corrosion*, *63*(9), 777–790. https://doi.org/10.1002/maco.201106282

[298] Ožbolt, J., Balabanić, G., & Kušter, M. (2011). 3d numerical modelling of steel corrosion in concrete structures. *Corrosion science*, *53*(12), 4166–4177. https://doi.org/10.1016/j.corsci.2011.08.026

[299] Ožbolt, J., Oršanić, F., Balabanić, G., & Kušter, M. (2012). Modeling damage in concrete caused by corrosion of reinforcement: Coupled 3d fe model. *International journal of fracture*, *178*(1), 233–244. https://doi.org/10.1007/s10704-012-9774-3

[300] Page, C. L. (1992). Nature and properties of concrete in relation to reinforcement corrosion. *Corrosion of Steel in Concrete*, 17–19.

[301] Page, C. L., Short, N. R., & El Tarras, A. (1981). Diffusion of chloride ions in hardened cement pastes. *Cement and concrete research*, *11*(3), 395–406. https://doi.org/10.1016/0008-8846(81)90111-3

[302] Pakkala, T. A., Köliö, A., Lahdensivu, J., & Kiviste, M. (2014). Durability demands related to frost attack for Finnish concrete buildings in changing climate. *Building and Environment*, *82*, 27–41. https://doi.org/10.1016/j.buildenv.2014.07.028

[303] Pandey, M. D., & Lounis, Z. (2023). Stochastic modelling of non-stationary environmental loads for reliability analysis under the changing climate. *Structural Safety*, *103*, 102348. https://doi.org/10.1016/j.strusafe.2023.102348

[304] Papadakis, V. G., Vayenas, C. G., & Fardis, M. N. (1991). Fundamental modeling and experimental investigation of concrete carbonation. *Materials Journal*, *88*(4), 363–373. https://doi.org/10.14359/1863

[305] Parrott, L. (1992). Carbonation, moisture and empty pores. *Advances in Cement Research*, *4*(15), 111–118. https://doi.org/10.1680/adcr.1992.4.15.111

[306] Patz, J. A., Campbell-Lendrum, D., Holloway, T., & Foley, J. A. (2005). Impact of regional climate change on human health. *Nature*, *438*(7066), 310–317. https://doi.org/10.1038/nature04188

[307] Peng, J., & Stewart, M. G. (2008). *Carbonation-induced corrosion damage and structural safety for concrete under enhanced greenhouse conditions* (tech. rep. Research Report No. 270.11.2008). Centre for Infrastructure Performance and Reliability, The University of Newcastle. NSW, Australia.

[308] Petoukhov, V., Claussen, M., Berger, A., Crucifix, M., Eby, M., Eliseev, A., Fichefet, T., Ganopolski, A., Goosse, H., Kamenkovich, I., et al. (2005). Emic intercomparison project (emip–co2): Comparative analysis of emic simulations of climate, and of equilibrium and transient responses to atmospheric co2 doubling. *Climate Dynamics*, *25*(4), 363–385.

[309] Pielke Sr, R. A., et al. (2011). Land use/land cover changes and climate: Modeling analysis and observational evidence. *Wiley Interdisciplinary Reviews: Climate Change*, *2*, 828–850. https://doi.org/10.1002/wcc.144

[310] Pimentel, M., Brühwiler, E., & Figueiras, J. (2014). Safety examination of existing concrete structures using the global resistance safety factor concept. *Engineering Structures*, *70*, 130–143. https://doi.org/10.1016/j.engstruct.2014.04.005

[311] Pour-Ghaz, M., Isgor, O. B., & Ghods, P. (2009). The effect of temperature on the corrosion of steel in concrete. part 1: Simulated polarization resistance tests and

model development. *Corrosion Science*, *51*(2), 415–425. https://doi.org/10.1016/j.corsci.2008.10.034

[312] Prieto, M., Tanner, P., & Andrade, C. (2016). Multiple linear regression model for the assessment of bond strength in corroded and non-corroded steel bars in structural concrete. *Materials and Structures*, *49*(11), 4749–4763. https://doi.org/10.1617/s11527-016-0822-8

[313] Qiao, Y., Dawson, A. R., Parry, T., Flintsch, G., & Wang, W. (2020). Flexible pavements and climate change: A comprehensive review and implications. *Sustainability*, *12*(3). https://doi.org/10.3390/su12031057

[314] Qing Li, C. (2004). Reliability based service life prediction of corrosion affected concrete structures. *Journal of Structural Engineering*, *130*(10), 1570–1577. https://doi.org/10.1061/(ASCE)0733-9445(2004)130:10(1570)

[315] Quan, Q., & Gengwei, Z. (2002). Calibration of reliability index of RC beams for serviceability limit state of maximum crack width. *Reliability Engineering & System Safety*, *75*(3), 359–366. https://doi.org/10.1016/S0951-8320(01)00133-8

[316] Rackwitz, R. (1976). Practical probabilistic approach to design. *Bulletin 112, Comite European, du Beton*.

[317] Rackwitz, R. (2000). Optimization — the basis of code-making and reliability verification. *Structural Safety*, *22*(1), 27–60. https://doi.org/10.1016/S0167-4730(99)00037-5

[318] Rackwitz, R., & Fiessler, B. (1976). Note on discrete safety checking when using non-normal stochastic models for basic variables. *Load Project Working Session*.

[319] Rackwitz, R., & Fiessler, B. (1978). Structural reliability under combined random load sequences. *Computers & structures*, *9*(5), 489–494.

[320] Randall, D. A. (2000). *General circulation model development: Past, present, and future* (Vol. 70). Elsevier.

[321] Rao, S., & Riahi, K. (2006). The role of non-co2 greenhouse gases in climate change mitigation: Long-term scenarios for the 21st century. *The Energy Journal*, *27*(3_suppl), 177–200.

[322] Raposo De M. Do N. E S. De Sotto Mayor, M., Dimova, S., Athanasopoulou, A., Rianna, G., Mercogliano, P., Villani, V., Nogal, M., Dos Santos Gervasio, H., Neves, L., Bastidas-Arteaga, E., & Tsionis, G. (2020). *Expected implications of climate change on the corrosion of structures*. Joint Research Center. https://publications.jrc.ec.europa.eu/repository/handle/JRC121312

[323] Raupach, M. (2006). Models for the propagation phase of reinforcement corrosion–an overview. *Materials and Corrosion*, *57*(8), 605–613.

[324] Ravindra, M. K., & Galambos, T. V. (1978). Load and resistance factor design for steel. *Journal of the Structural Division*, *104*(9), 1337–1353.

[325] Retief, J. V. (2022). Assessment of existing structures under climate change. *Acta Polytechnica CTU Proceedings*, *36*, 6–14. https://doi.org/10.14311/APP.2022.36.0006

[326] Riahi, K., Grübler, A., & Nakicenovic, N. (2007). Scenarios of long-term socio-economic and environmental development under climate stabilization. *Technological forecasting and social change*, *74*(7), 887–935.

[327] Riahi, K., Van Vuuren, D. P., Kriegler, E., Edmonds, J., O'neill, B. C., Fujimori, S., Bauer, N., Calvin, K., Dellink, R., Fricko, O., et al. (2017). The shared socioeconomic pathways and their energy, land use, and greenhouse gas emissions implications: An overview. *Global environmental change*, *42*, 153–168.

[328] Rianna, G., Reder, A., Sousa, M. L., & Dimova, S. (2023). Harmonised procedure to update thermal loads in the Eurocodes. Case study for Italy. *Climate Services*, *30*, 100391. https://doi.org/10.1016/j.cliser.2023.100391

[329] Richardson, M. G. (1988). *Carbonation of reinforced concrete: Its causes and management*. Citis.

[330] Rincon, L. F., Martı´n-Pérez, B., Matos, J. C. E., Moscoso, Y. F., & Bastidas-Arteaga, E. (2026). Experimental and numerical approaches to carbonation–chloride ingress effects on corrosion of reinforced concrete: A review. *Structural Engineering International*, 1–9. https://doi.org/10.1080/10168664.2025.2602862

[331] Robinson, J. D., Vahedifard, F., & AghaKouchak, A. (2017). Rainfall-triggered slope instabilities under a changing climate: Comparative study using historical and projected precipitation extremes. *Canadian Geotechnical Journal*, *54*(1), 117–127. https://doi.org/10.1139/cgj-2015-0602

[332] Robock, A. (2000). Volcanic eruptions and climate. *Reviews of geophysics*, *38*(2), 191–219.

[333] Rodriguez, J., Ortega, L., & Casal, J. (1997). Load carrying capacity of concrete structures with corroded reinforcement. *Construction and building materials*, *11*(4), 239–248.

[334] Rootzén, H., & Katz, R. W. (2013). Design Life Level: Quantifying risk in a changing climate. *Water Resources Research*, *49*(9), 5964–5972. https://doi.org/10.1002/wrcr.20425

[335] Rosenblatt, M. (1952). Remarks on a multivariate transformation. *The annals of mathematical statistics*, *23*(3), 470–472.

[336] Rosenblueth, E., & Mendoza, E. (1971). Reliability Optimization in Isostatic Structures. *Journal of the Engineering Mechanics Division*, *97*(6), 1625–1642. https://doi.org/10.1061/JMCEA3.0001521

[337] Rosowsky, D. V. (2018). Assessing climate change impacts on hurricane hazards. In *Climate change and its impacts: Risks and inequalities* (pp. 93–107). Springer.

[338] Rubinstein, R. Y., & Kroese, D. P. (2008). *Simulation and the monte carlo method*. John Wiley; Sons.

[339] Russell, D., Basheer, P. M., Rankin, G. B., & Long, A. E. (2001). Effect of relative humidity and air permeability on prediction of the rate of carbonation of concrete. *Proceedings of the Institution of Civil Engineers-Structures and Buildings*, *146*(3), 319–326. https://doi.org/10.1680/stbu.2001.146.3.319

[340] Saetta, A., Scotta, R., & Vitaliani, R. (1993). Analysis of chloride diffusion into partially saturated concrete. *Materials Journal*, *90*(5), 441–451. https://doi.org/10.14359/3874

[341] Saetta, A., Scotta, R., & Vitaliani, R. (1999). Coupled environmental-mechanical damage model of rc structures. *Journal of engineering mechanics*, *125*(8), 930–940. https://doi.org/10.1061/(ASCE)0733-9399(1999)125:8(930)

[342] Saetta, A., & Vitaliani, R. (2004). Experimental investigation and numerical modeling of carbonation process in reinforced concrete structures: Part i: Theoretical formulation. *Cement and concrete research*, *34*(4), 571–579. https://doi.org/10.1016/j.cemconres.2003.09.009

[343] Santos, S. R. d., Matioli, L. C., & Beck, A. T. (2012). New optimization algorithms for structural reliability analysis. *Computer Modeling in Engineering & Sciences(CMES)*, *83*(1), 23–55.

[344] Sarveswaran, V., & Roberts, M. B. (1999). Reliability analysis of deteriorating structures—the experience and needs of practising engineers. *Structural Safety*, *21*(4), 357–372. https://doi.org/10.1016/S0167-4730(99)00030-2

[345] Schlune, H., Plos, M., & Gylltoft, K. (2011). Safety formats for nonlinear analysis tested on concrete beams subjected to shear forces and bending moments. *Engineering structures*, *33*(8), 2350–2356. https://doi.org/10.1016/j.engstruct.2011.04.008

[346] Schlune, H., Plos, M., & Gylltoft, K. (2012). Safety formats for non-linear analysis of concrete structures. *Magazine of Concrete Research*, *64*(7), 563–574. https://doi.org/10.1680/macr.11.00046

[347] Schwartz, P. (1997). *Art of the long view: Planning for the future in an uncertain world*. John Wiley & Sons.

[348] Schwartz Jr, H. G. (2010). Adaptation to the impacts of climate change on transportation. *The Bridge*, *40*(3), 5–13.

[349] Seaby, L. P., Refsgaard, J. C., Sonnenborg, T., Stisen, S., Christensen, J. H., & Jensen, K. H. (2013). Assessment of robustness and significance of climate change signals for an ensemble of distribution-based scaled climate projections. *Journal of hydrology*, *486*, 479–493.

[350] Seneviratne, S. I., Zhang, X., Adnan, M., Badi, W., Dereczynski, C., Luca, A. D., Ghosh, S., Iskandar, I., Kossin, J., Lewis, S., Otto, F., Pinto, I., Satoh, M., Vicente-Serrano, S. M., Wehner, M., Zhou, B., & Allan, R. (2021). Weather and climate extreme events in a changing climate. In V. Masson-Delmotte, P. Zhai, A. Pirani, & S. L. Connors (Eds.), *Climate change 2021: The physical science basis. working group i contribution to the sixth assessment report of the intergovernmental panel on climate change* (pp. 1513–1766). Cambridge University Press.

[351] Seo, D.-W., & Caracoglia, L. (2015). Exploring the impact of "climate change" on lifetime replacement costs for long-span bridges prone to torsional flutter. *Journal of Wind Engineering and Industrial Aerodynamics*, *140*, 1–9. https://doi.org/10.1016/j.jweia.2015.01.013

[352] Sepúlveda, I., Haase, J. S., Liu, P. L.-F., Grigoriu, M., & Winckler, P. (2021). Non-Stationary Probabilistic Tsunami Hazard Assessments Incorporating Climate-Change-Driven Sea Level Rise. *Earth's Future*, *9*(6), e2021EF002007. https://doi.org/10.1029/2021EF002007

[353] Shi, X., Yao, Y., Wang, L., Zhang, C., & Ahmad, I. (2021). A modified numerical model for predicting carbonation depth of concrete with stress damage. *Construction and Building Materials*, *304*, 124389. https://doi.org/10.1016/j.conbuildmat.2021.124389

[354] Shibata, T., & Takeyama, T. (1977). Stochastic theory of pitting corrosion. *Corrosion*, *33*(7), 243–251. https://doi.org/10.5006/0010-9312-33.7.243

[355] Shine, K. P. (2000). Radiative forcing of climate change. *Space Science Reviews*, *94*(1), 363–373.

[356] Shirkhani, H., Lounis, Z., & Zhang, J. (2023). Life-cycle design of concrete highway bridge decks under climate change. In *Life-cycle of structures and infrastructure systems* (pp. 1609–1616). CRC Press.

[357] Shirkhani, H., Zhang, J., & Lounis, Z. (2020). Ensemble analysis of climate-change impacts on design-service life of reinforced concrete bridge decks across canada. *Natural Hazards Review*, *21*(3), 04020030. https://doi.org/10.1061/(ASCE)NH.1527-6996.0000397

[358] Shupe, T., Lebow, S., & Ring, D. (2008). *Causes and control of wood decay, degradation & stain*. Louisiana State University Agricultural Center.

[359] SIA. (2011). *SIA 269 - Existing structures – Bases for examination and interventions*. Swiss Society of Engineers; Architects.

[360] Skjolsvold, O. (1986). Carbonation depths of concrete with and without condensed silica fume. *Special Publication*, *91*, 1031–1048. https://doi.org/10.14359/10111

[361] Slobbe, A., Rózsás, Á., Allaix, D. L., & Bigaj-van Vliet, A. (2020). On the value of a reliability-based nonlinear finite element analysis approach in the assessment of concrete structures. *Structural Concrete*, *21*(1), 32–47. https://doi.org/10.1002/suco.201800344

[362] Smith, S. J., & Wigley, T. (2006). Multi-gas forcing stabilization with minicam. *The Energy Journal*, *27*(3_suppl), 373–392.

[363] Snaiki, R., Wu, T., Whittaker, A. S., & Atkinson, J. F. (2020). Hurricane wind and storm surge effects on coastal bridges under a changing climate. *Transportation research record*, *2674*(6), 23–32. https://doi.org/10.1177/0361198120917671

[364] Somerville, G., Andrade, C., Fagerlund, G., Lagerblad, B., Rodriguez, J., & Tuutti, K. (1995). *The residual service life of reinforced concrete structures* (Technical Report BRITE-EI-JRAM Project 4062). Commission of the European Communities.

[365] Sørensen, J. D., Kroon, I. B., & Faber, M. H. (1994). Optimal reliability-based code calibration. *Structural Safety*, *15*(3), 197–208. https://doi.org/10.1016/0167-4730(94)90040-X

[366] Sørensen, J. D., Hansen, S., & Nielsen, T. A. (2002). Calibration of partial safety factors in danish structural codes. *JCSS Workshop on Reliability Based Code Calibration*, *21*(22.03).

[367] Steenbergen, R. D. J. M., & Vrouwenvelder, A. C. W. M. (2010). Safety philosophy for existing structures and partial factors for traffic loads on bridges. *Heron*, *55*(2), 123–139.

[368] Steenbergen, R. D. J. M., Koster, T., & Geurts, C. P. (2012). The effect of climate change and natural variability on wind loading values for buildings. *Building and Environment*, *55*, 178–186. https://doi.org/10.1016/j.buildenv.2012.03.010

[369] Steenbergen, R. D. J. M., Sýkora, M., Diamantidis, D., Holický, M., & Vrouwenvelder, T. (2015). Economic and human safety reliability levels for existing structures. *Structural Concrete*, *16*(3), 323–332. https://doi.org/10.1002/suco.201500022

[370] Stefanoni, M., Angst, U., & Elsener, B. (2018). Corrosion rate of carbon steel in carbonated concrete–a critical review. *Cement and Concrete Research*, *103*, 35–48. https://doi.org/10.1016/j.cemconres.2017.10.007

[371] Stephens, G. L., & L'Ecuyer, T. (2015). The earth's energy balance. *Atmospheric Research*, *166*, 195–203.

[372] Stewart, M. G., Teply, B., & Kralova, H. (2002). The effect of temporal and spatial variability of ambient carbon dioxide concentrations on carbonation of rc structures. *9th international conference on durability of building materials and components, CSIRO, Paper*, *246*.

[373] Stewart, M. G. (2009). Mechanical behaviour of pitting corrosion of flexural and shear reinforcement and its effect on structural reliability of corroding rc beams. *Structural safety*, *31*(1), 19–30. https://doi.org/10.1016/j.strusafe.2007.12.001

[374] Stewart, M. G., & Al-Harthy, A. (2008). Pitting corrosion and structural reliability of corroding rc structures: Experimental data and probabilistic analysis. *Reliability engineering & system safety*, *93*(3), 373–382.

[375] Stewart, M. G., & Rosowsky, D. V. (1998). Structural safety and serviceability of concrete bridges subject to corrosion. *Journal of Infrastructure Systems*, *4*(4), 146–155. https://doi.org/10.1061(ASCE)1076-0342(1998)4:4(146)

[376] Stewart, M. G., Wang, X., & Nguyen, M. N. (2011). Climate change impact and risks of concrete infrastructure deterioration. *Engineering Structures*, *33*(4), 1326–1337. https://doi.org/10.1016/j.engstruct.2011.01.010

[377] Stewart, M. G., Wang, X., & Nguyen, M. N. (2012). Climate change adaptation for corrosion control of concrete infrastructure. *Structural Safety*, *35*, 29–39. https://doi.org/10.1016/j.strusafe.2011.10.002

[378] Stott, P. (2016). How climate change affects extreme weather events. *Science*, *352*(6293), 1517–1518. https://doi.org/10.1126/science.aaf7271

[379] Strydom, S., & Savage, M. J. (2017). Potential impacts of climate change on wildfire dynamics in the midlands of KwaZulu-Natal, South Africa. *Climatic Change*, *143*(3), 385–397. https://doi.org/10.1007/s10584-017-2019-8

[380] Sykora, M., Diamantidis, D., Holicky, M., & Jung, K. (2017). Target reliability for existing structures considering economic and societal aspects. *Structure and Infrastructure Engineering*, *13*(1), 181–194. https://doi.org/10.1080/15732479.2016.1198394

[381] Sykora, M., Holicky, M., & Marková, J. (2013). Verification of existing reinforced concrete bridges using the semi-probabilistic approach. *Engineering Structures*, *56*(0), 1419–1426. https://doi.org/10.1016/j.engstruct.2013.07.015

[382] Sykora, M., Holicky, M., Prieto, M., & Tanner, P. (2015). Uncertainties in resistance models for sound and corrosion-damaged RC structures according to EN 1992-1-1. *Materials and Structures*, *48*(10), 3415–3430. https://doi.org/10.1617/s11527-014-0409-1

[383] Sýkora, M., Holicky, M., & Diamantidis, D. (2016). Target reliability for existing civil engineering systems. *Second International Symposium on Stochastic Models in*

Reliability Engineering, Life Science and Operations Management (SMRLO2016), Beer Sheva, Israel, February 15-18, 2016., 109–114. https://doi.org/10.1109/SMRLO.2016.28

[384] Tanner, P., & Hingorani, R. (2010). Development of risk-based requirements for structural safety. In M. A. Hirt, J. Radić, & A. Mandić (Eds.), *Proceedings of the Joint IABSE-fib Conference: Codes in Structural Engineering: Developments and Needs for International Practice*. SECON-CSSE.

[385] Tanner, P., Lara, C., & Prieto, M. (2011). Semi-probabilistic models for the assessment of existing concrete structures. In M. H. Faber, J. Köhler, & K. Nishijima (Eds.), *Applications of Statistics and Probability in Civil Engineering: Proceedings of the 11th International Conference on Applications of Statistics and Probability in Civil Engineering (ICASP11), ETH Zurich, Zurich, Switzerland, August 1-4, 2011* (pp. 309–310). CRC Press/Balkema.

[386] Tanner, P., & Hingorani, R. (2015). Acceptable risks to persons associated with building structures. *Structural Concrete*, *16*(3), 314–322. https://doi.org/10.1002/suco.201500012

[387] Taylor, K. E., Stouffer, R. J., & Meehl, G. A. (2012). An overview of cmip5 and the experiment design. *Bulletin of the American meteorological Society*, *93*(4), 485–498.

[388] Tebaldi, C., & Knutti, R. (2007). The use of the multi-model ensemble in probabilistic climate projections. *Philosophical transactions of the royal society A: mathematical, physical and engineering sciences*, *365*(1857), 2053–2075. https://doi.org/10.1098/rsta.2007.2076

[389] Thoft-Christensen, P. (1998). Assessment of the reliability profiles for concrete bridges. *Engineering structures*, *20*(11), 1004–1009. https://doi.org/10.1016/S0141-0296(97)00196-X

[390] Thoft-Christensen, P., & Murotsu, Y. (2012). *Application of structural systems reliability theory*. Springer Science & Business Media.

[391] Thoft-Cristensen, P., & Baker, M. J. (1982). *Structural reliability theory and its applications*. Springer Berlin.

[392] Toll, D. G., Abedin, Z., Buma, J., Cui, Y., Osman, A. S., & Phoon, K. K. (2012). *The Impact of Changes in the Water Table and Soil Moisture on Structural Stability of Buildings and Foundation Systems: Systematic Review (CEE10-005 (SR90))* (Technical Report). Collaboration for Environmental Evidence. Durham, UK, Durham University Library.

[393] TRB. (2008). *Potential impacts of climate change on us transportation: Special report 290* (Vol. 290). Transportation Research Board.

[394] Trzaska, S., & Schnarr, E. (2014). *A review of downscaling methods for climate change projections*. U.S. Agency for International Development.

[395] Tuutti, K. (1982). *Corrosion of steel in concrete* (Doctoral dissertation). Lund University Research Portal. https://portal.research.lu.se/en/publications/corrosion-of-steel-in-concrete

[396] Tvedt, L. (1990). Distribution of quadratic forms in normal space—application to structural reliability. *Journal of engineering mechanics*, *116*(6), 1183–1197.

[397] Val, D. V., Andrade, C., Sykora, M., Stewart, M. G., Bastidas-Arteaga, E., Mlcoch, J., Truong, Q. C., & El Soueidy, C.-P. (2025). Probabilistic modelling of deterioration of reinforced concrete structures. *Structural Safety*, *113*, 102454. https://doi.org/10.1016/j.strusafe.2024.102454

[398] Val, D. V., & Melchers, R. E. (1997). Reliability of deteriorating rc slab bridges. *Journal of structural engineering*, *123*(12), 1638–1644. https://doi.org/10.1061/(ASCE)0733-9445(1997)123:12(1638)

[399] Val, D. V., & Stewart, M. G. (2002). Safety Factors for Assessment of Existing Structures. *Journal of Structural Engineering*, *128*(2), 258–265. https://doi.org/10.1061/(ASCE)0733-9445(2002)128:2(258)

[400] Valor, A., Caleyo, F., Alfonso, L., Velázquez, J., & Hallen, J. (2013). Markov chain models for the stochastic modeling of pitting corrosion. *Mathematical Problems in Engineering*, *2013*(1), 108386. https://doi.org/10.1155/2013/108386

[401] Van Nierop, S., Viljoen, C., & Lenner, R. (2017). Target reliability of concrete structures governed by serviceability limit state design. *Proceedings of the 15th International probabilistic workshop (IPW), Technische Universität Dresden, Dresden, Germany, Septemeber 27-29, 2017*.

[402] Van Vuuren, D. P., Den Elzen, M. G., Lucas, P. L., Eickhout, B., Strengers, B. J., Van Ruijven, B., Wonink, S., & Van Houdt, R. (2007). Stabilizing greenhouse gas concentrations at low levels: An assessment of reduction strategies and costs. *Climatic change*, *81*(2), 119–159.

[403] Vandamme, M., Zhang, Q., Ulm, F.-J., Le Roy, R., Zuber, B., Gartner, E., & Termkhajornkit, P. (2013). Creep properties of cementitious materials from indentation testing: Significance, influence of relative humidity, and analogy between csh and soils. In *Mechanics and physics of creep, shrinkage, and durability of concrete: A tribute to zdeňk p. bažant* (pp. 48–61). American Society of Civil Engineers. https://doi.org/10.1061/9780784413111.005

[404] van Vuuren, D. P., Edmonds, J., Kainuma, M., Riahi, K., Thomson, A., Hibbard, K., Hurtt, G. C., Kram, T., Krey, V., Lamarque, J.-F., Masui, T., Meinshausen, M., Nakicenovic, N., Smith, S. J., & Rose, S. K. (2011). The representative concentration

pathways: An overview. *Climatic Change*, *109*(1), 5. https://doi.org/10.1007/s10584-011-0148-z

[405] Velarde, J., Mankar, A., Kramhøft, C., & Sørensen, J. D. (2020). Probabilistic calibration of fatigue safety factors for offshore wind turbine concrete structures. *Engineering Structures*, *222*, 111090. https://doi.org/10.1016/j.engstruct.2020.111090

[406] Vergani, M. (2010). *Modellazione del degrado di strutture in calcestruzzo armato soggette a corrosione* (Master's Thesis in Civil Engineering). Politecnico di Milano.

[407] Vidal, T., Castel, A., & François, R. (2004). Analyzing crack width to predict corrosion in reinforced concrete. *Cement and concrete research*, *34*(1), 165–174. https://doi.org/10.1016/S0008-8846(03)00246-1

[408] Villain, G., Sbartaı, Z. M., Dérobert, X., Garnier, V., & Balayssac, J.-P. (2012). Durability diagnosis of a concrete structure in a tidal zone by combining ndt methods: Laboratory tests and case study. *Construction and Building materials*, *37*, 893–903. https://doi.org/10.1016/j.conbuildmat.2012.03.014

[409] Vousdoukas, M., Mentaschi, L., Mongelli, I., Ciscar Martinez, J., Hinkel, J., Ward, P., Gosling, S., & Feyen, L. (2020). *Adapting to rising coastal flood risk in the eu under climate change*. Joint Research Center. https://publications.jrc.ec.europa.eu/repository/handle/JRC118512

[410] Vrouwenvelder, A. C. W. M. (2002). Developments towards full probabilistic design codes. *Structural Safety*, *24*(2), 417–432. https://doi.org/10.1016/S0167-4730(02)00035-8

[411] Vrouwenvelder, A. C. W. M. (2012). Target reliability as a function of the design working life. *Proceedings of the 6th International Forum on Engineering Decision Making (IFED2012), Lake Louise, Canada, January 26-29, 2012.*

[412] Vrouwenvelder, A. C. W. M., & Scholten, N. (2010). Assessment Criteria for Existing Structures. *Structural Engineering International*, *20*(1), 62–65. https://doi.org/10.2749/101686610791555595

[413] Vrouwenvelder, A. C. W. M., & Siemes, A. J. M. (1987). Probabilistic calibration procedure for the derivation of partial safety factors for the netherlands building codes. *HERON*, *32*(4).

[414] Vu, K. A. T., & Stewart, M. G. (2000). Structural reliability of concrete bridges including improved chloride-induced corrosion models. *Structural safety*, *22*(4), 313–333. https://doi.org/10.1016/S0167-4730(00)00018-7

[415] Vuuren, D. v., Eickhout, B., Lucas, P., & Elzen, M. d. (2006). Long-term multi-gas scenarios to stabilise radiative forcing-exploring costs and benefits within an integrated assessment framework. *The energy journal*, *27*(3_suppl), 201–234.

[416] Walraven, J., & Dieteren, G. (2023). Approach to assessment of existing structures in the fib Model Code 2020. *Structural Concrete*, *24*(4), 4387–4395. https://doi.org/10.1002/suco.202300076

[417] Wang, X., Yang, Q., Peng, X., & Qin, F. (2024). A review of concrete carbonation depth evaluation models. *Coatings*, *14*(4), 386. https://doi.org/10.3390/coatings14040386

[418] Weart, S. (2010). The development of general circulation models of climate. *Studies in History and Philosophy of Science Part B: Studies in History and Philosophy of Modern Physics*, *41*(3), 208–217.

[419] Wilby, R. L., Charles, S. P., Zorita, E., Timbal, B., Whetton, P., & Mearns, L. O. (2004). *Guidelines for the use of climate scenarios developed from statistical downscaling methods* (tech. rep.) [Supporting material available from the IPCC Data Distribution Centre (DDC)]. Intergovernmental Panel on Climate Change (IPCC), Task Group on Data, Scenario Support for Impact, and Climate Analysis (TGCIA). Geneva, Switzerland.

[420] WMO. (2017). *Guidelines on the calculation of climate normals* (tech. rep. WMO-No. 1203). World Meteorological Organization. Geneva, Switzerland.

[421] WMO. (2018). Scientific assessment of ozone depletion: 2018.

[422] WMO. (2023). *Guidelines on the definition and characterization of extreme weather and climate events* (tech. rep. WMO-No. 1310). World Meteorological Organization. Geneva, Switzerland.

[423] World Bank. (2012). *Turn down the heat: Why a 4°c warmer world must be avoided* (Report). World Bank. Washington, DC. http://documents.worldbank.org/curated/en/865571468149107611

[424] WorldBankGroup. (2025). *Climate change knowledge portal*. https://climateknowledgeportal.worldbank.org (accessed: 07.07.2025)

[425] Wu, Y.-T., & Wirsching, P. H. (1987). New algorithm for structural reliability estimation. *Journal of Engineering Mechanics*, *113*(9), 1319–1336.

[426] Wu, Y.-Z., Lv, H.-L., Zhou, S.-C., & Fang, Z.-N. (2016). Degradation model of bond performance between deteriorated concrete and corroded deformed steel bars. *Construction and Building Materials*, *119*, 89–95. https://doi.org/10.1016/j.conbuildmat.2016.04.061

[427] Xi, F., Davis, S. J., Ciais, P., Crawford-Brown, D., Guan, D., Pade, C., Shi, T., Syddall, M., Lv, J., Ji, L., et al. (2016). Substantial global carbon uptake by cement carbonation. *Nature Geoscience*, *9*(12), 880–883.

[428] Xu, M., Du, J., Wang, C., & Li, Y. (2017). Hybrid uncertainty propagation in structural-acoustic systems based on the polynomial chaos expansion and

dimension-wise analysis. *Computer Methods in Applied Mechanics and Engineering*, *320*, 198–217. https://doi.org/10.1016/j.cma.2017.03.026

[429] Yalcyn, H., & Ergun, M. (1996). The prediction of corrosion rates of reinforcing steels in concrete. *Cement and concrete research*, *26*(10), 1593–1599. https://doi.org/10.1016/0008-8846(96)00139-1

[430] Yang, D. Y., & Frangopol, D. M. (2019). Physics-Based Assessment of Climate Change Impact on Long-Term Regional Bridge Scour Risk Using Hydrologic Modeling: Application to Lehigh River Watershed. *Journal of Bridge Engineering*, *24*(11), 04019099. https://doi.org/10.1061/(ASCE)BE.1943-5592.0001462

[431] Yoon, I.-S., Çopuroğlu, O., & Park, K.-B. (2007). Effect of global climatic change on carbonation progress of concrete. *Atmospheric Environment*, *41*(34), 7274–7285. https://doi.org/10.1016/j.atmosenv.2007.05.028

[432] Yousefpour, R., & Hanewinkel, M. (2016). Climate change and decision-making under uncertainty. *Current Forestry Reports*, *2*(2), 143–149.

[433] Zhang, D., Zhang, J., Yang, M., Wang, R., & Wu, Z. (2022). An enhanced finite step length method for structural reliability analysis and reliability-based design optimization. *Structural and Multidisciplinary Optimization*, *65*(8), 231.

[434] Zhang, H., Ellingwood, B. R., & Rasmussen, K. J. (2014). System reliabilities in steel structural frame design by inelastic analysis. *Engineering structures*, *81*, 341–348. https://doi.org/10.1016/j.engstruct.2014.10.003

[435] Zhang, H., Liu, H., Ellingwood, B. R., & Rasmussen, K. J. (2018). System reliabilities of planar gravity steel frames designed by the inelastic method in aisc 360-10. *Journal of Structural Engineering*, *144*(3), 04018011. https://doi.org/10.1061/(ASCE)ST.1943-541X.0001991

[436] Zhang, J., Shirkhani, H., & Lounis, Z. (2018). Climate change impact on design service life of concrete bridge decks exposed to chlorides. *Proc., 10th Int. Conf. on Short and Medium Span Bridges. Quebec, Canada: Canadian Society for Civil Engineering.*

[437] Zhang, R., Castel, A., & François, R. (2010). Concrete cover cracking with reinforcement corrosion of rc beam during chloride-induced corrosion process. *Cement and Concrete Research*, *40*(3), 415–425. https://doi.org/10.1016/j.cemconres.2009.09.026

[438] Zhang, Y., Ayyub, B. M., & Fung, J. F. (2022). Projections of corrosion and deterioration of infrastructure in United States coasts under a changing climate. *Resilient Cities and Structures*, *1*(1), 98–109. https://doi.org/10.1016/j.rcns.2022.04.004

[439] Zhang, Z., Jiang, C., Han, X., & Ruan, X. (2019). A high-precision probabilistic uncertainty propagation method for problems involving multimodal distributions.

Mechanical Systems and Signal Processing, *126*, 21–41. https://doi.org/10.1016/j.ymssp.2019.01.031

[440] Zhang, Z., Li, H., Xiong, J., Wang, F., Wei, L., & Ke, L. (2022). Determination of the Target Reliability Index of the Concrete Main Girder of Long-Span Structures Based on Structural Design Service Life. *Buildings*, *12*(12), 2249. https://doi.org/10.3390/buildings12122249

[441] Zhao, Y.-G., & Ono, T. (2001). Moment methods for structural reliability. *Structural safety*, *23*(1), 47–75. https://doi.org/10.1016/S0167-4730(00)00027-8

[442] Zhou, W., Xiang, W., & Hong, H.-P. (2017). Sensitivity of system reliability of corroding pipelines to modeling of stochastic growth of corrosion defects. *Reliability Engineering & System Safety*, *167*, 428–438. https://doi.org/10.1016/j.ress.2017.06.025

[443] Zhou, X. Y., Schmidt, F., & Jacob, B. (2012). Extrapolation of traffic data for development of traffic load models: Assessment of methods used during background works of eurocode. *Proceedings of the 6th Conference on Bridge Maintenance, Safety and Management (IABMAS2012), Lake Como, Italy, 8-12 July 2012*.

[444] Zhou, Y., Gencturk, B., Willam, K., & Attar, A. (2015). Carbonation-induced and chloride-induced corrosion in reinforced concrete structures. *Journal of Materials in Civil Engineering*, *27*(9), 04014245. https://doi.org/10.1061/(ASCE)MT.1943-5533.0001209

[445] Zorita, E., & Von Storch, H. (1999). The analog method as a simple statistical downscaling technique: Comparison with more complicated methods. *Journal of climate*, *12*(8), 2474–2489.